

Urotensin II in the development and progression of experimental chronic kidney disease

A thesis submitted to the University of Manchester for the degree of Doctor of
Philosophy (PhD) in the Faculty of Life Sciences

2015

Heather Eyre

Contents

List of Figures	6
List of Tables	13
List of Equations	15
Abstract	17
Declaration	18
Copyright statements	18
List of abbreviations	19
Acknowledgements	22
1: Introduction	23
1.1 Renal structure and function	23
1.1.1 Glomerular filtration	24
1.1.2 Tubular secretion and urine concentration	27
1.1.3 Renal haemodynamics	30
1.1.4 Renin, angiotensin and aldosterone	31
1.2 Chronic kidney disease	34
1.2.1 Prevalence	34
1.2.2 Causes and susceptibility	35
1.2.3 Pathophysiology and disease progression	39
1.2.4 Intervention	44
1.3 Animal models of chronic kidney disease	47
1.3.1 Genetic models of diabetic renal disease	47
1.3.2 Akita mouse strains	48
1.3.3 Streptozotocin induced type I diabetes mellitus	49
1.3.4 Induction of chronic renal failure by renal mass reduction	49
1.4 Urotensin II	51
1.4.1 Identification and isolation	51
1.4.2 Structure of urotensin II and urotensin II-related peptide	52
1.4.3 The urotensin II receptor (UT)	54

1.4.4	Urotensin II in physiology and disease	60
1.5	Aims and objectives	67
2:	Methods	69
2.1	Animals and regulations	69
2.2	5/6 th sub-total nephrectomy	69
2.3	Experimental design	73
2.4	Monitoring disease progression	81
2.5	Terminal sample collection	84
2.6	Urinary analysis	86
2.7	Blood sample analysis	89
2.8	Histological staining	91
2.9	Immunohistochemistry	95
2.10	Microscopy and image analysis	99
2.11	Validation of QuantiFast [®] SYBR Green RT-qPCR	100
2.12	Optimisation of QuantiFast [®] SYBR Green qPCR	112
2.13	SYBR Green qPCR for <i>Ywhaz</i> , <i>Uts2r</i> , <i>Uts2b</i> and <i>Uts2</i>	119
 The urotensin II system during the progression of chronic kidney disease following 5/6th subtotal nephrectomy		
3:	Results	125
3.1	Acute renal failure and survival	125
3.2	Physiological progression of chronic kidney disease	126
3.3	Terminal blood and urine analysis	132
3.4	Renal histology	134
3.5	Immunohistochemical staining of the extracellular matrix	145
3.6	The urotensin II system by immunohistochemistry	150
4:	Discussion	157
4.1	Initial phase	158
4.2	Stable phase	172
4.3	Late phase	177
4.4	Limitations of study design	187

4.5	Regression analysis	189
4.6	Conclusions	192
Expression of urotensin II system components by RT-qPCR		
5: Results		195
5.1	RNA quantification and quality control	195
5.2	<i>Ywhaz</i> - a potential reference gene	197
5.3	Urotensin II receptor - <i>Uts2r</i>	200
5.3.1	Example analysis of relative expression of <i>Uts2r</i>	203
5.4	Urotensin II related peptide - <i>Uts2b</i>	204
5.5	Urotensin II - <i>Uts2</i>	207
6: Discussion		209
6.1	mRNA extraction and quality control	209
6.2	Technical considerations of QuantiFast® SYBR Green qPCR	211
6.3.1	Controls and sample selection	211
6.2.2	Reference gene - <i>Ywhaz</i>	212
6.3	Expression of UII system components	213
6.3.1	Urotensin II receptor - <i>Uts2r</i>	213
6.3.2	Urotensin II related peptide - <i>Uts2b</i>	215
6.3.1	Urotensin II - <i>Uts2</i>	215
6.4	Experimental limitations and further considerations	216
6.5	Conclusions	216
Effects of intervention with UT receptor antagonist AZ13694621 on the progression of chronic kidney disease following 5/6th subtotal nephrectomy		
7: Results		219
7.1	Acute renal failure and survival	219
7.2	Physiological disease progression	220
7.3	Terminal data analysis	224
7.4	Histological profile	227
7.5	Immunohistochemistry for extra-cellular matrix	236

7.6	Immunohistochemical staining for urotensin II, urotensin II-related peptide and the urotensin II receptor	241
7.7	<i>Ywhaz</i> , <i>Uts2r</i> , <i>Uts2b</i> and <i>Uts2</i> analysis by RT-qPCR	247
8:	Discussion	263
8.1	Dosing regimen and tolerance	263
8.2	Physiological profile of intervention	266
8.3	Renal mass, histology and fibrosis	268
8.4	Expression of UII system components	269
8.5	Conclusions	270
9:	General Discussion	273
9.1	RT-qPCR for Urotensin II system components in the renal medulla	274
9.2	(Mal)adaption of the glomerular basement membrane	274
9.3	Scope for further intervention studies	275
9.4	Conclusion	277
	References	278
	Appendix A	309
	Appendix B	313

Word Count

63,379

List of Figures

1: Introduction

Figure 1.1	Schematic diagram of a nephron	24
Figure 1.2	The glomerular filtration barrier	25
Figure 1.3	Formation of urine in the nephron	29
Figure 1.4	The renin-angiotensin system	33
Figure 1.5	Interaction of factors in chronic kidney disease	36
Figure 1.6	Glucose homeostasis in diabetes	37
Figure 1.7	Structure and homology of the UT receptor	56
Figure 1.8	Signal transduction via the UT receptor	59

2: Methods

Figure 2.1	Schematic diagram of surgical 5/6 th sub-total nephrectomy	70
Figure 2.2	Fractional representation of renal tissue removed	73
Figure 2.3	Surgical and sampling timeline for the characterisation of the UII system following 5/6 th SNx in rat.	75
Figure 2.4	Pharmacokinetic profile of AZ13694621 in rat blood, following p.o. administration at 5 mg/Kg	78
Figure 2.5	Experimental protocol for UT antagonist study	80
Figure 2.6	Dissection diagram for cryogenic storage of renal tissue	85
Figure 2.7	Glomerulosclerosis scoring index, visual scale	93
Figure 2.8	A typical thermocycler profile for SYBR green qPCR	107
Figure 2.9	Pilot study results: gel electrophoresis of RNA extracts	109
Figure 2.10	Pilot study results: <i>Ywhaz</i> amplification and dissociation curves	110
Figure 2.11	Pilot study results: gel electrophoresis of <i>Ywhaz</i> qPCR products	111
Figure 2.12	Amplification and dissociation curves of <i>Uts2r</i> , <i>Uts2b</i> and <i>Uts2</i>	113
Figure 2.13	Gel electrophoresis of <i>Uts2r</i> qPCR products	115
Figure 2.14	Gel electrophoresis of <i>Uts2b</i> qPCR products	116
Figure 2.15	Gel electrophoresis of <i>Uts2</i> qPCR products	117

3: Results: Characterisation of the 5/6th subtotal nephrectomy model of chronic kidney disease

Figure 3.1	Kaplan-Meier survival plot of rats following 5/6 th SNx surgery	126
Figure 3.2	Growth curve of rats following 5/6 th SNx surgery	127
Figure 3.3	Comparison of systolic blood pressure in sham and SNx rats	128
Figure 3.4	Comparison of heart rate in sham and SNx rats	129
Figure 3.5	Albumin:creatinine ratio in SNx and Sham rats	131
Figure 3.6	Terminal urinary albumin creatinine ratio is elevated in SNx groups	132
Figure 3.7	Terminal blood biochemistry: blood urea nitrogen and blood creatinine in sham and SNx rats	133
Figure 3.8	Hypertrophy occurs in the remnant kidneys of SNx rats	133
Figure 3.9	Haematoxylin and eosin stained cortical sections of SNx rats and time-matched sham controls	135
Figure 3.10	Haematoxylin and eosin stained medullary sections of SNx rats and time-matched sham controls	136
Figure 3.11	Haematoxylin and eosin stained sections SNx rats: representative histological abnormalities	137
Figure 3.12	Glomerulosclerosis index from periodic acid Schiff stained sections of SNx and sham rats.	138
Figure 3.13	Representative periodic acid Schiff stained glomeruli from SNx and time-matched sham controls	140
Figure 3.14	Masson's trichrome stained cortical sections of SNx rats and time-matched sham controls	143
Figure 3.15	Masson's trichrome stained medullary sections of SNx rats and time-matched sham controls	144
Figure 3.16	Type IV collagen immunostaining in the renal cortex of SNx rats and time-matched sham controls	146
Figure 3.17	Laminin- β immunostaining in the renal cortex of SNx rats and time-matched sham controls	147
Figure 3.18	Type IV collagen immunostaining in the renal medulla of SNx rats and time-matched sham controls	148

Figure 3.19	Laminin- β immunostaining in the renal medulla of SNx rats and time-matched sham controls	149
Figure 3.20	UII-reactive immuno-reactivity in the cortex of SNx and time-matched sham controls	151
Figure 3.21	UII-reactive immuno-reactivity in the medulla of SNx and time-matched sham controls	152
Figure 3.22	UT immuno-reactivity in the cortex of SNx and time-matched sham controls	154
Figure 3.23	UT immuno-reactivity in the cortex of SNx and time-matched sham controls	155
Figure 3.24	UT immuno-reactivity in the medullary collecting ducts is not uniform	156

4: Discussion: Characterisation of the 5/6th subtotal nephrectomy model of chronic kidney disease

Figure 4.1	Renal mass removed, peak systolic blood pressure and peak urinary albumin:creatinine ratio	190
Figure 4.2	Predictive factors in the final survival model	191

5: Results: RT-qPCR analysis for *Ywhaz*, *Uts2r*, *Uts2b* and *Uts2*

Figure 5.1	Micro-volume spectrophotometer analysis of RNA extracts	196
Figure 5.2	Gel electrophoresis of RNA extracts	197
Figure 5.3	<i>Ywhaz</i> Amplification and dissociation curves	198
Figure 5.4	<i>Ywhaz</i> assay - Ct values	199
Figure 5.5	<i>Ywhaz</i> assay - gel electrophoresis of PCR products	200
Figure 5.6	<i>Uts2r</i> Amplification and dissociation curves	201
Figure 5.7	<i>Uts2r</i> assay - Ct values	202
Figure 5.8	<i>Uts2r</i> assay - gel electrophoresis of PCR products	203
Figure 5.9	Relative expression of <i>Uts2r</i>	204
Figure 5.10	<i>Uts2b</i> Amplification and dissociation curves	205
Figure 5.11	<i>Uts2b</i> assay - Ct values	206
Figure 5.12	<i>Uts2b</i> assay - gel electrophoresis of PCR products	207
Figure 5.13	<i>Uts2</i> Amplification and dissociation curves	208

7: Results: Intervention with UT antagonist AZ13694621

Figure 7.1	Kaplan-Meier survival plot of rats following 5/6 th SNx surgery	219
Figure 7.2	Growth curve of rats following 5/6 th SNx surgery	220
Figure 7.3	Systolic blood pressure in SNx and sham rats receiving UT antagonist or vehicle control	222
Figure 7.4	Heart rate in SNx and sham rats receiving UT antagonist or vehicle control	223
Figure 7.5	Urinary albumin creatinine ratio in SNx and sham and their treatment-matched controls	224
Figure 7.6	Terminal blood biochemistry: blood urea nitrogen and blood creatinine in sham and SNx rats receiving vehicle or UT-A	225
Figure 7.7	Terminal single kidney mass and estimated remnant kidney hypertrophy	226
Figure 7.8	Haematoxylin and eosin stained renal cortex sections	228
Figure 7.9	Haematoxylin and eosin stained sections of renal medulla	229
Figure 7.10	Haematoxylin and eosin stained sections SNx rats representative histological abnormalities	230
Figure 7.11	Glomerulosclerosis index from periodic acid Schiff stained sections	231
Figure 7.12	Representative periodic acid Schiff stained glomeruli from SNx and sham controls receiving UT-A or vehicle	232
Figure 7.13	Masson's trichrome stained cortical sections of SNx rats and sham controls receiving UT-A or vehicle	234
Figure 7.14	Masson's trichrome stained medullary sections of SNx and sham rats receiving UT-A or vehicle	235
Figure 7.15	Collagen IV immuno-reactivity in the cortex of SNx and sham rats and their treatment-matched controls	237
Figure 7.16	Laminin- β immuno-reactivity in the cortex of SNx and treatment-matched sham controls	238
Figure 7.17	Collagen IV immuno-reactivity in medullary sections of SNx and treatment-matched sham controls	239
Figure 7.18	Laminin- β immuno-reactivity in the renal medulla of SNx and time-matched sham controls	240

Figure 7.19	UII immuno-reactivity in the renal cortex of UT-A treated SNx and sham rats and vehicle-treated controls	242
Figure 7.20	UII immuno-reactivity in the renal medulla of UT-A treated SNx and sham rats and vehicle-treated controls	243
Figure 7.21	UT immuno-reactivity in the renal cortex of UT-A treated SNx and sham rats and vehicle-treated controls	244
Figure 7.22	UT immuno-reactivity in the renal medulla of UT-A treated SNx and sham rats and vehicle-treated controls	245
Figure 7.23	Cellular distribution of UT immuno-reactivity in the medulla of SNx rats	246
Figure 7.24	RNA quality by micro-volume spectrophotometer	248
Figure 7.25	Gel electrophoresis of RNA extracts	249
Figure 7.26	<i>Ywhaz</i> amplification plots and dissociation curve	250
Figure 7.27	Ct values from <i>Ywhaz</i> amplification	251
Figure 7.28	PCR product gel following <i>Ywhaz</i> qPCR	252
Figure 7.29	<i>Uts2r</i> amplification plots and dissociation curve	253
Figure 7.30	Ct values from <i>Uts2r</i> amplification	254
Figure 7.31	PCR product gel following <i>Uts2r</i> qPCR	255
Figure 7.32	Relative expression of <i>Uts2r</i>	256
Figure 7.33	<i>Uts2b</i> amplification plots and dissociation curve	257
Figure 7.34	Ct values from <i>Uts2b</i> amplification	258
Figure 7.35	PCR product gel following <i>Uts2b</i> qPCR	259
Figure 7.36	<i>Uts2</i> amplification plots and dissociation curve	260
Figure 7.37	PCR product gel following <i>Uts2</i> qPCR	261
Appendix B		
Figure B.1	Experiment 1 - Raw Ct values - <i>Col4a1</i>	316
Figure B.2	Experiment 1 - Raw Ct values - <i>Lamb1</i>	317
Figure B.3	Experiment 1 - Raw Ct values - <i>Fn1</i>	317
Figure B.4	Experiment 2 - Raw Ct values - <i>Col4a1</i>	318
Figure B.5	Experiment 2 - Raw Ct values - <i>Lamb1</i>	319
Figure B.6	Experiment 2 - Raw Ct values - <i>Fn1</i>	319

List of Tables

1: Introduction

Table 1.1	Components of the glomerular filtration barrier	27
Table 1.2	Stages of chronic kidney disease (CKD)	34
Table 1.3	Classification of hypertension	38
Table 1.4	The glomerular filtration barrier in chronic kidney disease	43
Table 1.5	Progression of CKD in the 5/6 th SNx	50
Table 1.6	Amino acid sequence of urotensin II and URP	53
Table 1.7	Summary of example isolated vessel responses to UII	61

1: Methods

Table 2.1	Structural and pharmacological properties of UT antagonists	77
Table 2.2	Staggered set-up and collection to allow regular sampling	79
Table 2.3	Acceptance criteria for systolic blood pressure measurement	83
Table 2.4	Processing protocol for paraformaldehyde fixed d tissues	91
Table 2.5	Optimisation of heat-induced antigen retrieval	96
Table 2.6	Summary of conditions for immunohistochemistry	97
Table 2.7	Properties of qPCR primer sets	102
Table 2.8	Reverse transcription reaction volumes	105
Table 2.9	qPCR standard curve preparation	106
Table 2.10	Concentration and purity of RNA extracts	108
Table 2.11	Optimisation pf qPCR standard curves for <i>Uts2r</i> , <i>Uts2b</i> and <i>Uts2</i> primer sets	114
Table 2.12	Refined assay qPCR assay conditions	118

4: Discussion 1

Table 4.1	Quick reference: conversion of ACR units	164
Table 4.2	Summary of urinary albumin - creatinine ratio in the literature	165
Table 4.3	Methodology-specific classification of albumin:creatinine ratio	166

7: Results: Intervention with UT antagonist AZ13694621

Table 7.1	Summary of statistical analysis for body weight, systolic blood pressure and heart rate	221
-----------	---	-----

Appendix A

Table A.1	QuantiTect® primer assay properties - <i>Ywhaz</i>	309
Table A.2	QuantiTect® primer assay properties - <i>Uts2</i>	310
Table A.3	QuantiTect® primer assay properties - <i>Uts2b</i>	311
Table A.4	QuantiTect® primer assay properties - <i>Uts2r</i>	312

Appendix B

Table B.1	QuantiTect® primer assay properties - <i>Col4a1</i>	313
Table B.2	QuantiTect® primer assay properties - <i>Lamb1</i>	314
Table B.2	QuantiTect® primer assay properties - <i>Fn1</i>	315

List of Equations

1: Introduction

Equation 1.1	Renal clearance (1)	30
Equation 1.2	Renal clearance (2)	30
Equation 1.3	Filtration fraction	31

2: Methods

Equation 2.1	Calculation of renal mass reduction	72
Equation 2.2	Curve fitting for urinary creatinine assay	86
Equation 2.3	Curve fitting for urinary albumin assay	88
Equation 2.4	Curve fitting for blood plasma creatinine assay	90
Equation 2.5	Calculation of urea nitrogen in blood plasma	90
Equation 2.6	qPCR reaction efficiency (E)	122
Equation 2.7	Calculation of expression ratio with Pfaffl modification	122

Chapter 4 Discussion 1

Equation 4.1	Linear regression - calculation of survival time from predictors	192
--------------	--	-----

Abstract

Urotensin II (UII) is a potent peptide hormone with a complex species and vessel-dependent vascular profile. UII and the homologous UII-related peptide (URP) bind to the G-protein coupled urotensin II receptor (UT) with high affinity. The peptide ligands and receptor have been detected in numerous human and rat tissues including heart, brain and kidney. The kidney is a major source of UII, which appears to act as both an endocrine and paracrine mediator of renal function. UII has been shown to influence renal blood flow, glomerular filtration rate and sodium handling in the renal tubules. More speculative actions of UII as a pro-fibrotic mediator include the activation of fibroblasts and promotion of collagen synthesis. Abnormally elevated UII, URP and UT expression has been highlighted in a number of cardio-renal disease states; particularly end stage renal disease, diabetes and diabetic nephropathy (DN). This work aims to investigate the role of the UII system in the development and progression of CKD using an experimental model of CKD in rodents.

The first aim of the current work involved establishing the surgical 5/6th subtotal nephrectomy (SNx) model of chronic kidney disease (CKD) in the laboratory and forming a profile of UII expression in late stage experimental CKD to complement UII clinical data which are exclusively from patients in the later stages of disease. UII/URP and UT were substantially over-expressed in the kidneys of SNx rats in late stage CKD. This novel insight complements the clinical profile of CKD/DN where over expression of the UII system is routinely reported.

In a second study the 5/6th SNx rat model was used to explore the effects of chronic UT receptor antagonism on the progression of CKD. Although there were no discernible differences in kidney mass or histological profile between the treatment groups at the end of the study, there was a small delay in the development of albuminuria and in the onset of systolic blood pressure elevation in the UT antagonist treated cohort. The study did not produce clear-cut evidence defining the potential therapeutic value of UT-antagonism in the treatment of CKD. Despite this the results are encouraging and suggest that the role of UT-inhibition in CKD is worth considering further.

Declaration

No portion of the work referred to in the thesis has been submitted in support of an application for another degree or qualification of this or any other university or other institute of learning.

Copyright Statements

The author of this thesis (including any appendices and/or schedules to this thesis) owns certain copyright or related rights in it (the 'Copyright') and she has given The University of Manchester certain rights to use such Copyright, including for administrative purposes.

Copies of this thesis, either in full or in extracts and whether in hard or electronic copy, may be made only in accordance with the Copyright, Designs and Patents Act 1988 (as amended) and regulations issued under it, or, where appropriate, in accordance with licensing agreements which the University has from time to time. This page must form part of any such copies made.

The ownership of certain Copyright, patents, designs, trademarks and other intellectual property (the 'Intellectual Property') and any reproductions of copyright works in the thesis, for example graphs and table ('Reproductions'), which may be described in this thesis, may not be owned by the author and may be owned by third parties. Such Intellectual Property and Reproductions cannot and must not be made available for use without the prior written permission of the owner(s) of the relevant Intellectual Property and/or Reproductions.

Further information on the conditions under which disclosure, publication and commercialisation of this thesis, the Copyright and any Intellectual Property and/or Reproductions described in it may take place is available in the University IP Policy (see <http://www.campus.manchester.ac.uk/medialibrary/policies/intellectualproperty.pdf>), in any relevant Thesis restriction declarations deposited in the University Library, The University Library's regulations (see <http://www.manchester.ac.uk/library/aboutus/regulations>) and in The University's policy on presentation of Theses.

List of Abbreviations

ACR	Urinary albumin creatinine ratio (expressed as mg/ μ mol or mg/g)
AGEs	advanced glycation end products
AKI	Acute kidney injury
Ang	Angiotensin
ANOVA	Analysis of variance
ARF	Acute renal failure
AT	Angiotensin II receptor
bp	Base pairs
BPM	Beats per minute
BSF	Biological services facility
BUN	Blood urea nitrogen
B _{wt}	Body weight
CKD	Chronic kidney disease
C _(x)	Renal clearance <small>(substance)</small>
CAMK	Ca ²⁺ /calmodulin-dependent kinases
CHO	Chinese hamster ovary
CO	Cardiac output
<i>Col4a1</i>	Collagen type IV, alpha 1
CR	Creatinine
CVD	Cardiovascular disease
DAB	3, 3'-diaminobenzidine
DAG	Diacyl glycerol
DM	Diabetes mellitus
DN	Diabetic nephropathy
ECL	Extra-cellular loop
ECM	Extra-cellular matrix
ERK	Extracellular signal-regulated kinase
ESL	Endothelial cell surface layer
FF	Filtration fraction
<i>FN1</i>	Fibronectin 1
FP	Foot processes
GAG(s)	glycosaminoglycan(s)
(e)GFR	(estimated) Glomerular filtration rate
GBM	Glomerular basement membrane

GEnC	Glomerular endothelial cell
GFB	Glomerular filtration barrier
gDNA	genomic DNA
GPCR	G-protein coupled receptor
GSI	Glomerulosclerosis index
HEK	Human embryonic kidney
HIER	Heat-induce epitope retrieval
HPLC	High-performance liquid chromatography
HR	Heart rate
HRP	Horse radish peroxidase
HSPG(s)	Heparan sulphate proteoglycan(s)
IHC	Immunohistochemistry
i.p.	intra-peritoneal
IP ₃	Inositol 1, 4, 5-trisphosphate
IP ₃ R	Inositol 1, 4, 5-trisphosphate receptor
IQR	Inter-quartile range
IUPHAR	The International Union of Basic and Clinical Pharmacology
JGA	juxtaglomerular apparatus
KDIGO	Kidney Disease: Improving Global Outcomes
K-S	Kolmogorov-Smirnov
K _{wt}	Kidney weight
<i>Lamb1</i>	Laminin-β ₁
MAPK	Mitogen-activated protein kinases
MAU	micro-albuminuria
MetS	Metabolic syndrome
MTC	Masson's trichrome stain
(N)IDDM	(None) insulin dependent diabetes mellitus
NKF	National Kidney Foundation
No RT	No reverse transcriptase
NTC	No template control
OD	Optical density
PAH	<i>para</i> -aminohippuric acid
PAS	Periodic acid Schiff
PBS	Phosphate buffered saline
PIP ₂	Phosphatidylinositol 4, 5-bisphosphate
PK	Pharmacokinetic
PKC	Protein kinase C

PLC	Phospholipase C
p.o.	Per os, oral administration
qPCR	quantitative polymerase chain reaction
RBC	Red blood cell
RBF	Renal blood flow
RPF	Renal plasma flow
RF	Renal failure
RM	Repeated measures
RRC	Renal reserve capacity
RRT	Renal replacement therapy
RT	Reverse transcriptase
RTmp	Room temperature
(S)BP	(Systolic) blood pressure
SD	Sprague-Dawley
SENR	Sensory epithelium neuropeptide-like receptor
SNx	Subtotal nephrectomy (5/6 th)
TBS	Tris buffered saline
TBS-T	Tris buffered saline with tween 20 (0.05%)
T _m	Melting temperature
TPF	Total peripheral resistance
UAE	Urinary albumin excretion
UCE	Urotensin II converting enzyme
UII	Urotensin II (gene: UTS2/ <i>Uts2</i> , human/rat respectively)
URP	Urotensin II related protein (gene: UTS2B/ <i>Uts2b</i> , human/rat respectively, previously <i>Uts2d</i>)
UT	Urotensin II receptor (gene: UTS2R/ <i>Uts2r</i> , human/rat respectively)
UT-A	UT receptor antagonist (AZ13694621 or SB-611812)

Acknowledgments

There are numerous individuals that have provided support, feedback and some not-so-gentle nudges throughout the duration of this project. First of all I would like to thank Dr Nick Ashton for the opportunity, demonstrations, discussions, feedback and encouragement. Thank you to Dr Donald Ward for academic support and guidance and to my industrial supervisor Dave Smith for problem solving with enthusiasm in all situations. I would also like to show my appreciation to Dr Jo Glazier for invaluable support, technical expertise and inspiration.

I also extend my thanks to Peter Walker, Peter March, Roger Meadows and the BSF team for their guidance and technical advice, along with John Swales and Mark Denn (both AstraZeneca) for chemical sample analysis.

I'd also like to thank fellow students Ellen Forty, Dan Squirell, Alla Alkhalefa and Kyle Davies for providing a variety of technical and not so technical support throughout this project. And lastly Shaun, for supporting me completely.

1: Introduction

The actions of urotensin II (UII) and urotensin II-related peptide (URP) via the urotensin II receptor (UT) have been described in a number of tissues, including the brain and spinal cord, kidneys and vasculature. The urotensin II system appears to be altered in a number of cardio-renal disease states including the increasingly prevalent chronic kidney disease (CKD). However the (patho)physiological role of UII in CKD remains undefined.

A review of the literature follows in this chapter considering the structure and function of the healthy kidney and the changes that occur in chronic kidney disease with a particular focus on the development and progression of glomerulosclerosis. The selection of the 5/6th sub-total nephrectomy model of CKD is described with a review of animal models of CKD. The final section will cover the discovery of the phylogenetically ancient UII system in mammals and the evidence of its role as a paracrine modulator of renal function and potential implications in CKD.

1.1 Kidney structure and function

The kidneys remove metabolic waste products such as urea and creatinine whilst also regulating blood volume, composition and pressure.¹ The functional unit of the kidney is a nephron ([Figure 1.1](#)); a healthy adult kidney has around 1 million nephrons although this number can vary drastically between individuals.^{2,3} The removal of toxic metabolites, such as creatinine and urea, is a complex process and occurs alongside excretion or retention of water and electrolytes and the reabsorption of glucose, vitamins and minerals.

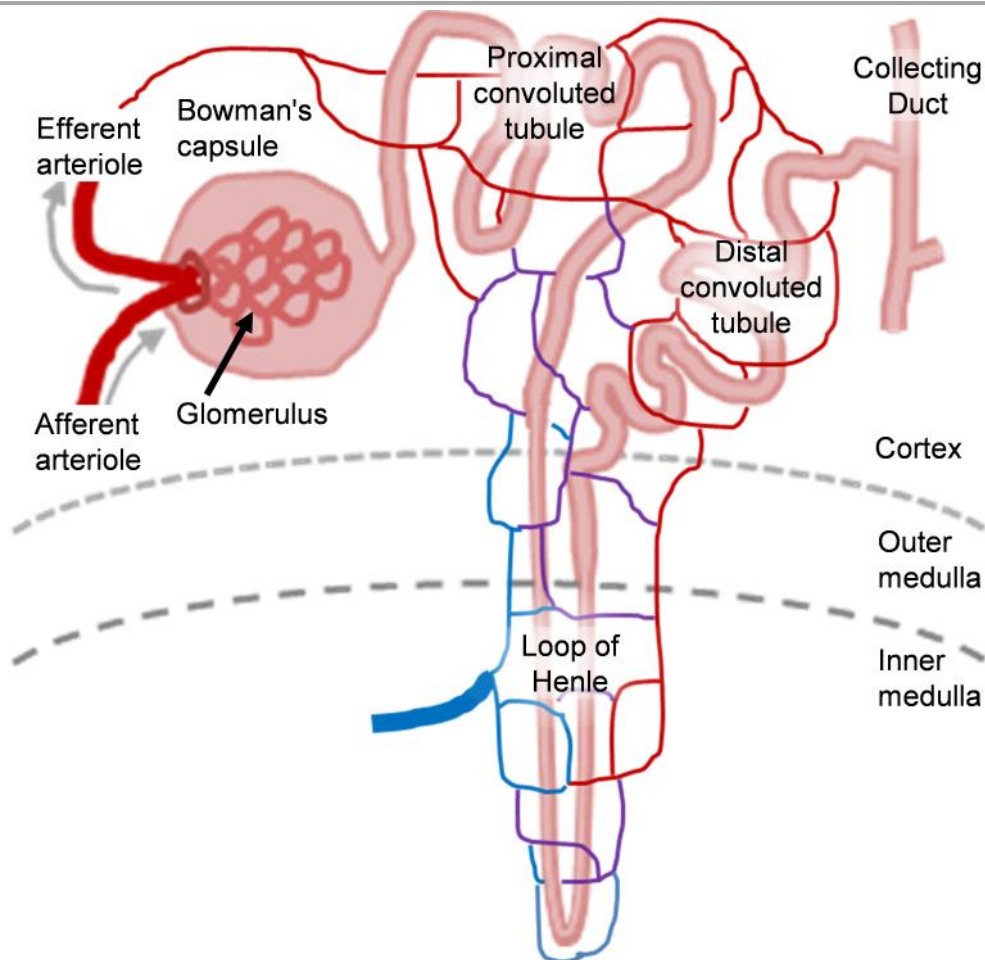


Figure 1.1 Nephron structure. Blood is filtered at the glomerulus, exchange of substances between the nephron tubules and interstitium/capillary network occurs throughout. The final filtrate is formed in the collecting duct, which can be further concentrated, in response to anti-diuretic hormone, as it passes further in to the medulla.

1.1.1 Glomerular filtration

Blood from the afferent arteriole enters the glomerulus, a bundle of capillaries where the plasma is filtered via the highly selective glomerular filtration barrier (GFB, [Figure 1.2](#)) under the influence of hydrostatic pressure. The resultant filtrate collects within the Bowman's space; this filtrate contains water, urea, glucose and electrolytes that entered the glomerulus. Only 20 % of the plasma volume that enters the glomerulus is filtered; the remaining 80 % exits into the efferent arteriole and contains an abundance of large (> 68 kDa) or highly charged molecules that cannot pass through the GFB, such as albumin.

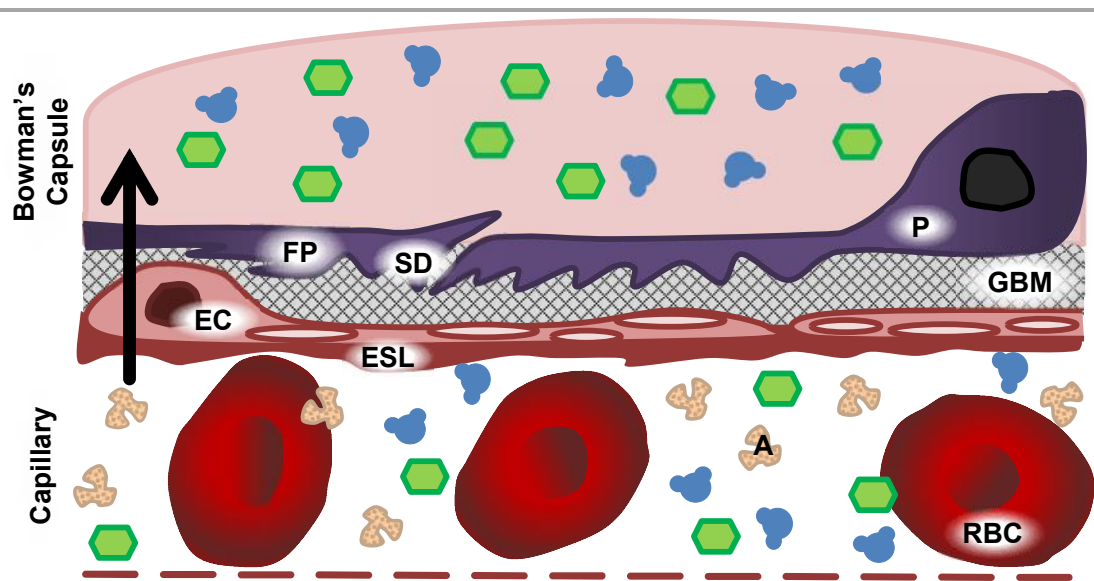


Figure 1.2 The highly selective glomerular filtration barrier is formed by interactions between capillary endothelial cells (EC, with glycocalyx and endothelial cell surface layer; ESL), the glomerular basement membrane (GBM) and podocytes (P). Podocytes have extended foot processes (FP) which encase the capillaries and interact with other podocytes to form highly selective slit diaphragms (SD). These slit diaphragms allow small molecules, such as glucose (■), water (●), small molecular weight waste products and electrolytes, into the Bowman's space whilst preventing larger objects such as red blood cells (RBC), albumin (A) and other proteins from leaving the capillaries. Arrow represents the directional movement of the filtrate.⁴⁻⁶

The GFB is a complex and highly selective structure made up of the fenestrated endothelium with glycocalyx coat and endothelial cell surface layer (ESL), glomerular basement membrane (GMB) and podocyte layer (organisation: [Figure 1.2](#), and major molecular components: [Table 1.1](#)).⁴⁻⁶ Until recently the role of the endothelial cell in glomerular selectivity had been contested as the size selectivity that could be attributed to the endothelium fenestrae, at 50 - 100 nM in diameter, had little impedance upon the movement of proteins such as albumin.⁶⁻⁸ However, substantial charge and size selectivity is purported to arise from the slime-like negatively-charged glycocalyx and ESL which are made up of glycosaminoglycans (GAGs), proteoglycans and glycoproteins that are anchored or secreted by the endothelial cells.⁸⁻¹² More recently the fenestrae have been shown to be spanned by diaphragms and filamentous structures which prevent the passage of smaller molecules such as albumin.^{6-8,10,13}

Moving in the direction of filtration the next structure to be encountered is the GBM, a thick (300 - 350 nm in healthy humans) and specialised basement membrane. The components of the GBM far outnumber those found in the other ECMs associated with either glomerular capillary endothelial cells (GEnCs) or podocytes independently.^{14,15} The long and filamentous coils of type IV collagen form a structural network supporting and separating the two cellular layers of the glomerular filtration barrier. This is formed predominantly by a heavily cross-linked network of $\alpha 3$, $\alpha 4$ and $\alpha 5$ chains and is thought to provide the physical strength required to cope with the hydrostatic filtration pressure.^{7,14} This contrasts with the BM of the renal tubules which are composed of an $\alpha 1$, $\alpha 2$ network.^{14,16-18} Laminin is a coiled heterotrimeric adhesion molecule and is also abundant within the GBM, specifically laminin-521 which is composed of $\alpha 5$, $\beta 2$, $\gamma 1$ proteins in a 1:1:1 arrangement. Laminins interact with cell to matrix adhesion molecules, integrins, forming physical contacts to the GMB and are involved in the activation of signalling pathways for cell survival, migration and proliferation via the recruitment of a plethora of adapter proteins.^{5,15,19} Laminin also interacts with other key components of the GMB including secreted extracellular heparan sulfate proteoglycans (HSPGs) such as agrin and perlecan.^{5,6,20} Agrin and nidogen, a ~200 kDa glycoprotein also known as entactin, interact with the collagen and laminin components of the GBM anchoring them together.^{5,16} As well as providing strength to the GFB the composition of this membrane is critical to endothelial and podocyte cell attachment for both cell survival and function; alterations in the expression of COL4 $\alpha 3$ and COL4 $\alpha 5$ have been implicated in impaired GFB function; mutations within these genes are implicated in Alport syndrome, an inherited condition typified by substantial haematuria, mild proteinuria and renal failure.^{7,21}

Glomerular filtration barrier component	Role	Components
Endothelial Cells	Cell surface layer	Proteoglycans, glycoproteins, glycosaminoglycans and sequestered albumin
	Adhesion	E-cadherin
Glomerular Basement Membrane		Collagen IV ($\alpha 3$, $\alpha 4$ $\alpha 5$) , laminin (heteromeric: $\alpha 5$, $\beta 2$, $\gamma 1$), Heparan sulfate proteoglycans (agrin, perlecan)
Podocytes	Attachment and foot process extension	Integrins ($\alpha_1\beta_3$), β -actin, synaptopodin, dystroglycan- $\alpha\beta$
	Slit diaphragm: cell-cell adhesion	Nephrin, NEPH family proteins, P-cadherin, podocin

Table 1.1 The function of the glomerular filtration barrier depends upon numerous components associated with the capillary endothelium, glomerular basement membrane and podocyte layer.^{5,6,8,9,11,16}

Podocytes also have a negatively charged glycocalyx, but the slit diaphragms which form between the foot processes are considered a key feature of a functional GFB.^{4,22} Podocytes have extensive primary processes that terminate in foot processes (FPs), which in turn wrap around the glomerular capillaries. The FPs effectively encase the capillaries and the junctions between individual FPs form these highly selective junctions, slit diaphragms. These modified tight junctions express unique components and a number of cell-cell adhesion molecules have been identified that are integral to these structures ([Table 1.1](#)). These cell-cell adhesion complexes are important to the maintenance of the cytoskeletal structure which supports the FPs.¹⁵ Reduced expression of slit diaphragm components, such as nephrin (NPHS1), nephrin family proteins (NEPH1/2/3) and P-cadherin, or changes in podocyte attachment molecules, $\alpha_3\beta_1$ integrin complex and $\alpha\beta$ dystroglycan for example, are associated with dramatically altered filtrate composition and albuminuria.^{4,6,21,23–25}

1.1.2 Tubular secretion, absorption and urine concentrating capacity

Although only 20 % of the renal plasma flow is filtered at the glomeruli some molecules are almost entirely removed by renal clearance in a single pass. Renal clearance (C) is the net product of solute filtration at the glomerulus and secretion in

to tubules, less any reabsorption that occurs ([Equation 1.1](#)). In the case of sodium, approximately 99 % of the filtered sodium ions are reabsorbed at different stages of the nephron. As a result only 1 % of filtered sodium is excreted in the final urine. Hence the clearance of sodium is low, relative to glomerular filtration rate. In contrast more potassium is excreted in the urine than is filtered at the glomerulus. This is possible because potassium ions are secreted into the filtrate in the distal part of the nephron. As a result the clearance of potassium is high, relative to glomerular filtration rate. Many channels and transporters are involved in this process and their effects are summarised in [Figure 1.3](#).

Along with the removal of metabolites and toxins the kidneys also regulate total plasma volume and composition; the human renal system produces around 180 L of primary filtrate per day, however only 2 L of urine is excreted. In order to achieve the reabsorption of such large quantities of water solutes, such Na^+ , Cl^- and urea, are transported out of the filtrate into the surrounding medullary interstitium, thereby creating an osmotic gradient which draws water out of the tubules, loop of Henle and collecting duct ([Figure 1.3](#)) through aquaporins (principally AQP1). Normally, although most of the water that passes through the kidneys is retained, the kidneys produce relatively dilute urine (100 mOsm/Kg). When excess water does not need to be retained the CD maintains a lower water permeability state, effectively carrying the dilute urine to the renal pelvis. Following dehydration (reduced blood volume) the CD becomes permeable to water, through the actions of vasopressin or anti-diuretic hormone (ADH) and the recruitment of aquaporin 2 (AQP2), and the osmolality of urine can be dramatically increased as water is reabsorbed by osmosis into the surrounding hypertonic medullary interstitium. These actions can produce comparatively large changes in urine concentration; human urine can be in excess of 1000 mOsm/Kg and the rat kidney can produce urine concentrated to 3000 mOsm/Kg.^{26,27}

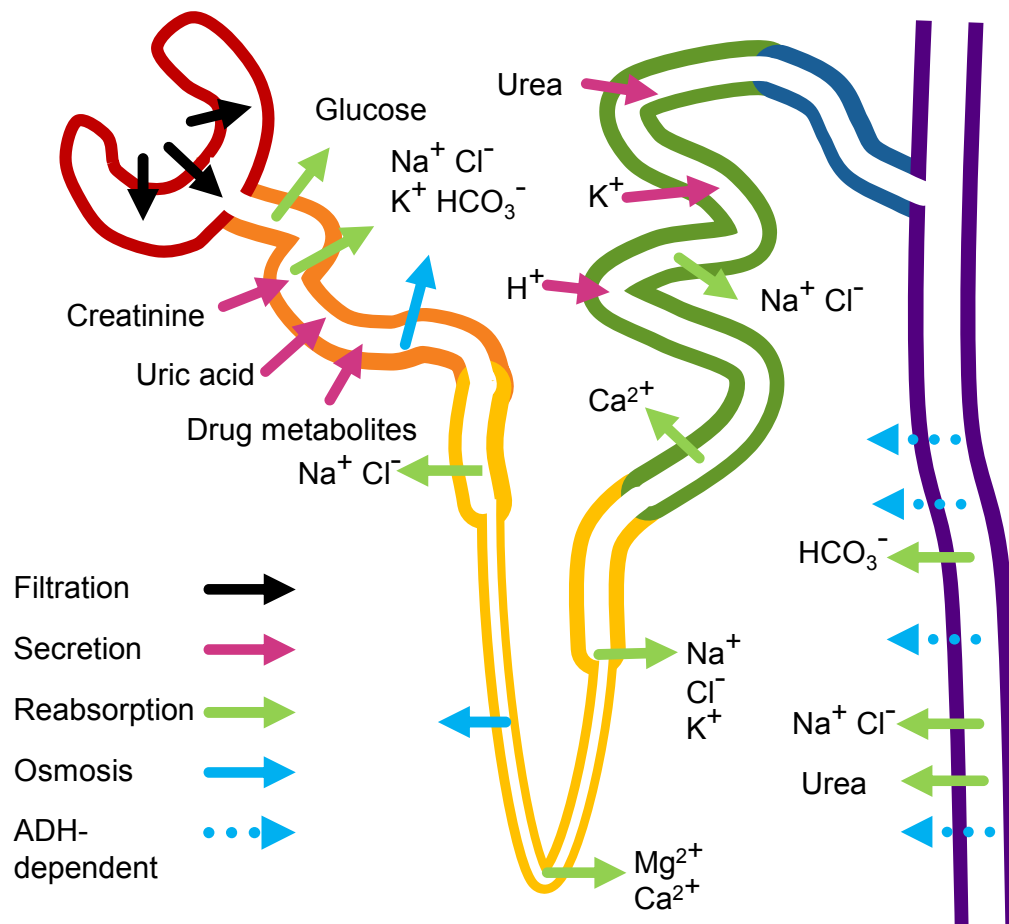


Figure 1.3 The composition of the primary filtrate formed at the glomerulus (Black arrows) changes considerably as it passes through the nephron. In the proximal convoluted (orange) nutrients (glucose, amino acids, vitamins) are reabsorbed along with electrolytes (eg, Na^+) whilst waste products (creatinine and drug metabolites) are secreted into tubule. The loops of Henle (yellow, particularly those of juxtaglomerular nephrons) create an osmotic gradient, as they descend towards the inner medulla, by transporting solutes (Na^+ , Ca^{2+} , urea) into the medullary interstitium. Further secretion of urea occurs in the distal convoluted tubules along with excess hydrogen ions (pH regulation) and potassium. The collecting ducts (purple) are selectively permeable to water in response to anti-diuretic hormone (ADH) and when required urine can be concentrated by further water reabsorption, some electrolytes are also reabsorbed.²⁶

1.1.3 Renal haemodynamics

When considering the role of the kidneys in the removal of metabolites and toxins from the body, the rate of removal is referred to as the renal clearance (C). Different substances are processed in differing ways and the rate of clearance depends upon filtration at the glomerulus, tubular secretion and tubular reabsorption ([Equation 1.1](#)).

$$\text{Renal clearance (C)} = (\text{Filtration} + \text{Secretion}) - \text{Reabsorption}$$

Equation 1.1

When a substance is at a steady-state concentration in the plasma, the renal clearance (in volume per unit time) can be calculated using [equation 1.2](#), using timed urine samples and a corresponding plasma sample. Generally renal clearance expressed in mL/min, or millilitres of blood plasma cleared of the substance per minute.

$$\text{Clearance (C)} = \frac{\text{Urine}_{\text{Conc}} \times \text{Urine}_{\text{Vol}}}{\text{Plasma}_{\text{Conc}}}$$

Equation 1.2

Renal function is often defined by glomerular filtration rate, or GFR, with decreases in GFR (below 90 mL/min/1.73 m²) indicating renal insufficiency. GFR is typically expressed as an indexed value using the standard body surface area of 1.73 m².²⁸ GFR is the volume of blood (plasma) filtered per unit of time. In healthy young adults GFR is typically in the region of 120 mL/min/1.73 m²; however GFR decreases with age and broadly values above 90 mL/min/1.73 m² are considered normal.²⁹ Clinical and experimental GFR can be measured using numerous methods, many of which are based upon the clearance of endogenous substances such as creatinine; other markers used include cystatin C, ⁵¹Cr-EDTA and ^{99m}Tc-DTPA.^{30–32} There are a number of complications with creatinine-based measures of GFR as approximately 15 % of cleared creatinine is actively secreted by the tubules and this over estimation of GFR can be problematic as GFR declines.³⁰ In addition factors such as age, gender and race should all be taken into account when using creatinine based measures of GFR as creatinine production is particularly influenced by muscle mass.³³ An alternative is the infusion of an exogenous substance with specific renal handling properties, primarily labelled forms of inulin or sinistrin. These molecules are filtered

at the glomerulus, but not reabsorbed or secreted by the tubules and are not metabolised by the kidney so their clearance rate ([Equation 1.2](#)) is equal to GFR.

Similarly, effective renal plasma flow (ERPF) can be estimated from the clearance of a substance, often *para*-aminohippuric acid (PAH), which is filtered and actively secreted into the tubules but not reabsorbed. As a result the substance is almost entirely removed from the plasma entering the kidney; a small proportion (~10 %) remains in plasma that is not processed by the nephrons.³⁴ Under normal circumstances only about 20% of the RPF is actually filtered through the glomeruli (GFR), this is termed the filtration fraction (FF, [Equation 1.3](#)).³⁵

$$\text{Filtration Fraction} = \frac{GFR}{RPF}$$

Equation 1.3

1.1.4 Renin, angiotensin and aldosterone

The renin-angiotensin system (RAS), or renin-angiotensin-aldosterone system (RAAS) as it is sometimes referred to, plays an important role in the regulation of blood volume and systolic blood pressure (SBP), and subsequently GFR.^{36,37} Reductions in blood pressure result in the release of renin from granular cells in the juxtaglomerular apparatus (JGA) of the kidney. Renin is an enzyme which converts angiotensinogen to angiotensin I (AngI, aa 1 -10); this is further processed into the highly active angiotensin II (AngII, aa. 1-9) by angiotensin converting enzyme (ACE, [Figure 1.4](#)). Chymase, an enzyme found in mast cells, also possess the catalytic ability to convert AngI to AngII.^{38,39} Once cleaved, AngII has multiple effects, both locally within the kidney and throughout the body. Most well characterised effects of AngII are mediated primarily by the type 1 angiotensin II receptor (AT₁). There are numerous other products derived from AngI or AngII by proteolytic cleavage (including AngIII, aa. 2-8, and AngIV, aa 3-8) which interact with AT₁, AT₂, AT₄ or other, yet to be defined, AT receptors. The role of AT₂ is less well defined. There is evidence that AT₂ mediates a vasodilator effect which counters AT₁-mediated vasoconstriction; AT₂ deficient mice have been shown to possess a heightened AngII pressor response.⁴⁰ A second isoform of ACE (ACE2) is involved in the production of Ang₁₋₇ a shortened angiotensin fragment that can be produced from both AngII and AngI (with further proteolytic cleavage by ACE) and ([Figure 1.4](#)).⁴⁰⁻⁴² The actions of Ang₁₋₇ are mediated by the Mas receptor and include vasodilation and inhibition of fibrosis and growth pathways. Ang₁₋₇ may also have physiological relevance as a

competitive inhibitor at AT₁ receptors.⁴³ For the purposes of clarity all discussions regarding the actions of angiotensin will be predominantly constrained to those of AngII via AT₁.

AngII acts as a potent vasoconstrictor within systemic arterioles, increasing vascular resistance via AT₁. AT₁ is considered to be typically coupled to the G_q g-protein, which activates phospholipase-C (PLC). This in turn culminates in contraction of vascular smooth muscle cells by Ca²⁺ mediated excitation-contraction coupling, with Ca²⁺ release from intracellular stores (inositol triphosphate at the IP₃ receptor) and the extracellular environment (Ca²⁺ channels).⁴⁴ The adrenal glands are also sensitive to AngII and release aldosterone when stimulated; and the pituitary gland releases vasopressin (ADH, produced in the hypothalamus); these hormones alter the reabsorption properties of the DCT and CD, respectively ([Figure 1.4](#)).

The regulation of blood (plasma) volume and pressure by the kidneys is dependent upon a number of feedback mechanisms. Firstly, dehydration leads to a decrease in blood (plasma) volume which reduces systemic blood pressure, simultaneously osmolality increases.^{26,45} This reduction in blood pressure impacts upon renal perfusion pressure and results in a temporary fall in intraglomerular pressure, GFR and filtration fraction. In a healthy individual GFR is normally restored by tubuloglomerular feedback, whereby the reduced filtrate flow and Na⁺ (and Cl⁻) concentration within the DCT/ThAL stimulates the macula densa, a collection of peritubular cells. Stimulation of the macula densa results in dilatation of the afferent arterioles and release of renin from the JGA.^{46,47} Systemically osmoreceptor activation triggers ADH release which increases water retention in the collecting ducts, reducing urine volume thus preserving plasma volume. These actions combine to restore SBP, blood volume and GFR, and the extent of these actions means that the RAAS system has remained a highly attractive target in the treatment of hypertension.

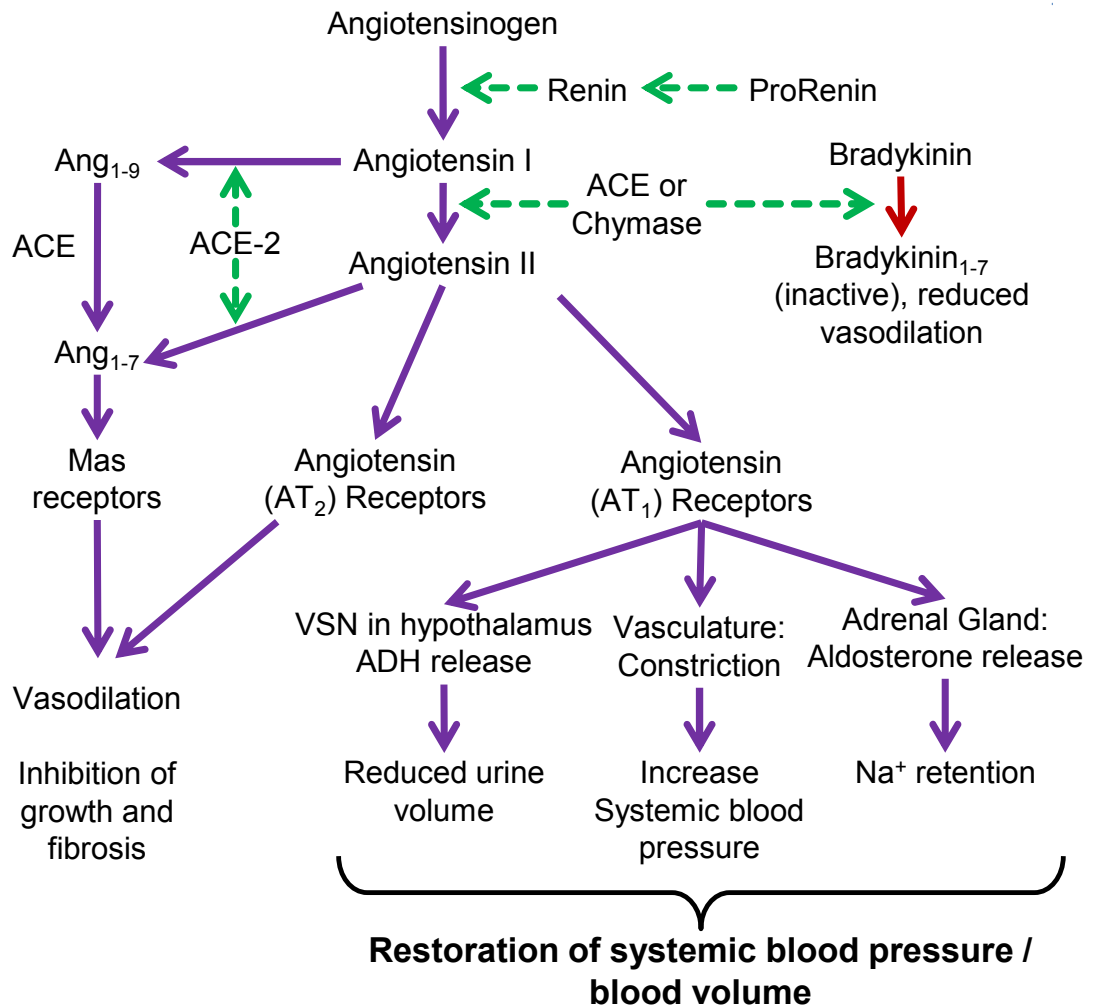


Figure 1.4 Overview of the production and actions of angiotensin II (AngII). AngII is produced by sequential proteolytic cleavage of angiotensinogen by renin then angiotensin-converting enzyme (ACE). Highly active AngII has potent vasopressor actions mediated by the angiotensin II receptor 1 (AT₁) expressed in vascular smooth muscle cells. AngII also mediates the release of aldosterone and anti-diuretic hormone (ADH) which alter sodium and water retention in the kidney; increasing blood volume and restoring systemic blood pressure. (VSN: vasopressin secreting neurones. ACE-2 produces the Ang₁₋₇ fragment which opposes traditional actions of AngII at AT₁.^{40,43}

1.2 Chronic kidney disease

Chronic kidney disease (CKD) is the progressive reduction in renal function, lasting 3 or more months and ultimately culminating in renal failure ($\text{GFR} < 15 \text{ mL} \cdot \text{min}^{-1} \cdot 1.73 \text{ m}^2$). At this stage, without renal replacement therapy (RRT; defined as transplant or dialysis), patients develop fatal uraemia. The progression of CKD is generally slow (months or years from diagnosis to failure) and has been divided into distinct stages that are described in [Table 1.2](#).^{48–51}

CKD stage	GFR	Clinical symptoms and pathology
1	>90	Normal GFR or hyperfiltration, CKD confirmed by the presence of histological changes or transient microalbuminuria ($30 < \text{UAE} < 300 \text{ mg/day}$)
2	60 - 89	Slightly decreased GFR, confirmed by structural abnormalities such as BM thickening and mesangial expansion and/or transient microalbuminuria
3	a 45 - 59	Moderate decrease in GFR. Persistent microalbuminuria, structural abnormalities progress and glomerulosclerotic lesions begin form.
	b 30 - 44	
4	15 - 29	Severe decrease in GFR. Extensive structural changes with advanced glomerulosclerosis and glomerular closure. Macroalbuminuria ($\text{UAE} > 300 \text{ mg/day}$)
5	< 15	Renal failure; Advanced lesions and vessel closure within the glomeruli, macroalbuminuria. Requiring transplant or dialysis.

[Table 1.2](#) Stages of CKD. Progression of CKD is divided into five stages based upon GFR (expressed in $\text{mL} \cdot \text{min}^{-1} \cdot 1.73 \text{ m}^2$), histological or structural abnormalities, or the presence of blood, protein or albumin in the urine. Compiled from Kidney Disease Outcomes Quality Initiative (K/DOQI) clinical guidelines from the National Kidney Foundation (NKF).^{48,49}

1.2.1 Prevalence

CKD is a major cause of global morbidity and mortality carrying substantial risk for the development of cardiovascular disease (CVD).^{52–54} Data from the National Health Service (2010) report over 1.7 million diagnosed cases of stage 3 - 5 CKD in the UK alone, with estimations from the NEOERICA project indicating that this number is almost certainly considerably higher with almost 4 million predicted cases, or 8.5% of

the population, of stage 3 - 5 CKD as of 2007.^{50,55} The situation is echoed in the US where it is estimated that 9.6 % of the general population have CKD (all stages).^{52,54} Improvements in health care and sanitation have started to markedly improve management of infectious diseases within developing populations increasing life expectancy substantially. As such chronic diseases, including CKD, are increasing in prevalence within these countries and are fast becoming a major health care burden making CKD a truly global issue.⁵⁶

This high prevalence of CKD, coupled with late intervention and the complex web of co-morbidities has led to a worldwide initiative from the International Society of Nephrology (ISN) and International Federation of Kidney Foundations (IFKF): World Kidney Day.^{54,57} Initially launched in 2006 the event aims to raise awareness of CKD, with the specific goals of improving detection of CKD in at risk populations and developing management strategies to decrease the rate of disease progression.^{48,52}

1.2.2 Causes and susceptibility

A range of factors can put individuals at an increased risk of developing CKD, while other factors are known to directly contribute to the initiation of CKD. Among the former, increasing age has a striking effect upon the prevalence of CKD. Data from the UK indicate that more than a third of people aged over 75 could have stage 3 - 5 CKD (Males: 75 - 84, 33.16 % and 85+ 44.75 %, females: 75 -84, 41.68% and 85+, 48.61 %). In contrast, in those under 55 rates were 10 times lower (3.08 and 2.79 % for males and females, respectively).⁵⁵ Other factors identified as increasing the risk of developing CKD are similar to these seen for many other chronic conditions; family history of the condition, complex socioeconomic factors (lower level of completed education and low income) and ethnicity.^{48,58-61}

This complex, non-communicable disease exists within a web of co-morbidities that can both initiate and aggravate the condition. In addition CKD itself is a risk factor for some of the risk factors for CKD ([Figure 1.5](#)). However it is helpful to discuss the relevance of these factors independently, if only to grasp the scale of the problem. It is estimated that diabetes and hypertension alone play a causative role in around two-thirds of all CKD cases.⁶¹⁻⁶³

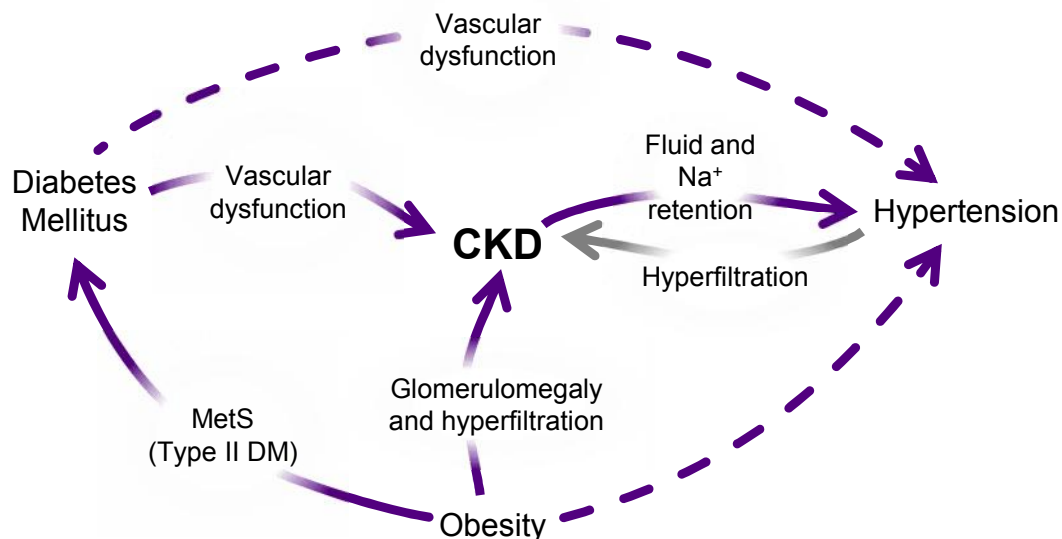


Figure 1.5 Diabetes mellitus (DM), hypertension and obesity are major contributors to the development and progression of chronic kidney disease (CKD). Many patients present with more than one predisposing factor, and these factors form an interconnected web rather than one directional cause: effect. For example: obesity is a risk factor for the development of CKD, but it is also linked to the development of hypertension and metabolic syndrome (MetS) which can lead to DM (type II).^{61,63}

1.2.2.1 Diabetes

Renal registry data from both the UK and US indicate that 26 % and 44 %, respectively, of all incidences of renal failure (patients requiring RRT) are attributed to diabetes mellitus (DM).^{64,65} DM is the leading cause of CKD and renal failure globally.^{53,66–70} CKD in diabetics is categorised differentially, as diabetic nephropathy (DN), and over a lifetime around one third of all diabetics develop the condition.⁷¹ Over the past 30 years the prevalence of DN has increased at an alarming rate, fuelled primarily by the epidemic rise in type II diabetes (non-insulin dependent DM, [Figure 1.6b](#)) across the globe and seconded by the improving long term survival of both type I (insulin dependent, [Figure 1.6c](#)) and type II diabetics.^{72–76} To give some perspective to the magnitude of this problem; in 2004 the World Health Organisation (WHO) estimated that 170 million people worldwide had diabetes, and predicted that 370 million people would be affected by diabetes by 2030.^{75,77} However just 10 years after those predictions, in 2014, 347 million people are classified as diabetic.⁷⁸

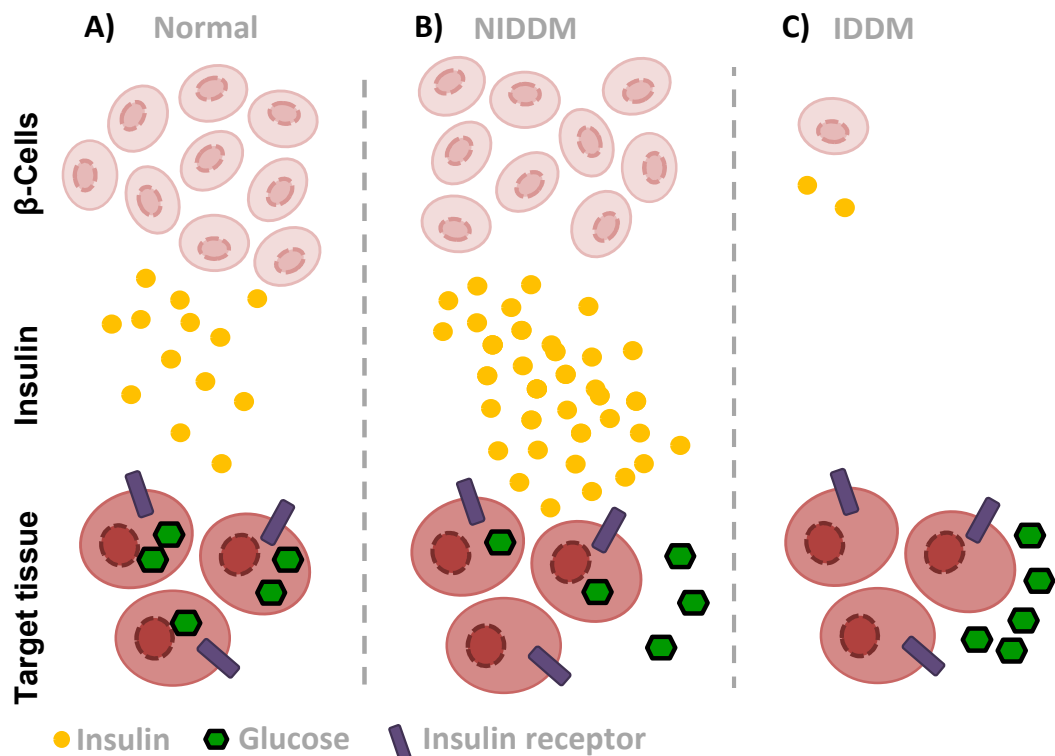


Figure 1.6 Diabetics have impaired glucose homeostasis. **A)** Healthy pancreatic β -cells release insulin which activates receptors on the surface of the target tissue (typically; liver, muscle and fat cells). These tissues then take up glucose from the blood, storing it as glycogen, ultimately lowering blood glucose concentration. **B)** In type II diabetes insulin signalling is ineffective, despite the release of adequate quantities of insulin by pancreatic β -cells. Insulin receptors at the target tissues do not respond appropriately and blood glucose levels remain elevated (> 6.0 mmol/L).^{72,73,80} When glucose concentrations fail to decrease the β -cells may compensate with exaggerated insulin secretion. **C)** In type I diabetes the pancreas does not produce sufficient insulin; this is often the result of autoimmune destruction of the β -cells. With no insulin the target tissues do not take up excess glucose from the blood leaving blood glucose elevated (> 6.0 mmol/L).^{74,80}

Although patients with both type I and type II diabetes (approximately 5 -10 and 90 - 95 % of the diabetic population, respectively) develop CKD which can progress to kidney failure, complications associated with type II DM mean that CVD mortality is high and often occurs in these patients before CKD progresses to renal failure.^{75,76} In addition, type II patients often present late and with multiple co-morbidities for CKD and CVD, including hypertension, obesity and dyslipidaemia.^{79,80}

1.2.2.2 Hypertension

Blood pressure (BP) is continuous within the population, meaning that there is no true definitive partition between normal blood pressure and hypertension. However, for the purposes of management and treatment a specific point of intervention at 140 / 90 mmHg or greater is generally accepted as hypertensive (Table 1.3).⁸¹⁻⁸⁴ Over a third of the global adult population meet this criterion, or over 950 million people have a BP over 140 / 90 mmHg (and/or are currently receiving anti-hypertensive treatment).^{85,86} According to WHO optimal adult blood pressure is 115 / 75 mmHg - 120 / 80 mmHg; worryingly the complications and risks of hypertension are tangible almost as soon as deviation from this range occurs.^{53,83,86} In addition to carrying an increased risk of CVD-related death; hypertension is also the second major cause of CKD, contributing to 28 % of renal failure cases in the US.⁶⁵

Grade		Blood Pressure (mmHg)	
		Systolic	Diastolic
Normal range		< 120	< 80
Pre-hypertension		120 - 139	80 - 89
Hypertension	Grade 1	140 - 159	90 - 99
	Grade 2	160 - 179	or 100 - 109
	Grade 3	≥ 180	≥ 110

Table 1.3 Hypertension is graded according to severity, although most of the risks associated with increased blood pressure are directly proportional and exist even when blood pressure is within the pre-hypertensive state.⁸¹⁻⁸⁴

1.2.2.3 Acute kidney injury

There are many causes of acute kidney injury (AKI) that have the potential to initiate, or worsen, CKD.⁸⁷ It is also worth considering that it is likely that the relationship between the two conditions is both bi-directional and complicated by the presence other covariates such as CVD or obesity.⁸⁷⁻⁹¹ The causes of AKI are numerous and the condition can arise from pre-renal, intrinsically renal and post-renal complications. For example decreased perfusion of the renal tissue resulting from

global hypotension is a pre-renal complication; in contrast physical renal injury, acute nephrotoxicity autoimmune disease and glomerulonephritis are causes intrinsic to the kidney. Post-renal complications can include urinary tract infection or obstruction.^{62,92,93}

All of these individual renal complications have the potential to develop into acute renal failure (ARF), or following recovery from AKI (with or without dialysis) there is potential for maladaptive repair which can result in progression to CKD and ultimately renal failure (CKD:5). Over 25 % of all patients receiving treatment for renal failure in the US had previously been identified as suffering at least one AKI incident.^{89,94} Retrospective studies suggest that the risk of progression to CKD:4-5 could be almost 30 times higher in patients receiving dialysis following AKI, and that this risk remains for patients suffering less serious AKI incidents.^{94,95} However, care must be taken interpreting these studies as they are based upon medical record data where there is the potential for AKI incidents to indicate undiagnosed CKD, rather than being purely causative.^{94–96}

1.2.3 Pathophysiology and disease progression

The stages of CKD ([Table 1.2](#)) are defined by three major criteria: changes in GFR, structural abnormalities within the kidney and the presence of albumin, protein or blood in the urine (albuminuria / proteinuria / haematuria, respectively). Stages 1 and 2 are typically silent and the associated mild to moderate change in GFR is not sufficient for diagnosis. Instead a diagnosis is made based upon histological anomalies following kidney biopsy, structural abnormalities identified by ultrasound scans or persisting albuminuria, proteinuria or haematuria. In contrast a diagnosis can be made based upon reduced GFR ($< 60 \text{ mL.min.1.73 m}^2$) alone from stage 3 onwards.^{49,54,61}

1.2.3.1 Glomerular damage

Although there are a number of initiating factors, glomerular damage is a primary characteristic of CKD. Glomerular hyper-filtration occurs early in the course of the disease. This hyper-filtration can be considered both the level of the whole kidney and the individual glomeruli. Whole kidney hyper-filtration can be a physiological response, effectively the use of reserve renal capacity; however persistent hyper-filtration is generally pathophysiological and ultimately damages the renal tissue.^{35,97} Physiological hyper-filtration arises from vasodilator actions of nitric oxide (NO) on

both the afferent and efferent arterioles; increased perfusion without increased intraglomerular pressure or filtration fraction.³⁵ The balance of afferent and efferent resistance impacts upon GFR, when the resistance of the afferent arteriole is low relative to the efferent arteriole intraglomerular pressure increases and there is a subsequent increase in GFR.⁴⁶

Whole kidney hyper-filtration is well documented in the early stages of DN, when GFR often exceeds that of a healthy adult.^{98–100} These changes are generally not, at least initially, accompanied by albuminuria.⁹⁸ Alterations in renal function appear to arise from changes in vascular control, primarily vasodilatation of renal vessels, which result in increased GFR accompanied by increased FF. Increases in GFR with a concurrent increase in FF can be indicative of increased intra-glomerular pressure, which can arise when there is an imbalance in vascular resistance between the afferent and efferent arterioles ([Figure 1.1](#)).

Although the mechanisms underlying these vascular changes are not fully understood a number of studies suggest that poor glycaemic control is central to the phenomenon. The precise process whereby persistent hyperglycaemia alters renal haemodynamics is still being explored; however there are two main areas of interest: changes which take place within the vasculature of the glomerulus where advanced glycation end products (AGEs) have been highlighted in a potentially causative role, and altered tubuloglomerular feedback resulting from increased glucose concentrations within the renal tubules.^{99,101} AGEs have been implicated in a number of diseases of the microvasculature, including nephropathy, retinopathy and atherosclerosis, and have been shown to alter vascular permeability and activate monocytes as well as affect nitric oxide-mediated vasodilatation.¹⁰² Elevated AGE is associated with activation of the AGE receptor (RAGE), a proposed self-perpetuating mediator of inflammation.^{102–104} Excessive glycation of basement membranes, particularly type IV collagen, is associated with decreased degradation by MMPs *in vitro* and is likely to directly contribute GBM thickening in diabetic CKD patients.¹⁰⁵ Persistently elevated insulin concentrations have also been highlighted as a potential instigator; however this does not explain the high number of DM type 1 patients with DN where some recovery of normal glomerular filtration is seen with the implementation of insulin therapy. In addition, data from subjects with impaired fasting glucose concentrations suggests that hyperinsulinaemia, in the absence of hyperglycaemia, does not result in hyper-filtration.¹⁰⁶

Metabolic syndrome (MetS) with impaired fasting glucose is sometimes included within non-diabetic causes of CKD but whether or not MetS can truly be considered outside the diabetic setting is questionable, given the state is effectively “pre-diabetes”.^{73,107}

In patients with non-diabetic CKD mechanisms other than hyperglycaemia must trigger the changes in renal haemodynamics that lead to an increase in GFR; however unlike in diabetics this generally occurs at the level of the individual nephron while total GFR remains normal or even decreases.^{35,108–110} Many factors have been implicated in these events; hypertension, obesity, increased age, genetic conditions, autoimmune diseases and AKI all have the potential to ultimately reduce the renal reserve capacity.^{35,46,87,94} For example, obesity can result in glomerulomegaly, where the nephrons enlarge to meet the increased metabolic demand of increased body mass. This also results in an increase in whole kidney RPF and GFR accompanied with increased FF and glomerular hypertension; the increase in RPF and GRF is not proportional.^{35,111,112} This particular situation arises as, unlike the liver, the kidney’s functional tissue cannot increase in mass; the number of functional nephrons is fixed (a healthy individual has roughly 1 million nephrons per kidney).³ Similarly, ageing reduces renal reserve capacity; around 40% of nephrons are lost by the age of 80 and AKI can lead to residual nephron ablation even after apparent recovery.^{2,113} This decrease in nephron number, regardless of cause, means that each filtration unit must increase its filtering capacity in order to meet metabolic demand.

Hypertension can be a consequence of CKD; it is also a contributory factor in 1/3rd of all cases of CKD.⁶⁵ Elevated blood pressure is also associated with other CKD causative factors such as obesity and DM.¹¹⁴ At a systemic level increased cardiac output (CO), plasma volume or vascular tone or conversely reduced vascular compliance can all contribute to elevated blood pressure. In healthy individuals renal autoregulation can compensate for transient fluctuations in blood pressure (and GFR) over a considerable range by modulation vascular tone in the afferent and efferent arterioles.¹¹⁴ When this autoregulation fails intra-glomerular pressure increase which can result in podocyte injury and (mal)adaptive changes within the glomeruli.^{35,115}

However it arises, a persistent increase in hydrostatic pressure is thought to be responsible for progressive and maladaptive changes in glomerular structure; the glomerular basement membrane (GBM) thickens whilst also becoming less

selective.^{13,116,117} Thickening of the GBM is a well-documented pathology of CKD and the membrane can end up 3 - 4 times thicker than in a healthy individual. The faltering filtration barrier is considered to be the result of pathological changes in the extracellular matrix, cell-cell interactions and podocyte dysfunction and death.^{13,23,24,116,118,119}

GBM thickening is primarily the result of an increase in ECM proteins, through increased deposition and decreased degradation.^{120,121} Altered expression of a number of GMB components ([Table 1.4](#)) has been reported at both the mRNA and protein level. This change in composition affects podocyte cell adhesion; integrins ($\alpha_1\beta_3$) which usually interact with laminin-521 and dystroglycan- $\alpha\beta$ which interacts with both agrin and laminin no longer adhere appropriately, initiating a cascade of intra-cellular signalling and ultimately resulting in actin reorganisation and foot process retraction which disrupts the highly selective slit diaphragm.^{4,7,16,22,122} This disruption of cell attachment can also result in podocyte cell death. Within the glomerular filtration barrier nephrin, podocin and P-cadherin have been shown to have central roles in the structure and function of the slit diaphragm, and are often down regulated in both diabetic and non-diabetic CKD.^{4,23,118,123} However as these molecules are generally podocyte-specific it is worth considering that the apparent reduction in expression could also be the result of the physical loss of podocytes. Podocytes, like any cell, are sensitive to changes in the immediate extra-cellular environment; however they have also been shown to be intrinsically sensitive to mechanical sheer forces not unlike those resulting from increased intra-glomerular pressure.¹²⁴ It has been suggested that this mechanical stress from increased filtering pressure results in reorganisation of β -actin networks, the very components that support the podocyte foot processes and slit diaphragms.^{4,125}

Target	Location	Evidence
Nephrin (NPHS-1)	Podocyte: slit diaphragm	Humans and mice with mutations in nephrin present with nephrotic syndrome, characterised by massive proteinuria
Collagen IV α_3 , α_4 and α_5	Glomerular Basement Membrane	Human mutations linked to albuminuria, and mice lacking the COL4 α_3 gene also suffer albuminuria as do those with reduced expression of COL4 α_3 , α_4
Podocin	Podocyte: slit diaphragm	Mutations in podocin are associated with albuminuria in humans
α -actinin-4	Podocyte: Foot process	Mutations in α -actinin-4 associated with albuminuria in humans
Laminin α_5 , β_2 and γ_1	Glomerular Basement Membrane	Congenital nephrotic syndrome

Table 1.4 Numerous changes in glomerular filtration barrier components are linked to the albuminuria and progressive glomerulosclerosis associated with chronic kidney disease.^{4,16,122}

The renin-angiotensin system has received particular attention following the realisation that inhibition of the actions of AngII (by inhibition of ACE or by angiotensin II receptor blockers, ARBs) leads to improvements in prognosis well beyond those expected from blood pressure reduction alone.^{126–128} Of note is a reduction in the severity of albuminuria, an effect seen predominantly in patients with DN. The mechanism of this reno-protection is not yet clear, though AngII acting through AT₁ appears to bolster the actions of AGE signalling through the AGE receptor (RAGE), with effects such as increasing expression of VCAM-1 and marked up-regulation of RAGE expression.^{129,130}

1.2.3.2 Albuminuria and inflammation in CKD

The degree of albuminuria (and proteinuria) has long been used as a marker to determine the severity of CKD and even predict outcomes; however it is now believed that albuminuria may play a role in driving the disease.^{131,132} While the mechanisms are not fully understood, albumin is believed to play a role in mediating inflammation within the tubular interstitium.¹³¹ Albumin and other plasma protein fractions have been shown to increase the production of numerous chemokines by

renal tubular cells *in vitro*; current evidence suggests that this results from increased generation of intracellular reactive oxygen species (ROS) and the activation of the nuclear factor kappa-light-chain-enhancer of activated β cells (NF- κ B) transcription factor. The NF- κ B pathway is well defined as pro-inflammatory.^{131,133} Corresponding studies *in vivo* also indicate that NF- κ B activity is higher in rats with proteinuria.¹³⁴ Downstream the result is up-regulation of numerous molecules which have the potential to act as inflammatory cell chemoattractants or pro-fibrotic mediators, such as: endothelin-1 (ET-1, shown to stimulate cell matrix production and attract monocytes), fractalkine (implicated in immune cell adhesion) and interleukin-8 (IL-8, immune cell chemoattractant).¹³¹ However, it is worth considering that proteinuria may actually be a marker for “leakiness” of the GFB and other active protein fragments, including protein bound growth factors that are too large to pass through a healthy GFB, could also modulate this phenomenon.¹³⁵

The final stages of CKD (CKD-4 and CKD-5) are often referred to as states of ‘low level’ inflammation with pro-inflammatory cytokines reported to be significantly higher in patients with renal failure. Interleukin 6 (IL-6) in particular is regularly reported to be 2 - 3 fold higher than in healthy controls.^{136–139} Furthermore, there also appears to be a correlation between CKD stage and IL-6 concentration in blood plasma. However, the implications of these findings are not entirely clear and the presence of any cause-effect relationship is yet to be determined. However IL-6 concentration in the blood may yet prove to be a useful surrogate marker for CKD severity.¹⁴⁰ It was suggested that this apparent build-up of inflammatory mediator is the result of inadequate clearance; however mRNA analysis of subcutaneous fat from patients with CKD demonstrated that IL-6 production was also higher than that of healthy controls.^{136,137,139,140}

1.2.4 Intervention

Diabetes and hypertension are both complex factors not only involved in the initiation of CKD but also in accelerating disease progression. As a result the majority of intervention strategies aim to slow disease progression by managing these aggravating factors.⁶¹ Early identification of at-risk individuals is vital, allowing intervention before substantial glomerular damage occurs so that renal function may be preserved for as long as possible.^{48,51,55} Effective management remains a specific challenge in those with multiple co-morbidities; the interaction between some of these can be seen in [Figure 1.5](#).

1.2.4.1 Management of hyperglycaemia

Poor glycaemic control is associated with poor prognosis.^{106,121} In DM type I the primary therapy is measurement of blood glucose concentration and the use of exogenous insulin to restore blood glucose to normal levels quickly following meals. Patient attitude to insulin therapy (and blood glucose monitoring) as well as dietary control are the key factors in successful management of hyperglycaemia.

In DM type II management of the condition is somewhat similar; prolonged increases in blood glucose should be avoided. However the methods of treatment vary immensely from those used in the management of type I DM. Generally type II DM is treated with a combination of weight management (diet and exercise), insulin sensitising drugs (metformin or peroxisome proliferator-activated receptor gamma (PPAR- γ) agonist pioglitazone) or insulin secretagogues (sulphonylureas such as glimepiride). It is common for dual even triple therapy to be implemented in order to reduce blood glucose and glycated haemoglobin (HbA_{1c}) to target levels (typically HbA_{1c} < 6.5 %).¹⁴¹ In addition insulin may also be used in the management of type II DM. The CKD implications of type II DM are often complicated by extended periods of hyperglycaemia prior to diagnosis of DM (or MetS) and subsequent late presentation. Worryingly these patients appear less likely to suffer RF, not because they are in better health, but because they often die from related conditions (primary: CVD) before renal function declines excessively. Despite this type II diabetics still account for 35% of all renal-failure cases.

1.2.4.2 Reduction of systemic blood pressure

Reducing systemic blood pressure, and by extension the propensity for glomerular hypertension, is a key point of therapeutic intervention, with implications for both CKD progression and CVD risk.¹⁴² Although less than 1/3rd of all CKD cases are directly attributed to hypertension, approximately 80% of CKD patients have hypertension.¹⁴³ In CKD patients (with and without diabetes) the regimens used to reduced blood pressure are typically more aggressive than in the general population, with blood pressure aims of $\leq 140 / 90$ mmHg in the absence and $\leq 130 / 80$ mmHg in the presence of elevated albumin excretion (ACR > 30 mg/mmol), respectively.

Whilst these targets are the ideal, many patients fail to meet them despite multi-drug intervention and the mechanism of blood pressure treatment varies depending upon whether or not albumin excretion is moderately or severely increased (ACR > 30 or > 300 mg/mmol, respectively). In patients without elevated urinary albumin excretion

treatment follows the typical course of anti-hypertensive treatment; diuretics to reduce blood volume and calcium channel blockers to reduce vascular resistance. In contrast in patients with elevated urinary albumin excretion the Kidney Disease Improving Global Outcomes (KDIGO) guidelines recommend blockade of the renin-angiotensin system.¹⁴⁴ This can be achieved through ACE inhibitors (ACE-I), reducing the conversion of AngI to AngII, AT₁ antagonists (AngII receptor blockers; ARBs) which block the actions of AngII, and the more recently developed renin inhibitors, which prevent conversion of angiotensinogen to AngI by renin.¹²⁶ Dual blockade (ACE-I plus ARB) of the RAS is common; however the addition of a renin inhibitor is linked to increased CVD risk in patients with diabetic renal impairment.¹⁴⁵

1.2.4.3 Albuminuria as a therapeutic target

The role of albuminuria and the associated protein fraction infiltration into the tubular interstitium in CKD has been revised following the realisation that not only did increasing urinary albumin excretion (expressed as UAE or ACR) correlate with poorer prognoses, it actually appears to play a causative role in the development of inflammation and worsening renal function.^{131,132,134} Inhibition of the RAS pathway has been shown to be useful in reducing albuminuria in both diabetic and non-diabetic CKD.^{146–151} However, optimal control over albuminuria has yet to be achieved and the interventions, while better than placebo or BP intervention alone, have yet to arrest to the progression of CKD.^{131,146–150,152} However, while the mechanisms are not completely understood, some vasoactive agents (namely; AngII and ET-1) have been implicated in this inflammatory response.^{133,134}

While therapeutically slowing the decline in renal function is desirable and encouraging, to date there is little evidence of successful reductions in all-cause mortality following RAAS system blockade, despite improvements in CKD management, BP and proteinuria.^{153–156} This is particularly poignant when considering renin inhibitors (with or without ARBs), where use in patients with diabetes increased CVD mortality.¹⁴⁵

1.3 *In vivo* models of CKD

In the human population CKD is a progressive disease with mixed aetiology and variable time course. There are numerous animal models of renal impairment which vary by method of induction, presence of co-morbidities and the rate and extent of renal impairment.^{157–160} Common methods of induction include toxic injury, inherited genetic mutations and surgical injury.

1.3.1 Genetic models of diabetic renal disease

A number of rat and mouse strains spontaneously develop diabetes with a range of diabetic complications. There are a number of models where the development of diabetes and/or renal failure is not consistent across the population. One example is the BioBreeding (BB), a diabetes prone strain that spontaneously develops type I DM due to immune destruction of pancreatic β -cells.^{160,161} Under normal circumstances only 50 % of a BB rat population will develop type I DM.¹⁶¹ The Otsuka Long-Evans Tokushima Fatty (OLETF) rat is a relatively new rat model of type II DM, the progression of diabetes in this model is slow (onset ~ 20 weeks) as are associated changes in renal structure. With age OLETF rats can develop glomerulosclerosis but it is typically diffuse and mild.^{159,162}

1.3.1.1 Mutations in the leptin signalling

Leptin, an adipocyte derived hormone, is involved in regulation of appetite and satiety.¹⁶³ There are a number of rodent models of type II diabetes resulting from mutations within the leptin signalling pathway. These include the ob/ob mouse, db/db mouse and Zucker *fa/fa* rats.¹⁵⁹ The changes in the models are driven primarily by hyperphagia.^{159,164}

Zucker^{fa/fa} diabetic obese rats

Zucker^{fa/fa} diabetic obese (ZDF) rat is model of type II diabetes mellitus. The strain is homozygous for a non-functional leptin receptor; as a result the rats develop hyperphagia. This is associated with elevated circulating insulin concentrations and impaired fasting glucose which rapidly progresses through MetS to overt type II DM with 3 months.¹⁶⁵ Unlike the BB rat, the ZDF strain reliably develops diabetes, cardiovascular complications and renal impairment due to its monogenetic basis.^{159,165,166} There is moderate glomerulosclerosis associated with the ZDF strain;

however hydronephrosis predominates and as such the renal profile of ZDF rats is not comparable to DN or CKD.¹⁶⁵

Diabetic (*db/db*) mice

Mice with the homozygous *db/db* (diabetic) genotype become obese at an early age due to hyperphagia and subsequently develop hyperinsulinaemia.¹⁶⁷ There is a period of compensatory hyperinsulinaemia before β -cell dysfunction and the development of hyperglycaemia and overt type II diabetes.¹⁶⁸ Analogous to the ZDF *fa/fa* rat, a non-functional leptin receptor underlies the model.¹⁶³ The renal profile of the *db/db* mouse is strain dependent but limited to persistent albuminuria, glomerular hypertrophy and mesangial expansion without substantial glomerulosclerosis.¹⁶⁴

Obese (*ob/ob*) mice

The phenotype of the *ob/ob* mouse is initially indistinguishable from that of the *db/db*. That is a fat, hyperphagic black mouse with persistent hyperinsulinaemia and impaired fasting glucose.^{163,164,168} Unlike the *db/db* mouse, the *ob/ob* has functional leptin receptors and consequently responds to exogenous leptin.¹⁶³ This model, along with the *db/db*, is widely used in the study of diabetes and associated complications; however the renal complications remain largely uncharacterised and are likely highly dependent upon the background strain.¹⁶⁹

1.3.2 Akita mouse strains

A mutation in the insulin II gene (*Ins2*) leads to type I DM in the akita mouse. The point mutation associated with the akita genotype is associated with protein misfolding.¹⁷⁰ Interestingly in *Ins2* null mice are not typically diabetic due to compensation by the retention of the duplicate *Ins1* gene.¹⁷¹ The pathology of the akita mouse is largely dependent upon background strain and gender; the symptoms are more severe in males than females.¹⁷⁰ C56BL/6^{akita/+} mice develop hyperglycaemia without many of the associated changes in renal histology; in contrast FVB/NJ^{akita/+} mice develop hyperglycaemia with more pronounced albuminuria and glomerular damage.^{170,172} Despite the more severe renal dysfunction on the FVB/NJ background the changes are typically limited to mesangial expansion, with little evidence of glomerulosclerosis.¹⁷⁰

1.3.3 Streptozotocin induced type I diabetes mellitus

Streptozotocin (STZ) can be used to induce diabetes in both rats and mice. The destruction of pancreatic β -cells induces a pronounced state of acquired type I DM that often requires exogenous insulin to manage. The STZ treated rodents do not develop consistent or marked glomerulosclerosis, but the STZ toxicity is not confined to the pancreas and can be associated with generalised toxicity which can confound the pathologies associated with this model.¹⁶⁹ This potential for non-specific nephrotoxicity and minimal renal impairment, despite substantial hyperglycaemia meant that this model was not best suited to the aims of this work.

1.3.4 Induction of chronic renal failure by renal mass reduction: a non-diabetic renal disease:

References to renal mass ablation as a method to induce progressive renal dysfunction date back over 100 years.¹⁷³ This approach has been carried out using a variety of methods including infarction, ligation and surgical removal of kidney tissue. The procedure has been carried out in a number different mammalian species such as rat, dog and mouse. The more standardised method for reduction in renal mass, now known as the 5/6th nephrectomy, was not established until the 1950s.¹⁶⁰ Today there remain a number of variations upon the model, but these variations relate not to the mass of tissue removed, rather to the method of mass reduction and the species used.

Achieving a 5/6th reduction in renal mass is most commonly carried out by removing the poles of the left kidney, leaving approximately 1/3rd of the kidney intact, or by ligation of branches of the left renal artery causing severe ischaemic damage within 2/3rd of the left kidney. In either case this is followed by complete removal of the right kidney some time later, leaving 1/6th of the original total renal mass.¹⁷⁴ The prevention of blood loss must be addressed during surgical resection of the poles; applying digital pressure, cauterisation or using a sealing substance to the cut-faces of the kidney are some ways in which this can be achieved. In contrast this issue is not met when ligating renal artery branches; however measuring the reduction in functional renal mass can be extremely difficult with this method and it is not applicable to mouse models due to minimal branching of the renal arteries.¹⁷⁵

In rats the induced renal disease progresses through three distinct phases that can be aligned to the course of CKD/DN in patients ([Table 1.5](#)); the development of

glomerulosclerosis is generally limited in mice.¹⁷⁶ The initial phase is relatively short (6 - 8 weeks) and represents the recovery of the remnant kidney. The remnant undergoes total and glomerular hypertrophy with associated mesangial expansions and thickening of the GBM which is associated with focal glomerulosclerosis. At this stage there is evidence of renal dysfunction including an increase in plasma concentration of metabolic waste products such as creatinine and urea.^{177,178} Albuminuria is mild but elevated compared to control rats. This is followed by a stable phase where albuminuria increases and systolic blood pressure become elevated.¹⁷⁹ There is variability in the length of the stable phase which is, in part, determined by the degree of hypertension and albuminuria; however glomerulosclerotic lesions become increasingly widespread and glomerular closure begins to occur.¹⁸⁰ The final decline phase is equivalent to the stage 5 CKD, severe renal insufficiency, gross morphological changes including glomerular closure and tubular atrophy and associated uraemia.

CKD stage	Clinical symptoms and pathology	Development in 5/6 th SNx Rat
1	Normal GFR or hyperfiltration, CKD. Presence of histological changes or transient microalbuminuria (30 < UAE < 300 mg/day)	Initial phase Normal GFR, hypertrophy, hyperfiltration and mesangial expansion
2	Slightly decreased GFR. BM thickening and mesangial expansion and/or transient microalbuminuria	
3	Moderate decrease in GFR. Persistent microalbuminuria, structural abnormalities progress and glomerulosclerotic lesions begin form.	Stable phase Declining GFR, persistent albuminuria, elevated systolic blood pressure and progressive glomerulosclerosis
4	Severe decrease in GFR. Extensive structural changes with advanced glomerulosclerosis and glomerular closure. Macroalbuminuria (UAE > 300 mg/day)	
5	Renal failure; Advanced lesions and vessel closure within the glomeruli, macroalbuminuria. Requiring transplant or dialysis.	Decline phase Renal failure, glomerular closure and uraemia

Table 1.5 Alignment of CKD stages with the progression of the 5/6th sub-total nephrectomy (SNx) in rat.^{175,177,179,180}

The 5/6th SNx model produces a robust and reproducible progressive chronic kidney disease with distinct phases relatable to clinical CKD.¹⁸⁰ There is a comparatively long course (6 - 9 months) of disease which is accompanied by progressive albuminuria and secondary hypertension.¹⁷⁵ Importantly the model develops substantial glomerulosclerotic lesions that are comparable to those seen in clinical CKD.¹⁷⁵ The extent and reliability of this glomerulosclerosis allows the potential role of UII in CKD to be studied more effectively than the diabetic models with milder changes in renal histology; particularly UII as a potential pro-fibrotic factor.¹⁸¹

1.4 Urotensin II

Originally isolated over 40 years ago, urotensin II (UII) is small peptide hormone which elicits an array of physiological responses. The complexity of these responses has made understanding the precise (patho)physiological roles of UII rather challenging. The urotensin II system is of particular interest as its role in CKD is largely unknown. There are a number of studies suggesting UII signalling is altered in the human CKD/DN and in animal models of CKD.^{178,182,183} As will be described, UII appears to be a complex vascular and renal modulator with some evidence suggesting a potential fibrotic role for the peptide.^{181,184,185}

1.4.1 Identification and isolation

Urotensin II (UII) was originally isolated, along with a number other active molecules, from the urophysis of the teleost fish *Catostomus commersoni* (White sucker). The neurosecretory urophysis is a ventral projection of the caudal spinal cord and is suggested to play a role in osmoregulation; particularly in the transition from fresh water to salt water, or vice versa.^{186,187} A pure form of UII was isolated using high-performance liquid chromatography (HPLC) from the urophysis of a different teleost species *Gillichthys mirabilis* (Goby) in 1980.^{188,189} Initial experiments identified UII as a general spasminogen, capable of contracting smooth muscle tissues from a variety of fish species, including trout bladder and intestine as well as goby sperm duct.¹⁹⁰ Since the neuro-secretory urophysis is a biological curiosity unique to the teleost infraclass this initial work was predominantly concerned with understanding the role of UII within a member of the teleost fish family. There was no immediate reason to look outside the teleosts as the urophysis is not present in other vertebrates nor are there any structural homologues.

Similarities were originally drawn to somatostatin-14, with which UII shares some structural resemblance. Specifically UII is a short cyclic peptide hormone with a F-W-K motif, and while the active forms of the two peptides do have some structural similarities, the genes which encode for them differ substantially.^{191,192} The wider physiological relevance of this newly identified molecule was expanded with the serendipitous discovery that non-vascular, mammalian tissues also respond to UII. Specifically UII produced relaxation of mouse anococcygeus muscle with a profile similar to that of somatostatin-14, though UII was substantially more potent in this assay producing responses at 0.1 - 6 μM compared to 10 - 80 μM for somatostatin-14.¹⁹³

1.4.2 Structure of urotensin II and urotensin II - related peptide

Over the next few years UII was isolated from numerous teleost fish species and comparisons revealed remarkable similarities within the amino acid (a.a.) sequence. Most notably a 6 a.a. fragment (Goby residues 6 -11: C-F-W-K-Y-C) towards the C-terminus was conserved in all species.¹⁹¹ The earlier discovery that UII could provoke responses from mammalian tissues heightened interest in the small peptide even though the mechanism of these effects and the receptor responsible remained unknown. Further studies demonstrated that mammalian cardiovascular tissues also responded to goby UII; for example pre-contracted rat aortic strips responded in a bi-phasic manner to UII in the nanomolar range.¹⁹⁴ At low concentrations it caused dilation whereas at higher concentrations it caused contraction.

Ultimately cDNA cloning identified the presence of a gene (*UTS2*, HGNC:12636) encoding a urotensin II precursor protein in human tissues. Complete with the conserved C-F-W-K-Y-C motif, this was the first indication that UII was present in a mammalian species. UII peptides have since been isolated from other mammalian species including rat (*Uts2*, RGD), mouse and monkey ([Table 1.6](#)).^{195–197} This high degree of conservation throughout a wide range of species fostered the search for the (patho)physiological role for UII, particularly in mammals.^{191,195} Initially UII binding sites were identified in rat aorta and a separate study in anaesthetised rats demonstrated apparent vasodilator activity of UII, suggesting that UII may play some role in cardiovascular regulation in mammals.^{198,199}

Urotensin II	Goby	N-terminus	Ala - Gly - Thr - Ala - Asp - Cys - Phe - Trp - Lys - Tyr - Cys - <u>Val</u>	C-terminal
	Frog		Ala - Gly - Asn - Leu - Ser - Glu - Cys - Phe - Trp - Lys - Tyr - Cys - <u>Val</u>	
	Human		Glu - Thr - Pro - Asp - Cys - Phe - Trp - Lys - Tyr - Cys - <u>Val</u>	
	rat		Gln - His - Gly - Thr - Ala - Pro - Glu - Cys - Phe - Trp - Lys - Tyr - Cys - <u>Ile</u>	
URP	Human		<u>Ala</u> - Cys - Phe - Trp - Lys - Tyr - Cys - <u>Val</u>	
	rat		<u>Ala</u> - Cys - Phe - Trp - Lys - Tyr - Cys - <u>Val</u>	

Table 1.6 Peptide sequence comparison of urotensin II (Ull) and urotensin II - related peptide (URP). The cyclic C-terminal region formed by a disulphide bridge between the two cysteine residues (Cys, shaded grey) is conserved. In Ull this is flanked by an acidic residue (aspartic or glutamic acid, red) and a small non-polar/aliphatic residue (valine or isoleucine, underlined). In URP both flanking residues are small and non-polar (alanine and valine, underlined).

Further cloning revealed that secondary immunoreactivity identified in the rat brain was in fact the product of a different gene (*Uts2b*) rather than a variant produced from the Ull gene.^{200,201} The mature octapeptide produced is now known as Ull-related peptide (URP) and shares the cyclic C-F-W-K-Y-C motif (Table 1.6). URP derived from human, rat and mouse share the same amino acid sequence.²⁰² This cyclic region confers biological activity to the peptides.²⁰³

Ull is produced as a precursor protein; pre-pro Ull. The biological activity of the mature peptide is markedly greater than that of the immature form and as such the proteolytic cleavage is considered a pre-requisite for Ull function.²⁰⁴ A number of putative “hormone convertase” cleavage sites have been identified in pro-Ull sequences from human, rat and frog; interestingly these sites are absent in pro-Ull from mouse.^{196,205–207} Chromatographic separation of isolates from human and mouse tissues have determined the predominant mature forms as hUll₁₁ and mUll₁₇, respectively.^{208,209} Despite isolation of the mature peptide forms the enzyme responsible for the conversion of pro-Ull to Ull, urotensin II converting enzyme (UCE), remains elusive. The conversion ability of furin and trypsin have been investigated; however current evidence suggests that prepro-Ull is processed by hormone convertase enzymes recognising a common tri, bi or monobasic cleavage motif rather than a substrate specific enzyme.^{208–211}

The brain and spinal cord are a major source of UII-immunoreactive peptides (where antibodies are used assays methods cannot distinguish URP, UII and pro-UII due to their structural similarities) in fish and mammals. Outside of the CNS evidence suggests that UII/URP production also occurs in skeletal muscle, kidney, liver and heart.^{208,212–216} Renal expression of UII has been described by radioimmunoassay using a number of methodologies. In rats, urinary UII/URP is over 1000 fold higher than in the plasma.²¹⁶ While this finding alone could be explained theoretically by secretion into the renal tubules, separate experiments in sheep demonstrate that there is also a gradient across the renal vasculature; UII/URP concentration in the renal vein is higher than in the renal artery suggesting that UII/URP is produced locally within the kidney.^{212,217,218} In addition, UII and URP mRNAs have been isolated from renal tissue.^{178,217} Within the kidney distribution of UII has been described using immunohistochemical staining; in rat, UII is expressed in the developing metanephros (the immature fetal kidney) and remains detectable in the adult. Typical expression patterns in adult kidney are diffuse but predominantly localised to the proximal convoluted tubules and collecting ducts, including those within the papilla.²¹⁶

More recently antibodies with a degree of selectivity for UII over URP have been combined with HPLC to develop assays capable of differentiating UII and URP in human plasma samples. Unfortunately this method is not applicable to immunohistochemical staining.²¹⁹

1.4.3 Identification of the urotensin II receptor

UII was identified as a ligand to the orphan rat G-protein coupled receptor (GPCR) GPCR14, also known as sensory epithelium neuropeptide-like receptor (SENR), in a functional *in vitro* assay using Chinese hamster ovary (CHO) cells expressing the receptor.^{206,220} Initial experiments used a peptide fraction derived from porcine spinal cord; eventually UII was identified as the ligand. Ultimately the receptor was shown to be highly sensitive to porcine UII-1 (pUII-1), pUII-2, hUII and fish UII but not to somatostatin-14.²⁰⁶ Simultaneously Nothacker et al.²²⁰ identified UII as the ligand to rat GPCR14, identifying a single peptide ligand in HPLC purified extracts from bovine hypothalamic tissue before challenging CHO cells expressing GPCR14 with various synthesised peptide ligands and ultimately identifying UII as the peptide in question. Concurrently the human homologue of SENR was identified using the SENR sequence to probe the human genome database. Human GPCR14 shares 75% homology with the rat equivalent and human embryonic kidney (HEK) 293 cells

expressing human or rat GPCR demonstrated positive functional responses (increased intracellular calcium) when challenged with gUll or hUll.²⁰⁷ GPCR14 was formally renamed and reclassified as the urotensin II receptor (UT) by The International Union of Basic and Clinical Pharmacology (IUPHAR) in 2000.²²¹

Since these initial discoveries UT receptors have been identified in numerous vertebrate species, the putative sequences of which share substantial homology; for example the mammalian species examined ([Figure 1.7a](#)) share around 75% homology with human UT.^{218,222–226} Following elucidation of the three-dimensional structure of the UT receptor it is clear that the variability within the sequence is not evenly distributed throughout the structure. When comparing UT from three mammalian species (human, rat and mouse) many regions appear to be very highly conserved (> 90 % homology) whilst others share only 50 % homology ([Figure 1.41b](#)).^{222,223,227–229} UT is a member of the class-A rhodopsin like GPCR super family, and was originally identified in part by recognition of putative transmembrane domains and the E/DRY motif during genome screening.^{223,227,228} The UT receptor is the product of a single exon and no subtypes have been identified to date.^{213,230}

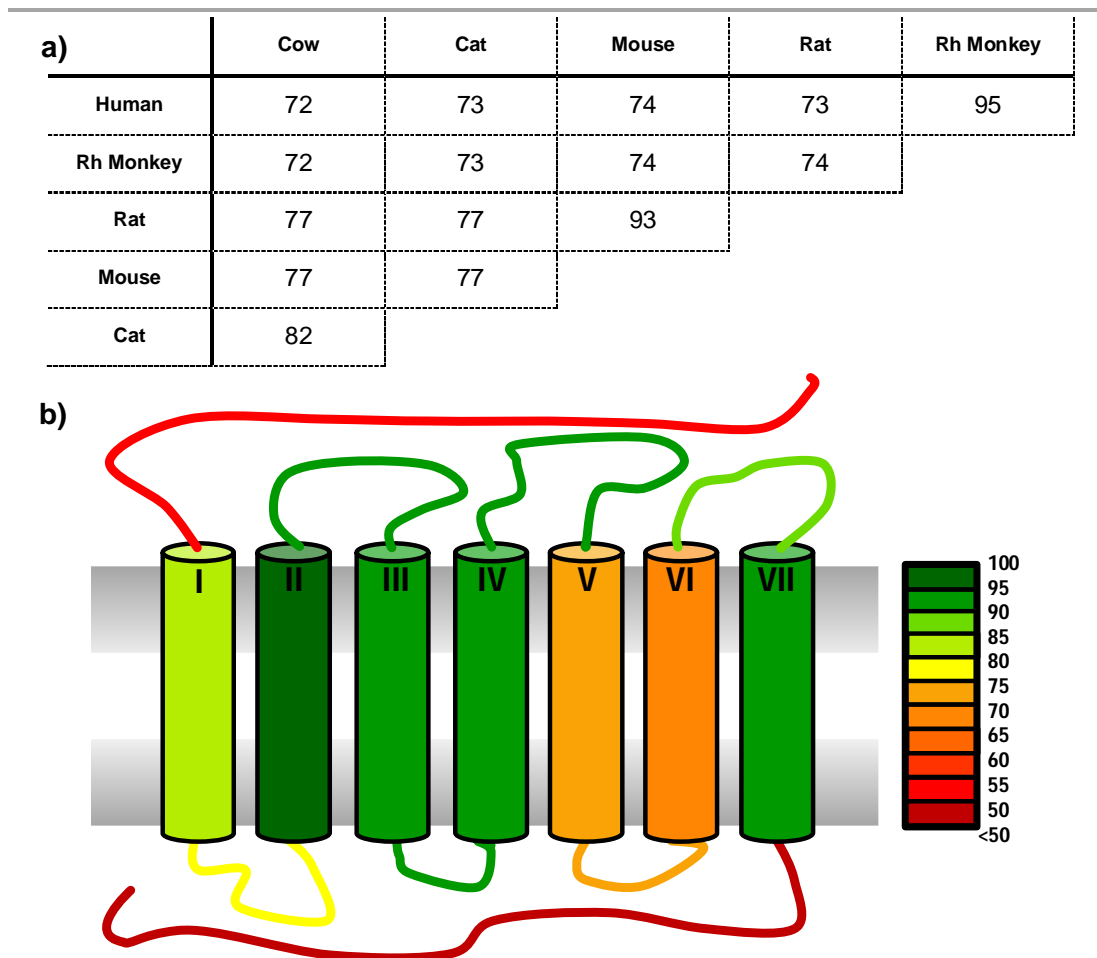


Figure 1.7 a) Amino acid sequence alignments^{224,225} of human (NP_061822.1), rhesus monkey (NP_001028066.1), rat (NP_065412.1), mouse (NP_663415.1), cat (NP_001041476.1) and cow (NP_001035574.1) urotensin II receptors (UT) highlights that there is a high degree of structural similarity across a range of mammalian species. Figures represent percentage homology (amino acid agreement).^{223,226} **b)** However comparing the rat, mouse and human UT reveals that the degree of sequence homology of the receptor structural domains is variable, with greater variability evident in the termini than in the transmembrane domains (TM).²²⁸ Homology is graded green (high) to red (low).

1.4.3.1 Receptor distribution

Apart from studies in fish, UT receptors were originally identified by the actions of Ull upon the vasculature. Binding sites (receptors) were localised using radio-labelled Ull; sites were identified within many vascular beds such as atrial myocardium, numerous brain regions, spinal cord, skeletal muscle and kidney (UT expression has been summarised in a review by Tölle and Van der Giet in 2008²³¹). Arterial tissue, specifically the thoracic aorta, as well as the heart are considered to express UT

highly.^{218,231} Renal expression of UT protein or mRNA has been detected in tissue from monkey, cat, rat and human and is typically more abundant in the renal medulla than cortex.^{216,218,223,232,233}

1.4.3.2 Pharmacology and intracellular signalling of UT

The natural ligands, UII and URP, are comparable in their affinity and efficacy at UT receptors across a range of species.^{202,234} There is substantial cross reactivity between UII orthologues both *in vivo* and *in vitro*, to such an extent that UT receptors are generally considered to be incapable of differentiating UII derived from different species.^{197,209,234} Many research groups have examined the structure-activity relationship of UII, and the findings have been used to produce antagonists which have been used in attempts to characterise the urotensin system. URP and the minimally active hUII fragment (residues 4 - 11, Asp-Cys-Phe-Trp-Lys-Tyr-Cys-Val with a disulphide bridge between the cysteine residues) share sequence homology at 7 of the 8 amino acid positions.^{234,235} This minimally active fragment has been modified to produce a series of peptidinerigic UT antagonists including the extremely potent urantide, which has proven useful when investigating the physiological effects of UII/UT.²³⁵

The endogenous ligands (UII and URP) have been shown to bind to UT with high affinity; hUII binds to hUT receptors with a pK_d 9.2 or $K_d < 1$ nM.²³⁶ Similarly UII was identified as highly efficacious at rat and human UT receptors with an effective concentration (of gUII) to produce a half-maximal response (EC_{50}) of just 0.78 nM and 0.47 nM, respectively.²⁰⁷ The high affinity binding of UII/URP to UT is such that it has been described as pseudoirreversible.^{214,237} This high affinity and efficacious binding, but apparent lack of efficacy *in vivo* has led to the suggestion that under normal circumstances UT receptors are occupied by endogenous UII species.²¹⁴

Systematic alteration of hUII has been used to demonstrate that removal of the preceding, variable, N-terminal region to leave just one single flanking residue (Asp₄) has little effect on the biological activity of UII at the rat UT receptor *ex vivo* or at hUT expressed within a cellular system.^{234,235,238} Further, removal of the remaining preceding amino acid in position four (Asp₄) results in reduced efficacy (roughly 100 fold vs. hUII); however substitution of this acid residue (to Ala₄) minimises this effect (4 fold reduction vs. native hUII).²³⁸ In contrast, alterations within the cyclic region have extensive effects on biological function: Trp₇, Lys₈ and Tyr₉ are vital to receptor binding and biological function whilst Phe₆ also plays an important role.²³⁸ Similar

studies have demonstrated that the same principles apply to the structure of hURP: the residues within the C-terminal ring structure are key to biological activity, which is unsurprising given the structural similarity of URP and the hUII₄₋₁₁ fragment.²⁰²

There are a number of domains within the UT receptor that are involved in recognition of ligands and receptor activation. The extracellular loops (ECL) II and III and the transmembrane domains (TM) IV, VI and VII of the UT receptor are proposed to be involved in ligand recognition.^{229,239,240} A methionine doublet (184/185 in rUT) in TM-IV was identified as a hUII binding site by Boucard et al. in 2003 using photolabelling methods.²²⁹ A further methionine residue in ECL-III has been identified using a similar photolabelling method.²⁴⁰ The role of EC-II and III were studied by Boivin et al. who reported that UII and URP interact with both EC-II and EC-III, whereas the peptide UT antagonist urantide interacts predominantly with EC-II and not EC-III.^{227,228} The UT receptor undergoes agonist-induced internalisation with cell surface expression reduced by approximately 70 % 30 minutes after stimulation with UII; however the mechanisms of this process remain unclear.^{239,241} One pathway thought to be involved in this process is internalisation into clathrin-coated pits mediated by arrestin3 (previously β -arrestin2) recruitment following agonist-induced phosphorylation of the conserved serine/threonine cluster located in the C-terminus of the receptor.²³⁹ Additional arrestin-independent mechanisms have also been described by Giebing et al. using HEK293 expressing rUT.²⁴¹

Studies using isolated tissues or UT transfected cell lines were used to determine that UII is capable of various cellular responses, which are primarily mediated by the UT coupling to G_q type G-protein ([Figure 1.8](#)); however, in common with many other GPCRs G-protein coupling type is not absolute and there is evidence of UT G_{i/o} coupling.^{239,242,243} Specifically, the actions of UT result from downstream activation of phospholipase C (PLC) and ultimately increases in intracellular Ca²⁺.^{243,244} In vascular smooth muscle cells (vSMCs) this pathway is generally associated with a contractile response whilst production of vasodilators can occur in endothelial cells.²⁴⁴ UII-dependent PLC-mediated production of inositol 1,4,5-trisphosphate (IP₃) and diacyl glycerol (DAG) from phosphatidylinositol 4,5-bisphosphate (PIP₂) has been demonstrably inhibited and results in reduced contraction.²⁴³ IP₃-mediated release of Ca²⁺ from intracellular stores (via the IP₃ receptor, IP₃R) represents only one component of the cellular response to UT activation. hUT expressing CHO cells incubated in the absence of extracellular Ca²⁺ lack the prolonged response component seen when incubated in a physiological (Ca²⁺ containing) buffer suggesting that Ca²⁺ entry, possibly via L-type calcium channels, is also important in

the signalling cascade associated with UT activation.²⁴⁴ Increases in intracellular calcium and production of DAG are implicated in the activation of protein kinase C (PKC). Downstream of these actions Ca^{2+} /calmodulin-dependent kinases (CAMKs), extracellular signal-regulated kinase (ERK 1/2) and mitogen-activated protein kinases (MAPKs) are potentially implicated in a variety of less immediate cellular responses such as differentiation, migration and proliferation.^{245,246}

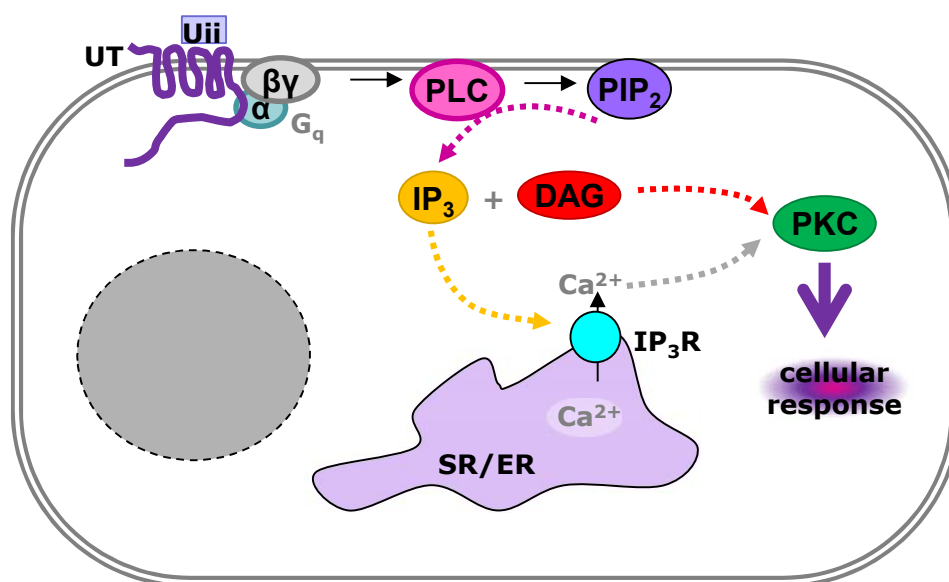


Figure 1.8 Urotensin II (UII) activates the urotensin II receptor (UT), a serpentine G-protein coupled receptor which has been shown to act principally through the G_q pathway. Activation of the G_q G-proteins activates phospholipase C (PLC), which converts phosphatidylinositol 4,5-bisphosphate (PIP_2) to inositol 1,4,5-trisphosphate (IP_3) and diacyl glycerol (DAG). IP_3 initiates the release of Ca^{2+} from the endoplasmic reticulum, via the IP_3 receptor (IP_3R), which leads to activation of protein kinase C (PKC); independent of this DAG can directly activate PKC. These signalling events can have a wide range of cellular outcomes.^{244,389}

1.4.3.2 Development of UT ligands

The development of UT ligands initially centred on substitution of amino acids in the minimal active fragment of human UII, hUT_{4-11} .²⁴⁷ This approach generated ligands with properties across the spectrum, super potent agonists (P5U) and potent antagonists (urantide).²⁰³ The disulphide bridge between the cysteine residues in position 5 and 10 is critical to the biological activity, in P5U cysteine₅ was substituted with penicillamine, another sulphur containing amino acid creating a super potent agonist at hUT receptors ($\text{pK}_i = 9.7$ and $\text{pEC}_{50} = 9.6$).²⁴⁸ At the other end of the

spectrum this process created urantide, a potent antagonist in rat aorta with no apparent agonist response but partial agonist activity documented in other assays.^{235,249,250} These ligands are particularly useful for studying the Ull system *in vitro* or *in vivo* by i.v. but are not practical for oral dosing due to their peptide structures. The non-peptide antagonist Palosuran was described as a potent hUT specific antagonist ($pK_i = 8.3 - 8.4$); however the potency of palosuran was substantially lower in whole cells and artery preparations for reasons that remain to be determined.^{251,252} More recently a series of aminomethylpiperazine compounds were generated from a κ -opioid receptor antagonist that was found to possess reasonable hUT potency in order to increase potency and minimise κ -opioid binding.²⁴⁶ Some of these compounds also demonstrated diminished activity in tissue preparations.²⁴⁶ A further UT antagonist is the arylsulfonamide compound SB-611812, which is less potent ($pK_i = 6.9$, rUT) than palosuran and urantide but has shown consistent results tissue based assays and demonstrated oral bioavailability.²⁵³

1.4.4 Urotensin II in physiology and disease

Ull, and the receptor UT, originally sparked interest due to the action of Ull as an ultra-potent spasminogen in isolated rat aorta.²⁰⁷ Particularly, *In vivo* hUll has been shown to cause vasoconstriction in isolated rat aorta, effects which are more potent than those seen with endothelin-1 (ET-1) and Ull remains the most potent (endogenous) vasoconstrictor characterised to date.²⁰⁷ Further studies using a range of isolated vessels from many mammalian species described considerable variability in the vasoactive properties of Ull; effects are vessel and species dependent ([Table 1.7](#)).^{194,213,237,254–257} Further studies were able to determine that vasodilator responses to Ull were endothelium dependent,¹⁹⁴ and that these responses are mediated by the production of endothelium-dependent hyperpolarising factor (EDHF) and increased production of nitric oxide (NO) by nitric oxide synthase (NOS).^{244,256}

Species	UII	Vessel	Response
Rat	goby	Thoracic aorta	Dose dependent :Dilate or Constrict* / Constrict*#
Rat	Human	Thoracic aorta	Constrict
Rat	Human	Abdominal aorta	Minimal constriction
Rat	Human	Jugular vein	No response
Rat	Human	Coronary artery	Dilate*
Human	Human	Pulmonary artery	Dilate*
Human	Human	Pulmonary artery	Constrict
Pig	Human	Thoracic aorta	Constrict
Rabbit	Human	Pulmonary artery	Minimal constriction
Guinea Pig	Human	Thoracic aorta	No response

Table 1.7 Summary of example isolated vessel responses to UII highlights variability of responses. * and # denote pre-constricted and endothelium denuded vessels, respectively. Compiled from Gibson,¹⁹⁴ Douglas et al.,²⁵⁴ Douglas,²³⁷ Stirrat et al.,²⁵⁵ Bottrill et al.,²⁵⁶ and Camarda et al.²⁵⁷

The immediately obvious actions of UII as a potent vasoconstrictor ultimately transpired to be substantially more complex. As described previously the actions of UII on isolated vessels is variable and is typically dependent upon distribution of UT receptors: UII can cause vasoconstriction in vessels where UT is expressed in the vSMCs or vasodilation when UT is predominantly localised in the endothelium, a reduction in detectable UT (eg. rat abdominal aorta) is associated with a lack of response.^{237,243,244,256} While numerous cardio-renal effects of UII have been described the physiological relevance of these actions remains largely undefined. In addition, further complexity arises due to variations in the method of administration; peripheral bolus, peripheral infusion and central bolus doses have very different cardiovascular response profiles.²⁴⁴ An extreme example of this variation is the vasoconstriction of cardiac arteries leading fatal cardiac dysfunction evoked by 300pg/Kg hUII administered by i.v bolus to non-human primates.²⁰⁷

To date altered expression of the receptor UT and/or the ligands UII and URP have been reported in a myriad of pathophysiological states. Elevated UT/UII/URP has been described in a number of disease states within the human population, including heart failure, (essential) hypertension^{258,259}, cirrhosis, metabolic syndrome and

diabetes^{260–264}, renal failure^{182,183} and atherosclerosis^{259,265}. Similarly variations within the urotensinergic system have been reported in animal models of hypertension^{178,266–268}, renal disease¹⁷⁸ and diabetes. The nature of these relationships remains unknown.^{213,269}

1.4.4.1 Blood pressure regulation and hypertension

The cardiovascular actions of UII in mammals were originally reported by Gibson et al.¹⁹⁸ almost 30 years ago. *In vivo* UII acts to lower blood pressure when delivered as a bolus i.v. in anaesthetised rats, actions which are suggested to arise from the chronic modulation of basal vascular tone particularly within resistance vessels such as those in the mesenteric bed.^{198,256,270} When infused at lower doses (6 pmol.min.100g) UII has little effect on blood pressure in the rat, a finding which has been attributed to a lack of unoccupied receptor capacity.^{214,268} More immediate roles, such as a regulator of total peripheral resistance, are considered unlikely due to the slow onset of responses and the nature of the interaction between UII and UT: UII dissociates from UT extremely slowly, with a K_d below 1 nM.^{207,213,214}

Elevated circulating and urinary concentrations of UII reactive peptides have been reported widely in patients with hypertension.^{258,271,272} For example a study of patients with essential hypertension plasma UII has been reported to be three-fold higher than in normotensive controls, and to correlate with the degree of hypertension.^{259,272} In addition, kidneys from spontaneously hypertensive rats (SHRs) have been shown to be more sensitive to exogenous UII administration and to express the mRNAs for both the protein and receptor more abundantly than their normotensive counterparts, with increased plasma UII concentrations also reported.^{216,268} Further to this, URP expression within the kidneys of pre-hypertensive (young) SHRs is elevated compared to non-predisposed (WKY) rats.^{178,267} Later in development (16 weeks) UT is also expressed more abundantly in SHRs than in WKY.¹⁷⁸ In contrast, UII is not different between the strains.^{178,267} In a separate study Hirose et al.²⁶⁶ described increased expression of UT, URP and UII mRNAs in cardio-renal tissues of SHRs; notably heart, kidney and aortic expression profiles were altered. Whilst these findings do not establish directionality of cause, the elevation in the components (URP) before the onset of hypertension could implicate the urotensin system in development of hypertension in SHRs.

Expression of UII and UT has been described cardiac tissue.²³⁷ In congestive heart failure (CHF) patients plasma UII has been reported to be elevated and to correlate

well with a number of established disease biomarkers, although whether or not UII contributes to disease progression has not been established.²⁷³ In rats cardiac hypertrophy induced by isoproterenol is exacerbated by administration of UII, resulting in increased cardiac fibrosis.¹⁸⁴ In contrast, cardiac function along with other disease markers were improved when obese (*ob/ob*) mice were treated with a urotensin II antagonist; similarly urantide has been shown to lessen monocrotaline-induced cardiac hypertrophy in rats.^{274,275} Another UT antagonist (SB611812) has also been suggested to improve outcomes in rats with experimental CHF.²⁷⁶ In contrast Zoccali et al. have suggested that UII is a protective factor in CHF patients.²¹⁵ These differences may result the ability of UII to act as both a vSMC-dependent vasoconstrictor and endothelium dependent vasodilator. The balance between these properties may differ between species and disease states.^{194,256}

In vitro there is evidence that UII is capable of inducing differentiation and collagen I synthesis in cultured fibroblasts isolated from the adventitia of rat aortae, with suggestions that PKC, MAPK and transforming growth factor- β (TGF- β) may be involved in signal transduction.^{277,278} Neonatal rat cardiomyocytes over expressing UT also undergo hypertrophy promoted through the MAPK/ERK pathway; however transactivation of the epidermal growth factor receptor (EGFR) is suggested to cause these effects rather than direct activation via PKC.²⁷⁹ Increased UII and UT mRNA expression has also been described in atherosclerotic lesions from human subjects, particularly within the immune cells recruited to the site.²⁸⁰ Further to this, circulating plasma UII has been reported to correlate with plaque scores in a hypertensive patient population.²⁵⁹ Conversely the UT knock out (K.O.), *Uts2r*^{-/-}, mouse appears curiously normal; while lacking any UII vasoconstrictor response the basal vascular phenotype appeared unaffected (heart rate, BP, CO).²⁸¹ Unfortunately the effects of the *Uts2r*^{-/-} on the kidney were not reported beyond the presence of renal mass, which was comparable to that of the wildtype *Uts2r*^{+/+} mouse.²⁸¹ Collectively these findings have been used to suggest a role for UII in vascular remodelling and disease.²⁸²

1.4.4.2 Renal function

Initial studies reporting the effects of UII on renal function, in rats, were contradictory.^{213,283} However, the development of reliable antagonists and insights into the physiological circulating concentrations of UII has allowed some of the renal actions of UII in the rat to be untangled.²³⁵

In anaesthetised rats infusion of UII (0.6 pmol/min per 100 g bodyweight) has been shown to cause a reduction in GFR and an associated reduction in urine flow, while at higher doses (6 pmol/min per 100 g bodyweight) these changes are accompanied by reduced effective renal blood flow (eRBF) and decreased urinary sodium excretion.²⁸⁴ Interestingly at lower doses (0.6 pmol/min per 100 g bodyweight) whilst total sodium excretion is unchanged, fractional excretion (FE_{Na}) is increased which is suggested to arise from altered handling of electrolytes in the renal tubules.²⁸⁴ In contrast, i.v. infusion of the potent peptide UT antagonist has been shown to cause transient increases in GFR, urine flow and urinary sodium excretion.²¹⁶

Immunohistochemical staining of renal tissue from rat highlights UT expression in the inner-medullary collecting ducts and ascending thin limbs of Henle within the medulla with no signal detected in the surrounding cells.^{216,232,268} UT expression in cortical sections has also been reported showing occasional staining within the glomerular tuft perhaps associated with the afferent arterioles.^{216,285}

1.4.4.3 The urotensin system in renal disease states

Differences between control and diseased cohorts are routinely documented for components of the UII system.²⁴⁴ However the role of UT, UII or URP as disease biomarkers or as potential therapeutic targets remains unclear. Totsune et al.¹⁸² reported increased concentrations of immuno-reactive UII (collectively; UII, URP and pro-UII) in the plasma of patients with chronic renal failure and those currently undergoing haemodialysis with levels two and three fold higher than controls, respectively. However, the difference between dialysis patients and those not receiving dialysis may be partly due to differential functional abilities of the kidney and dialysis machinery to remove the reactive species, so results from this particular group need to be interpreted with care.²⁸⁶ An Italian research group^{287,288} suggest that plasma UII is lower in patients with CKD (renal failure) and that this low UII is a marker for cardiovascular events and even death in these patients, a finding which contrasts with those of a separate study in renal failure (ESRD) patients from the same research group and those of Totsune et al., reporting two-fold higher plasma UII in patients with CKD (renal failure).^{182,289}

Elevated plasma UII (total reactive species) has also been reported in type II diabetic patients, and those with associated diabetic nephropathy.^{183,290} In addition, increased expression of UII and UT mRNAs have been described in renal biopsy tissues from patients with diabetic nephropathy.²³³ Interestingly variation in the urotensin II system

has also been described in 'pre-diabetes' or the metabolic syndrome (MetS) and insulin resistance. Ong et al.²⁶² describe variation in the prevalence of single nucleotide polymorphisms (SNPs) within the human UII gene (UTS2) and UT gene (UTS2R) in a Chinese (Hong Kong) population. Notably UTS2R haplotype (GGT) is associated with elevated fasting blood glucose and impaired glucose tolerance.²⁹¹ In a Japanese population a SNP within preproUll (Ser89Asn) has been identified to be significantly more prevalent within type II diabetic patients.²⁶¹ This finding is supported by Sáez et al.²⁹² who describe an association between the UTS2 gene and flanking region with insulin resistance in a European population.²⁹³

CKD is a multifaceted disease with complex aetiology defined by progressive decline in renal function and is associated with the development of glomerulosclerosis. In rats which have undergone a 5/6th sub-total nephrectomy, an established model of experimental (non-diabetic) chronic kidney disease, mRNAs for both the urotensin II receptor (UT) and ligands (Ull and URP) are more abundant than in the kidneys of sham controls 8 weeks after surgery.¹⁷⁸ This particular time-frame represents a relatively early phase in the disease, well before the onset of renal failure.^{61,294} As a result these data are not directly comparable to data from human studies as this is limited to patients with late-stage CKD, stage 4 or renal failure.¹⁸²

It is difficult to draw any firm conclusions from these previous cohort studies for multiple reasons. Methodological differences and specificity of the antibodies used to assay Ull in blood and urine are key sources of variation. Antibodies with selectivity for Ull demonstrate approximately 20% cross-reactivity with URP and preproUll. It is also important to consider the underlying cause of CKD (and renal failure), as the condition is a collection of pathophysiological traits rather than a single modality. This could be responsible for some of the variation seen between cohorts; for example diabetes is the leading cause of CKD and is associated with endothelial dysfunction which would likely not be a co-factor in non-diabetic CKD. Similarly hypertension is a major cause, and co-morbidity, of CKD a condition where altered Ull has been widely reported in patients and animal models.^{178,267,268,272} If the results from these studies could be reconciled through identification of differences in study design and cohort selection, they could provide insight into correlation but not into the role of Ull in CKD; no determination of a causative vs. reactive role can be made without intervention.²⁹⁵

Data from intervention studies in humans and rats are limited. The non-peptide UT antagonist palosuran showed promise, improving pancreatic and renal function in

diabetic rats. Palosuran also reduced acute renal injury risk following reflow hypoxia in male Wistar rats and improved some haemodynamic parameters in the bile-duct ligation model of cirrhosis.^{251,296,297} In contrast clinical studies using the UT antagonist have been largely disappointing; initial trials in healthy male subjects showed that 125 mg twice daily was well tolerated.²⁹⁸ Following this reduced albuminuria was reported in a short term, 2 week, intervention study using the same dosing regimen in diabetic nephropathy patients with macro-albuminuria (> 300 mg/day), but these findings were not replicated in a longer, cross-over controlled study in DN patients with less prominent albuminuria.^{299,300} At first sight the reasons for the poor performance of palosuran in human trials compared with the rat studies is unclear. In membrane preparations palosuran shows selectivity for hUT over rUT, being about 100 fold less potent at the rat receptor. However the inhibitory potential of the antagonist is substantially lower in whole cells, a factor which would undoubtedly influence *in vivo* application and dosing.²³¹ Indeed Douglas and colleagues have criticized the design of the clinical trials and point to the very low bioavailability of palosuran in humans. They estimate that $\leq 10\%$ of UT receptors would have been occupied at the dose employed in the trial.²⁵²

The absence of substantial UII targeted intervention-based human data or CKD specific intervention in animal models make determining the potential role of the urotensin system in the development or progression of CKD extremely difficult. This current work aims to provide insight in to the expression of the UII system in a model of late stage CKD thus providing a point of comparison to clinical data where early stage data are lacking. The extensive glomerulosclerotic lesions associated with the 5/6th SNx also provide an opportunity to investigate the potential of UT antagonism in the development of CKD associated glomerulosclerosis.

1.5 Aims and Objectives

1. Establish the 5/6th sub-total nephrectomy model of CKD in rat within the laboratory group and refine monitoring methods to allow collection of (near) renal failure data.
2. Examine structural changes within the kidney using histological staining techniques and light microscopy; particularly the use of periodic acid Schiff stain to detect glomerulosclerosis and ECM staining for fibrosis.
3. Generate a renal expression profile for Ull, URP and UT at protein and mRNA levels in the model using immunohistochemical techniques and SYBR Green RT-qPCR, respectively. This (near) renal failure data will provide insight into the expression of the Ull system in the later stages of experimental CKD for the first time.
4. The model and profile data can then be used to investigate whether chronic UT-antagonism is an effective intervention to delay the progression of CKD following 5/6th SNx in the rat during the initial and stable phase of disease.

2: Methods

All work was carried out in accordance with The Animals (Scientific Procedures) Act 1986, Amendment Regulations 2012 (SI 2012/3039) and received local ethical approval.

2.1 Animals

Male Sprague-Dawley (SD) rats (8 – 10 weeks, 285 ± 28 g) were obtained from Charles River (Margate, Kent, UK) and housed for 1 week within the Biological Services Facility (BSF) prior to any experimental procedure. Throughout all studies rats were housed in individually ventilated, green line cages (Techniplast, Buguggiate, Italy) in a 12: 12 hour light: dark cycle with controlled temperature (22-24 °C) and relative humidity. Food (RM1, expanded pellet diet, Special Diet Services, Witham, Essex, UK) and water were provided *ad libitum*. Rats were allocated to cages at random (3 per cage) by technical staff on arrival to the unit.

2.2 5/6th sub-total nephrectomy: surgical reduction in renal mass

To establish a progressive renal disease male SD rats underwent a two-stage surgical reduction in renal mass.¹⁸⁰ This sub-total nephrectomy (SNx) was achieved by removing 2/3rd of the left kidney followed by the removal of the right kidney a week later. This results in the removal of 5/6th of total renal mass.

The one week recovery period between the two procedures reduces the risk of acute renal failure substantially.^{174,180,301} Surgery was carried out in groups of 9 animals per day (6 SNx and 3 controls, [Section 2.2.5](#)). All procedures were carried out in the BSF theatre space using aseptic technique.

2.2.1 Surgical preparation

Anaesthesia was induced using 4 % isoflurane (Baxter, Newbury, Berkshire, UK) delivered in 2 L/min oxygen (BOC Healthcare, Manchester, Greater Manchester, UK) via a vaporiser (Vapomasta5, Anmedic, Stockholm, Sweden) before clipping of the fur on the appropriate flank and cleaning the skin with iodine solution (BSF). Anaesthesia was then maintained with 2 % isoflurane in 2 L/min oxygen throughout

the procedure. For all procedures buprenorphine analgesia (0.06 mg/procedure, Sogeval UK, York, North Yorkshire, UK) and fluid replacement (1 mL, 154 mM sodium chloride for injection, Braun Medical Ltd., Sheffield, South Yorkshire, UK) were administered subcutaneously between the shoulders. Buprenorphine was administered at the start of the procedure as it takes approximately 20 minutes for it to exert its effects.

With the animal positioned on the appropriate side, starting posterior to the ribcage and close to the muscle block that runs parallel to the spine, an incision was made at 45° on the flank ([Figure 2.1a](#)) using a number 10 scalpel (Swan Morton, Sheffield, Wet Yorkshire, UK). The kidney was located and exteriorised before careful separation from the renal capsule, which was returned to the abdominal cavity to avoid damage to the adrenal gland, before continuing with the procedures described below.

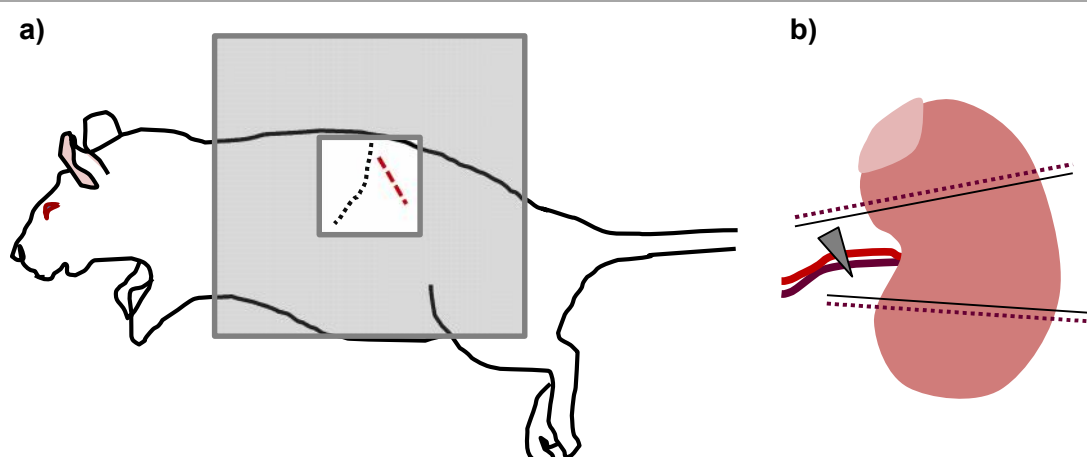


Figure 2.1 Schematic diagram showing (a) the position and orientation of the surgical incision (red dashed line) relative to the ribcage (black dotted line), and (b) the exteriorised kidney; the left renal artery was temporarily occluded (grey arrow head) before ligation (black solid line) and cutting (dark red dotted line) of the renal poles for removal. The adrenal gland (pale pink) was carefully dissected away from the kidney along with the renal capsule prior to removal of the poles.

2.2.2 Left kidney; procedure one

With the capsule detached, the left renal artery was temporarily occluded with a loop of braided and coated, non-absorbable, silk suture (4/0, Mersilk®, Ethicon, Livingston, West Lothian, UK) before the poles were ligated using non-absorbable suture (4/0, Mersilk®, Ethicon) and then removed using a square razor ([Figure 2.1b](#)).

The cut faces were sealed with (n-butyl-2-cyanoacrylate) tissue glue (Histoacryl[®], Braun Medical Ltd.). The suture loop was removed as soon as the cut faces were fully sealed, restoring blood flow to the tissue (typically this part of the procedure took less than 5 minutes). The kidney remnant was returned to the abdominal cavity and the wound closed ([Section 2.2.4](#)). The removed renal tissue was weighed in order to calculate the estimated reduction in renal mass and snap frozen in liquid nitrogen for future analysis ([Equation 2.1](#)). Typical procedure duration was 15 - 20 minutes.

2.2.3 Right kidney; procedure two

One week later the capsule and adrenal gland were dissected away from the right kidney before the renal artery and vein were ligated at two points, approximately 5 mm apart, using non-absorbable suture (4/0, Mersilk[®], Ethicon). The vessels were then cut between the two ligatures and the kidney removed whole before the wound was closed. The weight of the kidney was recorded and used to calculate renal mass reduction ([Equation 2.1](#)). Completion of this second procedure is considered time zero. Typical procedure duration was 10 - 15 minutes.

2.2.4 Wound closure and recovery

Wound closure was carried out with absorbable suture (3/0, Polyglactin 910[®], Ethicon), using continuous running sutures for the underlying peritoneal wall and continuous, sub-dermal, mattress sutures for skin closure. Following each surgery the animal was allowed to recover in a warmed environment, under close observation, until mobile and displaying normal behaviour (grooming, feeding) before being transferred back to normal housing.

Following return to normal housing animals were provided with pre-soaked food to ensure adequate hydration for at least 24 hours. Close observation was maintained for 48 hours post-surgery until the risk of acute renal failure or wound opening had abated.

The incidence of acute renal failure was extremely low (5.6 %): a total of 54 animals underwent the established SNx procedure ([Section 2.2](#)), of which 3 went into acute renal failure within 72 hours of the second procedure. Additionally, 1 sham animal (out of the total of 24) required re-suture of the peritoneal wall after developing a

hernia following the first procedure. This took approximately 10 minutes (from anaesthesia to completion) and the animal was able to complete the study.

2.2.5 Control animals

Control animals underwent an equivalent two stage sham operation where the abdominal cavity was opened and the kidney exteriorised and manipulated before being returned to the cavity intact. All preparation, anaesthesia, analgesia, fluid replacement therapy, wound closure and recovery procedures were the same as those used for SNx animals. The typical procedural duration was 10 - 15 minutes.

2.2.6 Calculation and analysis of renal mass reduction

To estimate the reduction in functional renal mass the following equation was used:

$$\frac{(2 \times \text{Right Kwt}) - (\text{Right Kwt} + (\text{Weight of Poles} + 100\text{mg}))}{(2 \times \text{Right Kwt})}$$

Equation 2.1

This calculation is subject to the following assumptions: the right and left kidney are equal in size, the right kidney does not change in size in the time between the two procedures and approximately 50 mg of tissue at the cut face of each pole becomes ischaemic and is no longer functional. Results are expressed as a fraction (where 10% would be represented as 0.1).

To determine consistency of the procedure, renal mass reduction was calculated for all SNx animals and the results between the experimental groups compared using a Kruskal-Wallis test. The fraction of kidney tissue removed was not significantly different between any of the groups (Overall mean: 0.736, n = 54, p = 0.509), [Figure 2.2](#).

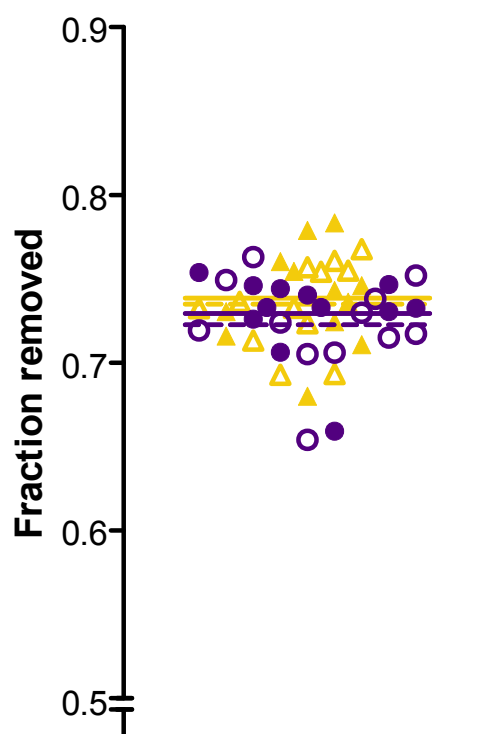


Figure 2.2 The fraction of renal tissue removed was not significantly different between experimental groups. Early (filled circles) and late (open circles) groups were used in the characterisation study ([Section 2.3.1](#)) whilst vehicle (filled triangles) and UT antagonist (open triangles) groups were used in the intervention experiment ([Section 2.3.2](#)) as described below. Group means represented by colour matched lines (solid line/solid shapes and dashed lines/open shapes).

2.3 Experimental design

For both experimental protocols ([Sections 2.3.1](#) and [2.3.2](#)) each group required five perfusion-fixed tissue samples and five frozen tissue samples at the endpoints. For sham animals one kidney could be fixed independently of the other, meaning that one animal could provide both sample types. In contrast, SNx rats only had one remaining kidney which could be either fixed or perfused. As a result the n numbers for SNx rats were twice as large as the shams.

2.3.1 Characterisation of the 5/6th SNx model

In order to establish the SNx model within the laboratory a profile of the progressive renal disease associated with the 5/6th subtotal nephrectomy was generated. These data were then compared with the literature for the associated pathophysiology in order to validate the model.

A number of physiological parameters were monitored ([Section 2.4](#)) in order to monitor disease progression. Of particular importance were: time to renal failure, systolic blood pressure (SBP) and changes in renal function, as reflected by urinary albumin:creatinine ratio (uACR). Terminal blood plasma samples were analysed for urea nitrogen products (BUN) and creatinine concentration as the build-up of these

products is indicative of inadequate renal function. Changes in renal structure ([Section 2.8](#)) were examined using histological staining techniques; basic histology was examined using haematoxylin and eosin stain, periodic acid Schiff (PAS) stain was used to determine the extent of glomerulosclerosis and Masson's trichrome (MTC) stain used to visualise collagen fibres.

2.3.1.1 The UII system in late-stage CKD following 5/6th SNx

In addition to confirmation of the pathophysiology, the later part of this work aimed to examine the changes in UII, URP and UT mRNA expression, beyond those up to 8 weeks post-surgery that have been described previously.²⁶⁶ Expression of mRNAs for UT, UII and URP have been shown to be up-regulated 8 weeks post-surgery; this time-frame represents the transition from the initial (hyper-filtering) phase to the stable phase of the CKD associated with 5/6th SNx model. There is currently no information available regarding the expression of these targets in the latter stages of the stable phase (week 8 - 20), or the decline phase (week 20 onwards); this contrasts the data from CKD patients where expression profiles represent exclusively late stage (CKD stages 4-5) data.

The expression of UII/URP and UT were examined at the protein level by immunohistochemical staining of tissue sections ([Section 2.9](#)), and was further explored using SYBR green RT-qPCR for UII, UT and URP mRNAs ([Section 2.11](#)).

To achieve this, nephrectomised rats, and time-matched sham controls, were followed to the stage of renal dysfunction (early, 8 weeks) or (near) end-stage renal failure (late, 30 ± 3 weeks). The time points used represent patients at CKD stages 1 - 2 and 4 - 5 respectively, [Table 1.2](#)). At each time ([Figure 2.3](#)) point n = 12 (SNx) and n = 6 (sham) rats were culled by cardiac puncture, under terminal anaesthesia and samples collected as described in [Section 2.5](#).

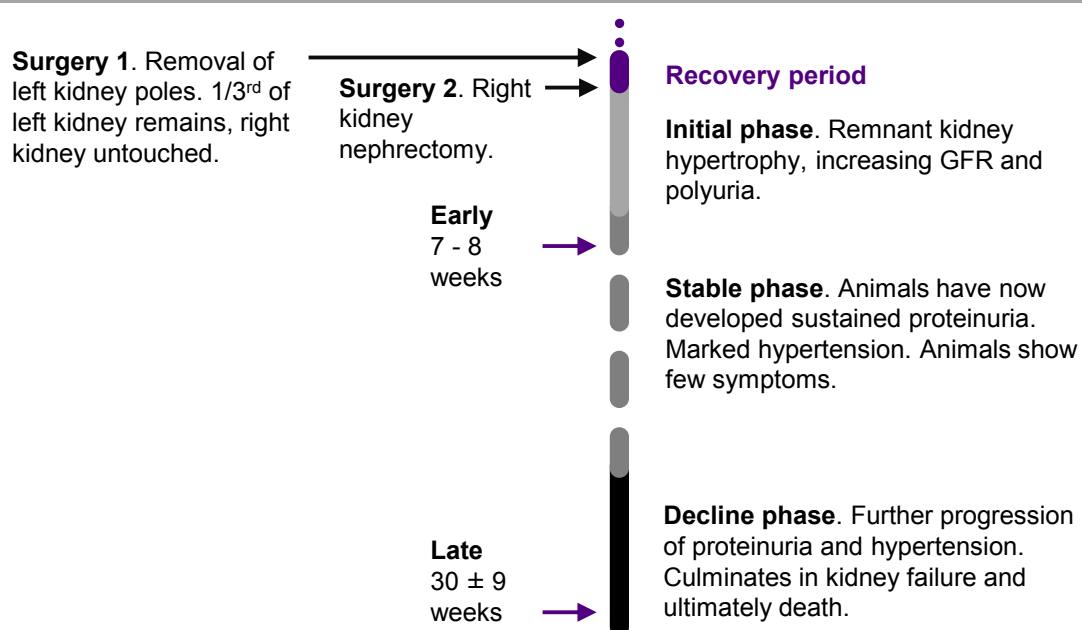


Figure 2.3 Surgical and sampling timeline for the characterisation of the UII system following 5/6th SNx in rat. Terminal samples were collected at two time points: early (7 - 8 weeks) and late (30 ± 3 weeks) after procedure 2.

2.3.1.2 End point determination

Samples from the late stage animals were collected as late as possible in the disease course; this was to ensure that the pathology would be representative of ESRD. These criteria meant that strict monitoring procedures were employed in order to minimise any distress; these checks were initially made on a daily basis with frequency increasing in the later stages of the study. Decisions about continuation were made based primarily on a warning system pertaining to The Animals (Scientific Procedures) Act 1986, Amendment Regulations 2012 (SI 2012/3039) project licence. Amber markers for close monitoring included: visual inspection of appearance (dirty coat, paling of the eyes) and behaviour (withdrawal from social interactions and reduced energy) along with changes in SBP (> 200 mmHg), ACR > 1.5 mg/μmol and body weight (> 10 % from peak body weight). If these changes were persistent a termination under anaesthesia was carried out. Red (immediate termination by Schedule 1 method) markers included unresponsiveness to stimuli, piloerection, impaired mobility and weight loss (> 15 %). While more informative of the underlying pathophysiological condition of the animal, biochemical analyses were considered too slow when a rapid decision was required regarding impending humane endpoints.

2.3.1.3 Sampling and data collection

Over the course of the experiment, physiological parameters were monitored as detailed in [Section 2.4](#) below. Body weight was measured every 1 – 4 days. Urine samples and systolic blood pressure (SBP) data were collected regularly throughout the course of the experiment (typically every 2-4 weeks).

2.3.1.4 Statistical analysis

For the purpose of statistical analysis the following groups were used: early vs. late and SNx vs. sham. This produced a two-way (end-point) analysis with two levels of comparison. Where repeated measures (within subject measures, time) were required early and late data were analysed independently as 2-way ANOVA (with RM). All data analysis was carried out in SPSS (version 22.0, IBM SPSS Statistics) or Prism (version 5.0, GraphPad Software Inc.). Full details of the individual analyses used can be found within the appropriate sections below.

2.3.2 Intervention with a urotensin II receptor antagonist

In order to determine whether inhibition of the UII system altered the rate of progression of CKD induced by the SNx, the effects of a non-peptide UT antagonist, AZ13694621, were investigated.

2.3.2.1 Confirmation of compound bioavailability in SD rat

Several UT antagonists ([Table 2.1](#), kindly synthesised by AstraZeneca, Alderley Edge, Cheshire, UK) were tested for their suitability for use in a chronic exposure study (oral dosing) in the SD rat. To do this the bioavailability and the clearance profiles of each UT antagonist were determined using a 24 hour pharmacokinetic (PK) protocol. Once collected, all PK samples were analysed by John Swales and Mark Denn, AstraZeneca, Alderley Park.

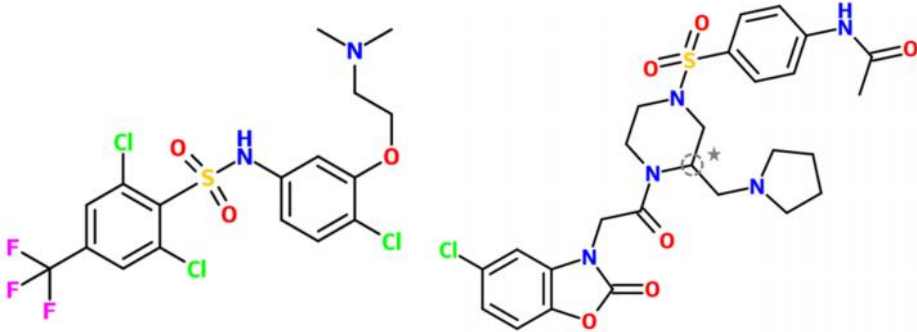
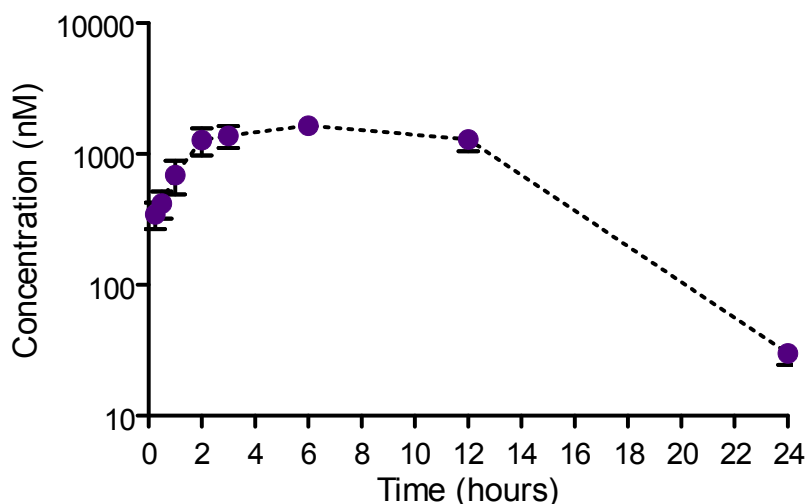
	L and S enantiomers	
	AZ13631437	AZ13631439
	AZ13694621	
Structure		
Name	SB-611812 2, 6-dichloro-N-[4-chloro-3-[2-(dimethylamino) ethyloxy] phenyl]-4-(trifluoromethyl) benzenesulfonamide	Compound 37 9-(2-{4-(p-Acetylamino)phenylsulfonyl}-2-[(1-pyrrolidinyl)methyl]-1-piperazinyl}-2-oxoethyl)-3-methyl-7-oxa-9-azabicyclo[4.3.0]nona-1,3,5-trien-8-one
K _i (Rat UT) (nM)	121	4.0
K _b (rat aorta) (nM)	-	13.1 ± 3.6
pA ₂	6.59 (257 nM)	-
Selectivity	No change in rat aorta response to KCl, phenylephrine, endothelin-1 or angiotensin-II at 10 µM	Opioid receptor (κ) EC ₅₀ : 1300

Table 2.1. Properties of the compounds used in this study. Structures and properties reproduced from published sources.^{246,302} ★ Denotes a chiral carbon atom, the R and S- enantiomers were tested independently for the purposes of the PK study.

Each compound was administered orally (p.o.) at 5 mg/Kg to male SD rats (220-300 g, n=2-4). Compounds were suspended in 0.5% hydroxyl-propyl methylcellulose (HPMC, Sigma, Gillingham, Kent, UK) with 0.1% Tween20 (Sigma) in deionised water at a concentration of 2 mg/mL. Blood samples (100 µL) were collected at 0.25, 0.5, 1, 2, 3, 6 and 12 hours (h) via the lateral tail vein, using a 23G needle, into chilled, heparinised, 0.5 mL centrifuge tubes. A final sample (24 h) was collected via cardiac puncture under isoflurane (Baxter, Newbury, Berkshire, UK) anaesthesia. Each 100 µL sample was diluted 1:1 with phosphate-buffered saline (PBS, pH 7.4, Sigma) and stored in a 96 well microplate at – 20 °C for analysis.

Compounds AZ13631437 and AZ13631439 were synthesised from a published structure (L and S enantiomers, Compound 37, [Table 2.1](#))²⁴⁶ and showed no exposure in the blood of SD rats following oral dosing, indicating that the substance was not present in an appreciable concentration. This could, for example, be the result of poor absorption in the gastrointestinal tract or rapid first pass metabolism. An alternative compound, AZ13694621, was synthesised (AstraZeneca) and was detectable in the blood and had a suitable clearance profile ([Figure 2.4](#)).



[Figure 2.4](#) Concentration of AZ13694621 in rat blood, following p.o. administration at 5 mg/Kg, (n=4). Concentration of AZ13694621 in rat blood peaked at 1643.1 nM, 6 hours after dosing.

Once bioavailability was confirmed a larger quantity of AZ13694621 was synthesised for the 14 week dosing study (Pharmaron, Beijing, China).

2.3.2.2 Dosing

AZ13694621 was administered once daily p.o. by flexible gavage (8 Fg x 80 mm, VetTech, Congleton, Cheshire, UK) from day 7 post-surgery, for 13 weeks. AZ13694621 was suspended in 0.5% HPMC (Sigma) with 0.1% Tween20 (Sigma) in deionised water at a concentration of 12 mg / mL. Both vehicle and AZ13694621 suspension were sonicated for 10 min (U100H sonication bath, Ultrawave, Cardiff, Glamorgan, UK) before use to ensure particles were small enough to allow a consistent suspension. Animals received 2.5 mL/Kg of UT antagonist (AZ13694621) suspension to achieve a daily dose of 30 mg.Kg⁻¹.day⁻¹, time and age-matched control animals received vehicle at 2.5 mL.Kg⁻¹.day⁻¹. This dosing regimen has been

used previously in *in vivo* rat studies and was chosen based upon a reported clearance half-life of 4 - 5 h.³⁰²

The animals were grouped, per date of surgery, into subgroups A, B, C and D (each containing 6 SNx and 3 Sham, in total n = 36). To allow disease progression to be monitored effectively, surgery was carried out over 3, overlapping, weeks ([Table 2.2](#)). Early subgroups (A and B) were randomly allocated to a treatment group independently of late subgroups (C and D). The final allocations were: subgroups A and C formed the treatment (UT antagonist; AZ13694621) group and subgroups B and D formed the control (vehicle) group.

Mon	Tues	Wed	Thurs	Fri	Notes
	A, Surgery 1		B, Surgery 1		
	A, Surgery 2	C, Surgery 1	B, Surgery 2	D, Surgery 1	Week 0 (A and B)
		C, Surgery 2		D, Surgery 2	Week 0 (C and D)

[Table 2.2](#) Staggering of surgical preparation was necessary to allow implementation of fortnightly blood pressure measurements and urine sample collection throughout the study period.

2.3.2.3 Sampling and data collection

Body weights were recorded every 2-4 days for monitoring purposes and to allow accurate adjustment of drug dose in line with bodyweight ([Section 2.4.1](#)). SBP data and urine samples were collected every two weeks (2, 4, 6, 8, 10, 12 and 14 weeks post-surgery), terminal samples ([Figure 2.5](#)) were collected under anaesthesia in week 14 ([Section 2.5](#)). Following data from the characterisation experiment ([Section 2.3.1](#)) and published data on the SNx model 14 weeks post-surgery was deemed to be broadly representative of the stable phase of disease, providing sufficient time for changes in renal function and structure to become apparent; yet reducing the likelihood of renal failure associated with the decline phase.¹⁷⁸

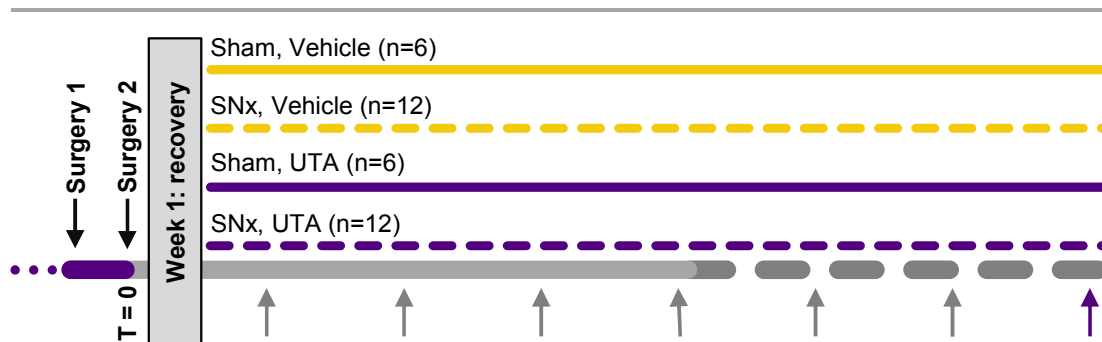


Figure 2.5 SNx (dashed, $n = 12$ per treatment) and sham controls (solid, $n = 6$ per treatment) underwent two-stage surgery followed by a one week recovery period, surgery 2 = T0. After recovery animals were randomly allocated to receive vehicle (yellow) or UTA (purple) by daily gavage for 13 weeks. Blood pressure data and urine samples were collected at 2, 4, 6, 8, 10 and 12 weeks (grey arrows) post-surgery, with final blood pressure data and terminal blood, urine and tissue samples collected at 14 weeks (purple arrow).

2.3.2.4 Statistical analysis

For the purpose of statistical analysis the groups were defined as follows: UT-A vs. vehicle and SNx vs. sham. This produced a two-way analysis with only two levels comparison between subjects, plus repeated measures where appropriate. Full details of the analyses used can be found within the appropriate sections below. All data analysis was carried out in SPSS (version 22.0, IBM SPSS Statistics) or Prism 5 for Windows (version 5.0, GraphPad Software Inc.).

2.4 Monitoring disease progression

2.4.1 Body weight, appearance and behaviour

Animals were checked visually at least once per day; of particular note are changes in appearance (dirty coat, porphyrin staining, paling of the eyes and piloerection) or behaviour (reduced mobility, alertness or food intake, social withdrawal and lack of normal grooming). Body weight was measured using a balance with averaging function (LC4200, 10 point moving average, Sartorius Stedim, Epsom, Surrey, UK), with weighing frequency increased as required.

Decisions regarding the humane endpoint for the late SNx group were based primarily upon regular inspection and interaction, with a loss of 15 % body weight (vs. peak) forming a secondary measure. Additional monitoring was implemented for all gavage dosed animals with close observation for signs of respiratory distress in the hour immediately after dosing.

2.4.1.1 Analysis of changes in body weight

Although monitoring took place every 2 - 4 days, body weight data are presented in a weekly format in all tables and figures.

Data are presented as mean \pm SEM, unless otherwise stated. Absolute weights are presented throughout. Weight data were analysed as two 2-way (repeated measures) ANOVA for experiment 1 ([Section 2.3.1](#)) or 3-way (repeated measures) for data in experiment 3 ([Section 2.3.2](#), all in SPSS version 22.0, IBM SPSS statistics).

2.4.2 Urine sample collection

Spot urine samples were collected in order to determine the urinary albumin: creatinine ratio (ACR) rather than housing rats in metabolic cages for over 24 hours to calculate albumin excretion rates (UAE), in order to minimise distress. Rats were individually housed in oblong metabolic cages (Techniplast) for a period of 1- 4 hours until sufficient sample (minimum 0.5 mL) was produced (typically 1 – 2.5 hours). All collections were initiated between 10 am and midday.

Throughout the collection period the animals had *ad libitum* access to water; however food was withheld to prevent sample contamination. Samples were

collected into chilled 2 mL centrifuge tubes and remained on ice for the duration of the sampling period.

Once collected, samples were transported on ice, before being split into aliquots (100 - 200 μ L) for storage at -20 °C until needed. Following complete analysis ([Section 2.6](#)) samples were transferred to -80 °C for long term storage.

2.4.3 Blood pressure

SBP and HR data were collected at intervals described above ([Section 2.31 and 2.32](#)) using non-invasive tail cuff piezoelectroplethysmography. Following some initial acclimatisation, the animals would remain still enough to measure blood pressure effectively with only minimal manual restraint. Resting one hand across the shoulders and back of the animal was often more than sufficient; a blanket was also used to provide comfort and a visual barrier. To maintain sufficient blood flow to the tail the animals were placed on a warming mat (Morphy Richards, Mexborough, South Yorkshire, UK) as required.

After an acclimatisation period (5-25 minutes) the first 20 suitable readings were recorded; specific acceptance criteria were pre-determined and can be found in [Table 2.3](#).


Criterion	Notes
Acclimatisation period	For reliable readings the rat needs to be settled, this period varied from 5-25 minutes.
SBP \geq 100 mmHg	Small movements of the tail can cause the reading to cut out prematurely. To remove these readings a low cut-off was employed, below which readings could be considered outside of the physiological range in SD rats above 12 weeks of age. (Butterfield, Lu)
	
SBP < 300mmHg	The storage meter and probe are only designed to read SBP < 300 mmHg, occasional artefactual readings occurred above this. (Typically SBP > 500 mmHg)
No movements of the tail during read	Movements can disrupt the read, resulting in artefacts
HR < 550 BPM	HR readings above 550 BPM can be a sign of stress, wait until calmed down
No bowel movements during read	Causes a temporary increase in SBP, wait until re-settled

Table 2.3 Acceptance criteria for SBP recording using tail cuff piezoelectroplethysmography. Image represents an 'erroneous' low read.

2.4.3.1 Analysis of blood pressure data

The acceptance criteria (specifically rejection of readings where SBP < 100 mmHg) created a potential risk of skew towards higher SBP values. To account for this the data were ranked and the tails trimmed to leave 12 replicates per animal. Data trimming was performed blind to the individual animals' experimental group and before any means had been calculated, using an automatically updating spreadsheet (Excel 14).

Once trimmed, the data were tested for normality using the Shapiro-Wilk test; normality was assumed if $p > 0.05$. All SBP and HR data that passed the normality test were analysed using two-way ANOVA with repeated measures (RM), with Tukey post-test. The structure of the RM ANOVA required matched data from each subject at each included time point; if analysed to study completion over half of all cases were excluded. As a result data were analysed up to and including week 28. Similarly data from experiment 2 ([Section 2.3.2](#)) were analysed by three-way ANOVA with RM, with Tukey post-test (SPSS version 22.0, IBM SPSS statistics).

Outliers were defined, considering both inter-subject (matched subjects at the corresponding time) and intra-subject (over-time) using median absolute distribution (MAD) with values lying more than 3 x MAD from the median were excluded from further analysis.

2.5 Terminal sample collection

Kidney samples were collected either as frozen (for qPCR and protein analysis) or fixed (for histology and immunology) tissue. For sham control animals the left kidney was perfusion-fixed with 4% paraformaldehyde and the right kidney frozen. For SNx animals the remaining remnant kidney was collected as fixed or frozen tissue; the collection method was allocated using a list randomiser available at RANDOM.ORG. Randomisation was carried out per surgical group in order to distribute animals from each group between the collection methods. Occasionally the pre-arranged allocations required adjustment due to the uneven loss of animals from the study for other reasons.

Terminal samples were collected under anaesthesia, induced using 4 % isoflurane (Baxter) delivered in 2 L/min oxygen (BOC Healthcare) via a vaporiser (Vapomax5, Anmedic). Body weight was recorded and anaesthesia maintained with intraperitoneal (i.p.) thiobutabarbital ($100 \text{ mg.Kg}^{-1}.\text{mL}^{-1}$) in water (water for injection, Braun Medical Ltd.); once a suitable level of surgical anaesthesia was achieved, samples were collected as follows:

Blood was collected by cardiac puncture using a chilled, heparinised 5 mL syringe with 1 ¼ inch, 23G needle (BD, Oxford, Oxfordshire, UK), into a heparin (Braun Medical Ltd.) coated 15 mL falcon tube and kept on ice before centrifugation at $2000 \times g$ for 10 minutes at 4 °C (MSE Mistral 3000i centrifuge, Sanyo, Leicestershire, UK). Plasma was separated from the erythrocyte fraction, transferred to 2 mL centrifuge tubes and stored at -80 °C for later analysis.

The abdomen was then opened and urine was collected directly from the exposed bladder using a chilled 2 mL syringe with 1 inch, 23G needle (BD), and transferred to 1.5 mL centrifuge tubes for storage at -20 °C.

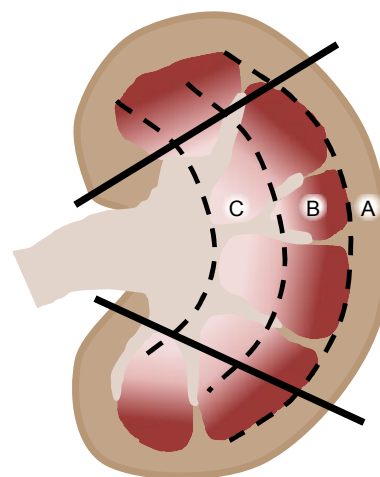
2.5.1 Frozen tissues for qPCR

In sham control animals the right kidney, and for the allocated SNx animals the remnant left kidney, were collected as fresh tissue, which was macro-dissected and

then snap frozen in liquid nitrogen. Once the kidney was removed the process was carried out as quickly as possible, using chilled instruments and a chilled dissection surface.

The kidney was dissected into sections enriched for cortex, outer medulla and inner medulla (Figure 2.6). Some tissue was also collected as an un-enriched fraction. When separating the remnant kidneys from SNx animals care was taken to remove any remaining tissue glue and to orientate the kidney appropriately. Dissected tissue was transferred to pre-chilled cryovials and frozen rapidly in liquid nitrogen. Once frozen the samples were transferred directly from liquid nitrogen to -80 °C freezers for storage.

Figure 2.6 Kidneys were bisected longitudinally before the outer cortical surface was removed and the remaining tissue macro-dissected to create enriched fractions of **(a)** cortex (including previously removed outer surface), **(b)** outer medulla and **(c)** inner medulla.



2.5.2 Fixed tissues

In sham control animals the left kidney, and for the allocated SNx animals the remnant left kidney were perfusion-fixed for histology and immunohistochemistry. A polythene cannula (Portex fine bore tubing, 0.96/0.58 mm outside/inside diameter, Smiths Medical, Hythe, Kent, UK) was inserted, retrogradely, into the aorta below the left renal artery branch as follows: the aorta was tied-off 2 - 3 cm below the left renal artery branch and occluded just above the branch using a clip before the cannula was inserted and tied in place. Once the cannula was in place, and the blood flow checked, the aorta was tied-off above the left renal artery. This allowed direct perfusion of the kidney at pressure in order to open up the tubules and preserve the structure of the tissue. The kidney was flushed with 50 mL of PBS (pH 7.4, Sigma) at a rate of 15 mL/min; this was followed by 50 mL of 4% paraformaldehyde (Sigma, prepared in 1 x PBS, at pH 7.4, and filtered through Whatman No. 1 filter paper

before use) at the same rate. A small incision in the renal vein relieved the pressure and allowed the perfused fluid to exit the kidney.

Once fixed the kidney was removed, bisected longitudinally and submerged in 4% PFA solution for 24 hours at 4 °C, before transfer into 70 % industrial methylated spirit (IMS) for longer term storage at 4 °C.

2.6 Urinary analysis

Urinary albumin creatinine ratio (uACR) was calculated following analysis of completely thawed urine samples for both creatinine and albumin. This provides an estimation of progression of proteinuria / albuminuria from spot urine samples, removing the need for lengthy individual housing of animals in metabolic cages (48 hour holding for 24 hour samples).³⁰³

2.6.1 Urinary Creatinine

Creatinine concentrations in urine samples were quantified using a colorimetric assay based upon the Jaffe reaction (DetectX® urinary creatinine kit, Arbor Assays, Ann Arbor, Michigan, US). All samples were initially diluted 1 in 20 using deionised water prior to analysis. Standards (20, 10, 5, 2.5, 1.25, 0.625, 0.3125 mg/dL) were diluted as described in the product insert. Once diluted all standards and samples were used within 1 hour. All reagents were allowed to equilibrate to room temperature for 30 minutes before use.

Prepared samples and standards were loaded into wells of a clear 96-well polystyrene microplate (Starlab UK, Milton Keynes) in duplicate, 50 µL per well. Colour reagent was added to each well (100 µL) and incubated for 30 minutes at room temperature. Each plate was shaken for 5 seconds before reading the optical density (OD) at 490 nm with a 570 nm correction (Biotek Synergy HT plate reader with Gen5 software).

Data were exported to Excel (Version 14.0, Microsoft) for standard curve generation and interpolation of results. Net OD (490 nm – 570 nm) data with background subtracted were fitted to a linear model, forced through 0, 0 ([Equation 2.2](#)).

$$Y = Mx \text{ (Where } M = \text{gradient)}$$

Equation 2.2

Values from the assay were in mg/dL; for use in uACR calculations all values were converted to $\mu\text{mol/mL}$ by multiplying by a factor of 0.0884.

2.6.2 Urinary Albumin

A sandwich enzyme-linked immunosorbent assay (ELISA) was used to assay urinary albumin. High protein binding, clear, 96-well flat-bottom microplates (Nunc MaxiSorp[®], ThermoFisher, Loughborough, Leicestershire, UK) were coated with 100 $\mu\text{L/well}$ unconjugated sheep anti-rat albumin antibody (1 mg/mL, Bethyl Laboratories, Inc. Texas, USA) diluted 1:100 in carbonate-bicarbonate buffer (pH 9.6, Sigma), and incubated at room temperature (22-25 °C) for 1 hour. All incubations were carried out under plate seals to prevent dehydration (Starlab UK, Milton Keynes). The coating antibody was removed and the plate washed four times with wash buffer (pH 8, 50 mM tris base, 140 mM sodium chloride with 0.05% tween20 in deionised water, all Sigma). Plates were blocked with 200 $\mu\text{L/well}$ 1 % bovine serum albumin (Melford, Suffolk, UK in 50 mM tris base, 140 mM sodium chloride at pH 8 in deionised water, both Sigma) overnight at 4 °C.

Standards were prepared from rat reference serum (30 mg/ mL albumin, Bethyl Laboratories, Inc. Texas, USA) to produce standards of 1000, 333, 111, 37, 12.3, 4.1, 1.37 and 0 ng/mL by dilution in assay diluent (1 % bovine serum albumin (Melford, Suffolk, UK)) in pH 8, 50 mM Tris base, 140 mM sodium chloride with 0.05% tween20 (Sigma) in deionised water. Urine samples were diluted 1:100 – 1:1000000 in assay diluent prior to use.

After removal of the blocking solution and a further 4 washes with wash solution, prepared standards or sample were loaded in to the plate in duplicate, 100 $\mu\text{L/well}$, and incubated at room temperature (22-25 °C) for 1 hour. Samples were aspirated out of the wells and washed 4 times with wash buffer before application of 100 $\mu\text{L/well}$ horseradish-peroxidase (HRP) conjugated sheep anti-rat albumin detection antibody (1 mg/mL, Bethyl Laboratories, Inc. Texas, USA), diluted 1:50000 in assay diluent, for 1 hour at room temperature (22-25 °C). After a final round of four washes, samples were incubated with 100 $\mu\text{L/well}$ TMB substrate (TMB Ultra one-step reagent, Pierce, Rockford, USA) for 15 – 30 minutes at room temperature before stopping the reaction with 100 $\mu\text{L/well}$ ELISA stop solution (Sigma).

The OD of the resulting yellow substrate was read at 450 nm with 570 nm correction (Biotek Synergy HT plate reader with Gen5 software). Data were exported to Prism 5

for Windows (Version 5.0, GraphPad Software Inc.) and standards converted to \log_{10} (albumin concentration) for curve fitting to a 4 parameter logistic curve ([Equation 2.3](#)) which was used to interpolate the concentration of albumin in the samples. Interpolated values were exported to Excel (Version 14.0, 32-bit, Microsoft) and corrected for any dilution before calculation of uACR.

$$Y = Bottom + (Top - Bottom)/(1 + 10^{((LogEC50 - X) * HillSlope)})$$

Equation 2.3

Values from the assay were in ng/mL; for use in uACR calculations all values were converted to mg/mL by dividing by a factor of 1000000.

2.6.3 Urinary albumin creatinine ratio

Values are expressed in mg/ μ mol with 0.05 and 0.50 approximately representing micro and macroalbuminuria, respectively.

2.6.4 Statistical analysis

This ratio-based measurement is derived from two continuous measures; as such data were tested against a normal distribution using the Shapiro-Wilk test ($p < 0.001$ to 0.258) and found to be predominantly non-normally distributed. Data are presented as median: inter-quartile range (IQR). Data were transformed before analysis using \log_{10} of (ACR + 0.0001) and the distribution re-tested. All transformed data that passed the normality test were analysed using two-way ANOVA with repeated measures (experiment 1, [Section 2.3.1](#)), followed by Tukey post-test. The structure of the RM ANOVA required matched data from each subject at each included time point; if analysed to study completion over half of all cases were excluded. As a result data were analysed up to and including week 28. Similarly data from experiment 2 ([Section 2.3.2](#)) were analysed by three-way ANOVA with RM, with Tukey post-test (SPSS version 22.0, IBM SPSS statistics)

2.7 Blood sample analysis

Terminal plasma samples were analysed for both creatinine and urea-nitrogen as markers of renal dysfunction.

Under normal circumstances creatinine is cleared from the blood by the kidneys at a relatively constant rate and so the circulating plasma concentration remains between 0.2 - 0.8 mg/dL (47.7 - 70.7 $\mu\text{mol/L}$) in the rat.^{304,305} When kidney function is reduced creatinine concentrations in the blood increase as the metabolite is no longer removed effectively.

Urea, $\text{CO}(\text{NH}_2)_2$, is a nitrogenous waste product biochemically involved in the excretion of excess nitrogen in the urine. When renal function declines urea is no longer excreted effectively leading to uraemia / azotaemia, a build-up of nitrogen products in the blood. The normal range for blood urea nitrogen (BUN) in the rat is 15 - 21 mg/dL (5.4 - 7.5 mmol/L).³⁰⁴

2.7.1 Creatinine in blood plasma

Creatinine standards (4, 2, 1, 0.5, 0 mg/dL) were prepared following the manufacturer's instructions from the stock solution supplied (Arbor Assays). Standards and samples were analysed in duplicate using half-area 96 well plates. For each sample or standard 25 μL of sample was diluted 1:1 with 25 μL assay diluent (supplied) in the 96 well plates, taking care to avoid the formation of bubbles. 100 μL of colour reagent (Detect X[®], Arbor Assays) was added to each well before reading the plate in a colormetric plate reader at 490 nm (BioTek, Synergy HT with Gen5 software) after incubation at room temperature for 1 minute and again after 30 minutes. The use of change in optical density, rather than a single point reading as used in the equivalent urinary assay, allows the assay to remain robust despite the variation in initial sample colour which can be the result of varying degrees of sample haemolysis.

Data were exported to Excel (Version 14.0, 32-bit, Microsoft) for standard curve generation and interpolation of results. OD values for 1 minute were subtracted from the read data at 30 minutes to give Δ OD. Δ OD was fitted to a linear model, where x = concentration and y = Δ OD ([Equation 2.4](#)). Interpolation of values was carried out using a template file provided by the product manufacturers.

$$Y = Mx + c \text{ (Where } M = \text{gradient and } c = \text{intercept)}$$

Equation 2.4

2.7.1.1 Statistical analysis

Data which passed tested a Shapiro-Wilk test for normality were analysed by two-way ANOVA with Tukey post-test and presented as mean \pm SEM. Significance was assumed when $p < 0.05$.

2.7.2 Blood urea-nitrogen

Samples were quantified for urea-nitrogen using an enzymatic colorimetric assay kit (Stanbio Laboratory, Boerne, Texas, USA). In duplicate, 2.5 μ L of sample or standard (30 mg/dL) was treated with 250 μ L enzyme reagent for 10 minutes at room temperature. 250 μ L of enzyme reagent incubated in the absence of sample or standard formed a blank. Blank, standard and samples were then incubated with 250 μ L colour reagent for 10 minutes at room temperature. 100 μ L of each replicate was loaded into a well of a 96 well micro plate in order to measure the OD at 600 nm (BioTek, Synergy HT with Gen5 software).

Mean OD data were calculated from replicates and, after deducting background (OD of blank), the concentration of the samples was calculated using [equation 2.5](#).

$$\text{Urea - Nitrogen (mg/dL)} = \frac{OD (\text{unknown})}{OD (\text{standard})} \times 30$$

Equation 2.5

2.7.2.1 Statistical analysis

Data which passed tested a Shapiro-Wilk test for normality were analysed by two-way ANOVA with Tukey post-test and presented as mean \pm SEM. Significance was assumed when $p < 0.05$.

2.8 Histological staining

PFA-fixed tissue samples ([Section 2.5.3](#)) were processed overnight ([Table 2.4](#)) using an automated tissue processor (Microm, STP 120 Spin) before embedding the tissue in paraffin wax blocks using an embedding station (Histocentre2, ThermoShandon, Fisher).

Treatment	Duration	Purpose
70 % EtOH	Pre-processing	Begin dehydration of tissue
95 % EtOH	60 min	Further dehydrate tissue
100 % EtOH	60 min	Dehydration, it is important to ensure that the tissue has an extremely low water content.
100 % EtOH	90 min	
100 % EtOH	90 min	
100 % EtOH	120 min	
Xylene	60 min	Displaces ethanol. Also removes some fats resulting in sample shrinkage.
Xylene	60 min	
Paraffin wax	60 min	Infiltrates the tissue resulting in a stabilised tissue that can be sectioned down to 5 µm in thickness.
Paraffin wax	60 min	

[Table 2.4](#) Tissue processing protocol followed using a tissue processing station on an overnight protocol. Water is displaced by successive changes of ethanol, ethanol is displaced by xylene which is in turn displaced by wax to produce a stable sample which is embedded to form a block.

2.8.1 Sectioning and mounting

PFA-fixed, paraffin embedded tissues were sectioned to 6 µm using a manual microtome (manufacturer, Cambridge, UK) with disposable blades (S35 disposable blades, Feather Safety Razor Co, Osaka, Japan). Cut sections were floated on the surface of a deionised water bath at 50 - 60 °C to remove wrinkles in the wax, before mounting individually onto twin frost standard slides (Blue Star, Smethwick, West Midlands, UK). Slides were dried overnight on a heat block (Laboratory Thermal Equipment, Greenfield, Greater Manchester, UK) at 55 °C before storing for later use.

2.8.2 Haematoxylin and eosin stain

Mounted sections were deparaffinised through two 5 minute changes of xylene (ThermoFisher) before rehydrating through a series of ethanol baths (99, 99, 95, 95 and 70 % in deionised water, ThermoFisher) before rinsing in deionised water.

Nuclei were stained with Mayer's haematoxylin for up to 7 minutes before rinsing in lukewarm running tap water for 5 minutes. Sections were rinsed in deionised water before transferring to 95 % ethanol for 1 minute with agitation. Cytoplasm and other cellular components were then counterstained with Eosin-Phloxine B solution (0.1% eosin Y (Philip Harris, Hythe/Stockport, UK), 0.01% phloxine B (BDH, Poole, Dorset, UK) in 74 % ethanol in water and acidified with 1 % acetic acid) for 1 minute.

Sections were dehydrated through a series of increasingly concentrated ethanol solutions (95, 99, 99 % in deionised water, 5 minutes each, ThermoFisher) before clearing in two 5 minute changes of xylene (ThermoFisher). Sections were then permanently mounted with a coverslip (No. 1.5, 22 mm x 50 mm, Appleton Woods, Birmingham, West Midlands, UK) using xylene-based mounting media (Pertex, Leica Biosystems, Illinois, USA) and allowed to dry overnight.

2.8.3 Periodic acid Schiff (PAS) stain for glomerulosclerosis

Mounted sections (n = 3 - 5 per experimental group) were deparaffinised and rehydrated as described ([Section 2.8.2](#)) before immersion in periodic acid (0.5 % in water, Sigma) for 5 minutes. Sections were washed in five changes of deionised water and stained with Schiff's reagent (0.5 % basic fuchsin (Sigma) with 1 % potassium metabisulphite (ThermoFisher) in 0.1 M hydrochloric acid (Fisher)) for 15 minutes. The colour was developed in warm running tap water for 5 minutes.

Nuclei were counterstained with Gill III haematoxylin (Merck Millipore, Feltham, Middlesex, UK) for 90 seconds before washing in running tap water for 5 minutes and rinsing in deionised water. Stained sections were dehydrated and mounted as described previously ([Section 2.8.2](#)).

2.8.3.1 Analysis

Slides stained with PAS were blinded using opaque tape, and coded using an arbitrary numbering system, before imaging at 20x magnification as described in [Section 2.10](#). For each section 50 individual glomeruli were tagged and scored.

Coded images of single glomeruli were given a glomerulosclerosis score (GSI) of 0 – 4 based upon the extent of the lesions present ([Figure 2.7](#)). Once scored, and the data inputted, the code was deciphered and the scores allocated to the appropriate experimental group.

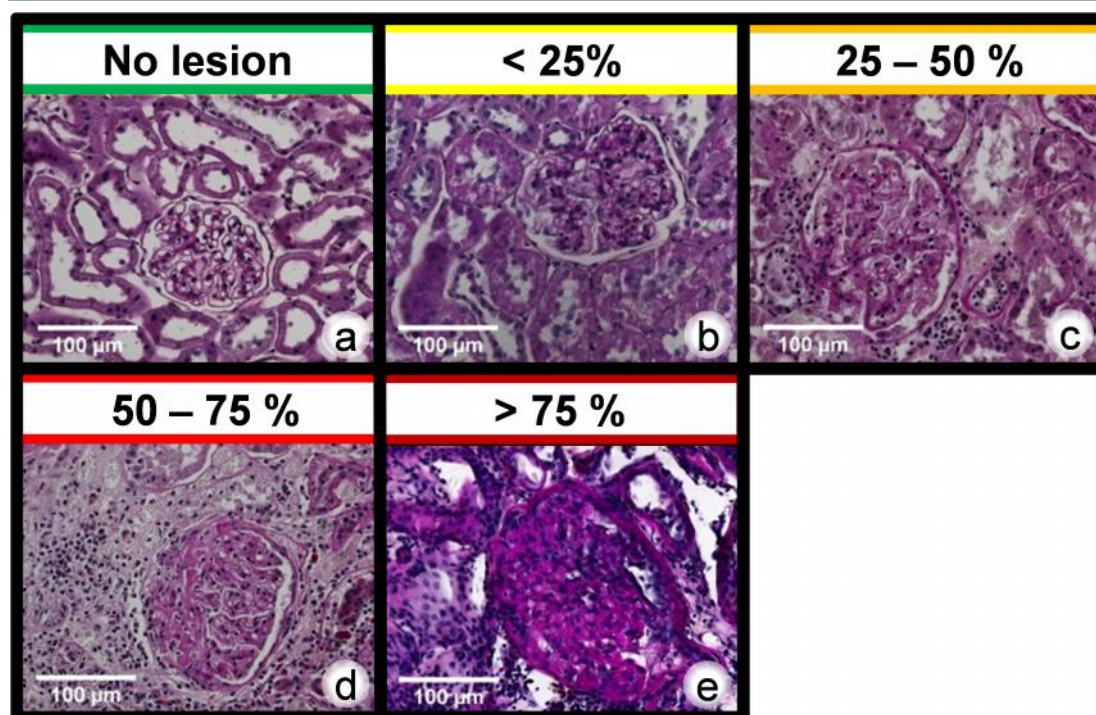


[Figure 2.7](#) Glomeruli were scored on the presence of sclerotic lesions. Scoring as follows; 0 **(a)** no lesion was present, 1 **(b)** less than 25 % affected, 2 **(c)** 25 - 50 % sclerotic, 3 **(d)** 50 - 75 % glomerular area affected, and 4 **(e)** full glomerular closure, more than 75 % affected.

Individual glomerulosclerosis scores were pooled per experimental group before analysis by non-parametric ANOVA (Kruskal-Wallis test).

2.8.4 Masson's trichrome stain for collagen

Mounted sections (n = 3 - 5 per condition) were deparaffinised and rehydrated as described ([Section 2.8.2](#)). To improve the quality of staining, tissues were then re-fixed in Bouin's solution (per 100 mL; 71.4 mL saturated picric (1.3%) acid, 23.8 mL 37-40% formaldehyde and 4.8 mL glacial acetic acid) for 1 hour at 56 °C and rinsed under running tap water to remove any yellow colour before continuing with the staining protocol.

Nuclei were stained with Weigert's iron haematoxylin (0.5 % haematoxylin (Acros Organics, Geel, Belgium) and 0.58 % iron III chloride (ThermoFisher) with 0.05 % glacial acetic acid (ThermoFisher) in 47.5 % ethanol (in deionised water) for 10 minutes. Sections were then rinsed in running tap water for 10 minutes to remove any excess before rinsing in deionised water.

Sections were transferred to biebrich scarlet-acid fuchsin stain (0.9 % biebrich scarlet (ThermoFisher) and 0.1% acid fuchsin (Acros Organics) in deionised water with 1 % glacial acetic acid (ThermoFisher)) for 15 minutes and rinsed in deionised water before immersion in phosphomolybdic-phosphotungstic acid solution (2.5 % phosphomolybdic acid (Sigma) and 2.5% phosphotungstic acid (Sigma) in deionised water) for 10 minutes to differentiate the collagen fibres. Sections were transferred, without rinse, to 2 % aniline blue (Acros Organics) solution (aqueous, acidified by addition of 2 mL glacial acetic acid per 100 mL, ThermoFisher) and stained for 10 minutes before rinsing in deionised water and then 1 % acetic acid (ThermoFisher) for 3 minutes.

Sections were rinsed in deionised water before dehydration and mounting.

2.9 Immunohistochemistry

PFA fixed tissues were processed and embedded as described in [Section 2.8](#). Serial sections were mounted on to Superfrost plus, positively charged slides (Menzel-Gläser, Brunswick, Germany) as described in [Section 2.8.1](#).

2.9.1 Antigen Retrieval

The tissue samples generated in this work were quite large and often included voids formed when sectioning across cysts within the renal tissue. These properties resulted in section sloughing during epitope retrieval when following the standard laboratory protocol (TEG buffer, pH 9, for 10 minutes at 95 -100 °C in a water bath).³⁰⁶

In order to determine the optimal conditions for antigen retrieval in SNx tissue samples, a range of buffers and incubation periods were trialled ([Table 2.5](#)). The buffers tested were:

- TEG (Tris base (10mM) EGTA (0.5 mM), pH 9.0)
- Sodium Citrate (Trisodium citrate dihydrate (10 mM) with 0.05 % Tween20, pH 6.0)
- Tris EDTA (Tris Base (10mM) EDTA (1 mM) with 0.05 % Tween20, pH 9.0)
- Tris EDTA (Tris Base (10mM) EDTA (1 mM), pH 9.0)

All buffers were prepared in deionised water and the pH adjusted, using 2 M hydrochloric acid or 5 M sodium hydroxide, as appropriate (Hydrochloric acid; ThermoFisher, all other components; Sigma). For all conditions buffer solutions were pre-heated to 94-96 °C in lidded, polypropylene Coplin jars using a covered water bath (Grant JB1, Grant Instruments Ltd, Cambridge, UK). Slides were incubated for 10 to 20 minutes in the antigen-retrieval buffer. During incubation the lids were left off the jars in order to prevent boiling (n = 4 slides per condition).

After the incubation period the slides were transferred to deionised water to cool, before checking the integrity of the tissue sections. Slides where sections had detached were discarded before continuing with the staining protocol. Briefly, polyclonal goat anti-rat UT (sc-10194, Santa Cruz Biotechnology, Heidelberg, Germany) used at 1:100, followed by HRP-conjugated, polyclonal rabbit anti-goat IgG secondary antibody (1:100, Dako, Ely, Cambridgeshire, UK) detected with 3,3'-

diaminobenzidine HRP substrate (SigmaFAST™, Sigma). Full details can be found in [Section 2.9.2](#).

Buffer	pH	Time	Outcome
TEG: Tris (10mM) EGTA (0.5mM)	9	10	All sections lost
		20	N/A
Sodium citrate (10mM) with 0.05% Tween 20	6	10	All sections intact: staining not strong
		20	All sections intact: staining not strong
Tris (10mM) EDTA (1mM) with 0.05% Tween 20	9	10	Sections lost
		20	N/A
Tris (10mM) EDTA (1mM)	9	10	All sections intact: staining good
		20	All sections lost

[Table 2.5](#) Test condition matrix and results for heat-induced antigen retrieval optimisation. Although both Tris EDTA pH 9.0 (without Tween 20) and sodium citrate pH 6.0 resulted in stable sections, antigen sites were retrieved more reliably using Tris EDTA pH 9.0 for the antibody tested.

Based upon these results, and in the absence of specific instructions from the antibody suppliers, all antigen retrieval was carried out in Tris (10 mM) EDTA (1 mM) without Tween20 for 10 minutes as standard.

2.9.2 Standard protocol

This standard protocol was used for all IHC staining; the specific modifications for each target protein can be found in [Table 2.6](#). IHC techniques were used to visualise protein expression of urotensin II (Ull), collagen IV, laminin-β and the urotensin II receptor, UT. The anti-Ull antibody detects an antigenic sequence located within the conserved cyclic region of the peptide; as a result it detects Ull across all species. As this cyclic region is also shared with URP, the antibody cannot distinguish between Ull and URP.²¹⁶ The final URP product (**ACFWKYCV**) is shorter than Ull (**QHGTAPECFWKYCI**), and the extent of this similarity means that it is not possible to distinguish between the two proteins using this or commercially available antibodies. Consequently in subsequent descriptions of immuno-staining using this antibody, positive staining refers to both immuno-reactive Ull and URP.

Prepared slides were passed through two 5 minutes baths of xylene (ThermoFisher) to remove the paraffin wax from the sections before rehydration through a series of 5

minute changes of ethanol (ThermoFisher) at 99 %, 99 %, 95 %, 95 %, 70 % and 50 % in water, finishing in deionised water.

Antigen sites were unmasked using heat-induced antigen retrieval (HIER) carried out in a water bath (JB1, Grant Instruments, Shepreth, Cambridgeshire, UK) at 94-96 °C for 10 minutes. Tris-EDTA buffer (pH 9.0, prepared as described in [Section 2.9.1](#)) was preheated in lidded polypropylene Coplin jars prior to use, the lids were removed during the incubation period to prevent turbulence associated with boiling. The Coplin jars were removed from the water bath after which the slides were transferred to deionised water and allowed to cool for 10 minutes before proceeding with the staining protocol.

Immunogen	1° Antibody	2° Antibody	Controls
Urotensin II / URP	1:100, rabbit polyclonal raised against goby UII (P Ingleton, University of Sheffield, UK)	1:100, polyclonal goat anti-rabbit IgG (Dako)	5 / group
Urotensin II receptor	1:100, goat polyclonal to rat UT. (sc-10194, Santa Cruz Biotechnology, Heidelberg, Germany)	1:100, polyclonal rabbit anti-goat IgG (Dako)	5 / group
Collagen IV	1:250, rabbit polyclonal to human Col IV (ab 6586 AbCam, Cambridge, UK)	1:100, polyclonal goat anti-rabbit IgG (Dako)	2 / group
Laminin	1:100 rabbit polyclonal to laminin- β (pan) (ab11575, AbCam, Cambridge, UK)	1:100, polyclonal goat anti-rabbit IgG (Dako)	2 / group

[Table 2.6](#) Antibody dilutions and additional conditions for the immunohistochemical detection of UII / URP, UT, collagen IV and laminin. Controls indicate the number negative (primary antibody omitted) slides per treatment condition.

Slides were dried carefully and a closed ring drawn around the sample with a hydrophobic barrier pen (ImmuEdge™, Vector Labs, Peterborough, Cambridgeshire, UK). The following incubations were carried out in a darkened humidified chamber. As soon as the hydrophobic barrier was dry slides were washed briefly (3 x 1 minute rinses) with Tris buffered saline containing 0.1 % tween20 (TBS-T, pH 8.5, All components; Sigma), before blocking with 1 % bovine serum albumin (BSA, Melford, Ipswich, Suffolk, UK) in TBS-T (pH 8.4) for 1 hour at room temperature (200 μ L per slide). Blocking solution was removed and the slides incubated with primary antibody (100 μ L per slide, prepared as described in [Table 2.6](#)) diluted in TBS-T (pH 8.5) with

1 % BSA (Melford). The incubation was carried out overnight (typically 16 hours) at 4°C.

The following day the slides were allowed to equilibrate to room temperature for 1 hour before the primary antibody solution was removed and the sections washed with TBS-T (5 x 1 minute washes). Endogenous peroxidases were blocked with 0.3 % hydrogen peroxide solution (Sigma) in TBS for 15 minutes at room temperature. The hydrogen peroxide solution was removed and the slides washed three times with TBS-T (1 minute each) before application of a horseradish peroxidase (HRP)-conjugated secondary antibody diluted in TBS-T (pH 8.5) with 1 % BSA (Melford, Ipswich, UK) for 30 – 45 minutes at room temperature ([Table 2.6](#)).

Secondary antibody solution was washed off with TBS-T (3 x 1 minute quick washes and 3 x 10 minute washes) prior to application and development of the chromogenic HRP substrate; 3,3'-diaminobenzidine (ImmPACT™ enhanced DAB substrate, Vector Laboratories) for 5-10 minutes. Colour development was stopped by immersion in deionised water for 5 minutes (twice) at room temperature.

Nuclei were counterstained with Mayer's haematoxylin (Sigma) for 2-7 minutes (time adjusted for the age of the solution). The colour was developed by rinsing in warm, running, tap water for 5 minutes before returning to deionised water.

Sections were dehydrated through a series of increasingly concentrated ethanol solutions (50, 70, 95, 95, 99, 99 % in water, ThermoFisher) for 5 minutes each before clearing in two 5 minute changes of xylene (ThermoFisher). Sections were then permanently mounted with a coverslip (No 1.5, 22 mm x 50 mm, Appleton Woods) using xylene based mounting media (Pertex, Histolab Products AB, Gothenburg, Sweden) and allowed to dry overnight in the dark.

2.9.3 Controls

Negative control slides were incubated with antibody diluent in the absence of primary antibody. For UT and Ull serial sections were included for all samples as negative controls (n = 5 per group). For collagen IV and laminin-β serial sections were included as controls from 2 or 3 animals per group. All negative control slides were examined for any spurious staining prior to the acceptance and inspection of any positive staining.

2.10 Microscopy and image analysis

Images presented in this thesis were collected on an Axiovision Axioskop, upright microscope using a 40x/0.95 Plan Apochromat oil, or 20x/0.55 Plan Apochromat air, objective and captured using an AxioCam colour CCD camera through Axiovision LE software (version 4.8.2 with service pack 3, all Carl Zeiss Ltd., Cambridge, Cambridgeshire, UK). Images were then processed and analysed using ImageJ (<http://rsb.info.nih.gov/ij>).

Whole section images for analysis purposes were acquired using a 20x/0.80, Plan Apo, objective using the 3D Histech Panoramic 250 Flash slide scanner, managed by the University of Manchester Bioimaging Facility.

2.11 Validation of QuantiFast® SYBR Green RT-qPCR for *Ywhaz*, *Uts2r*, *Uts2b* and *Uts2* gene expression

The mRNA expression of *Ywhaz* (tyrosine 3-monooxygenase/tryptophan 5-monooxygenase activation protein, zeta), *Uts2r* (UT), *Uts2b* (URP) and *Uts2* (UII) was explored using two-step RT-qPCR with SYBR green as the reporter dye. To facilitate the extraction of RNA from tissues that had been previously snap-frozen, the use of RNA/ater®-ICE (Ambion, Paisley, Renfrewshire, UK) transition solution was evaluated. This reagent allows transition of frozen tissues to a thawed state at -20°C with preservation of RNA. An initial pilot was conducted on a small selection of rat kidney samples to determine the suitability of this reagent for the application of RNA extraction, reverse transcription and qPCR assay. This also afforded the opportunity to undertake optimisation of qPCR assays for the genes of interest prior to application to the experimental tissues.

2.11.1 Extraction of RNA from RNA/ater-ICE® treated samples

Snap-frozen tissues (collected as described in [Section 2.5.1](#)) are sensitive to fluctuations in temperature even over short periods of time, including those experienced during the tissue disruption and homogenisation processes required for reliable RNA extraction. To reduce the likelihood of RNA degradation during the extraction process, samples were stabilised and transitioned to -20 °C storage using RNA/ater®-ICE solution.

This solution was previously untested within this laboratory so it was important to validate the quality of the RNA extracted from renal cortex when using RNA/ater-ICE®. For quality control purposes RNA/ater®-ICE treated tissues were compared against the gold standard in RNA stabilisation in fresh tissue, RNA/ater® (Sigma).

2.11.1.1 Sample preparation and experimental design

Matched renal cortex samples were collected from male SD rats (kindly provided by Alla Alkhalefah) under terminal anaesthesia. Samples were either treated immediately with RNA/ater®, or snap frozen using liquid nitrogen ([Section 2.5.1](#)) and stored at -80 °C for one week before treatment with RNA/ater®-ICE.

Samples were treated as follows: for RNA/ater®, 200 mg renal cortex was immersed in 1 mL of room temperature RNA/ater® solution and stored at 4 - 8 °C for 16 hours before storage at -20 °C; this treatment formed a benchmark for RNA quality. In

contrast, RNA/*later*[®]-ICE was pre-chilled to -80 °C overnight in 2 mL aliquots in 3 mL cryovials (Starlab) prior to the addition of 200 mg snap-frozen renal cortex per vial. Each sample was inverted 5 times before storage at -20 °C.

To ensure the RNA/*later*[®]-ICE solution was also suitable for treating previously stored samples, two representative samples, one sham control and one 5/6th SNx, from long term -80 °C storage (> 6 months) were also treated with RNA/*later*[®]-ICE as described above.

2.11.1.2 Tissue homogenisation and disruption

Lysis buffer (Buffer RLT plus, Qiagen) was prepared by the addition of 10 µL beta-mercaptoethanol (β-ME, Sigma) per 1 mL. Renal cortex tissue (100 mg, approximately) was homogenised in 1.5 mL of prepared buffer using a homogenisation drill (Powergen 125, Fisher), ramping the speed slowly from setting 1 up to 6 over 15 - 20 seconds before homogenising on full speed for a further 30 - 45 seconds. Lysates were stored on ice immediately, before continuing with RNA extraction as detailed below. Unless stated otherwise, samples remained chilled on ice throughout the extraction process.

2.11.1.3 RNA extraction and purification using Qiagen RNeasy[®] plus mini kit

Some of the primer assays used ([Table 2.7](#))^{307,308} did not span an exon/exon boundary and so had the potential to amplify transcripts from genomic DNA (gDNA). To prevent amplification from gDNA the RNeasy[®] plus mini kit (Qiagen) was employed; this contains gDNA eliminator columns which selectively bind gDNA fragments that may be present in tissue lysates. This gDNA elimination step was reinforced by a further gDNA elimination step included in the QuantiTect[®] reverse transcription kit, which was carried out immediately prior to the reverse transcriptase (RT) reaction ([Section 2.11.2](#)).

Name	Gene Symbol	Entrez Gene ID	RGD Id	Accession (mRNA)	Primer pair (Qiagen)	Exons amplified	Amplicon length
tyrosine 3-monooxygenase/tryptophan 5-monooxygenase activation protein, zeta	<i>Ywhaz</i>	25578	3980	NM_013011 (1815 bp)	QT02382184	2/3	99 bp
Urotensin II	<i>Uts2</i>	29180	3930	NM_019160 (527 bp)	QT00193018	3/4	82 bp
Urotensin II Receptor	<i>Uts2r</i>	57305	621884	NM_020537 (1161 bp)	QT01082690	N/A, does not span exon-exon junction	116 bp
Urotensin II related peptide / urotensin 2B	<i>Uts2b</i>	378939	727977	NM_198133 (747 bp)	QT00438767	N/A, does not span exon-exon junction	120 bp

Table 2.7 Details of mRNA transcripts targeted for qPCR analysis. Primer sequences were not provided for these commercially available primer pairs (Qiagen QuantiTect® primer assays) so the approximate location (25 bp increments) of the amplicon centre is provided (estimated from the appropriate GeneGlobe specification which can be found in appendix A).

Lysates were centrifuged at 18800 x G (Heraeus Pico 21, ThermoFisher) for 3 minutes and 700 μ L supernatant transferred to a gDNA eliminator column (Qiagen). This was then centrifuged at 19600 x G for 45 seconds. The liquid flow through was retained and the column discarded along with any bound gDNA.

The gDNA-free lysate was then treated with 1 volume (700 μ L) 70 % Ethanol (Fisher, in PCR grade water, Sigma) and mixed 10 times using a manual pipette, before transferring 700 μ L to an RNeasy[®] mini spin column (Qiagen). The column was centrifuged at 9600 x G for 30 seconds before discarding the flow through.

The RNeasy[®] mini spin column (Qiagen) was washed three times; once with 700 μ L buffer RW1 (Qiagen) centrifuged for 30 seconds at 9600 x G, then 500 μ L buffer RPE (Qiagen) for 30 seconds at 9600 x G, and finally 500 μ L buffer RPE centrifuged at 9600 x G for 2 minutes to dry the column matrix. The column was then transferred to a clean, labelled, 1.5 mL centrifuge tube and the RNA eluted by addition of 50 μ L PCR grade water (Sigma) which was left to stand for 1 minute before centrifuging at 9600 x G for 1 minute. RNA extracts were transferred to ice immediately ready for quantification and storage.

2.11.1.4 Quantification of RNA by Nanodrop™

Concentration of RNA was measured using a micro-volume spectrophotometer (Nanodrop2000c, ThermoFisher) with NanoDrop 2000 / 2000c Operating Software (version 1.5, Updated July 2013). The pedestal was cleaned using 3 μ L of PCR grade water (Sigma) and a tissue before allowing the system to perform a routine verification.

After setting the system to measure RNA the blank was set using 1 μ L PCR grade water (Sigma). Each RNA sample (1 μ L) was measured and the pedestal cleaned with PCR grade water in between each reading. Concentration was recorded and the A_{260}/A_{280} and the A_{260}/A_{230} ratios noted as measures of RNA purity and chemical contamination, respectively. For RNA the A_{260}/A_{280} ratio should be approximately 2.0. Traditionally, the A_{260}/A_{230} ratio should be approaching 2.0, however the importance of this particular measure has been contested.^{309,310}

2.11.1.5 RNA integrity by non-denaturing gel electrophoresis

RNA extracts were run out on a 1.5 % agarose gel in order to determine their quality and integrity. Gels were prepared freshly as required using 1.5 g agarose (Bioline, London, UK) per 100 mL 1 x Tris-acetate-EDTA (TAE, 40 mM Tris, 20 mM acetic acid, 1 mM EDTA, Cleaver Scientific, Rugby, Warwickshire, UK) buffer. Agarose was dissolved in TAE buffer by heating in a microwave (NN-SD466M, Panasonic, Bracknell, Berkshire, UK) at full power for up to 2 minutes. Once the agarose had dissolved, the solution was stirred gently and cooled, to approximately 50 °C, before the addition of 10 µL GelRed nucleic acid stain (Biotium, Hayward, California, USA). Any skin which forming on the surface of the molten agarose was removed before pouring slowly into an electrophoresis tray (standard horizontal gel tray, Anachem, Luton, Bedfordshire, UK). Combs were inserted and the gel allowed to set.

Once set, the gel combs were removed and the gel electrophoresis tank filled with running buffer (1 x TAE buffer, Cleaver Scientific) until the surface of the gel was just submerged. The RNA extracts were prepared by dilution to 100 ng/µL (with PCR grade water, Sigma); 8 µL of each diluted RNA sample was then mixed with 2 µL 5 x loading buffer (Bioline) and loaded in to the lanes. The samples were run at 120 V (200 / 400 GPS gene power supply, Pharmacia, Sandwich, Kent, UK) for 30 - 45 minutes.

Bands were visualised using an ultraviolet gel dock (InGenius, Syngene, Cambridge, Cambridgeshire, UK) and images captured using Syngene Genesnap software (version 7.07 for Windows, exported as 8-bit bitmap files). For printing purposes images were inverted to reduce ink usage.

2.11.2 QuantiTect[®] Reverse transcription with gDNA wipe-out treatment

Prior to cDNA production RNA extracts were treated with gDNA wipe-out buffer (Qiagen) as follows: RNA extracts were diluted in thin-walled PCR strips (Multiply-µStrips, Sarstedt, Leicester, Leicestershire, UK) to contain 2 µg RNA in 24 µL by addition of PCR grade water (Sigma), to which 4 µL gDNA elimination buffer (Qiagen) was added. Samples were mixed well before incubation at 42 °C for 2 minutes (Stratgene Mx3000/3005P Thermocycler, Agilent Technologies, Les Ulis, France) and storage on ice. For control purposes a no template control (NTC, RNA

replaced with PCR grade water, Sigma) and no reverse transcriptase control (No RT, 2 µg RNA sample blend) were included.

The gDNA wipe-out treated RNA samples were then reverse transcribed using QuantiScript® reverse transcriptase, primer mix and reaction buffer (containing deoxynucleotide triphosphate mix (dNTPs) and Mg²⁺ provided (all Qiagen)). A master mix was prepared as described in [Table 2.8](#) with a 10% contingency for repetitive pipetting losses.

Component	Volume per 2 µg reaction	No RT control
Quantiscript® RT enzyme	2 µL	-
Reaction buffer (buffer, Mg ²⁺ , dNTPs)	8 µL	8 µL
RT primer mix (OligodT and random hexamers)	2 µL	2 µL
Water	-	2 µL

[Table 2.8](#) Preparation of reverse transcription reactions. Each reaction was set up as a double volume reaction following supplier instructions (final volume: 2 µg RNA in 40 µL).

The prepared master mix was then distributed to each reaction tube (12 µL per tube making the final reaction volume 40 µL) excluding the No RT control. For this reaction the components were added individually with the RT enzyme substituted for PCR grade water (Sigma). All reactions were then incubated at 42 °C for 15 minutes before inactivation of the RT enzyme at 95 °C for 3 minutes using a 96 well thermocycler (Stratgene Mx3000/3005P, Aligent Technologies). Samples were placed on ice immediately before storage at - 20 °C.

2.11.3 Pilot Study: QuantiFast® SYBR Green RT-qPCR for *Ywhaz*, *Uts2r*, *Uts2b* and *Uts2*

To confirm capacity for DNA amplification by primer pairs ([Table 2.7](#)) targeting the genes of interest in renal cortex samples, the qPCR assays were validated. All qPCR preparation was carried out in a laminar flow cabinet (Airstream.DUO, ESCO Rotherham, South Yorkshire, UK) to reduce the risk of environmental contamination.

2.11.3.1 Standard reaction conditions

A standard curve was established from pooled cDNAs by 2-fold serial dilution in PCR grade water (Sigma). Standards used were as follows: 50, 25, 12.5, 6.25, 3.125, 1.563, 0.781 and 0.391 ng (assuming 100 % RNA to cDNA conversion efficiency) in 10 μ L. Standards were prepared in bulk to allow the same set of standards to be used for multiple qPCR assays ([Table 2.9](#)).

	Addition	Of	Water	Total cDNA (ng)^a	Final cDNA (ng in 10 μL)^b
Std1	10 μ L	50 ng/ μ L stock	-	500	50
Std2	10 μ L	50 ng/ μ L stock	10 μ L	250	25
Std3	10 μ L	Std2	10 μ L	125	12.5
Std4	10 μ L	Std3	10 μ L	62.5	6.25
Std5	10 μ L	Std4	10 μ L	31.25	3.125
Std6	10 μ L	Std5	10 μ L	15.63	1.563
Std7	10 μ L	Std6	10 μ L	7.81	0.781
Std8^c	10 μ L	Std7	10 μ L	3.91	0.391

[Table 2.9](#) Preparation of standard curve by two-fold serial dilution. Each standard was prepared to a final volume of 10 μ L^a, before a final addition of 90 μ L water to all standards. 10 μ L of standard was used per qPCR reaction.^b (Note; 10 μ L was removed from standard 8 and discarded before addition of the water).^c

cDNAs (including NTC and No RT controls) were diluted 1 in 100 with qPCR grade water (Sigma) before use in reactions. Alongside the standards, samples, No-RT control and NTC control, a water (buffer) control was also included as a negative for the qPCR assay conditions. Reactions were set up in thin-walled 0.2 mL reaction strips (Sarstedt) as follows: in duplicate, 10 μ L cDNA was mixed with 15 μ L assay mastermix (prepared to contain 12.5 μ L QuantiFast[®] SYBR Green PCR mix and 2.5 μ L QuantiTect[®] primer blend per reaction, all Qiagen).

Samples were gently mixed (finger flicked) before being centrifuged for 10 seconds (tube-strip PicoFuge, Stratgene) to ensure all assay components were at the bottom of the tubes. The sealed strips were loaded into a 96-well thermocycler (Stratgene Mx3000/3005P, Aligent Technologies), the HotStarTaq Plus DNA Polymerase was

activated by incubation at 95 °C for 5 minutes before running 40 cycles (denaturation; 95 °C for 10 seconds, combined annealing/extension; 60 °C for 30 seconds, with collection of SYBR Green I and ROX (reference dye) fluorescence data at the end of the annealing/extension phase of each cycle). A dissociation curve (55 °C to 95 °C ramp, reading fluorescence every 0.1 °C) was completed after the final cycle, Segment 3 in [Figure 2.8](#).

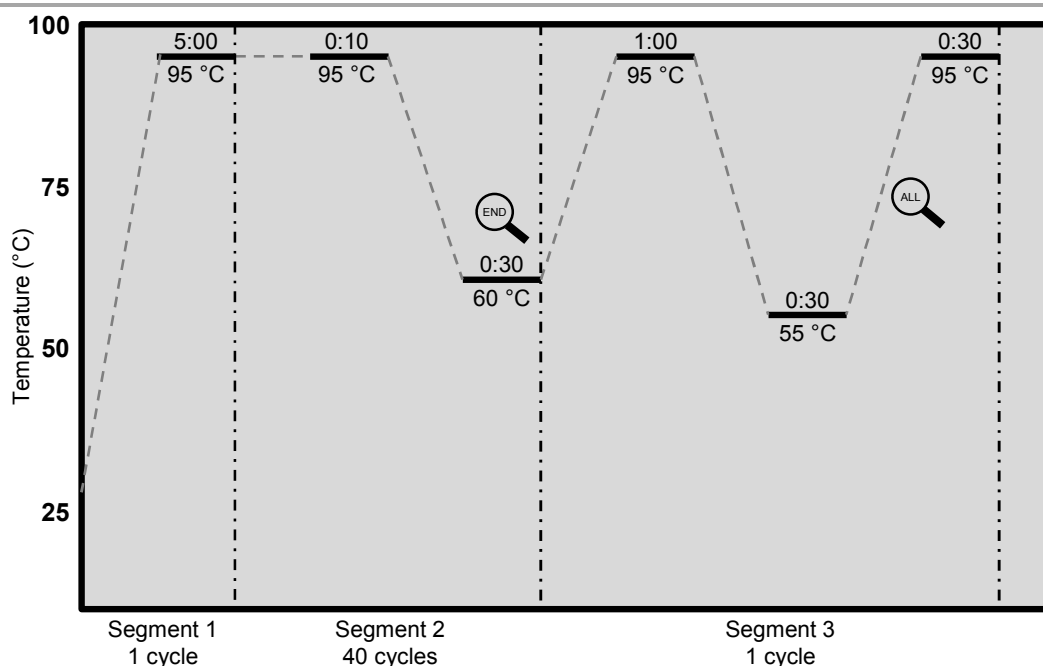


Figure 2.8 A typical thermocycler profile for qPCR. Segment 1 represents HotStarTaq Plus DNA Polymerase (Qiagen) activation. Segment 2; the rapid cycling profile recommended for use with the QuantiFast[®] SYBR green assays (Qiagen). Segment 3 is the standard dissociation curve protocol when using the Mx3005P software (Stratgene).

2.11.3.2 PCR product gel

Amplicon size was visualised under non-denaturing conditions on a 2.5 % agarose gel (prepared as described in [Section 2.11.1.5](#)). Routinely, 16 µL PCR reaction was mixed with 4 µL 5 x loading buffer (Bioline) before running at 120 V for 45 minutes alongside size markers (5 µL/lane, HyperLadder II and HyperLadder IV run in lanes 1 and 16 respectively, both Bioline). Product bands were visualised as described in [Section 2.11.1.5](#).

2.11.4 Results

The pilot study data suggest that there is no difference between the quality and quantity of RNA extracted from samples treated with RNA/ater[®]-ICE rather than RNA/ater[®], and no difference in the amplification potential of cDNAs produced from the RNA extracts.

2.11.4.1 RNA quantity, quality and integrity

RNA extracts were of reproducibly high nucleic acid concentration (226.9 - 379.3 ng/ μ L) and A_{260}/A_{280} ratios were consistent with pure RNA (2.03 - 2.06, [Table 2.10](#)).

Sample ID	Conc (ng / μ L)	A_{260}/A_{280}	A_{260}/A_{230}
Left - RNA/ater [®]	275.4	2.03	1.97
Right - RNA/ater [®]	360.0	2.06	1.55
Left - RNA/ater [®] -ICE	323.5	2.04	1.48
Right - RNA/ater [®] -ICE	226.9	2.04	1.75
Sham - RNA/ater [®] -ICE	228.0	2.04	1.40
SNx - RNA/ater [®] -ICE	379.3	2.04	1.77

[Table 2.10](#) Concentration and purity of RNA extracts from samples treated with RNA/ater[®] or RNA/ater[®]-ICE as determined by spectrophotometric analysis.

18S and 28S bands were clearly visible in all samples ([Figure 2.9](#)), with no discernible difference between samples treated with RNA/ater[®] (lanes 1 and 2) and those treated with RNA/ater[®]-ICE (lanes 3 and 4). The previously stored samples also had intact 18S and 28S bands (Lanes 5 and 6), suggesting that RNA/ater[®]-ICE was a suitable reagent for the extraction of concentrated and intact RNA from previously cryogenically stored tissue.

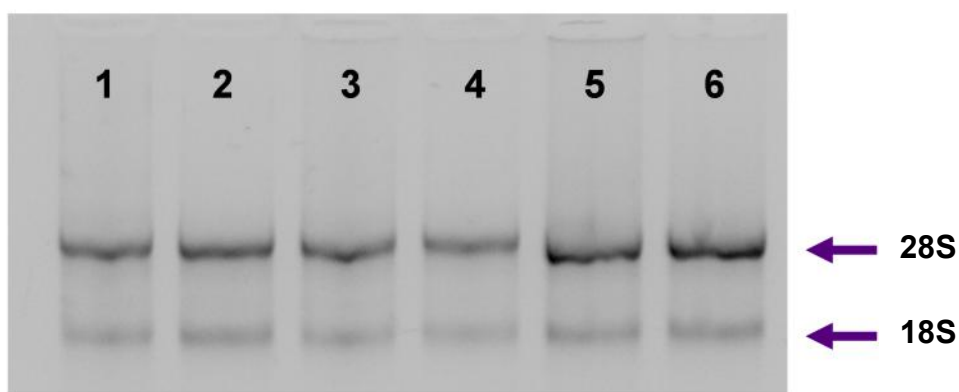


Figure 2.9 Gel electrophoresis of RNA extracts showed intact bands for the 28S and 18S ribosomal subunits in all samples. In all samples the heavier 28S band was approximately twice as intense as the lighter 18s band. RNA extracts from samples treated with RNA/ater[®]-ICE (lanes 4-6) were comparable to those from samples treated with RNA/ater[®] (Lanes 1 -3).

2.11.4.2 *Ywhaz* qPCR

cDNA quality was verified first by amplification of *Ywhaz* by qPCR using the protocol described in [Section 2.11.3.1](#). This ubiquitously expressed gene coding a 14-3-3 adapter protein (tyrosine 3-monooxygenase/tryptophan 5-monooxygenase activation protein, zeta) is used regularly as a reference gene as it is highly conserved and widely expressed at relatively high levels.

The *Ywhaz* primer assay confirmed amplification potential in all tissue samples (C_t range: 20.66 - 21.97, [Figure 2.10a](#)), producing a single PCR product with a melting temperature (T_m) of 79.9 - 80.6 °C ([Figure 2.10b](#)) in all tissue samples, except the No RT, NTC and water controls (No C_t). In addition, the qPCR results for *Ywhaz* suggested that there was no discernible difference in amplification capacity between samples with lower A_{260}/A_{230} ratios (1.40 - 1.97, [Table 2.10](#)).

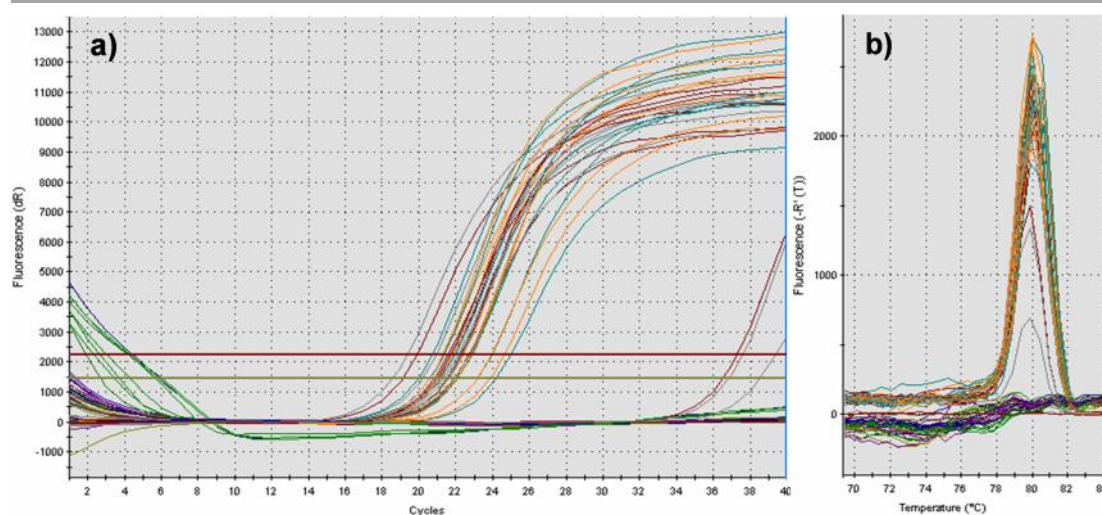


Figure 2.10 qPCR for *Ywhaz* demonstrated amplification capacity for all samples and standards, producing **a)** typical sigmoidal-shaped amplification plots (C_t : 18.61 - 24.22) and **b)** a single peak on the dissociation curve. There was slight environmental amplification in some of the negative controls, however this occurred at much higher cycle numbers ($C_t > 36.5$) than any other sample.

A single dissociation peak was consistent with the presence of a single band, of approximately 100 bp (Figure 2.11), the predicted *Ywhaz* amplicon size (99 bp; Table 2.7) when the completed PCR reactions were run out on a 2.5% non-denaturing agarose gel as described in Section 2.11.3.2.

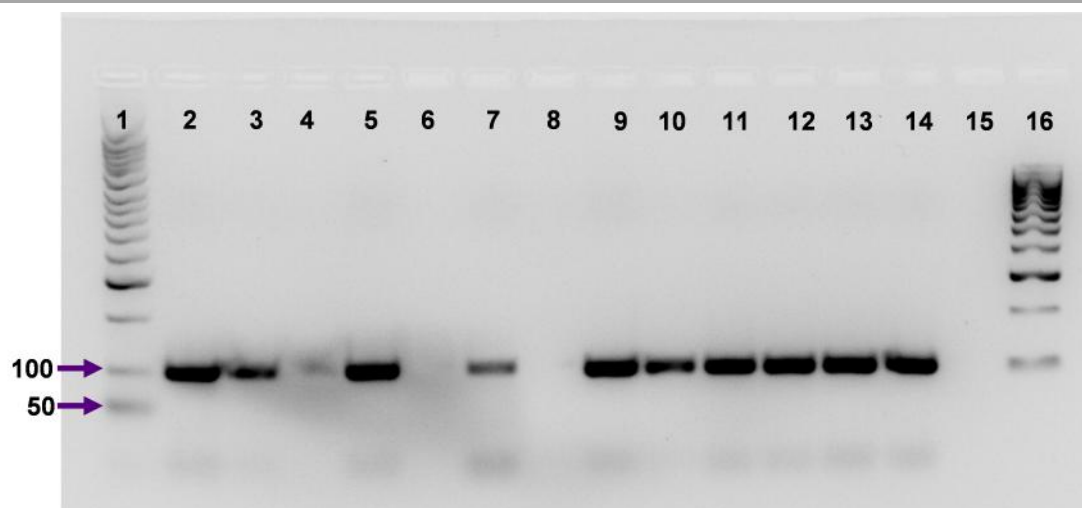


Figure 2.11 qPCR for Ywhaz yields a single PCR product with an approximate size of 100 bp. Size estimated from known bands in HyperLadder II (lane 1; 50 bp ladder) and HyperLadder IV (lane 16; 100 bp ladder). Lanes 2 and 3 contain standards (50 and 3.125 ng, respectively) with negative controls (NTC, No RT and buffer) in lanes 6, 7 and 8 respectively. The test samples can be visualised in lanes 9 - 14 as follows; Left - RNA/ater[®], Right - RNA/ater[®], Left - RNA/ater[®]-ICE, Right - RNA/ater[®]-ICE, Sham - RNA/ater[®]-ICE and SNx - RNA/ater[®]-ICE. Lane 5 contained an additional standard (12.5 ng).

The results of this qPCR assay were encouraging, with reliable amplification of a single PCR product in all samples. Importantly, there was no discernible difference between samples treated with RNA/ater and those treated with RNA/ater-ICE (C_t values (mean \pm SEM); 21.23 ± 0.46 vs 21.77 ± 0.19 , respectively), which validates the use of RNA/ater-ICE as a suitable method for the extraction of good quality RNA from renal cortex tissue. It can also be inferred that extracted RNA was successfully converted to cDNA using the QuantiTect[®] (Qiagen) reverse transcription kit. This positive qPCR outcome further suggests that the QuantiFast[®] SYBR Green assay chemistry (Qiagen) is suitable for use with renal cortex when investigating genes of interest. There was a slight contamination issue with the No RT control sample in this particular assay (lane 7, [Figure 2.11](#)), but this did not impact upon the quality of the remaining samples, or the NTC and buffer controls (lanes 6 and 8 respectively). This was issue was rectified in later assays.

2.12 Optimisation of QuantiFast® SYBR Green qPCR conditions for *Uts2r*, *Uts2b* and *Uts2* in rat renal cortex

Initial attempts to amplify *Uts2r*, *Uts2b* and *Uts2* transcripts were carried out using cDNA diluted to 1 in 100. The results of these assays were largely negative (below detectable threshold), despite increasing the cycle number up to 60 cycles.

The qPCR assays for *Uts2r*, *Uts2b* and *Uts2* were repeated using cDNAs diluted at 1 in 5 with a revised standard curve (per reaction; 500, 250, 125¹, 62.5, 31.25, 7.81, 3.90, 1.95 ng). This process placed a substantial burden on cDNA stocks so, for these initial investigatory processes, a single replicate determination was performed for individual samples. An alternative tissue was also sourced as a potential positive control. The tissue chosen was placenta from Sprague-Dawley rat as, although data were not available for rat placenta, human placenta has been shown previously to express *Uts2r* and *Uts2* at higher levels than that of the whole kidney in either rat or human.²⁰⁰ cDNA from rat placenta was used in these initial qPCR assays at a 1 in 20 dilution. To increase the potential for amplification, cycle number was extended to 60.

The results of these trials were promising, with amplification of products seen with all three primer sets. The primer assays for *Uts2r* ([Figure 2.12.a and b](#), C_t ; 33.84 ± 1.19) and *Uts2b* ([Figure 2.12.c and d](#), C_t ; 33.39 ± 0.55) resulted in amplification products with a single T_m (86.8 - 87.3 °C and 83.1 - 83.7 °C, respectively). The *Uts2* primer assay gave more mixed results producing a number of products in the dissociation curve; however this appeared to be the result of low gene copy number in the tissue of interest as the threshold was not reached until later in the assay ([Figure 2.12.e and f](#), C_t 38.41 ± 1.31).

¹ The 500, 250 and 125 ng cDNA loads were above the maximum recommended by the suppliers (Qiagen)

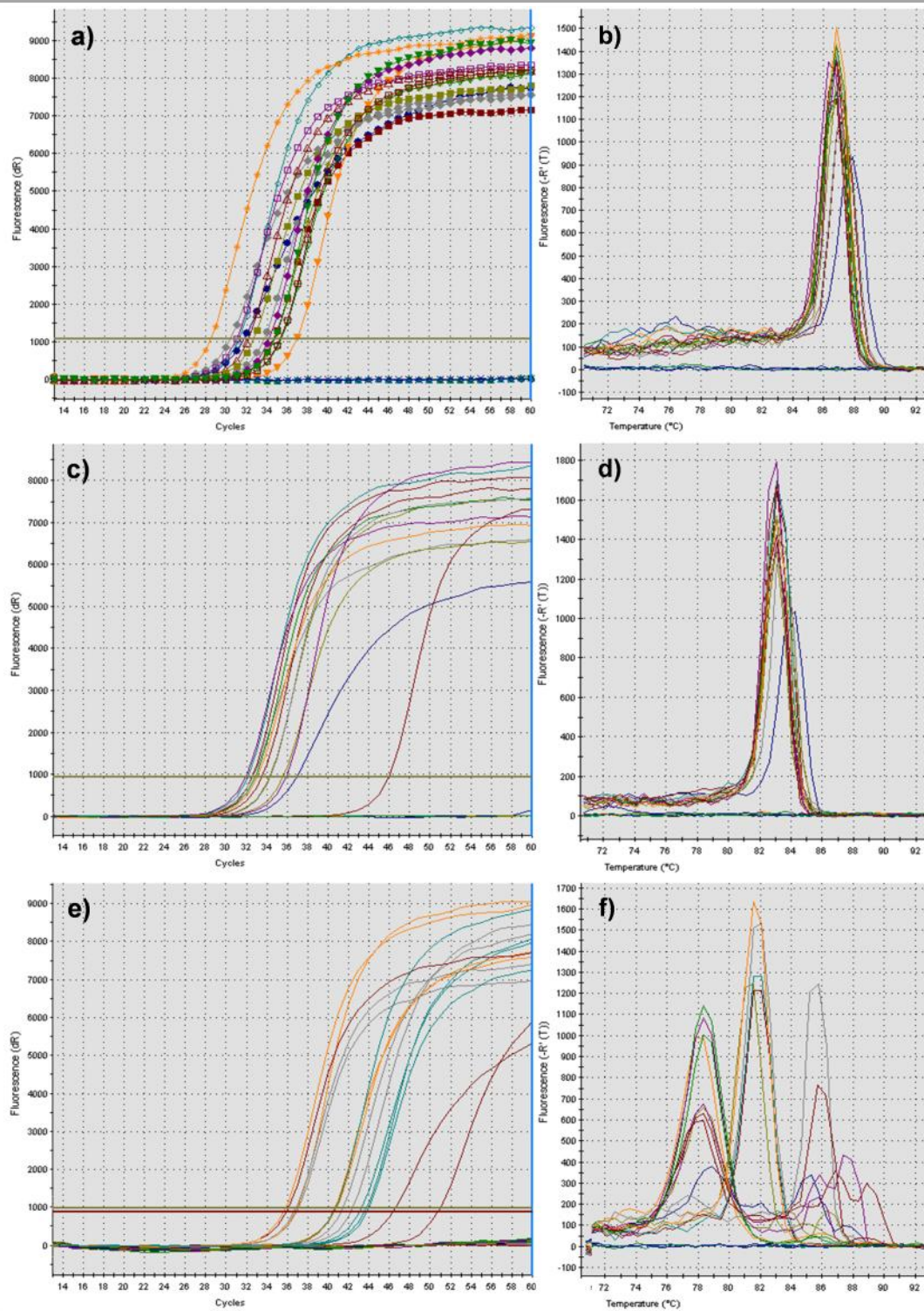


Figure 2.12 Primer sets for *Uts2r* (a and b) and *Uts2b* (c and d) appeared to amplify well (C_t 28.56 - 36.94 and 32.58 - 35.62, respectively), producing a single peak on the dissociation curve (T_m 86.8 - 87.3 and 83.1 - 83.7 °C, respectively). In contrast the primer pair for *Uts2* (e and f) amplified products later in the cycle (C_t 35.82 - 43.80) with multiple peaks visible in the dissociation curve.

It was clear that loading 500 and 250 ng cDNA per qPCR reaction (standards: undiluted and 1 in 2 dilution of cDNA) generally had an inhibitory effect on the reaction kinetics ([Table 2.11](#)).

Standard load (ng)	<i>Uts2r</i>	<i>Uts2b</i>	<i>Uts2</i>
500 (undiluted)	31.73	36.95	46.64
250 (1 in 2)	30.45	32.63	50.94
125 (1 in 4)	31.01	32.13	43.31
62.5 (1 in 8)	32.14	33.53	41.47
31.25 (1 in 16)	33.73	34.39	40.67
15.625 (1 in 32)	34.21	35.92	40.75
7.813 (1 in 64)	35.32	46.00	42.43
3.906 (1 in 128)	34.78	No C _t	44.01

[Table 2.11](#) Estimated C_t values for the standards across the three primer assays indicate that using cDNA at dilutions less than 1 in 4 has an inhibitory effect on the reaction kinetics, decreasing the sensitivity and accuracy of the assay

2.12.1 *Uts2r*

To confirm amplicon sizes the qPCR products were run out on gels as described above ([Section 2.11.3.2](#)). The primer set for *Uts2r* yielded positive results and the presence of an intense band with a size slightly greater than 100 bp is consistent with the predicted amplicon size of 116 bp ([Figure 2.13](#)). This band was prominent in all standards tested (lanes 1 to 3), samples (6 to 11) and placenta (lane 15). There were no amplification products in the negative controls (NT, No RT and water, lanes 12, 13 and 14, respectively). This result supported the result from the pilot qPCR where a single peak was seen on the melt curve ($T_m = 86.8 - 87.3$ °C) and the negative controls did not amplify (No C_t).

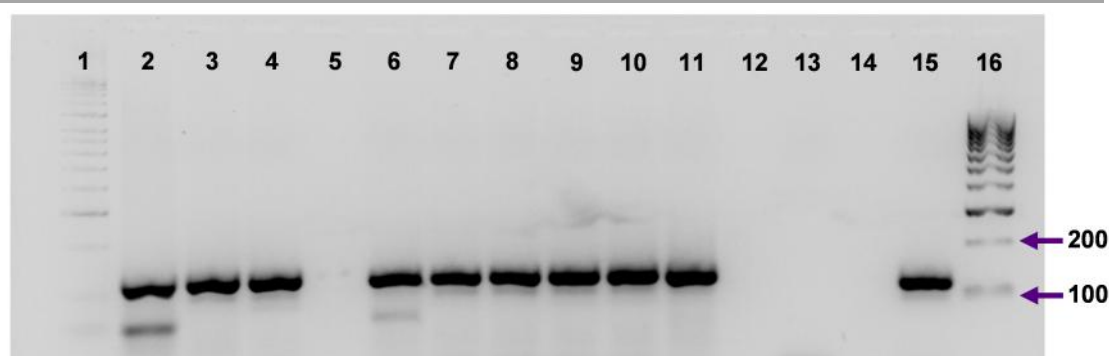


Figure 2.13 qPCR for *Uts2r* primarily yields a single PCR product with approximate size slightly greater than 100 bp. Size estimated from known bands in HyperLadder II (lane 1; 50 bp ladder) and HyperLadder IV (lane 16; 100 bp ladder). Lanes 2 - 4 contain standards (500, 250 and 62.5 ng, respectively) with negative controls (NTC, No RT and buffer) in lanes 12, 13 and 14. The test samples can be visualised in lanes 6 - 11 as follows; Left - RNA/*ater*, Right - RNA/*ater*, Left - RNA/*ater*-ICE, Right - RNA/*ater*-ICE, Sham - RNA/*ater*-ICE and SNx - RNA/*ater*-ICE. Lane 15 contains qPCR products from placental cDNA (1 in 20 dilution). Lane 5 was empty.

2.12.2 *Uts2b*

The primers for *Uts2b* produced a major product between 100 and 200 bp in size (lying closer to 100 bp, in accord with predicted size of 120 bp) in all standards (lanes 2 - 4) and samples (lanes 6 - 11) (**Figure 2.14**). There were no visible bands in the negative controls (lanes 12 - 14) or in the placental sample (1 in 20 dilution, lane 15). The poor amplification of the highest standards (500 and 250 ng load) was also visible in the gel, although this was not quantified.

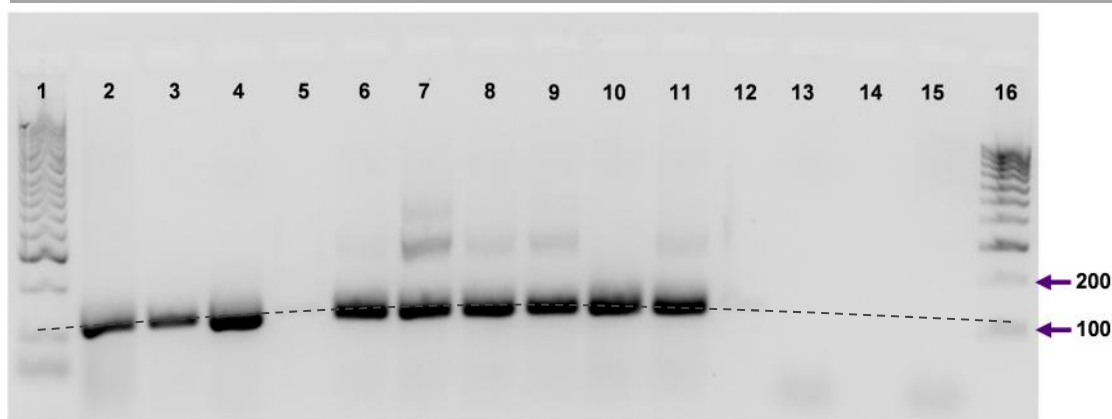


Figure 2.14 qPCR for *Uts2b* yields a major PCR product with approximate size greater than 100 bp. Size estimated from known bands in HyperLadder II (lane 1; 50 bp ladder) and HyperLadder IV (lane 16; 100 bp ladder). Lanes 2 - 4 contain standards (500, 250 and 62.5 ng, respectively) with negative controls (NTC, No RT and buffer) in lanes 12, 13 and 14. The test samples can be visualised in lanes 6 - 11 as follows; Left - RNA/*later*, Right - RNA/*later*, Left - RNA/*later*-ICE, Right - RNA/*later*-ICE, Sham - RNA/*later*-ICE and SNx - RNA/*later*-ICE. Lane 15 contains placenta, which did not amplify a product in this assay, at a 1 in 20 dilution. Note: there is a curvature in the gel; as a result the bands in the central lanes (6 - 11) appear heavier. Lane 5 is empty.

2.12.3 *Uts2*

The variability in melting temperature seen in the *Uts2* assay was replicated when the PCR products were visualised in a 2.5% agarose gel as described in [Section 2.11.3.2](#), with multiple bands seen in most lanes. This primer pair spanned an intron so it is unlikely that these products were the result of amplification from gDNA, and the products were instead the result of mispriming. This amplification of non-specific products occurred at higher cycle numbers ($C_t > 38 - 40$). Despite the high cycle numbers used, no amplification occurred in any of the negative control reactions (No C_t reached for NTC, No RT or buffer). This observation was supported when products were visualised on a 2.5% agarose gel; there were no visible bands in any negative control ([Figure 2.15](#), lanes 11, 12 and 13). A single product was amplified ($C_t = 36.94$) in the placental sample with a melt temperature of 82 °C, and this single band (< 100bp) can be seen in [Figure 2.15](#) (lane 14). This product appears consistent with the predicted 82 bp amplicon. Interestingly, the late SNx sample included (SNx - RNA/*later*-ICE) in this assay produced a major band in the same position as that of the placental sample ([Figure 2.15](#), lane 10).

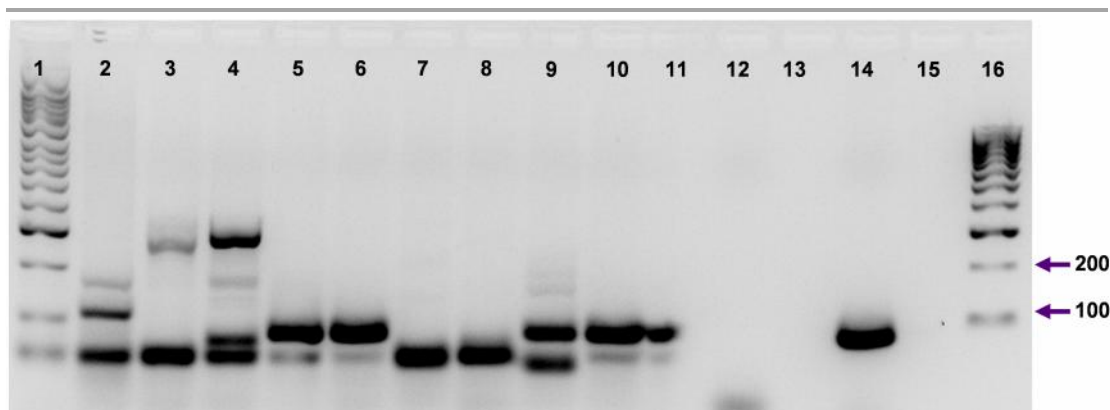


Figure 2.15 qPCR for *Uts2* was complicated by apparent low copy number and as a result of the high cycle number required to reach a threshold of detection there was a problem with mispriming and the production of non-specific products. This problem was particularly evident in the standards (500, 125 and 31.25 ng, Lanes 2 - 4). Negative controls (NTC, No RT and buffer) in lanes 11, 12 and 13 produced no visible banding. Lane 14 contains placenta, which produced a single band <100 bp in size. Band sizes estimated from known bands in HyperLadder II (lane 1; 50 bp ladder) and HyperLadder IV (lane 16; 100 bp ladder). The test samples can be visualised in lanes 5 - 10 as follows; Left - RNA/ater[®], Right - RNA/ater[®], Left - RNA/ater[®]-ICE, Right - RNA/ater[®]-ICE, Sham - RNA/ater[®]-ICE and SNx - RNA/ater[®]-ICE. Note: signal in lane 11 is carryover from lane 10. Lane 15 is empty.

2.12.4 Revised assay conditions

The results of the above assays were used to develop an optimised assay design ([Table 2.12](#)) for the analysis of *Uts2r*, *Uts2b* and *Uts2* expression in the experimental tissues of interest. An interesting finding was that amplification of *Uts2* and *Uts2r* in the placental sample was consistent. This amplification occurred around the same cycle number as the kidney samples for *Uts2r* and earlier than kidney for *Uts2*; despite the difference in starting dilution. In contrast, at this dilution (1 in 20), *Uts2b* did not amplify. This also influenced the assay design.

Assay	cDNA dilution factor	Top Std (ng)	Cycles	Expected T_m (°C)	Placenta
<i>Ywhaz</i>	100	50	40	79.9 - 80.6	+ve
<i>Uts2r</i>	10	125	50	86.8 - 87.3	+ve
<i>Uts2b</i>	10	125	50	83.1 - 83.7	-ve
<i>Uts2</i>	10	125	50	82.1	+ve

Table 2.12 Refined assay conditions for *Ywhaz*, *Uts2r*, *Uts2b* and *Uts2* RT-qPCR.

2.12.4.1 PCR assay inclusion criteria

Strict acceptance criteria were implemented for qPCR assays. Individual samples must: (i) be consistent between replicates, (ii) produce a single dissociation peak of appropriate temperature within the dissociation curve and (iii) produce a sigmoidal-shaped amplification plot. Assays failing to meet these criteria were excluded from analysis entirely. In addition, for interpolation of unknowns, the standard curve must produce an efficiency approaching 100 % (accepted range: 85 % to 115 %) over a minimum of 4 data points.

2.13 QuantiFast® SYBR Green qPCR for *Ywhaz*, *Uts2r*, *Uts2b* and *Uts2* in rat renal cortex.

To examine the expression of mRNAs for *Uts2r*, *Uts2b* and *Uts2* in rat renal cortex over the course of the progressive renal failure following 5/6th SNx ([Section 2.3.1](#)), and when intervening in this model with a non-peptide UT antagonist ([Section 2.3.2](#)), the cryogenically-stored samples (collected as described in [Section 2.5.1](#)) were first stabilised and transferred to -20 °C storage using RNAlater®-ICE ([Section 2.11.1.1](#)).

Samples from the two studies, progression of CKD in the 5/6th SNx model ([Section 2.3.1](#)) and UT antagonist intervention in the 5/6th SNx model ([Section 2.3.2](#)), were treated independently throughout. *Ywhaz* was used as an internal reference gene for both studies.

2.13.1 RNA extraction, quantification and quality control

Briefly: approximately 100 mg renal cortex was homogenised in 1.5 mL lysis buffer RLT (Qiagen, prepared with 10 µL β-ME per 1 mL, Sigma) using a homogenisation drill (Powergen 125, Fisher, [Section 2.11.1.2](#)). RNA was then extracted and purified using the RNeasy® plus mini kit (Qiagen) as described in [Section 2.11.1.3](#).

RNA extracts were quantified using a micro-volume spectrophotometer (Nanodrop 2000c, ThermoFisher) before storing at -80 °C ([Section 2.11.1.4](#)).

Following quantification RNA extracts (800 ng per lane, in loading buffer, Bioline) were run on a 1.5 % agarose gel (Bioline), under non-denaturing conditions, and examined for the presence of intact 28S and 18S bands ([Section 2.11.1.5](#)). The presence of these bands provided a visual indication of RNA quality and was considered a mandatory prerequisite for sample inclusion in the subsequent reverse transcription reactions and qPCR assays.

2.13.1.1 Renal disease progression in the 5/6th SNx model

Following the inclusion criteria described above the group numbers were as follows: early sham (ES): n = 6, late sham (LS): n = 6, early SNx (EN): n = 7 and late SNx (LN): n = 7. One sample was excluded for failing these criteria: LS8 (late sham 8) had a poor final RNA concentration of 79.1 ng / µL, much lower than that obtained for all other samples.

2.13.1.2 Intervening with a UT antagonist in the 5/6th SNx model of CKD

Following the inclusion criteria described above the final group numbers were as follows: sham (vehicle): n = 5, sham (UT-A): n = 5, SNx (vehicle): n= 5, SNx (UTA): n= 5. One sample was excluded for failing these criteria: AN3 (UT-A SNx 3) with a final RNA concentration of 43.3 ng / μ L, again very much more dilute than other samples.

2.13.2 QuantiTect[®] Reverse transcription with gDNA wipe-out treatment

Samples of satisfactory concentration (>83.3 ng/ μ L) and quality (18S and 28S bands intact) were converted to cDNA using the QuantiTect[®] reverse transcription kit (Qiagen) along with NTC and No RT controls, as described in [Section 2.11.2](#). Each sample was transcribed as three 40 μ L reactions to provide substantial cDNA stocks (total volume 120 μ L); these individual reactions were carried out together and the replicates pooled prior to dilution and use in qPCR reactions.

Briefly: RNA samples were diluted in PCR reaction strips (Sarstedt) to contain 2 μ g RNA in a volume of 24 μ L (using PCR grade water, Sigma). To this, 4 μ L gDNA wipeout buffer was added and the strips incubated at 42 °C for 2 minutes (Stratgene Mx3000/3005P, Aligent Technologies) before placing on ice. To each tube; 12 μ L reverse transcription master mix was added ([Table 2.8](#)) before mixing and incubation at 42 °C for 15 minutes before the RT enzyme was inactivated at 95 °C for 3 minutes (Stratgene Mx3000/3005P, Aligent Technologies). Samples were placed on ice immediately before storage at - 20 °C.

2.13.3 cDNA pool for preparation of standard curves

A cDNA pool was prepared using 10 μ L of each; LN1, LN2, LN3, LN4, LN5, LN6, LN7, early sham 3 (ES3), late sham 2 (LS2) and early SNx 6 (EN6). Late nephrectomy samples formed the majority of the cDNA as it was hoped that this would decrease the cycle number required to reach threshold, improving sensitivity. A representative sample was included from the other groups to reduce the volume of cDNA taken from any one individual sample. This blend was used to produce two sets of standards: one for highly expressed transcripts (*Ywhaz*) composed of 50, 25, 12.5, 6.25, 3.125, 1.563, 0.781 and 0.391 ng / 10 μ L, and a second for transcripts expected to have lower expression (*Uts2r*, *Uts2b* and *Uts2*) comprising 125 , 62.5,

31.25, 7.813 and 3.906 ng / 10 μ L. These standards were prepared once and used for both studies.

2.13.4 *Ywhaz*

For detection of the reference gene *Ywhaz*, cDNAs were diluted 1 in 100 and samples, standards (50, 25, 12.5, 6.25, 3.125, 1.563, 0.781 and 0.391 ng, [Table 2.9](#), from cDNA pool enriched with increased proportion of late SNx samples) and controls were run, in duplicate, in PCR reaction strips (Sarstedt) using the standard protocol described in [section 2.11.3.1](#) for 40 cycles in a thermocycler (Stratgene Mx3000/3005p). Following completion of the cycles, and dissociation curve, the PCR products were stored at -20 °C for product analysis by non-denaturing gel electrophoresis.

2.13.5 *Uts2r*

For detection of *Uts2r*, cDNAs were diluted 1 in 10 and samples, standards (125, 62.5, 31.25, 15.625, 7.813 and 3.906 ng) and controls were run, in duplicate, in PCR reaction strips (Sarstedt) using the standard protocol described in [Section 2.11.3.1](#) modified as described in [Table 2.12](#) (row 2, [Section 2.12.4](#)) for 50 cycles in a thermocycler (Stratgene Mx3000/3005p). Following completion of the cycles, and dissociation curve, the PCR products were stored at -20 °C for product analysis by non-denaturing gel electrophoresis.

2.13.6 *Uts2b*

For detection of *Uts2b*, cDNAs were diluted 1 in 10 and samples, standards (125, 62.5, 31.25, 15.625, 7.813 and 3.906 ng) and controls were run, in duplicate, in PCR reaction strips (Sarstedt) using the standard protocol described in [Section 2.11.3.1](#) modified as described in [Table 2.12](#) (row 3, [Section 2.12.4](#)) for 50 cycles in a thermocycler (Stratgene Mx3000/3005p). Following completion of the cycles, and dissociation curve, the PCR products were stored at -20 °C for product analysis by non-denaturing gel electrophoresis.

2.13.7 *Uts2*

For detection of *Uts2*, cDNAs were diluted 1 in 10 and samples, standards (125, 62.5, 31.25, 15.625, 7.813 and 3.906 ng) and controls were run, in duplicate, in

PCR reaction strips (Sarstedt) using the standard protocol described in [Section 2.11.3.1](#) modified as described in [Table 2.12](#) (row 4, [Section 2.12.4](#)) for 50 cycles in a thermocycler (Stratgene Mx3000/3005p). Following completion of the cycles, and dissociation curve, the PCR products were stored at -20 °C for product analysis by non-denaturing gel electrophoresis.

2.13.8 Analysis of qPCR data

For each assay qPCR data were processed using MxPro software (version: 4.10, Aligent technologies) with threshold fluorescence calculated automatically from all wells meeting the acceptance criteria ([Section 2.12.4.1](#)) providing the raw threshold cycle (Ct) data used in all further analysis.

2.13.8.1 Reference gene stability

Ywhaz has previously been used as a reference gene in renal tissue from healthy young SD rats.^{232,306} Basic analysis of reference gene stability was carried out by two-way ANOVA on data transformed to aligned ranks generated from the Ct value (SPSS version 22.0, IBM SPSS statistics).

2.13.8.2 Relative expression of *Uts2*, *Uts2b* and *Uts2r*

Where a minimum of 4 consecutive standards (from two replicates per standard) amplified well a standard curve was generated and the reaction efficiency was calculated ([Equation 2.6](#)).³¹¹

$$Efficiency (E) = 10^{(-1/slope)}$$

Equation 2.6

Where standard curve fit was good ($R^2 > 0.95$) and reaction efficiencies were between 85 and 115 % the relative expression was determined using the Pfaffl modification to account for differing reaction efficiencies ([Equation 2.7](#)).^{311,312}

$$Ratio = \frac{E_{GOI}^{\Delta Ct_{GOI}(control-sample)}}{E_{Ref}^{\Delta Ct_{Ref}(control-sample)}}$$

Equation 2.7

E_{GOI} and E_{Ref} represent the reaction efficiencies of the qPCR assay for gene of interest (GOI, *Uts2r*, *Uts2b*, *Uts2*) and reference gene (Ref, *Ywhaz*), respectively. Efficiencies are calculated according to [equation 2.6](#) where 100% efficiency = 2.³¹¹ ΔCt for GOI or REF is calculated using the replicate means. Details of the control group used are stated within the appropriate results section.

Where no suitable standard curve could be produced (due to non-conformance to the inclusion criteria) data are expressed as Ct values, and no further analysis was carried out.

For graphing purposes (Prism 5, GraphPad Software Inc.) sample values were calculated from qualifying replicates ($n = 1$ or 2) and the each individual biological sample presented as a single point within the appropriate group. The group mean is represented by a line. Relative expression data is presented on a \log_{10} scale so that a 10 fold up or down regulation appear equidistant from 1 (no change).

2.13.9 Visualisation of qPCR products

To confirm amplicon size and the generation of a single amplification product, PCR products were examined under non-denaturing conditions on a 2.5 % agarose gel (prepared as described in [Section 2.11.1.5](#)). For representative samples ($n=2$, from each treatment group), negative controls, placenta and two select standards (Assay dependent: high and low or high) a 16 μL of the final reaction was mixed with 4 μL 5 x loading buffer (Bioline) before running at 120 V for 45 minutes alongside weight markers (5 $\mu\text{L}/\text{lane}$, HyperLadder II and HyperLadder IV run in lanes 1 and 16 respectively, both Bioline). Product bands were visualised as described in [section 2.11.1.5](#).

2.13.9.1 Excision and elution of product bands for sequencing

PCR products were visualised using a UV transilluminator and gel slices containing the amplified PCR product were carefully excised using a clean scalpel blade (No. 23, Swann-Morton). Gel slices were sealed into pre-weighed tubes (30 mL universal tube, ThermoFisher) and the tubes were weighed again to calculate gel slice weight before storage at 4 °C.

3: Progression of chronic kidney disease following 5/6th subtotal nephrectomy

Animals were monitored regularly for changes in health and renal function associated with the progression of chronic kidney disease (CKD) induced by the 5/6th SNx procedure. Details of end point determination can be found in [Section 2.3.1.2](#).

3.1 Acute renal failure incidence and survival

Animals underwent the 5/6th SNx procedure in two-stages ([Section 2.2](#)) in order to reduce the risk of acute renal failure (ARF); the reduction in renal mass was highly consistent across the SNx rats (73.6 ± 3.5 % resection, $n = 30$, mean \pm SD). Of the 30 animals in this study that underwent the 5/6th SNx, 2 went into ARF; an incidence rate of 6.7 %. All cases of ARF occurred within 48 hours of the second surgical procedure. All of these cases were in the pilot group. Data from 1 animal (G2 SNx4) were excluded from data analysis following an adverse reaction (apparent stroke, with no evidence of advanced renal disease) in week 13, leaving a cohort of 15 in the late SNx (LN) group, and 12 in the early SNx (EN) group. One sham control from the pilot study was also culled as over-grooming left an open wound that could not be closed surgically, leaving 12 shams in the late (LS) group and 6 in the early (ES) group.

For the LN animals ($n = 15$) the mean time to renal insufficiency was 30.9 ± 8.5 weeks (mean \pm SD), with a steady decline in numbers seen from week 20 to week 45 ([Figure 3.1a](#)).

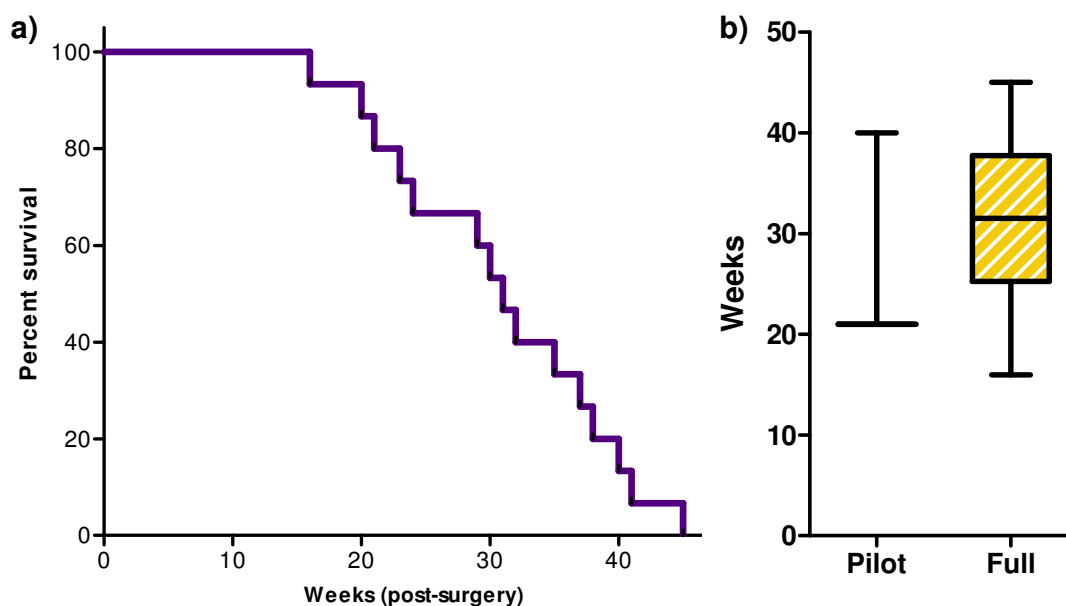


Figure 3.1 (a) Kaplan-Meier survival plot of rats undergoing 5/6th SNx highlights variable survival time, with half of the cohort reaching the defined endpoint by 31 weeks post-surgery. There was a steady decline in numbers from 16 weeks post-surgery until the end of the study at 45 weeks. (b) Survival was not different between the pilot study animals (LN/pilot, n = 3) and the full late nephrectomy (LN/full) group, (n = 12).

The pilot data were comparable ($p = 0.575$) with the full long-term study group: the pilot animal survival times of 27.3 ± 11.0 weeks (mean \pm SD, $n = 3$) were not significantly different from the main long-term study group (30.8 ± 8.8 weeks, mean \pm SD, $n = 12$, [Figure 3.1b](#)). Therefore the data from the pilot animals are included in all analyses and are collectively referred to as the late SNx (LN) group from now on.

3.2 Physiological progression of CKD

Disease progression was monitored using a number of physiological parameters including changes in body weight ([Section 2.4.1](#)), systolic hypertension ([Section 2.4.3](#)) and renal function by albumin: creatinine ratio (ACR) in spot urine samples ([Section 2.4.2](#)).

3.2.1 Body weight

Rats in the ES, LS and EN groups gained weight steadily throughout the study; in the LN group weight gain halted in the later stages of renal disease ([Figure 3.2](#)) and the rats began to lose weight, ultimately losing 9.5 ± 1.2 g. The time to renal failure

was variable; this is reflected by the visible divergence of the groups by approximately 20 weeks post-surgery. Towards the end of the study there is an apparent rapid gain in weight within the LN group in particular. This artefact was the result of reducing subject numbers as the pre-defined end-points were reached. This was compounded as any weight-loss in the remaining subjects has a greater effect on the group mean with a smaller group size. A similar pattern is noticeable within the LS group with variations in weight arising from (near) time-matched culling, despite no weight losses in this group.

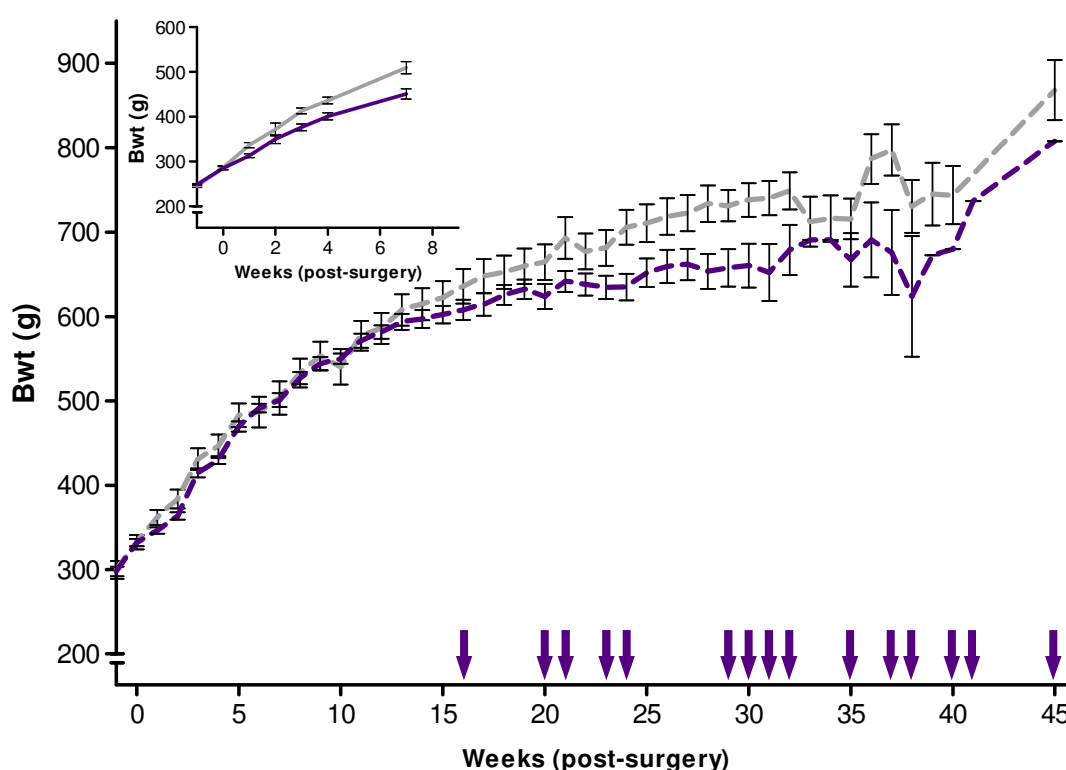


Figure 3.2 Growth curves for all groups demonstrate steady growth between start weight and approximately 600 g, after which weight gain slows substantially. **Inset:** Early SNx (EN, solid purple line, $n = 12$) and early shams (ES, solid grey line, $n = 6$) started the experimental protocol ($t = -1$ week) at a lower weight (247.5 ± 1.6 g) than (**main panel**) late SNx (LN, dashed purple line, $n = 15$ at $t = \text{week } -1$ and 0 , with arrows representing termination points of LN group animals) and late sham animals (LS, dashed grey line, $n = 12$) which weighed 298.7 ± 5.6 g prior to surgery 1.

Rats within the LN and LS groups weighed 296.4 ± 6.0 and 299.7 ± 10.6 g, respectively, at the start of the study (at surgery 1, $t = -1$ week). Despite the visible divergence of the two groups (Figure 3.2, main panel) the differences between them were not statistically significant. This is likely to be the result of decreasing statistical power (reducing n numbers) as the study progressed.

3.2.2 Systolic blood pressure and heart rate

Early SNx (EN) rats started to develop increased systolic blood pressure (154.5 ± 2.9 mmHg, $n = 12$) compared with the sham controls (ES) by 7 weeks post-surgery (141.9 ± 1.9 mmHg, $n = 6$, $p = 0.020$, [Figure 3.3b](#)); however this was not allowed to progress further as terminal samples were collected at 7 - 8 weeks post-surgery for histological, immunological and gene expression analysis. Late SNx (LN) rats developed systolic hypertension over the course of the study; in contrast there was no change in SBP in the sham controls ([Figure 3.3a](#)). SBP was significantly higher in the LN group compared with the sham controls by 12 weeks post-surgery (LN, 156.7 ± 2.5 , $n = 15$ vs. 132.0 ± 2.2 mmHg, $n = 12$, $p < 0.001$), and remained elevated for the remainder of the study. This hypertension was progressive ($p < 0.001$), increasing in severity with time, reaching 175.4 ± 5.7 mmHg after 28 weeks (LN, $n = 10$) compared with 141.3 ± 2.8 mmHg ($n = 9$) in the LS group.

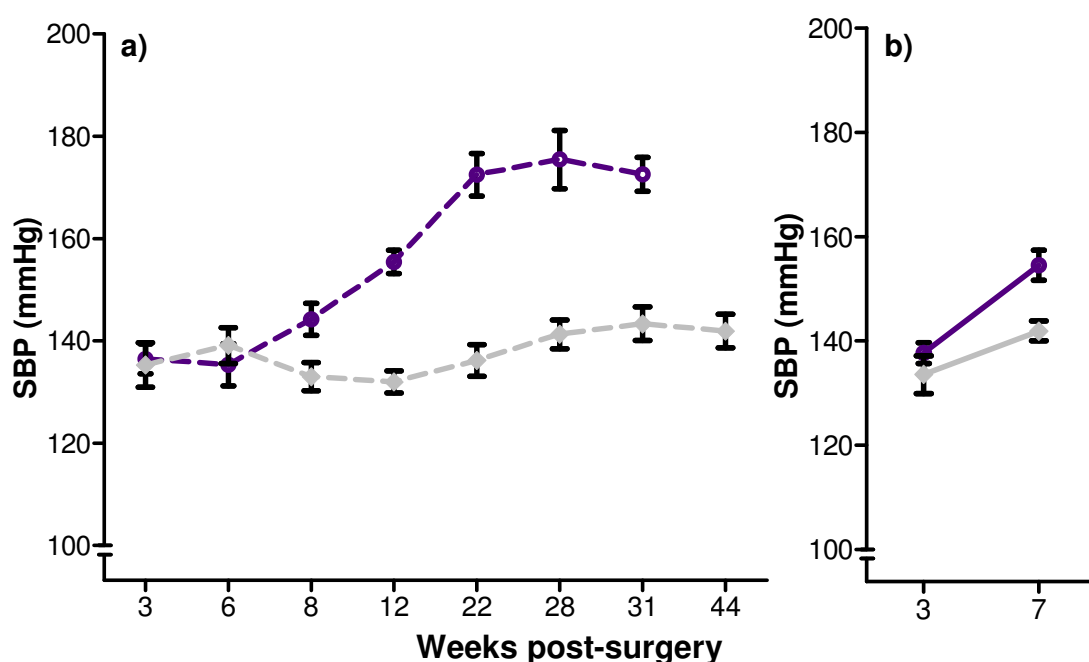


Figure 3.3 (a) SNx rats developed progressive systolic hypertension over the course of the experiment ($p < 0.001$). Systolic blood pressure (SBP) was significantly higher than in the sham controls from 12 weeks post-surgery (Late SNx; dark dashed line, 156.7 ± 2.5 , $n = 15$, vs. Late sham, light dashed line, 132.0 ± 2.2 mmHg, $n = 12$, $p < 0.001$), and there was no significant change in blood pressure in the sham controls over the time-course. **(b)** SBP was higher in SNx rats at 7 weeks post-surgery than in the age-matched controls (154.5 ± 2.9 mmHg, $n = 12$ vs. 141.9 ± 1.9 mmHg, $n = 6$, $p = 0.020$). Data were analysed by 2-way ANOVA with Tukey post-test.

In contrast, heart rate (HR) was not significantly different between the SNx and sham groups in either cohort ([Figure 3.4](#)). HR tended to decrease slightly after the first two readings, before levelling off over the remainder of the study. This pattern was seen in all groups ([Figure 3.4a](#)).

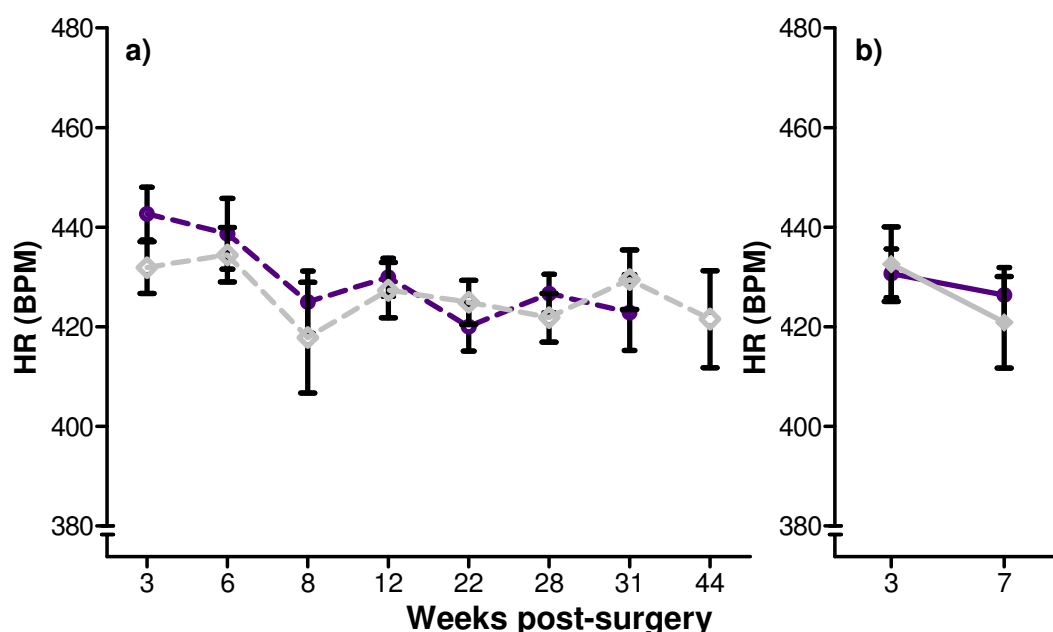


Figure 3.4 (a) In the long term experimental groups there were no time-dependent effects on heart rate (HR) in SNx or sham animals, and no difference between the SNx and sham groups (overall mean: 429.6 ± 3.1 vs. 426.2 ± 2.0 beats per minute (BPM), respectively) **(b)** Over the course of the short term experiment, there was no difference between SNx and sham animals or between 3 and 7 weeks post-surgery, (overall mean: 428.6 ± 2.2 vs. 426.7 ± 5.9 BPM, respectively).

The nature of this study resulted in occasional missing values; these absent data points prevented the application of the appropriate statistical analysis (2-way ANOVA with repeated measures, following K-S test for normality). For the late group; out of 218 potential data points for SBP, data existed for 165 and three of these were removed having failed outlier testing (described in [Section 2.4.3.1](#), 28 weeks, group 3 sham 2 and sham 3 along with 6 weeks, group 1 SNx4), leaving 162 points. For many of these points data were missing due to subjects reaching the defined end point (near renal failure, [Section 2.3.1.2](#)) at differing rates. For HR, out of 218 potential data points, data existed for 165 and there were no outliers. There were no missing values in the early group data for either measure.

To rectify this the data were transformed, replacing missing values by linear trend using SPSS (version 20.0.0, for Windows, IBM SPSS statistics). The following criteria were applied: a maximum of one missing value per case was replaced, and any values missing at the tails of the data set were not replaced. A total of 12 missing SBP values were replaced, along with 10 HR values. This process was completed automatically with no user influence over the final values. These replaced values were included for the purposes of statistical analysis only and were not graphed. This process allowed the analysis of the LN and LS groups up to and including week 28 by two-way RM ANOVA (with $n = 10$ per group).

3.2.3 Renal function by albumin: creatinine ratio

Albumin: creatinine ratio (ACR) was calculated as described in [Section 2.6.3](#). The resulting raw ratio data were non-normally distributed, and as a result the values presented are median: IQR.

SNx rats developed progressive albuminuria: ACR increased significantly over the course of the experiment ($p_{\text{time}} < 0.001$) and ACR was higher than that of the controls by 7 weeks post-surgery (0.061: 0.015 - 0.938 mg/ μ mol, $n = 15$ vs. 0.005: 0.002 - 0.010 mg/ μ mol, $n = 12$, $p = 0.007$) and remained elevated for the remainder of the study ([Figure 3.5](#)). The difference between the SNx and sham group was not significant at week 28 (0.391: 0.077 - 2.858 mg/ μ mol, $n = 10$ vs. 0.086: 0.011 - 0.180 mg/ μ mol, $n = 10$); however there was a progressive reduction in n numbers from $n = 12$ sham and $n = 15$ SNx to $n = 10$ in both groups by week 28. Since those animals with less severe renal dysfunction survived the longest, the lack of statistical significance at week 28 can be attributed to the prior loss of SNx rats with more pronounced albuminuria. There was no time-dependent effect seen within the sham control animals over the course of the study.

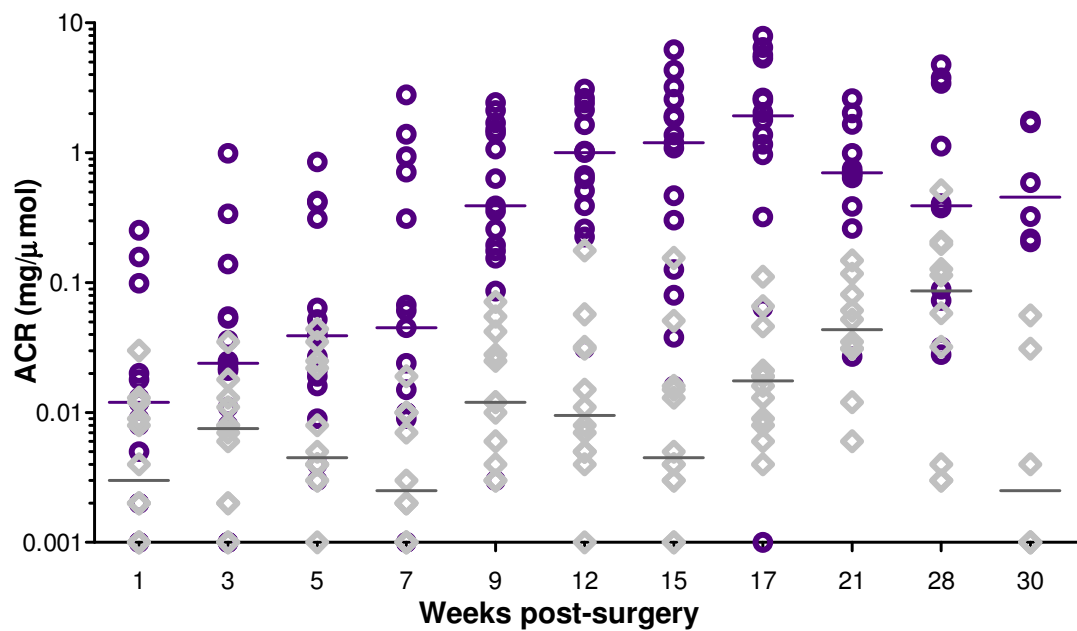


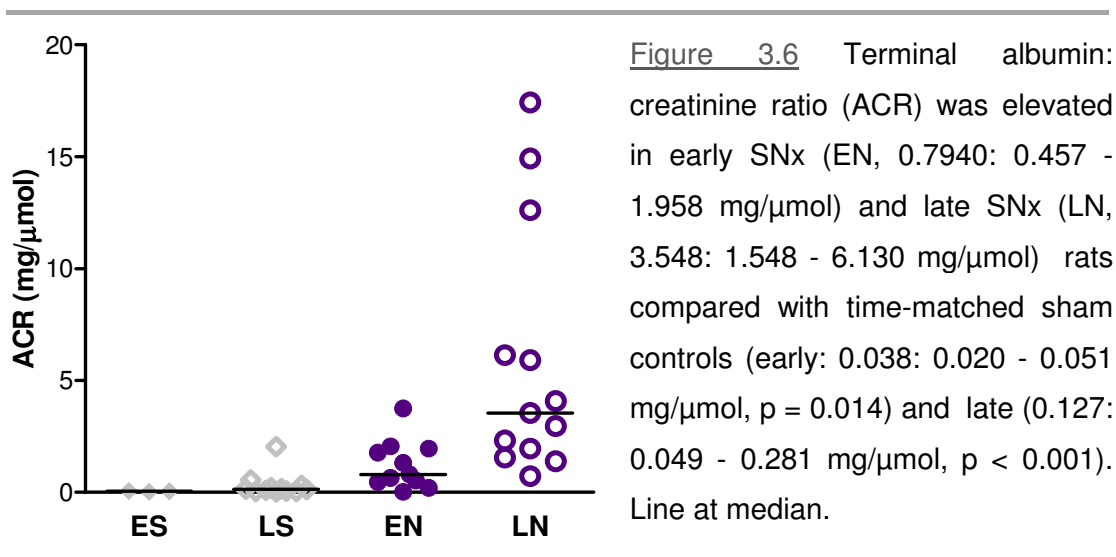
Figure 3.5 SNx rats developed marked and progressive albuminuria over the course of the study. ACR was significantly higher in SNx ($n = 15$, circles) rats than time-matched controls ($n = 12$, diamonds) by 7 weeks post-surgery (0.045: 0.010 - 0.823 vs. 0.003: 0.002 - 0.01 mg/μmol, $p = 0.002$). Analysed by 2-way RM ANOVA on log transformed data; horizontal lines represent median.

Within the SNx cohort ACR peaked at 17 weeks post-surgery (1.920: 1.115 - 3.324 mg/μmol, $n = 13$) which was substantially higher than in the matched sham controls (0.018: 0.009 - 0.027 mg/μmol, $n = 12$, $p < 0.001$). Data from the SNx rats were more variable than the age-matched sham controls; this is illustrated by the spread of the individual points (open circles, purple) compared to the controls (open diamonds, grey; [Figure 3.5](#)). ACR in the sham animals was consistently low over the course of the study (range in group median and IQR over course of the study: 0.003: 0.002 - 0.010 mg/μmol, $n = 12$, in weeks 1 and 7, to 0.086: 0.011 - 0.180 mg/μmol, $n = 10$, week 28).

3.3 Terminal data

Terminal samples were collected as described in [Section 2.5](#). Terminal urine samples ($n = 3, 12, 11$ and 13 for early sham (ES), late sham (LS), early nephrectomy (EN) and late nephrectomy (LN), respectively) were analysed for ACR and terminal plasma samples ($n = 6, 12, 11$ and 13 for ES, LS, EN and LN, respectively) were analysed for creatinine and BUN.

Terminal urine samples revealed that SNx rats within the early group (EN) developed albuminuria ([Figure 3.6](#)), with ACR higher than that of the time-matched sham controls ($0.7940: 0.457 - 1.958 \text{ mg}/\mu\text{mol}$ vs. $0.038: 0.020 - 0.051 \text{ mg}/\mu\text{mol}$, $p = 0.014$). In addition, ACR was significantly higher in the SNx rats in the late group (LN, $3.548: 1.548 - 6.130 \text{ mg}/\mu\text{mol}$) when compared to time-matched sham controls (LS, $0.127: 0.049 - 0.281 \text{ mg}/\mu\text{mol}$, $p < 0.001$).



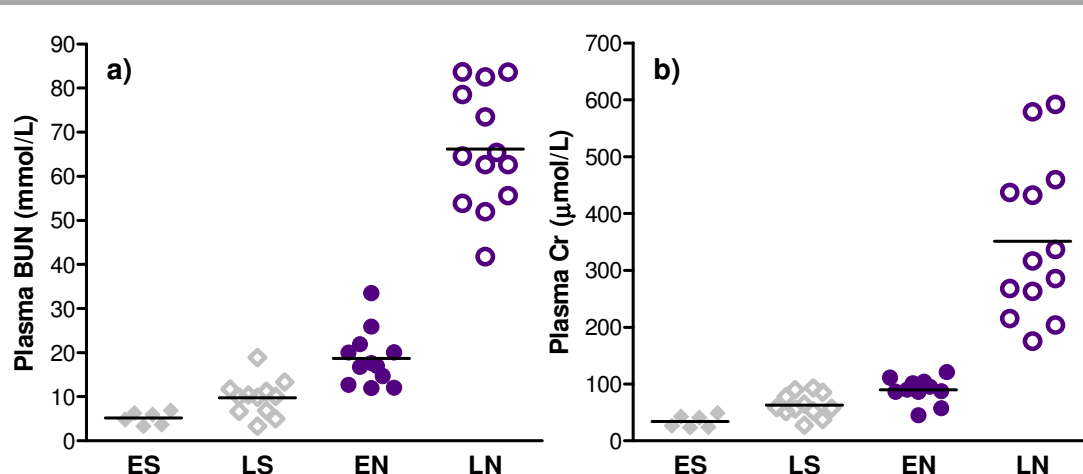


Figure 3.7 Terminal plasma analysed for **(a)** blood urea nitrogen (BUN) and **(b)** creatinine were 5-fold higher in late SNx (LN) animals ($n = 14$) than in time-matched sham controls (LS, $n = 12$, both $p < 0.001$). BUN was significantly higher in the early SNx (EN) group ($p = 0.014$); however the difference in plasma creatinine was not statistically significant ($p = 0.522$). There were no differences between ES and LS groups. Horizontal lines represent group mean

The mass of the remnant kidneys increased substantially ([Figure 3.8](#)) in both EN and LN rats ($123.3 \pm 28.0 \%$, $n = 6$ and $320.4 \pm 36.3 \%$, $n = 8$, respectively). Initial kidney weight was calculated as right kidney weight minus weight of the removed poles. There was no difference in the estimated starting weight of the kidneys from EN (0.97 ± 0.12 g) compared to LN (0.96 ± 0.06 g). Final kidney weights are based on the weight of tissue prior to freezing; samples that were fixed *in situ* were excluded as the process of PFA-fixation artificially increased tissue weight.

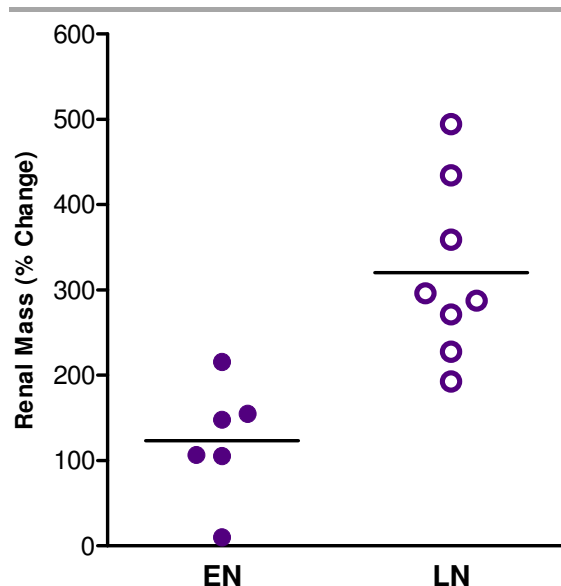


Figure 3.8 The remnant kidney portion increased in mass by 7-8 weeks post-surgery (EN, solid circles: start weight 0.97 ± 0.12 , increased by $123.3 \pm 28.0 \%$) approximately doubling in size. The change was greater in the (near) renal failure group (LN, open circles: start weight: 0.96 ± 0.06 g, $320.4 \pm 36.3 \%$). Line represents group mean.

3.4 Histology

Haematoxylin and eosin (H&E) staining highlighted some of the general structural changes that occurred during the progression of renal failure. There were no clear differences between the ES and LS groups within either cortical ([Figure 3.9, a and b](#)) or medullary sections ([Figure 3.10, a and b](#), respectively). However, there were noticeable changes in EN rats including dilation of the renal tubules ([Figure 3.9, panel c](#), labelled P) and peritubular expansion and hyper-cellularity (black arrow). Within LN cortical sections these changes were more extensive, with widespread tubular distortion, peritubular hyper-cellularity ([Figure 3.9 panel d](#), white star) and the formation of peritubular spaces and tubular casts (C, [Figure 3.9d](#)). There was a clear decrease in the number of intact tubular structures and a high proportion of glomeruli with abnormal appearance (G, [Figure 3.9d](#)).

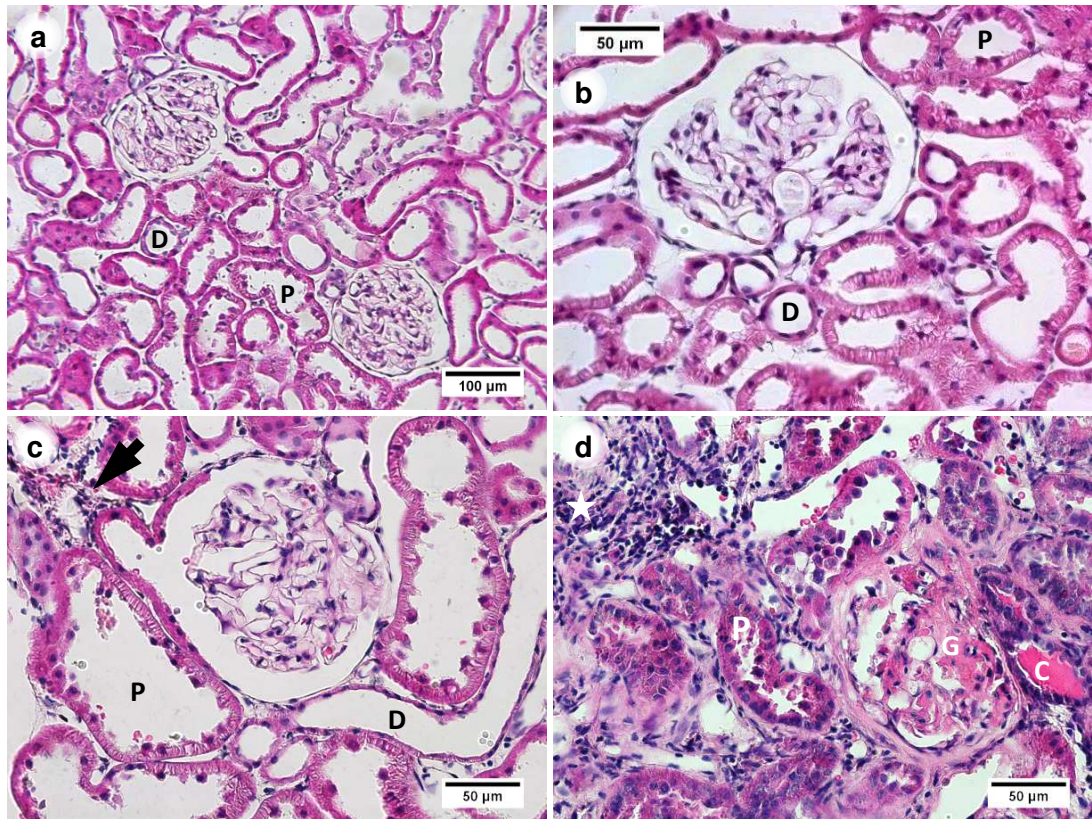


Figure 3.9 Haematoxylin and eosin staining of cortical sections from **(a)** early sham (ES), **(b)** late sham (LS) were packed tightly with proximal (P) and distal (D) tubules. Glomeruli in these sections were uniform and occupied a substantial portion of the Bowman's capsule. The gross structure of the **(c)** early nephrectomy (EN) sections appeared normal. The tubules appeared dilated (P) and there are small areas of sporadic peritubular hyper-cellularity (marked with a black arrow). Changes in the cortex of late nephrectomy (LN) rats **(d)** were extensive, particularly proliferation of cells between the tubules (P), many of which appear to have closed entirely. All images captured at x 40 except panel **a** captured at x 20 magnification.

Changes in renal structure in the EN group were primarily located within the cortex, leaving the structure of the medulla generally intact, at least at the level visible with light microscopy (**Figure 3.10c**, transverse section). Thick (T) and thin (t) limbs from the loop of Henle, collecting tubules (CT) and erythrocyte filled vasa recta (v) are all identifiable. The extent of these changes was not limited to the cortex in the LN group. Gross changes in structure were visible including cellular expansion between the various tubular structures and the formation of peritubular spaces or voids (**Figure 3.10d**).

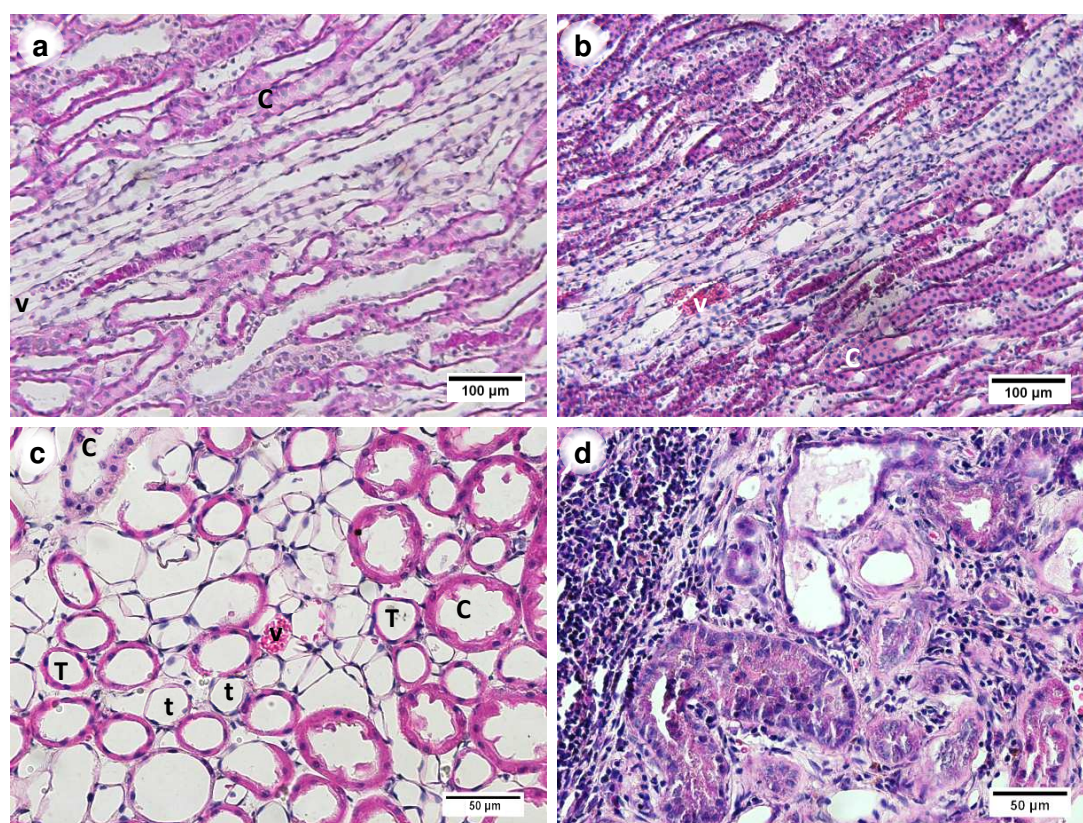


Figure 3.10 Haematoxylin and eosin staining of medullary sections from **(a)** early sham (ES), **(b)** late sham (LS) were packed tightly with parallel bundles of collecting tubules/ducts (C) and vasa recta (V). The gross structure of the **(c)** early nephrectomy (EN) sections generally appeared normal, containing thick (T) and thin (t) limbs from the loop of Henle, collecting tubules (C) and erythrocyte filled vasa recta (v). In contrast changes in the medulla of late nephrectomy (LN) rats **(d)** often made histological identification difficult as voids and sporadic cellular proliferation were common. Panels **a** and **b** are captured at x 20 magnification, whilst panels **c** and **d** are at x 40.

Whilst areas of tissue from EN rats did appear normal there was evidence of fibrotic lesions; these were found predominantly in the form of tubular casts (black arrowhead) and small areas of potentially fibrotic hyper-cellularity (black arrows) within the cortex ([Figure 3.11a](#)). Similar abnormalities were occasionally seen in the medulla (Black arrow, [Figure 3.11b](#)). These lesions were particularly extensive within the cortex of the LN rats where typical gross cortical structure was absent, replaced by voids of varying sizes and areas of disorganised cellular proliferation ([Figure 3.11c](#)).

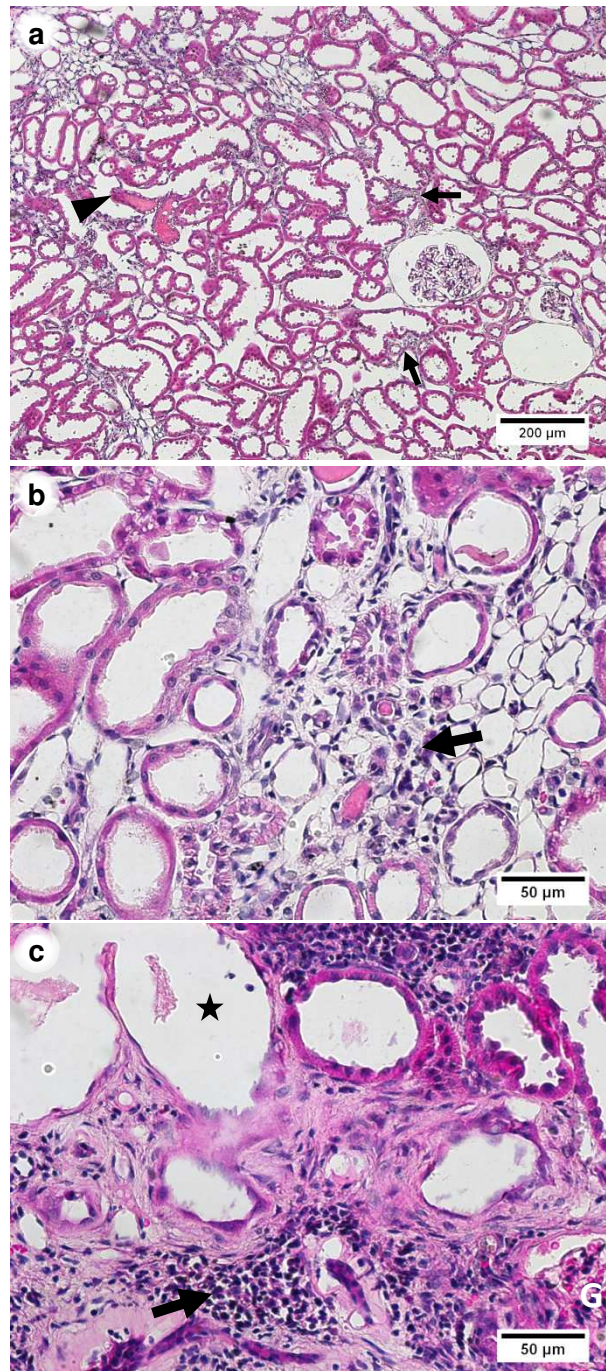
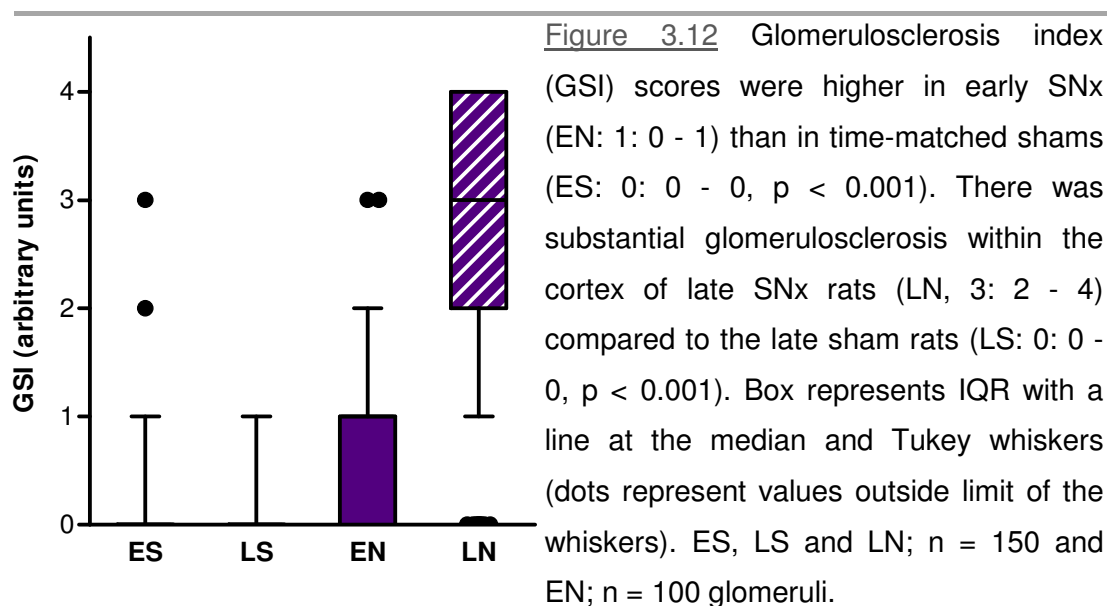


Figure 3.11 Structural changes in the cortex **(a)** and medulla **(b)** of early nephrectomy rats included the formation of tubular casts (arrowhead, panel **a**) and peritubular hyper-cellularity (black arrows panel **a** and **b**). Gross disruption of renal structure in the cortex of late SNx rats **(c)** included areas of peritubular hyper-cellularity (black arrows) and the formation of large voids (star).

3.4.1 Periodic acid Schiff stain for glomerulosclerosis

Glomeruli stained with periodic acid Schiff (PAS) were scored on a glomerulosclerosis index (GSI, 0 - 4, as described in [Section 2.8.3](#)) with results presented as median: IQR ([Figure 3.12](#)). There were no discernible differences between the glomeruli from ES (0: 0 - 0, panel (a), [Figure 3.13\(1\)](#)) and LS (0: 0 - 0, panel (c), [Figure 3.13\(2\)](#)) rats, with no obvious glomerulosclerotic lesions present within either group (p). Changes in the EN glomeruli were noticeable (1: 0 - 1, [Figure 3.13\(1\)](#) panel (b)) and significant when compared to the time matched controls ($p < 0.001$). The PAS staining highlighted extensive (panel (d), [Figure 3.13\(2\)](#)) and widespread glomerulosclerosis in the renal cortex of LN animals (3: 2 - 4, [Figure 3.12](#), $p < 0.001$ when compared with LS or EN rats), including full closure of some glomeruli (42 out of 150 glomeruli had a GSI score of 4 in the LN group). GSI scoring data were analysed using a Kruskal-Wallis test.



Fine staining of the basement membrane (deep pink) is clearly visible within the glomeruli of ES ([Figure 3.13\(1\)](#)a black arrowhead) and LS rats ([Figure 3.13\(2\)](#)(c), white arrow). This staining was visible but less defined in the EN rats ([Figure 3.13\(1\)](#)b, black arrowhead) and was, in places, replaced by patches of PAS-positive material ([Figure 3.13\(1\)](#)b, white arrow). These changes were further developed in the LN rats in which very little 'typical' glomerular structure remained and, where still visible, the basement membrane appeared thickened ([Figure 3.13\(2\)](#)d, black arrow). There are areas of sclerosis clearly visible within these glomeruli, identified by dense deep pink PAS stain in the absence of visible capillary loop structure ([Figure](#)

3.13(2)d, white arrow). In addition the exterior surface of the Bowman's capsule also stained with a much greater intensity in sections from the LN group.

Further changes were noticeable in the surrounding cortical structure. The renal tubules (proximal convoluted tubule, PCT and distal convoluted tubule (DT)) were densely packed with very little space between them in both the ES (Figure 3.13(1)a) and LS rats (Figure 3.13(2)c). The brush border on the apical surface of the PCT cells (luminal surface) in both ES and LS rats stained pink (ES: Figure 3.13(1)a and LS: Figure 3.13(2)c, black arrow) as did the basement membrane of both the PCT and DT (basal surface, fine staining, not labelled). In the EN group the PCT retained a distinct brush border (Figure 3.13(1)b, black arrow) and gross tubule structure was generally intact. There was evidence of peritubular hyper-cellularity (white arrowhead, Figure 3.13(1)b) and the occasional presence of tubular casts (white star, Figure 3.13(1)b). Further to these changes, the kidneys of LN rats showed gross disruption of renal structure and extensive peritubular hyper-cellularity (Bottom right hand corner, Figure 3.13(2)d). Dilatation of the tubules was also evident, along with loss of the PCT brush border (labelled as P), formation of peritubular spaces (marked with a black star) and increased BM deposition (white arrowhead, Figure 3.13(2)d).

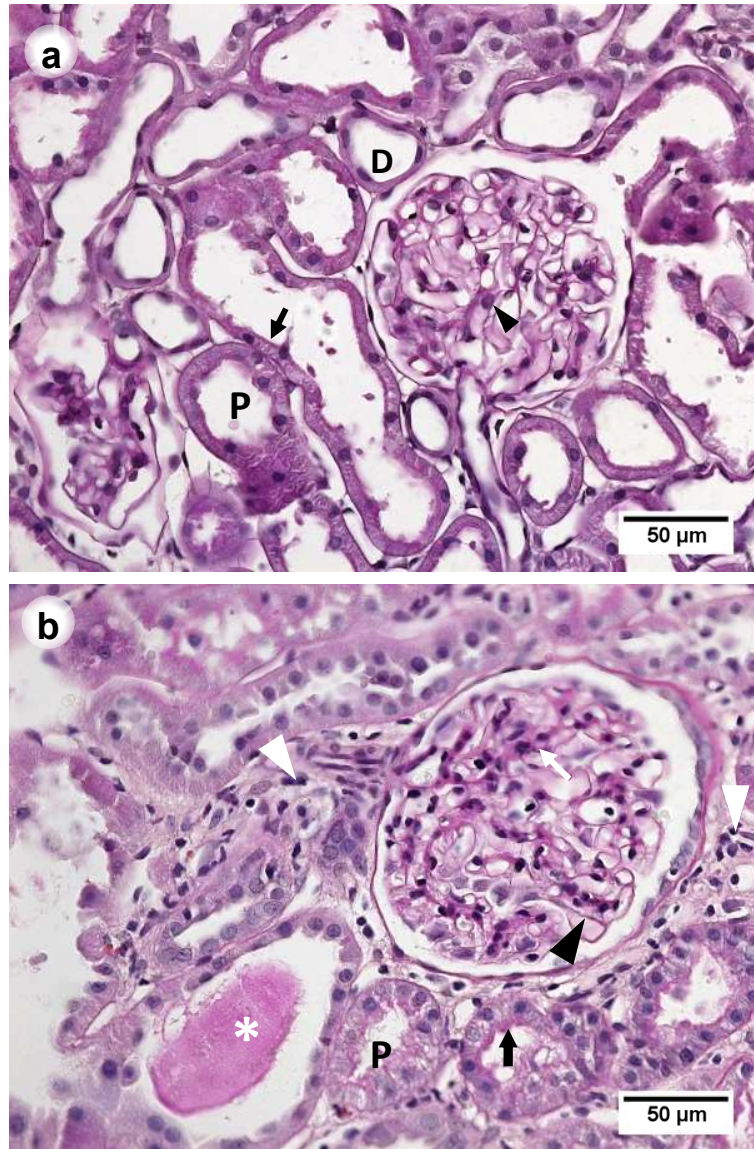


Figure 3.13(1) PAS stained glomeruli from **(a)** early sham (ES) and **(b)** early SNx (EN). Fine staining of the glomerular basement membrane (black arrowheads) is clear within glomeruli from both ES **(a)** and EN **(b)** rats. Proximal convoluted tubules (P, with apical brush border, black arrow, panel **a**) and distal convoluted tubules (D) in the ES rats had clear defined structures, and whilst the P of the EN rats were less defined the apical/luminal brush border was still visible (black arrow, panel **b**). Abnormalities had started to appear in the EN tissues **(b)** such as peritubular hypercellularity (white arrowheads), tubular casts (white star) and focal glomerulosclerotic lesions (white arrow).

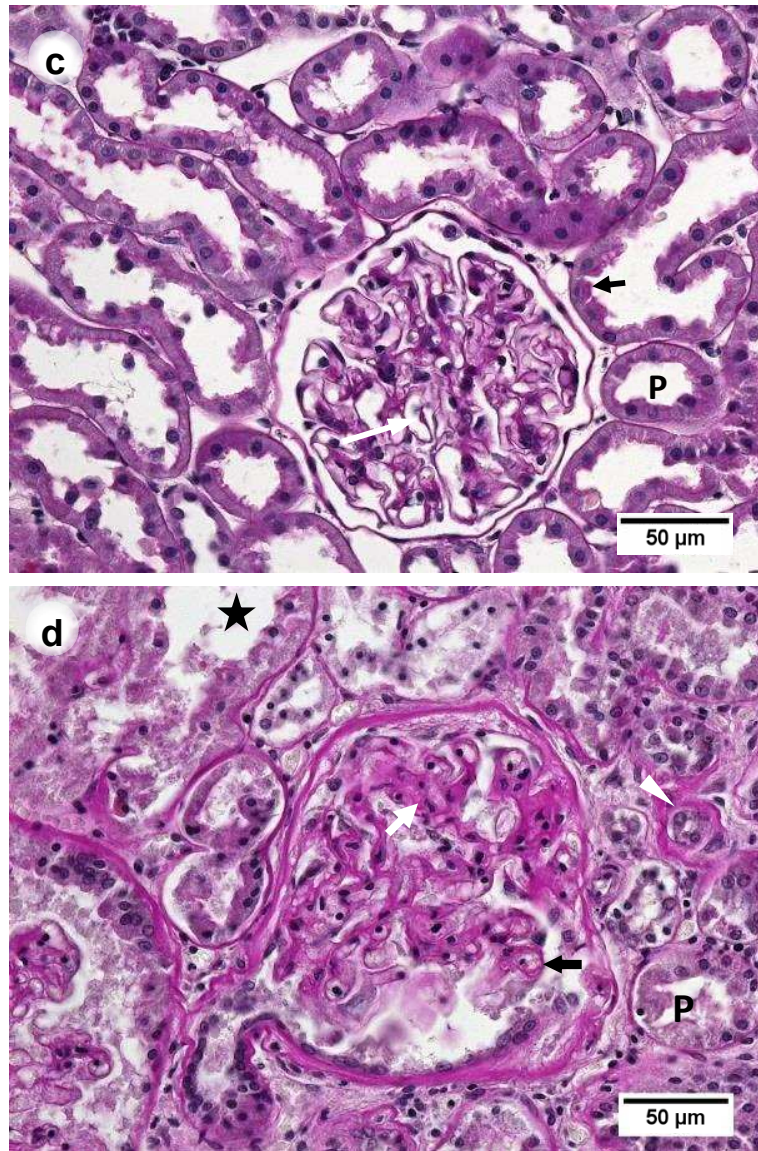


Figure 3.13(2) Fine staining of the glomerular basement membrane (GBM) was clear in PAS stained glomeruli from **(c)** late sham (LS, white arrow) but not in **(d)** late SNx (LN) rats. In tissues from the LN group **(d)** sections of remaining GBM appeared thickened (black arrow) and there were considerable glomerulosclerotic lesions (white arrow). Changes in gross tubular structure were apparent; LS rats had a defined brush border in the proximal convoluted tubule (P, panel **c**, black arrow) that was disrupted in the LN rats (panel **d**, P). In the LN tissue **(d)** there was also tubular expansion (black star), more prominent tubular basement membranes (white arrowhead) and peritubular hyper-cellularity.

3.4.2 Masson's Trichrome Stain for Collagen

Masson's trichrome (MTC) staining of the renal cortex highlighted changes in collagen distribution as renal disease progressed. In ES and LS kidneys the blue component staining was minimal ([Figure 3.14 a and b](#)), generally confined to areas surrounding arteries/arterioles and the surface of the Bowman's capsule. There was more pronounced staining within sections from EN kidneys; with increased staining visible around the renal capsule ([Figure 3.14c](#)). Aniline blue staining was particularly prominent in LN sections, particularly within the glomeruli. Increased blue collagen staining was also seen around the tubules and around the peritubular spaces ([Figure 3.14d](#)). Tubular casts seemed to stain strongly with both aniline blue and beibrich-scarlet acid fuchsin stains, although this appeared to be predominantly non-specific.

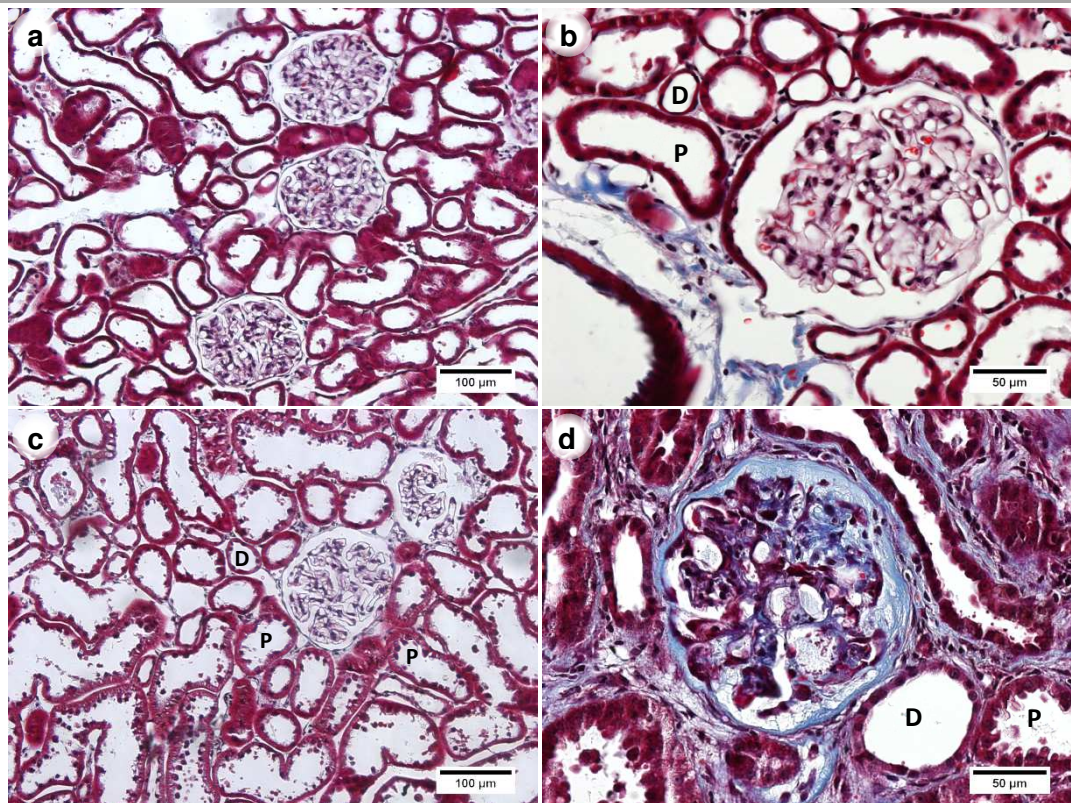


Figure 3.14 Masson's trichrome staining of the renal cortex of **(a)** early sham (ES), **(b)** late sham (LS), **(c)** early nephrectomy (EN) and **(d)** late nephrectomy rats (LN). Blue collagen staining was faint in ES, LS and EN rats and typically localised to the renal arteries and the exterior surface of the Bowman's capsule. In contrast changes in blue staining was intense and wide spread in the cortex of LN rats **(d)** often appearing to fill the Bowman's space and surrounding the glomeruli. Blue staining was also prominent in areas of peritubular proliferation adjacent to the proximal (P) and distal (D) tubules. Panels **a** and **c** are captured at x 20 magnification, whilst panels **b** and **d** are at x 40.

Within the medulla (**Figure 3.15**) there was minimal blue staining in the **(a)** ES, **(b)** LS and **(c)** EN sections, and whilst there was widespread staining within the **(d)** LN medullary sections some of the characteristic structures remained identifiable. Collecting ducts (stained red) were visible but were surrounded by an intense blue staining pattern which was not seen in the other groups.

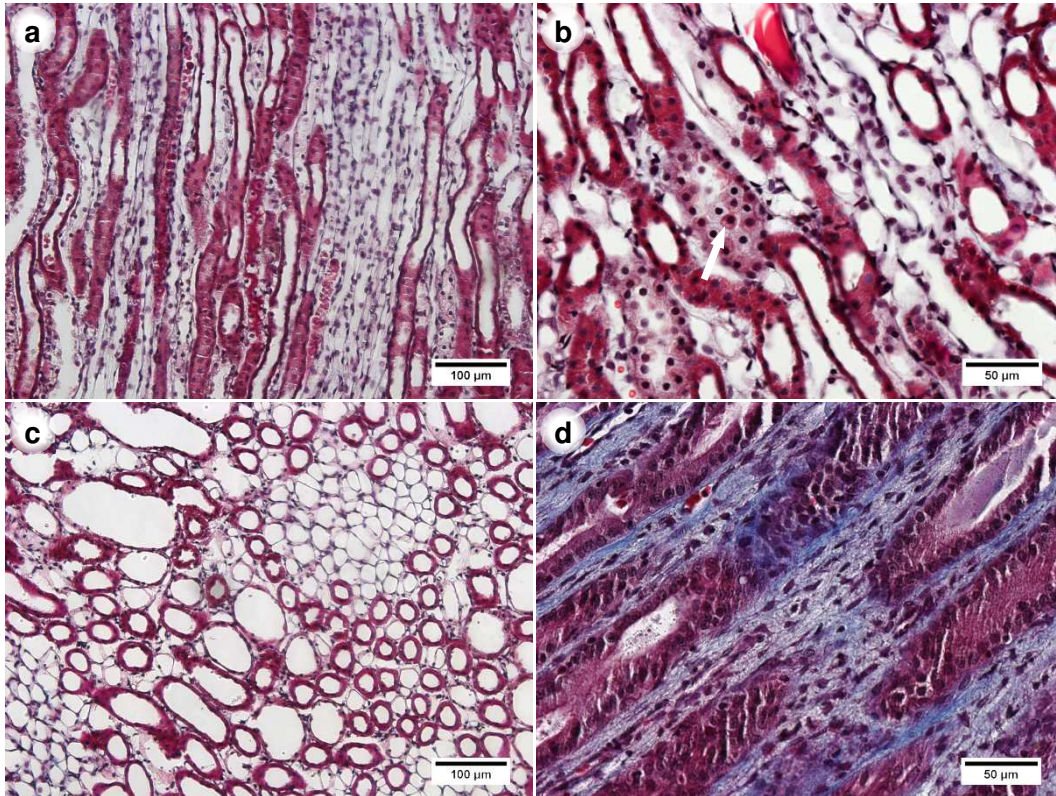


Figure 3.15 Masson's trichrome staining of the renal medulla of **(a)** early sham (ES), **(b)** late sham (LS), **(c)** early nephrectomy (EN) and **(d)** late nephrectomy rats (LN). Blue collagen staining was faint or absent in ES, LS and EN rats. In contrast blue staining was intense and wide spread in the medulla of LN rats **(d)** particularly around the collecting ducts (stained dark red). Panels **a** and **c** are captured at x 20 magnification, whilst panels **b** and **d** are at x 40.

3.5 Immunohistochemical staining of basement membrane components

In addition to MTC staining for collagen, antibodies were used to allow the specific staining of basement membrane components; collagen (IV) and laminin (pan β). In the cortex of sham rats (panels **a** and **b**) the distribution of staining was similar for both proteins. Staining was localised to the basement membranes of the proximal and distal tubules and the surface of the glomerular capsule in the cortex ([Figure 3.16](#) and [3.17](#), collagen IV and laminin- β respectively); staining was also seen in the glomerular basement membranes, although this was more prominent in sections stained with the collagen IV antibody than with the laminin- β . Tissues from EN rats stained with a distribution and intensity highly comparable to that of the sham control rats for both collagen IV ([Figure 3.16c](#)) and laminin- β ([Figure 3.17c](#)). In contrast, staining for both collagen IV ([Figure 3.16d](#)) and laminin- β ([Figure 3.17d](#)) was more extensive and more intense in the cortex of LN rats. The renal tubules were disrupted and surrounded by areas of cellular hypertrophy; these peritubular areas often stained for collagen IV and to a lesser extent for laminin- β . Within some tubules casts could be seen, and these stained positively for collagen IV ([Figure 3.16d](#)). Within the glomeruli (G) the basement membranes were much less defined, with areas of strong atypical staining occasionally noted ([Figure 3.17d](#)).

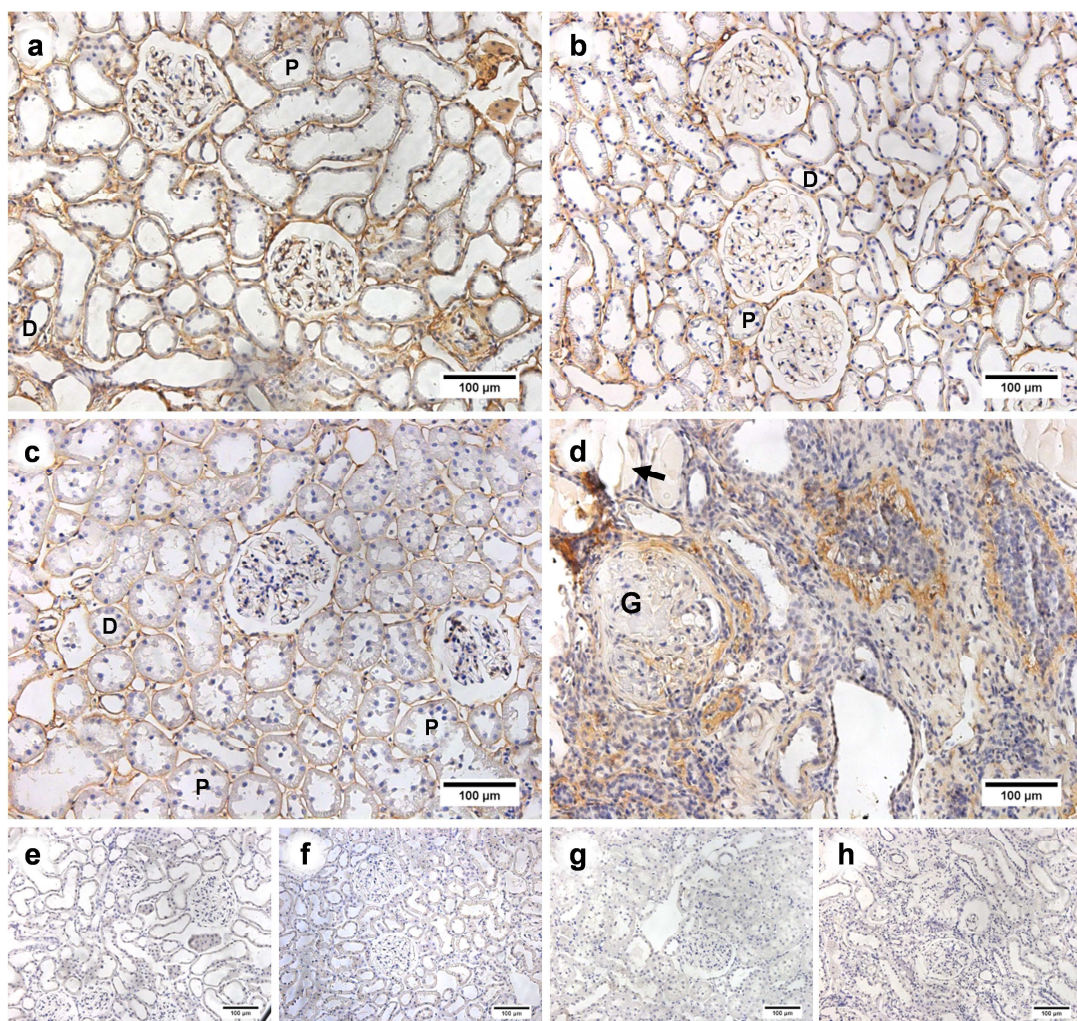


Figure 3.16 Immunohistochemical staining of collagen IV in the cortex of **(a)** early sham (ES), **(b)** late sham (LS), **(c)** early SNx (EN) and **(d)** late SNx (LN) rats. Staining was typically seen in the basement membranes of the proximal (P) and distal (D) tubules, around the Bowman's capsule and associated with the glomerular basement membrane. The staining distribution and intensity was retained in the EN rats **(c)**. Within the cortex of LN rats diffuse staining was seen throughout the cortex, with increased staining intensity around some tubules. The general structure of the tissue was grossly disrupted. **(e - h)** Representative negative controls (primary antibody omitted) from ES, LS, EN and LN, respectively. All images captured at x20 magnification with 100 µm scale bar.

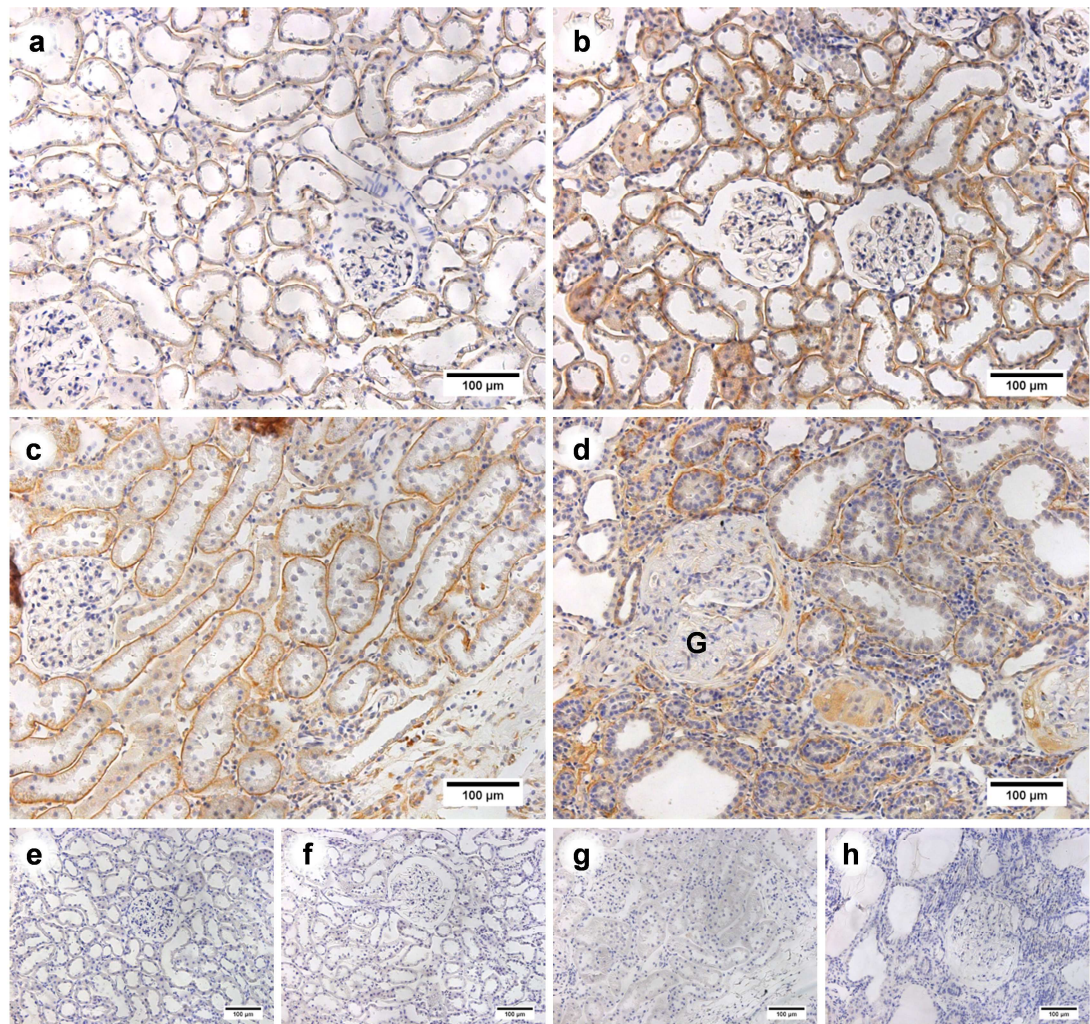


Figure 3.17 Immunohistochemical staining of laminin- β in the cortex of **(a)** early sham (ES), **(b)** late sham (LS), **(c)** early SNx (EN) and **(d)** late SNx (LN) rats. Staining was typically seen in the basement membranes of the proximal (P) and distal (D) tubules and around the Bowman's capsule; staining in the LS group appeared more intense. The staining pattern was similar in the EN rats **(c)** but with greater intensity compared to the time-matched shams. Within the cortex of LN rats diffuse faint staining was seen throughout the cortex, with increased staining intensity around the basement membranes of the renal tubules. The general structure of the tissue was severely disrupted. **(e - h)** Representative negative controls (primary antibody omitted) from ES, LS, EN and LN, respectively. All images captured at x20 magnification with 100 μ m scale bar.

In the medulla of sham rats (ES and LS) staining for collagen IV ([Figure 3.18](#)) and laminin- β ([Figure 3.19](#)) was less intense than in the cortex. For both proteins the staining pattern appeared to be localised to the basement membranes of tubular structures (collecting tubules and loops of Henle). This pattern was also seen in the

EN rats, with staining for laminin- β (Figure 3.19c) and collagen IV (Figure 3.18c) localised to the basement membranes and with a similar staining intensity to that of the time-matched sham controls (ES). Changes in the late SNx were more obvious and more complex. Staining for collagen IV was more widespread and of greater intensity than in any other group (Figure 3.18d), appearing as quite intense but diffuse staining between the inner medullary collecting ducts. In contrast, medullary staining for laminin- β was less extensive and generally associated with plaques/casts (Figure 3.19d).

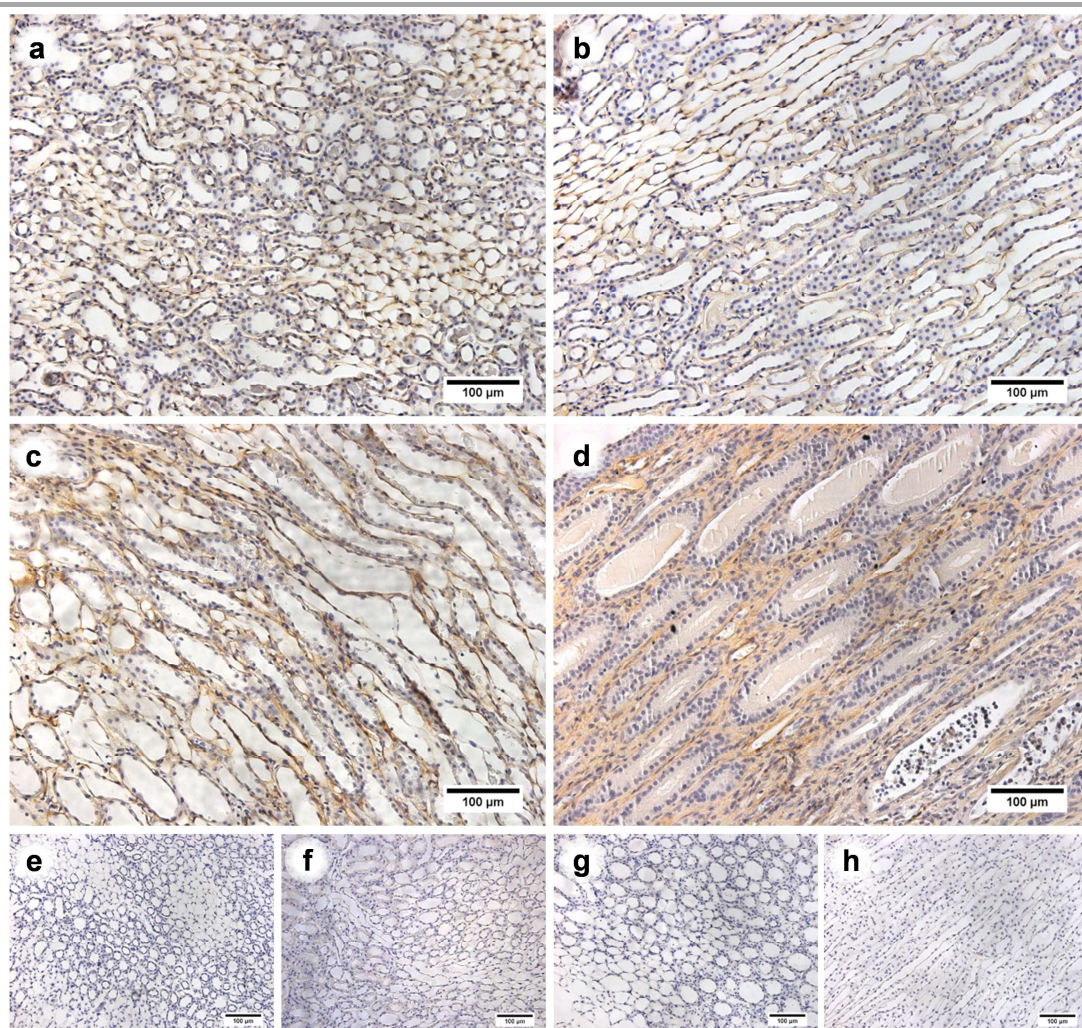


Figure 3.18 Immunohistochemical staining of collagen IV in the renal medulla of **(a)** early sham (ES), **(b)** late sham (LS), **(c)** early SNx (EN) and **(d)** late SNx (LN) rats. Staining was typically seen in the basement membranes of the collecting tubules and loops of Henle. The staining pattern was similar in the EN rats **(c)**. Widespread staining was seen in the medulla of LN rats **(d)**. **(e - h)** Representative negative controls (primary antibody omitted) from ES, LS, EN and LN, respectively. All images captured at x20 magnification with 100 μ m scale bar.

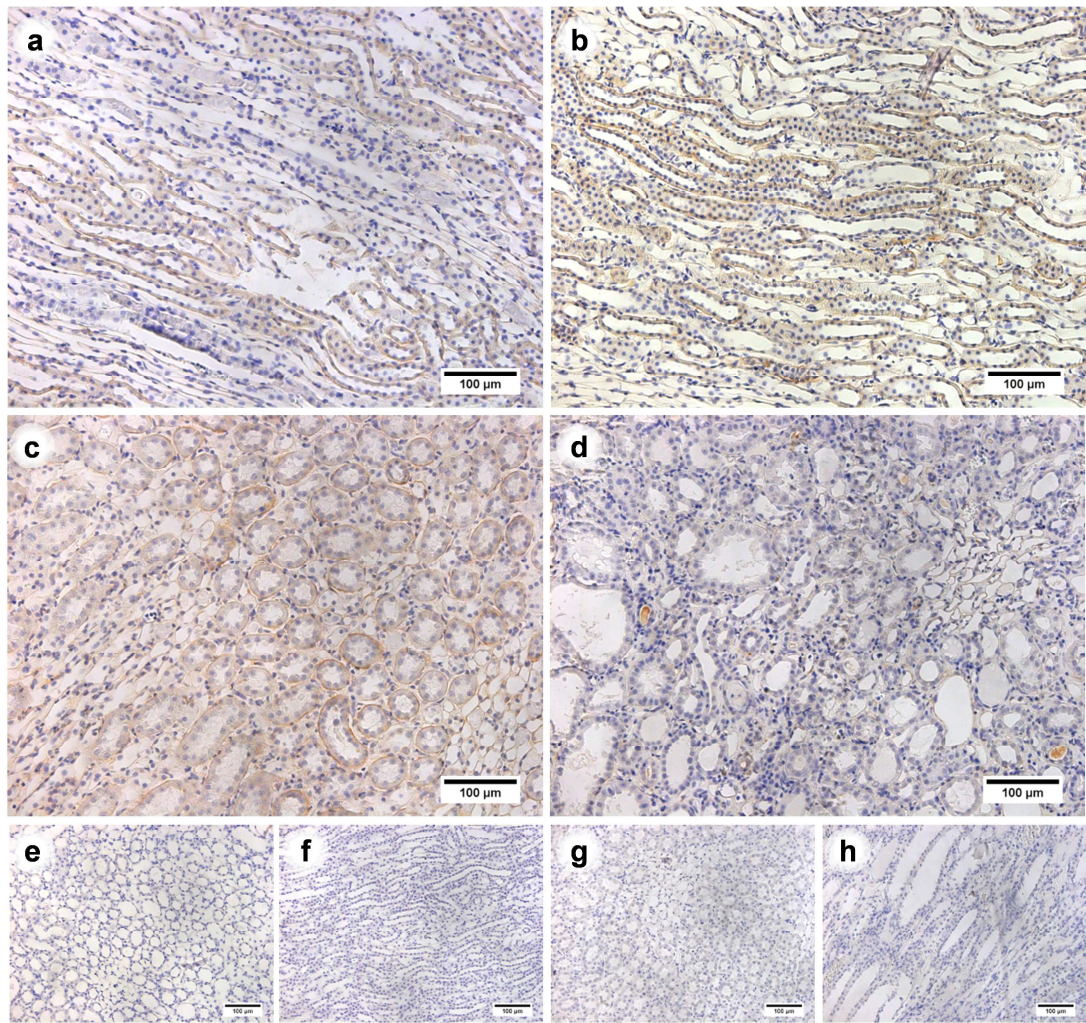


Figure 3.19 Immunohistochemical staining of laminin- β in the renal medulla of **(a)** early sham (ES), **(b)** late sham (LS), **(c)** early SNx (EN) and **(d)** late SNx (LN) rats. Staining was typically seen in the basement membranes of the collecting tubules and loops of Henle. This staining pattern was also seen in the medulla of EN rats **(c)**. In the medulla of LN rats **(d)** staining tended to be less intense and typically associated with small casts. **(e - h)** Representative negative controls (primary antibody omitted) from ES, LS, EN and LN, respectively. All images captured at x20 magnification with 100 μ m scale bar.

3.6 Staining of UII, URP and UT by immunohistochemistry

UII-immunoreactivity encompasses the mature UII and URP peptides as staining was carried out using an antibody raised against the conserved cyclic region of flounder UII, which is common to both peptides. The antibody has also been shown to detect pro-UII. The high degree of structural homology between UII and URP (all species) means that it is not possible to differentiate between the two peptides with this, or any commercially available antibody.²¹⁶

3.6.1 UII-immunoreactive staining

In both early ([Figure 3.20a](#)) and late ([Figure 3.20b](#)) sham rats UII-immunoreactivity was relatively faint and diffuse. Within cortical sections the staining was most intense within the epithelial cells of the proximal convoluted tubules (P). Further staining was also visible in the distal tubules. Staining appeared more intense in EN rats ([Figure 3.20c](#)) which presented with generally intact cortical structure and staining was localised in a manner similar to the sham controls ([Figure 3.20a](#) and [b](#)). Additional faint staining was noted within the glomeruli and in areas of proliferation. UII-immunoreactive staining was particularly intense in the late SNx rats ([Figure 3.20d](#)), again with the most intense staining seen within the epithelial cells of the tubules (arrows). There was additional staining visible within glomeruli and in areas of proliferative expansion (white star).

Within the medulla ([Figure 3.21](#)) UII-reactive staining was seen in the epithelial cells of collecting ducts and continued to the inner medullary collecting ducts in all groups. UII-reactive staining in the EN rats ([Figure 3.21c](#)) appeared more intense than in the ES rats ([Figure 3.21a](#)) and whilst generally localised within the (inner medullary) collecting ducts there was staining in the surrounding cells. Similarly in the late cohorts the staining in the SNx group (LN, [Figure 3.21d](#)) appeared more intense and more widespread than in the sham counterparts (LS, [Figure 3.21b](#)). Negative control slides (primary antibody omitted) were included for all groups and representative sections are presented for both cortex ([Figure 3.20e - h](#)) and medulla ([Figure 3.21e - h](#)).

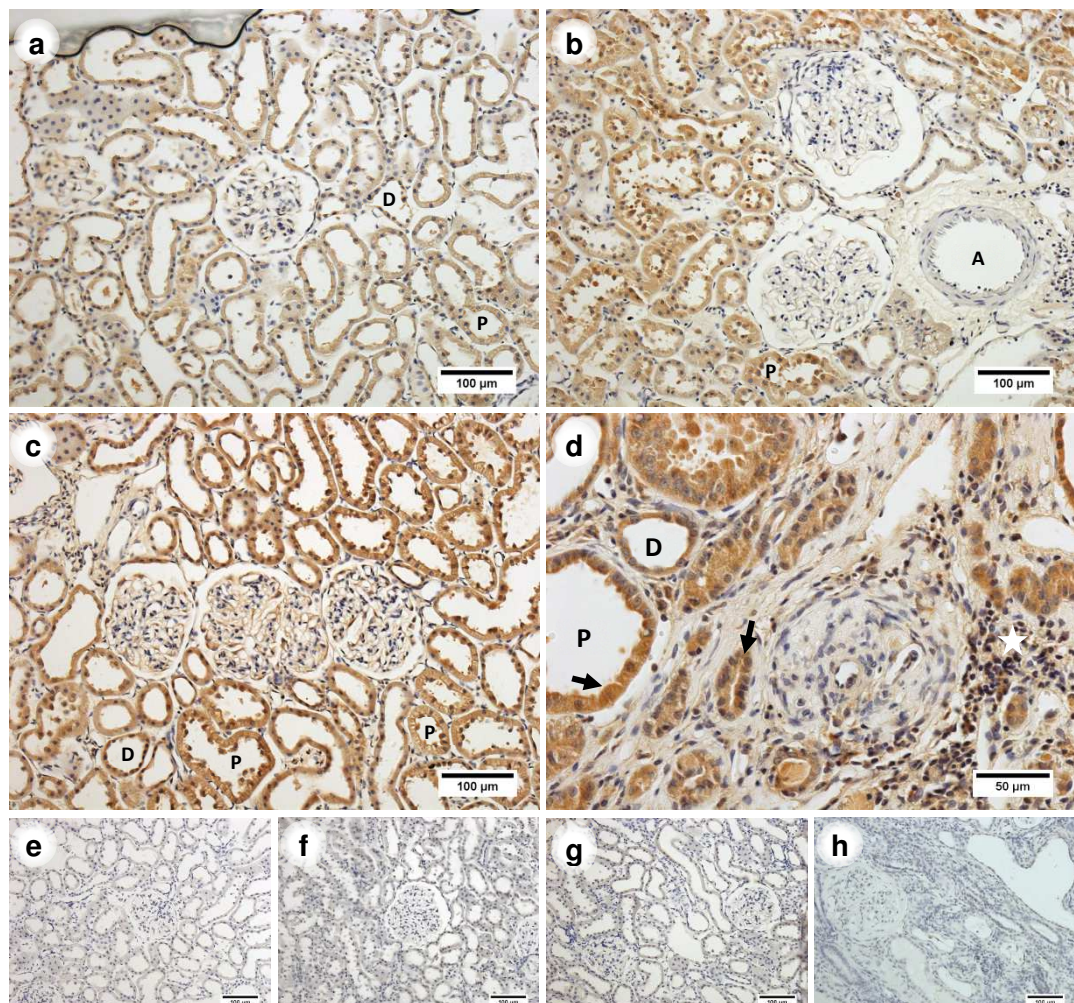


Figure 3.20 Immunohistochemical staining of urotensin II reactive proteins in the cortex of **(a)** early sham (ES), **(b)** late sham (LS), **(c)** early SNx (EN) and **(d)** late SNx rats. Staining was generally diffuse and localised to the cytoplasm of epithelial cells of the proximal convoluted tubules (P) with some staining also seen in the distal tubules (D). The staining pattern was retained in the ES rats **(c)** but with greater intensity and additional faint staining visible within the glomeruli. Within the cortex of LN rats strong staining was seen in the tubular epithelia (arrows), further diffuse staining was seen within the glomeruli and in areas of peritubular hypercellularity (white star). **(e - h)** Representative negative controls (primary antibody omitted) from ES, LS, EN and LN, respectively. All images captured at x20 magnification with 100 μ m scale bar, except **(d)** at x40 with 50 μ m scale bar.

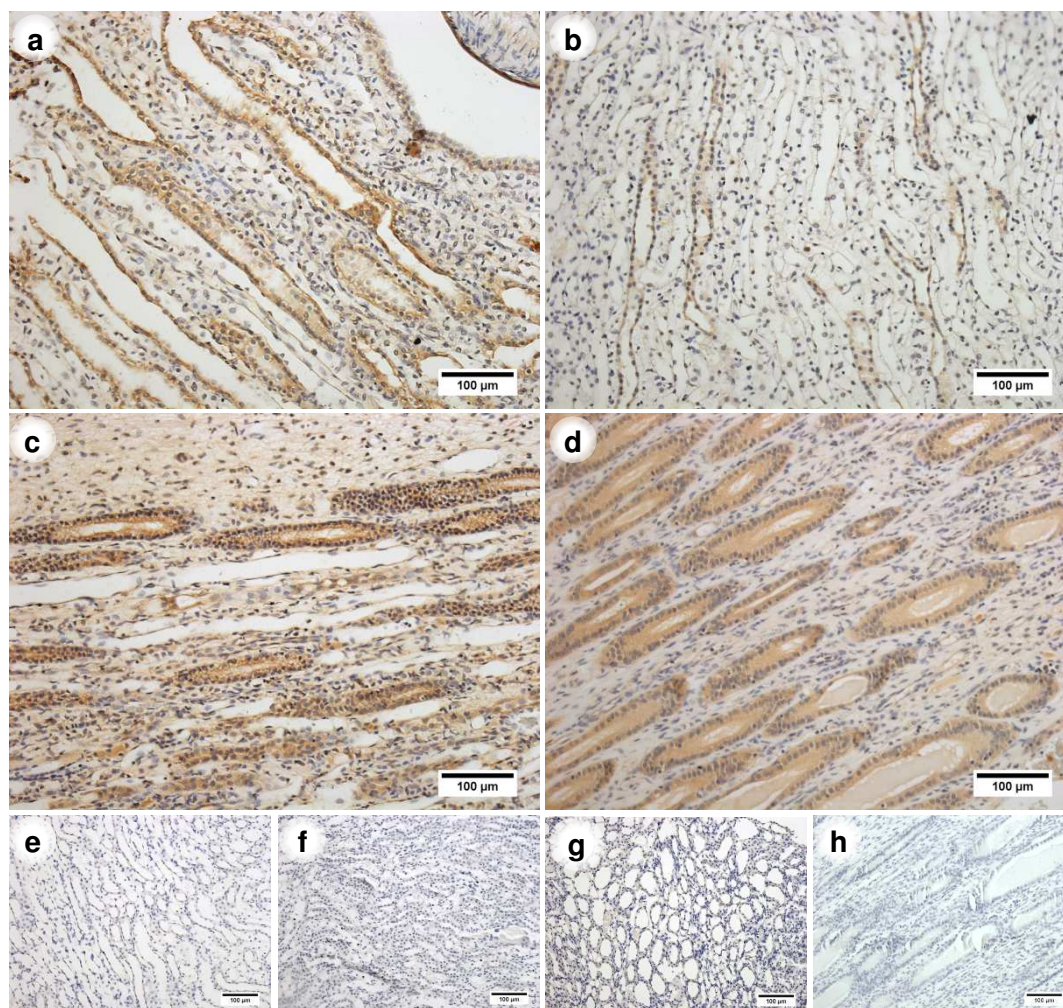


Figure 3.21 Immunohistochemical staining of urotensin II reactive proteins in the medulla of **(a)** early sham (ES), **(b)** late sham (LS), **(c)** early SNx (EN) and **(d)** late SNx rats was typically localised within the cytoplasm of collecting duct epithelial cells. In the EN (c) and LN (d) the staining was similarly localised but tended to be more intense; additional faint staining was visible in the surrounding interstitium. **(e - h)** Representative negative controls (primary antibody omitted) from ES, LS, EN and LN, respectively. All images captured at x20 magnification with 100 µm scale.

3.6.2 Immunohistochemistry for UT receptor

The most intense staining for the Ull receptor (UT) is predominantly localised within the collecting ducts of the medulla ([Figure 3.23](#)) with very little staining seen in the cortex ([Figure 3.22](#)) of ES (**a**), LS (**b**) or EN (**c**) rats. In contrast LN rats presented with staining for UT in cortical regions ([Figure 3.22d](#)), typically seen within areas of peritubular hypertrophic expansion (arrows) and within some cells in the renal tubule structures. Medullary staining was most intense in the LN cohort, where staining was associated with the apical membrane ([Figure 3.23d](#)); in the other ES and LS groups staining was clearly localised to the collecting ducts, and the less intense staining appeared to form a punctate pattern ([Figure 3.24a](#) and **b**). In these groups staining was not distributed equally within all collecting duct cells. Areas within the medulla of LN rats sometimes presented with particularly intense UT staining outside of the collecting ducts; this staining appears to be associated with the thin limbs (arrows) and surrounding areas of hypertrophy ([Figure 3.24c](#)).

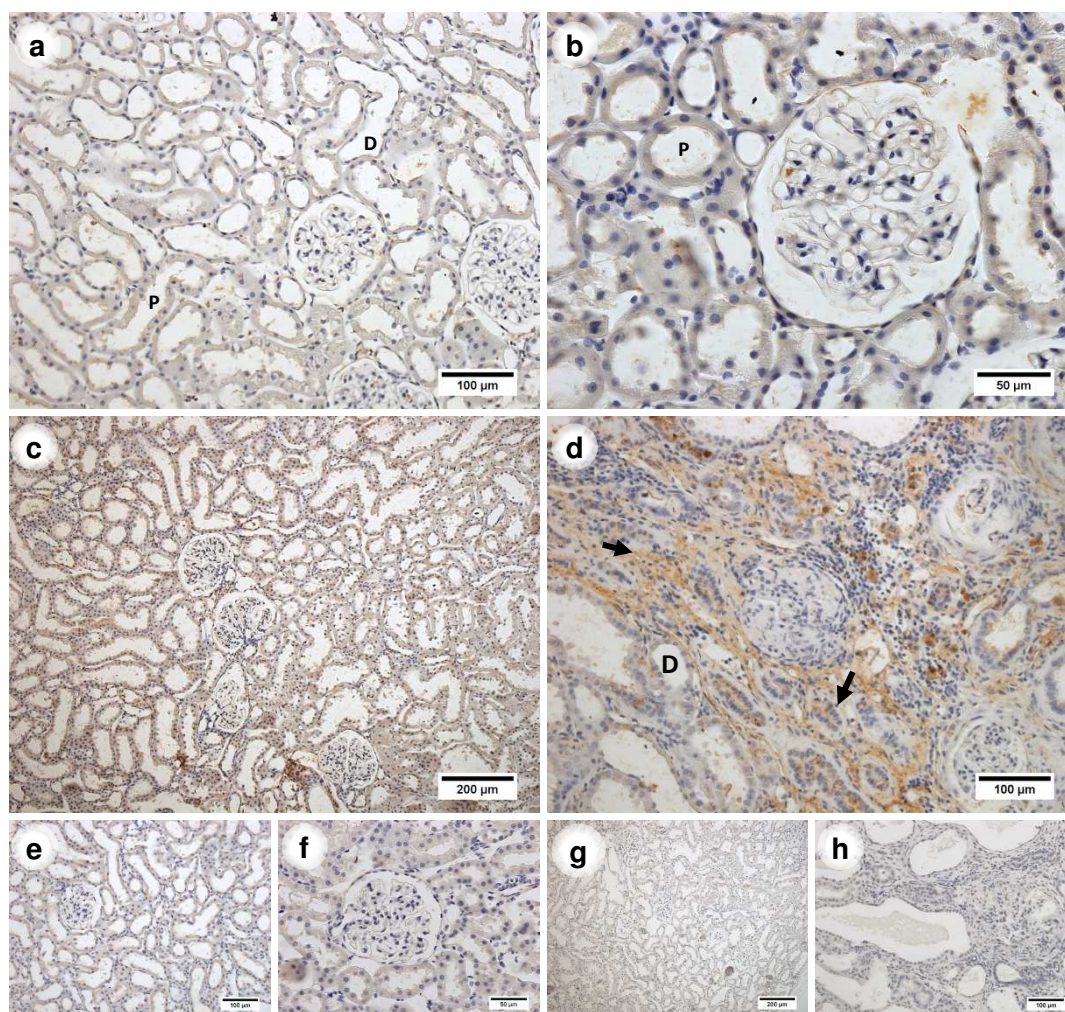


Figure 3.22 There was little evidence of immunohistochemical staining for the urotensin II receptor (UT) in the cortex of **(a)** early sham (ES) or **(b)** late sham (LS) rats. In the SNx groups staining was more pronounced, appearing diffuse in both the early SNx (EN) **(c)** and late SNx (LN) **(d)** rats. More intense staining was seen in the LN cohort and was most pronounced in areas of peritubular hyper-cellularity (arrows). **(e - h)** Representative negative controls (primary antibody omitted) from ES, LS, EN and LN, respectively. Images captured at; x40 magnification with 50 μm scale bar **(b, f)**, x20 magnification with 100 μm scale bar **(a, d, e and h)** or x10 magnification with 200 μm scale bar **(c, g)**.

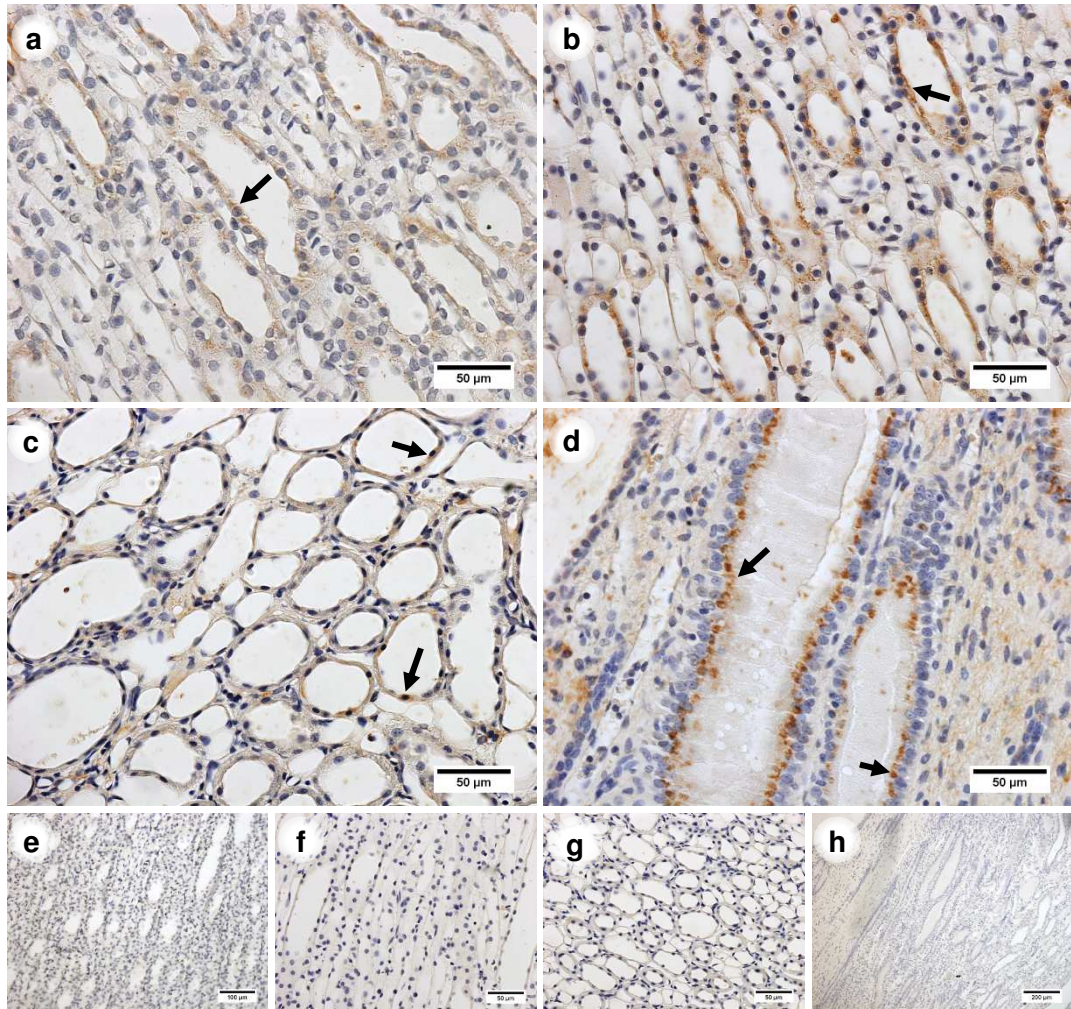


Figure 3.23 Immunohistochemical staining of the urotensin II receptor (UT) in the medulla of **(a)** early sham (ES), **(b)** late sham (LS), **(c)** early SNx (EN) and **(d)** late SNx (LN) rats was typically localised within the collecting duct epithelial cells (arrows). In the LN group **(d)** the staining was localised in a pattern similar to that of the time-matched shams but tended to be more intense, with pronounced apical distribution and additional faint staining was visible in the surrounding cells. **(e - h)** Representative negative controls (primary antibody omitted) from ES, LS, EN and LN, respectively. All images captured at x40 magnification with 50 µm scale bar, except **(e)** at x 20 and **(h)** at x10 with 100 µm and 200 µm scale bars, respectively.

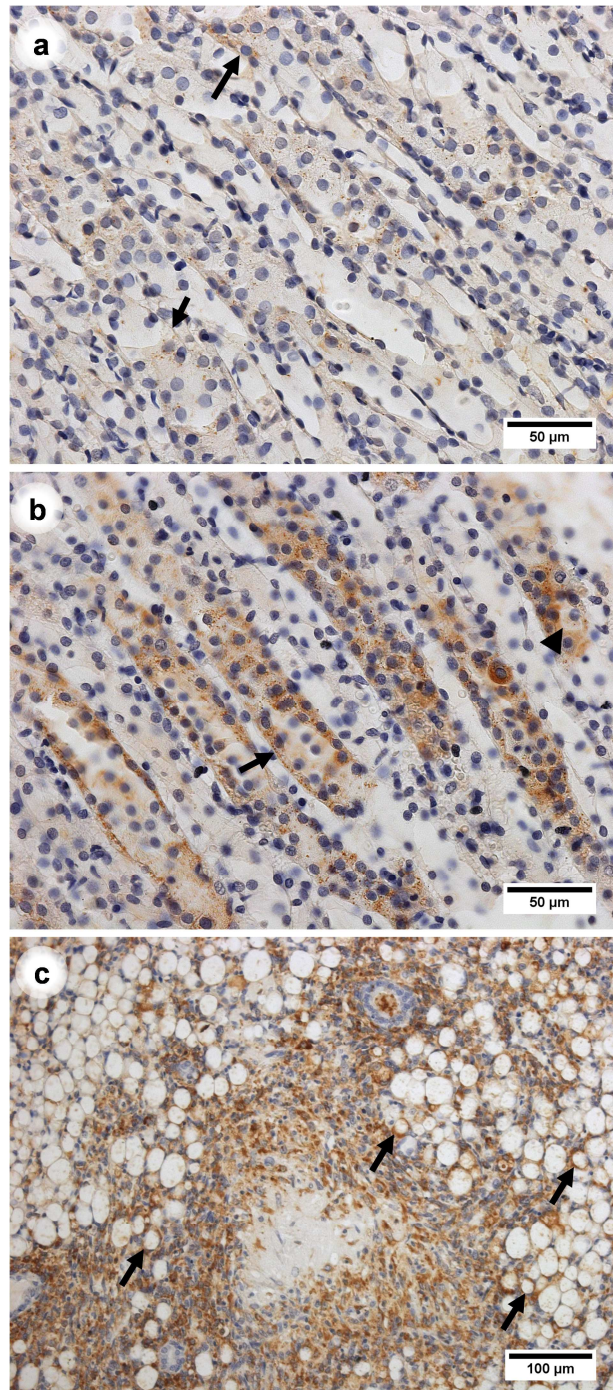


Figure 3.24 UT staining in appeared punctate in the collecting ducts of **(a)** early sham and **(b)** late sham rats (arrows). This staining was not uniformly distributed within the cells of the collecting duct **(b, arrowhead)**. **(c)** Intense staining within the medulla of late SNx rats is associated with the thin limbs of the loop of Henle (arrows) and accompanied by staining in the surrounding abnormal (fibrotic) tissue.

4: Discussion - Progression of chronic kidney disease in the 5/6th SNx rat

The 5/6th SNx is a previously validated model of chronic renal dysfunction, culminating in renal failure.^{177,266} However, prior to this study the model had not been established in this laboratory. As a result it was necessary to characterise the physiological progression of the disease fully prior to any experimental interventions. The physiological data demonstrated that the 5/6th SNx model could be set up with minimal variation in the fraction of renal mass removed and produced progressive renal dysfunction characterised by increasing albuminuria, decreased urinary concentrating capacity with concurrent, progressive raised systolic blood pressure.

The rate of disease progression was variable, which is comparable to previous studies using renal mass reduction as a method of inducing CKD.¹⁷⁹ This is also reflective of CKD within the human population where the rate of disease progression is dependent upon a myriad of co-factors including co-morbidities (such as hypertension, dyslipidaemia and diabetes), body weight and age. As a result of this variability there is an emphasis on clinical monitoring for progression markers and aggressive management of co-morbidities; in particular diabetes and hypertension.^{52,313}

The proportion of renal mass removed was highly consistent (73.6 ± 3.5 %, $n = 30$, mean \pm SD) across both SNx groups. Although the fraction removed is slightly below the 83.3 % required for an exact 5/6th resection it is comparable to other studies using this model.^{314,315} It is also important to consider that there will be variability in the tissue death that occurs at the cut faces (estimated at 100 mg) as well as the size difference between the left and right kidney and potential tissue growth of the right kidney between the procedures when considering the calculation applied to estimate the reduction in renal mass ([Equation 2.1](#)). Refinement of the procedure resulted in very few cases of acute renal failure. In the rats where acute renal failure occurred the reduction in renal mass was near to 83.3 % (75.5 and 85.0 %). Whilst the degree of renal tissue removed will ultimately influence disease progression consistency is more important than the exact reduction, providing the surgery removes sufficient tissue to induce progressive renal disease without causing acute failure. The work was ultimately successful in meeting this aim.

Despite the consistency in renal mass reduction the progression of CKD following the 5/6th SNx surgery was variable, with time to (near) renal failure (RF) ranging from 16 to 44 weeks. This degree of variation was an expected feature of the model, with rate of progression known to be affected by co-factors such as the degree of ischaemia within the remnant kidney and subsequent hypertension.^{179,180,316} However, time to failure at 30.9 ± 8.5 weeks (Mean \pm SD) and the steady decline in numbers was not different from the expected survival time for this model.¹²⁰

Data collection, with the exception of weight, began two weeks post-surgery to allow recovery before the increased handling required for sample collection procedures. For reference; time zero (t = 0) is the day of procedure 2 (right nephrectomy or the equivalent sham procedure in control animals, as described).

4.1 Initial phase

Following recovery from procedure two the rates of post-operative complications and acute renal failure (ARF) were extremely low (2.1 % and 6.7 %, respectively). In these initial 6 - 8 weeks physiological data showed only minor deviation from that of the sham controls. Weight gain following surgery was similar across all groups and towards the end of the period the SNx groups presented with moderate but significant increases in systolic blood pressure (SBP) and urinary albumin creatinine ratio (uACR). In contrast blood creatinine and blood urea nitrogen concentration (BUN) tended to be higher than in time-matched controls, but not significantly so.

During the initial weeks general appearance and behaviour was not distinguishable from that of the sham controls with rats showing grooming, nesting and social behaviours. Other markers of stress, such as porphyrin staining, were minimal; it was important to become acutely aware of normal and abnormal behaviours during this period to allow more effective monitoring in the later stages. This is as these minor behavioural changes, combined with weight-loss, urinary albumin excretion and significantly elevated blood pressure, formed the basis of humane end point determination later in the study.

4.1.1 Growth, appearance and renal mass

Comparison of the growth curves from early (sham: ES and SNx: EN) groups and late (sham: LS and SNx: LN) groups suggest that there was an estimated age difference of approximately 5 to 11 days at procedure 1. The combined average

body weight (Bwt) for the early group animals (ES and EN) on the day of procedure one ($t = -1$ week) was 247.5 ± 1.6 g ($n=18$), lower than that of the late group (LS and LN) animals: 298.7 ± 5.6 g ($n=27$). This translates to approximate ages of 55 - 58 days (8 weeks) and 63 - 67 (9 - 9.5 weeks at the time of procedure 1 in the early and late groups, respectively).³¹⁷ This factor had to be considered when comparing growth rates between the compound sham (ES plus LS) and SNx (EN and LN) groups as weight gain is typically faster in the earlier stages, with rapid weight gain particularly evident in the first 12 weeks of life.³¹⁷⁻³²⁰

For the purposes of growth curve comparison, compound groups ES/LS and EN/LN are used during the weeks 0 to 7 only. These differences were considered by transposing the early group data by 1 week, effectively aligning procedure two ($t = 0$ weeks) data from the ES/EN group with procedure one ($t = -1$ week) data of the LS/LN group; subsequently data are expressed as percentage change from weight at procedure 1 (LS/LN group) or weight at procedure 2 (ES/EN group). This allowed analysis of all bodyweight during this period over the larger compound groups, for the amalgamated groups initial weights were as follows: sham (ES/LS: $n = 18$) 295.4 ± 7.2 g and SNx (EN/LN: $n = 27$) 292.1 ± 3.7 g. During these initial weeks weight gain in the sham and SNx groups was comparable; by week 6 (week 7 early) rats in the sham group had increased in weight by 68.5 ± 5.1 % whilst those in the SNx group weight gain was typically 62.5 ± 2.6 %. This is not surprising considering weight-loss was not expected to occur until much later in disease progression, when the compensatory mechanisms fail and renal function declines.

For this purpose the 'sham' operation is an effective control procedure and any effects on weight and health from the surgical procedures were experienced in both groups. Between procedure 1 and procedure 2 sham rats gained 13.5 ± 1.6 % whilst SNx rats gained a comparable 10.9 ± 0.9 % body weight. Recovery was generally swift in all groups, with growth following the growth estimates from the suppliers regardless of experimental group.^{317,319}

Kidneys (expressed as g per Kg of body weight, g/Kg) from the EN group were significantly heavier (5.61 ± 0.53 g/Kg, left kidney, $n = 6$) than those from rats in the ES group (3.10 ± 0.08 g/Kg, right kidney, $n = 6$) when harvested. This difference indicates the occurrence of a substantial renal hypertrophy of the remnant kidney fraction during this initial period, as only $1/3^{\text{rd}}$ of the left kidney was left intact following the $5/6^{\text{th}}$ SNx procedure. This comparison underestimates the true extent of the difference as the right kidney is typically larger than the left, in opposition to

humans where the left kidney generally is larger.³²¹ It was not possible to take this difference into consideration since the SNx animals only had a single remnant kidney (left) whilst in the shams the left kidney was perfusion-fixed with PFA during terminal sample collection as the vessels required for the perfusion procedure are more accessible than on the right kidney. The PFA penetrates the tissue and thus artificially increases tissue weight.³²² In contrast the right kidney in the shams was collected as fresh tissue and weighed before dissection and rapid freezing in liquid nitrogen.

This change in kidney weight in the SNx animals represents an increase of 123.3 ± 28.0 % in the weight of the remnant kidney. Interestingly very little of this change is the result of normal organ growth associated with increasing body weight. The weight of the right kidneys removed from the EN rats during the SNx procedure (1.55 ± 0.06 g at body weight of 285.0 ± 0.9 g, $n = 12$) at the start of the experiment (week 0) was not different from those removed from the ES rats at the end of the experiment 7 weeks later (1.58 ± 0.02 g at a body weight of 509.7 ± 5.1 g, $n = 6$) despite a significant difference in body weight. This would suggest that the rate of gain for body weight far exceeds that of the kidneys after the initial period of growth. This disparity means that care must be taken when comparing kidney weight between rats of differing sizes and to literature where values are expressed as relative weight such as g/Kg or % bwt. A kidney weight of approximately 5 g/Kg is reported for healthy male SD rats weighing 358 ± 12.3 g (mean \pm SD), which compares well to the initial, healthy, right kidney weights of both the LN (4.9 ± 0.1 g/kg at 333 ± 1.2 g, $n = 15$) and EN groups (5.4 ± 0.2 g/Kg at 285 ± 0.9 g, $n = 12$).³²³ In older and heavier rats the kidney weight per kilogram of body weight is reduced; at 509.7 ± 5.1 g the ratio was 3.1 ± 0.1 g/Kg (ES, week 7, $n = 6$) and at 793.7 ± 10 g this reduced to 3.0 ± 0.1 g/Kg (LS, week 32*, $n = 12$). This type of correlation between body weight and organ size has also been described for the heart and kidney in WKY, but not SHR rats.³²⁴ An alternative method of normalisation relies upon tibia length. This correlates with animal size and overall growth more accurately than body weight due to increasing weight caused by fat gain without increase in organ or skeleton size.³²⁵

4.1.2 Blood pressure and heart rate

At the beginning of the experiment SBP was comparable between all rats and group mean values ranged from 133.6 ± 3.7 mmHg to 140.2 ± 6.3 mmHg. Blood pressure in young rats is generally lower than in adults, with values typically reaching

a plateau at around 16 weeks of age in healthy rats.³²⁶ The SBP data recorded from the sham rats throughout the experiment, and baseline values from the SNx rats, are in agreement with veterinary guidance of 84 - 134 mmHg (SBP) and previously documented values (134 ± 8 mmHg, $n = 6$, age unspecified, > 550 g and 138.4 ± 5.8 mmHg, $n = 30$, 20 weeks old) for SBP from conscious adult SD rats measured by tail-cuff plethysmography.^{177,304,326} These data are also comparable with telemetry based recordings in 20 week old SD rats (131 ± 2 mmHg, $n = 8$).³²⁷ During the first 6 weeks SBP remained stable in both the sham and SNx rats. After 6 weeks SBP was 139.1 ± 3.5 mmHg ($n = 12$) and 135.5 ± 4.1 mmHg ($n = 14$) in the LS and LN groups, respectively; no data were recorded for the ES or EN groups in week 6.

Other studies have shown that during this initial period (6 - 8 weeks) the method by which the renal mass reduction is achieved may play a role in the development of hypertension; particularly infarction and the associated hypoxic injury appears to produce a substantial effect on systemic blood pressure well beyond that evoked by the reduction of renal mass alone.³²⁸ Specifically Griffin et al. demonstrated that SBP was not elevated after six weeks in the current 5/6th SNx surgical model (120 ± 2 mmHg). In contrast when unilateral nephrectomy is combined with the infarction of 2/3rd of the remaining kidney SBP is elevated (156 ± 5 mmHg), compared to sham controls (117 ± 5 mmHg).³²⁸ The data presented by Griffin et al.³²⁸ were recorded using 24-hour telemetry and as such are influenced by the diurnal nature of SBP in the rat. While this accounts for much of the disparity between the control data reported by Griffin et al.³²⁸ and the data from this current work, the SBP data from Griffin et al.^{323,328} are lower than data reported by other groups using similar telemetry-based methods in the SD strain.³²⁹ This variability highlights the vital need for robust internal experimental controls (age-matched shams, repeated measures experimental design) when reporting SBP data, as numerous experimental variations can arise that affect the measurement of SBP in rat.^{328,329} Regardless of this technical variation the data from Griffin et al. suggest that there is little change in SBP during the first 6 weeks following an entirely surgical 5/6th reduction in renal mass; a finding which was confirmed in this study.^{323,328}

The consistency of the LS and ES cardiovascular parameters throughout the course of the study are encouraging and suggest that the tail-cuff plethysmography is a reliable and reproducible method for the measurement of SBP and HR in this model. Although it is not rapid the method is reproducible providing the methodology applied is consistent. For this study a series of carefully considered criteria were used to collect and process the data. In addition, while a heating mat was used in this study,

in a warmer environment heating may not be necessary. These data collection criteria were particularly important as the method can be variable as it is sensitive to factors such as temperature, movement and stress.

Beyond 6 weeks, and towards the end of the initial phase, SBP was higher in the SNx cohort, significantly so in the EN group (154.5 ± 2.9 mmHg, $n = 12$ vs. ES: 141.9 ± 1.9 mmHg, $n = 6$, $p < 0.001$, week 7), but not within the LN group where SBP had increased to a lesser degree (144.3 ± 2.5 mmHg, $n = 11$ vs. LS: 133.0 ± 2.7 , $n = 6$, $p = 0.751$, week 8). It is worth noting here that within the LN and LS data a large number of statistical comparisons (2 groups x 6 time points) were made during post-hoc testing. As a result whilst applying an individual un-paired t-test would suggest the groups are different ($p = 0.031$) this is not the case when the p-values are adjusted appropriately for the multiple comparisons made (within SPSS, Tukey post-test). Although the populations (ES and EN) had diverged there was still considerable overlap between the groups, arising from the nature of the increase in SBP within the SNx population, which was not homogenous.

Initial heart rate (HR) data were within the accepted range for healthy rats in the waking period (350 - 450 bpm) and consistent across the groups: mean values ranged from 430.7 ± 4.9 BPM to 442.7 ± 5.3 BPM.³⁰⁴ These results lie towards the high end of the normal range for HR in rats and while minimal restraint was used, the animals were disturbed and removed from their normal housing environment in order to record blood pressure. In contrast, ambulatory (24 - hour) HR measured using telemetry, an initially invasive technique, can provide more representative HR data by eliminating the need to remove the animals from normal housing. Consequently a disparity can arise when comparing these data to values gathered using tail-cuff plethysmography due partly to the diurnal nature of CV regulation in the rat. Blood pressure and HR are typically lower during the light hours when the animals are least active and accordingly telemetry data from the active period (night) in SD rats places a normal HR in the region of 350 - 400 BPM, whilst a 275 - 300 BPM is normal in undisturbed rats during the light period, although it is common to present 24-hour averages.³²⁹

HR was used as a measure of both procedural stress for SBP measurement and a marker of physiological condition over the course of the experiment. The minimally invasive nature of tail-cuff plethysmography was an important factor given the length of the experimental protocol and the invasive nature of the 5/6th SNx procedure. At the start of the procedure the rats were not full adult size (< 300 g) and were

expected to grow considerably throughout the experiment. Considering this substantial growth there was a risk of displacement of a telemetry transducer making this method less favourable to the tail-cuff in this situation.

4.1.3 Renal function by albumin - creatinine ratio

Insight in to the underlying glomerular damage, and by surrogate renal functional decline, was gained by measuring urinary albumin-creatinine ratio (ACR, mg/ μ mol). As described previously ([Section 1.1.1](#)) the glomerular filtration barrier (GFB) is both highly permeable and highly selective.^{4,6,7,13,21,330,331} Crucially, changes in glomerular permeability are a hallmark of CKD and recent evidence suggests that increased permeability to proteins may play a causative role in the progression of CKD.^{131,132,313} In patients with CKD albuminuria is categorised diagnostically as microalbuminuria or macroalbuminuria: microalbuminuria is generally considered below the detection limit of basic dipstick type tests which are also sensitive to fluctuations in urine concentration. To account for these variations urinary albumin is commonly normalised to creatinine.

The 5/6th SNx model of CKD is particularly recognised for the development of glomerulosclerotic lesions with progressive albuminuria over the course of the disease.¹⁷⁵ Even during the early stages, ACR was elevated in the SNx rats compared to the controls ([Figure 3.5](#) and [3.6](#)).

Published figures for urinary albumin excretion are variable and this is complicated by the range of units used to report urinary protein excretion in the literature. One source of variation is the assay type: general protein assays (e.g. Bradford, Lowry and spectrophotometer analysis) or albumin specific assays (ELISA and other antibody based methodologies).^{332,333} Protein assays provide results based on a mixture of protein molecules and the presence of individual protein moieties will be influenced by the permeability of the GFB.³²⁴ Further variation arises as a result of differing collection methodologies: 24 hour sampling yields data typically referred to in grams or milligrams per day (g/day or mg/day); however results from 24 hour samples are sometimes analysed and reported in a ratio-metric manner to a marker molecule (typically creatinine). There are a number of ways to express ACR data; mg/g (or g/mg), mg/ μ mol, mg/mmol and mg/mg_{Cr} being the most common. Clinically mg/mmol and mg/g appear most often; and mg/g is particularly useful as it roughly represents urinary albumin excretion (UAE) in mg/day, a useful measure for defining

microalbuminuria (30 - 300 mg/day) and macroalbuminuria (> 300 mg/day). Conversion between these units is not overly complex ([Table 4.1](#)).

FROM→	mg/μmol	mg/mmol	mg/mg _{Cr}	μg/mg	mg/day
TO↓					
mg/mmol	X 1000			X 0.113	
mg/g	X 8840	X 8.84	X 1000	Equiv.	≈ in human

[Table 4.1](#) Conversion of ACR units, for reference. ^{334,335}

4.1.3.1 Sham controls

There are a range of uACR units reported in the literature a matter which is further complicated by strain and gender differences which are outlined in [Table 4.2](#).^{314,336–340} For ease of comparison values reported have been converted to mg/g when direct comparisons are drawn. It is clear from these data that while 30 mg/g is the generally accepted threshold for microalbuminuria in humans, the range of values from healthy rats is more varied and typically greater (6.5 - 597 mg/g). During the early stage of the current study (up to and including week 7) the overall average for the sham control cohort was 0.009 ± 0.013 mg/μmol (82.8 ± 111.9 mg/g, mean \pm SD): this is the average of 2 - 7 samples over 7 weeks from 16 individuals (a total of 62 samples). These values are within the range of other reported values for male SD rats of a similar age.^{337,339} Although comparable, the variability within the cohort and in the values reported in the literature highlights the need for an appropriate control group. Specifically as the measure is ratio-metric small variations in protocol, such as time of collection, dietary protein or method of analysis, could theoretically lead to a marked shift in the outcome, making comparisons to other datasets problematic in the absence of model and methodology specific normal ranges.

Study	Strain	Gender	Age / weight	Reported value	Converted to mg/g
Current work	SD	M	250 - 600g	0.009 ± 0.013 mg/μmol	82.8 ± 111.9
Han³³⁷	SD	M	≈ 340 g	0.07 ± 0.01 mg/mg _{Cr}	70
Sung³³⁹	SD	M	8 weeks	197.4 ± 218.2 mg/day	197.4 ± 218.2*
				3.78 ± 7.48 mg/mmol	31.8
			32 Weeks	579.72 ± 229.3 mg/day	579.72 ± 229.3*
				11.14 ± 10.5 mg/mmol	98.5
Advani¹⁷⁷	SD	M	≈ 682 g	0.10 ×/÷ 1.18 mg/μmol [#]	88.4 [#]
McCarthy³⁴¹	SD	F (preg)		19 ± 3 mg/mmol	168.0
So³³⁶	LETO	M	38 weeks	6.41 ± 0.34	
	OETF			486.59 ± 30.79	
Oldroyd³¹⁴	Wistar	M	≈ 480 g	9.9 ± 1.1 mg/day	9.9 ± 1.1*
Johnson¹²⁰	Wistar	M	≈ 414 g	6.5 ± 0.7 mg/day	6.5 ± 0.7*
Ahmed³⁴²	Wistar	M	≈ 400 g	61.9 ± 12.7 mg/day	61.9 ± 12.7*

Table 4.2 Summary of literature values for urinary albumin in healthy rats which vary by gender, age and species. High sugar diet OETF rats (diabetic) included for comparison. Data are represented as mean ± S.D or geometric mean ×/÷ tolerance factor. Calculation of mg/g values carried out using the conversion factors in [Table 4.1](#) * indicates the approximation of mg/day ≈ mg/g.³⁴³ # indicates total protein, rather than albumin. Strain abbreviations: SD = Sprague-Dawley, LETO = Long-Evans Tokushima Otsuka rats, OETF = Otsuka Long-Evans Tokushima Fatty rats.

The data in this study are based upon an albumin-specific ELISA assay and as such are used to calculate an albumin: creatinine ratio. Values reported elsewhere use a mixture of both general protein and albumin-specific methodologies and there is no clear way to interchange these ACR and protein based results. While human urinary albumin concentrations are well defined (normal ACR < 30 mg/g; microalbuminuria 30 ≤ 300 mg/g and macroalbuminuria ≥ 300 mg/g) proteinuria is not clearly defined beyond the acceptance that normal urinary protein excretion should be less than 150 mg/day (protein: creatinine ratio < 15 mg/g). In humans albumin typically accounts for approximately 20 % of this total urinary protein and the 30 mg/day for albumin or 150 mg/day for protein are often used in an interchangeable manner. In healthy rats values from 10 - 50 % have been suggested making conversion from protein:

creatinine ratio to ACR problematic.^{344,345} Using the data from the control cohorts (ES and LS) a grading was created to define the normal ACR values specific to the methodology used in this work. This was then combined with data from the SNx cohorts (EN and LN) to produce an ACR severity scale (Table 4.3).

	mg/g		mg/ μ mol
Normal	≤ 149		≤ 0.017
High Normal	150 - 499		0.0017 - 0.056
Mild	500 - 4999		0.057 - 0.565
Moderate	5000 - 14999		0.566 - 1.697
Severe	≥ 15000		≥ 1.697

Table 4.3 Methodology-specific classification of albumin: creatinine ratio results

During the early post-operative stage the ACR in the sham animals tended to fall well within the previously defined normal range (0.009 ± 0.013 mg/ μ mol or 81.6 ± 112.4 mg/g, mean \pm SD) with occasional results falling in the elevated normal range (max: 0.035 mg/ μ mol or 313.7 mg/g). During this time such increases in ACR were transient rather than persistent; hence the sham cohort provides a stable baseline against which the SNx data can be compared.

4.1.3.2 ACR in the SNx cohort

During the early phase (up to 7 weeks) mean ACR in the SNx cohort was elevated considerably to 0.142 ± 0.394 mg/ μ mol (1251.0 ± 3479.5 mg/g, $n = 76$, overall period mean \pm SD), approximately 15-fold greater than the time-matched control data (0.009 ± 0.002 mg/ μ mol, or 82.87 ± 14.2 mg/g, $n = 62$, overall mean \pm SD). Even at this early stage there was substantial variability within the cohort; however most values fell within the normal (< 150 mg/g, 36 data points), high normal (150 - 499 mg/g, 18 points) or mildly elevated ranges (500 - 4999 mg/g, 17 data points). There were very few results in the highest categories, moderate (5000 - 14999 mg/g, 4 data points) and severe (≥ 15000 mg/g, 1 data point). The general lack of extreme values at this stage suggests that the effect of reduced renal capacity, and by extension persistent glomerular hyperfiltration at the single nephron level, causes a delayed and progressive (cumulative) degeneration in the GFB and renal function rather than instantaneous damage similar to that associated with acute renal failure. Transient hyper-filtration is generally not considered problematic as although the

increased intraglomerular pressure can lead to increased protein excretion the changes are generally a result of the increased hydrostatic pressure and filtered load, rather than altered permeability. In contrast, persistent increases in intraglomerular pressure and the associated mechanical stresses have been shown to result in podocyte death *in vitro*.^{124,125}

4.1.4 Blood chemistry

Blood chemistry analysis for both blood urea nitrogen (BUN) and serum (plasma) creatinine was carried using previously validated, commercially available kits. BUN analysis was carried out using an enzyme-based colorimetric assay modified as described for use with small sample volumes. Plasma creatinine was analysed using a modified Jaffe reaction against a standard curve. BUN and plasma creatinine in the ES control rats were measured at 4.9 ± 0.6 mmol/L and 34.5 ± 4.5 μ mol/L, respectively. BUN in this group was slightly lower than the reference range of 15 - 21 mg/dL (conversion to mmol/L by factor $\times 0.357$: 5.4 - 7.5 mmol/L); however this is not a major discrepancy as only elevated BUN is considered pathological.³⁰⁴ Plasma creatinine values were in the middle of the 0.2 - 0.8 mg/dL reference range (conversion factor $\times 88.4$, 17.7 - 70.7 μ mol/L) and comparable to data from another study also using sham controls (12 weeks post-surgery, 0.48 ± 0.05 mg/dL or 42.4 ± 4.4 μ mol/L).^{178,266,304} Together these data suggest that the control rats were healthy and free from renal impairment whilst additionally providing validation of the methodologies used to analyse these substrates.

BUN (17.8 ± 1.7 mmol/L) and plasma creatinine (89.6 ± 6.7 μ mol/L) tended to be higher in the plasma from EN rats than in the controls; this 2.5-fold difference represented a significant increase in BUN but not plasma creatinine ($p = 0.014$ and 0.522 , respectively).¹²⁰ In contrast to the results from the ES group those from the EN group were outside of the expected healthy range for both BUN and p-Cr, indicating a degree of renal insufficiency within these animals and the significant increase in BUN, but not plasma creatinine, is likely to result from a tendency for BUN to rise more rapidly than serum creatinine in most circumstances.^{301,316} This suggests that whilst the rats are still gaining weight, behaving normally and have only moderately increased blood pressure, the hypertrophy that occurs within the remnant kidney during this initial period does not restore renal function adequately. This is the beginning of established and progressive kidney disease.¹⁸⁰

4.1.5 Renal histology

Histological staining of sham (ES) and SNx (EN) kidneys highlighted subtle changes within the EN renal tissue. At this stage of the disease changes are predominantly localised to the cortex and specifically within the glomeruli. Within the renal cortex general staining with haematoxylin and eosin revealed some dilatation of the renal tubules in the EN samples; there were also small areas of hyper-cellularity around the tubules, but at the level of basic structure there were few real noticeable differences. Sections of medulla from EN rats appeared remarkably normal when stained with H & E although small areas of cellular expansion were occasionally seen. This was expected since the damage to the glomeruli caused by the induced hyperfiltration would result initially in glomerular damage and tubulo-Interstitial fibrosis before eventual redundancy and closure of the tubules leading to the formation of tubular vacuoles and ultimately changes within the collecting ducts and other medullary structures. The increased protein concentration within the tubules appears to play a role in this fibrotic process; however the mechanism is not completely understood with opinion divided over the role of protein per se compared to specific active fractions (TGF- β or IGF-I for example).¹³⁵

4.1.5.1 Renal fibrosis

The EN rats, by the nature of the procedure, had fewer remaining glomeruli; but it was also clear from PAS staining that of those remaining glomeruli a significant proportion had at least some degree of focal glomerulosclerosis whereas glomeruli from time-matched sham animals appeared normal. Tissues from EN rats also presented with a typically normal staining pattern for collagen using Masson's trichrome stain (MTC), with minimal blue staining which was generally localised to the exterior surface of the Bowman's capsule in the cortex and areas surrounding renal blood vessels throughout the section. This staining pattern was highly comparable to the staining seen in the time-matched controls. There was little evidence of peritubular expansion or cortical fibrosis, areas which would also stain for collagen. These results also suggest that while changes in renal structure and function are starting to occur in SNx rats the gross structure of the kidneys remain remarkably normal during this early stage of the disease.

It is worth noting that the intensity of the aniline blue component (collagen) of the MTC stain is less than that of collagen-specific immunohistochemical staining (discussed below); this difference is particularly noticeable in the basement

membranes of the renal tubules which did not stain strongly with the aniline blue. There was substantial optimisation of this staining protocol in order to balance the contrast (Weigert's haematoxylin nuclear stain) and primary stains (Biebrich scarlet-acid fuchsin cytoplasmic stain and aniline blue collagen stain) across the variable amounts of collagen present in different experimental groups. The result of this optimisation over a wide range of conditions is lower intensity collagen staining in the normal and near-normal tissues which is generally confined to areas surrounding renal blood vessels, and not detectable in the fine basement membranes of the renal tubules. The more intense collagen staining seen in the late SNx sections demonstrates the efficacy of the staining protocol and the need for such optimisation.

In sham rats immunohistochemical staining for type IV collagen was associated with the tubular basement membranes in both cortical and medullary tissue. Within the cortex staining was also seen in the Bowman's capsular membrane and glomerular basement membranes. Staining of collagen IV in these regions is well documented within the kidney and the differential expression of $\alpha_3\alpha_4\alpha_5$ isoforms within the GBM has been described in both human and rat.^{16,346} Laminin- β was similarly distributed, although staining within the glomeruli was less extensive. At the superficial level staining for both type IV collagen and laminin- β staining in the SNx cohort was comparable to the controls. It is important to consider that the proportions of specific type IV collagen ($\alpha_3\alpha_4\alpha_5$) or laminin- β ($\alpha_5\beta_2\gamma_1$) species may be altered without impacting the intensity of immunostaining due to the cross-reactivity of the antibodies used. These polyclonal (pan) collagen IV and (pan) laminin- β antibodies produced reliable staining; further insights in to the expression of specific species could be gained by qPCR which will be discussed in [Section 9](#).

The lack of obvious changes in gross renal structure, despite evidence of deteriorating renal function and reduced glomerular selectivity, indicates that the changes go beyond those immediately visible under a light microscope. Increased permeability of the glomerular filtration barrier (GFB) to proteins (detected as increased urinary ACR) suggests that significant changes in functionality of the GFB are already occurring. This is much like the changes in the glomerular basement membrane (GBM) that are seen during the early stages of CKD, in DN patients particularly, where the GBM thickens whilst becoming more permeable.^{347,348} These structural changes are used as a diagnostic marker for early CKD, where GFR may be normal or even elevated.^{99,100}

4.1.6 Immunohistochemical staining of urotensin II system components

Substantial modification of the laboratory's standard immunohistochemistry protocol was necessary to overcome problematic antigen retrieval. These problems are believed to be the result of differing tissue section properties, as the slides and equipment used throughout were consistent with previous works in the laboratory.³⁰⁶ In this work the sections from adult rat kidney were much larger than those from young rats which have been the focus of earlier studies in the lab. In addition the tissues from late group SNx rats often presented with voids. These larger void-filled tissues appeared susceptible to bubbles in the antigen retrieval fluid and even following extensive optimisation the process remained extremely sensitive to any deviation in procedural temperature and duration. Modified blocking and washing processes resulted in minimal background staining which is evident in the negative control sections.

4.1.6.1 UII and URP

Despite these methodological changes the immunohistochemical staining of UII reactive peptides (as described earlier the antibody used detects both UII and URP) in the sham control tissues was consistent with previous work. There was diffuse staining throughout the renal cortex with the most intense staining seen in the proximal tubules. In healthy cortical sections the diffuse nature of the stain often requires a contrasting negative control in order to identify positive staining as it is not always immediately clear; however staining was typically absent from the glomeruli, a finding noted previously in this laboratory and others.^{178,216,268} Staining in the medulla was less abundant and generally localised within the cells of the collecting duct rather than a widespread pattern of staining, which is also consistent with previous studies.^{216,268}

UII reactive staining in the early SNx rats tended to follow the distribution seen in the time-matched controls; however staining intensity was noticeably greater. This increased intensity was noted in sections from both the cortex where staining was diffuse and localised to the tubules and in the medulla where collecting duct epithelia appeared to express the UII/URP peptide with marked intensity.

These results add support to the findings of Mori et al. describing an up-regulation in UII system components at mRNA level in the remnant kidneys of rats with

experimental CKD induced by the infarction method of 5/6th SNx.¹⁷⁸ In the current work it is not possible to dissect the apparent increase in UII/URP reactivity beyond the suggestion that total UII-reactivity is increased in the cortex and medulla of SNx rats after just 7-8 weeks post-surgery. It is conceivable that URP, UII or both components could be expressed more abundantly in SNx rats. Indeed the data from Mori et al.¹⁷⁸ would suggest that both UII and URP are more abundant in the kidneys of rats 8 weeks after establishing CKD by 5/6th SNx.

4.1.6.2 UT receptor

Immunohistochemical staining for UT was minimal in the cortex of both sham and SNx animals at the early time point (7 weeks post-surgery), a finding which is consistent with previous work which reported only sporadic/occasional UT-reactive staining in the renal cortex.²¹⁶ It has been suggested that cortical staining with UT-specific antibodies may be associated with the arterioles of the glomerular tuft which could indicate a role in the regulation of intraglomerular pressure by modulation of afferent and efferent vascular resistance, although this hypothesis is yet to be confirmed. There was a distinct lack of positive staining in the cortex of time-matched controls; there was however a faint and diffuse staining pattern seen in the SNx cohort. In the medulla staining was typically seen in the cells of the collecting ducts with comparable intensity in both the sham and SNx cohorts. Increased UT (*Uts2r*) mRNA has been reported in the kidneys of rats just 8 weeks after undergoing the 5/6th SNx procedure (infarction model);¹⁷⁸ however this was not reflected in the accompanying immunohistochemical staining, nor was this difference apparent in the current work. However, there is evidence that the distribution of UT expression (protein) has altered in EN with staining evident in the cortex of SNx but not control animals. Whilst an increased signal was not seen in the medulla the small but widespread change in cortical expression is compatible with increased UT expression in the kidney of SNx rats at the whole kidney level¹⁷⁸ as the cortex accounts for a large proportion of total renal tissue. It is also important to consider that mRNA and protein expression are not always equivalent and the relationship between the two are subject to factors such as transcript stability and protein turnover rates.

When staining the collecting ducts of the medulla for a protein with relatively low expression such as UT there are certain technical considerations relating to the orientation of tissue that greatly improve imaging and identification of positively stained structures. The hypertrophy and physical change in the remnant kidneys

resulted in a loss of landmarks that allow accurate dissection and orientation of the tissues at the point of collection and as a result it became more difficult to capture images of stained structures in these tissues than in the control tissues, an issue that became even more prominent in the later samples. The less than optimal orientation of the tissues sometimes resulted in less than ideal imaging opportunities, although in later tissues the increase in signal counteracted this effect.

4.1.7 Summary of the initial phase

Whilst SNx rats appear outwardly normal during the initial period, gaining weight and displaying normal social behaviours for example, changes are already occurring within the kidney. These changes present as mild but noticeable histological alterations within the cortex and formation of focal glomerulosclerotic lesions within a proportion of the remaining glomeruli; this is accompanied by altered GFB permeability presenting as increased urinary albumin excretion (measured by uACR). There was little to indicate global changes in kidney structure; outside of the glomeruli the tubules appeared slightly dilated but otherwise intact. Staining for basement membrane proteins, whether tubular or glomerular, remained comparable to the sham controls. Renal changes were also beginning to affect physiological parameters. SBP was elevated and blood urea nitrogen and blood creatinine were both higher in EN rats than in the time-matched controls which is indicative of renal dysfunction/insufficiency. Immunohistochemical staining for UII tended to be more intense in both cortex and medulla of the EN rats (compared to time-matched sham controls); UT staining in the cortex also appeared more intense in this group, with minimal UT staining seen in cortical samples from either sham cohort. It is not possible to compare the UII/URP and UT specific findings to clinical data as UII/URP and UT expression have only been described in patients with late stage CKD (frequently referred to as end stage renal disease, ESRD) and often in patients with clinical renal failure receiving dialysis, and not during the earlier stages of CKD.

4.2 Stable phase

After the initial hypertrophic period (~ 6 - 7 weeks) disease progression rate became more variable. The rate of progression in the stable phase is considered to be dependent upon numerous aggravating factors; this is similar to clinical CKD where appropriate control of factors such as albuminuria, hypertension and diabetes forms a substantial portion of the treatment regimen.^{48,51} The terminal data from the early group (ES and EN) were collected on the perceived cusp of this stable phase, before

further increases in SBP or substantial albuminuria. The duration of this period was variable and precedes the short decline phase into renal failure/dysfunction. During this period rigorous monitoring was vital for both animal welfare and identification of the decline phase for appropriate sample collection. When reviewing the data during this period the variability in progression rate has to be taken into consideration since the animals with comparably worse underlying pathology progressed at a faster rate; there are some points within the time courses (SBP and ACR in particular) where the group average is particularly influenced by the drop-out of these individuals. For sham rats the stable phase is represented by data from week 8 - 19, in the SNx cohort data from week 8 until up until the last two time point measures are taken as the stable phase; in this group the end of the stable phase varied from week 9 to week 27. During this phase behaviour and appearance were not immediately distinguishable from that of the controls; however the SNx cohort did develop persistent and increasingly severe albuminuria along with increasingly elevated SBP.

4.2.1 Progression monitoring

When analysing body weight the two-way RM ANOVA highlighted the substantial effect of time which is referred to as “growth” from this point onwards. Whilst this effect was most noticeable in the first 12 - 15 weeks, most rats continued to gain weight until the end of the study; this is particularly true in the sham controls. Over time a visible divergence of the groups was clear in the growth curves; however although the LS and LN group means visibly separate at around week 14 (LS: 614.8 ± 18.9 g, $n = 12$, vs LN: 595.5 ± 9.7 , $n = 14$) the difference between the groups was not significant. Of particular note is the general pattern of continual weight gain even in the SNx cohort during the stable phase.

Similarly behaviour of the rats was not different during this phase with most exhibiting grooming behaviour, social interaction and normal feeding patterns. As a result weight data, SBP and ACR were used to track disease progression and identify the transition into the decline phase on an individual basis.

4.2.2 Blood pressure and heart rate

In all groups in the long term study there was a slight, but significant, reduction in HR as the experiment progressed. A similar pattern was seen in the early groups, but this change was not significant, despite being of a similar magnitude. This phenomenon occurred at the point where the animals progressed into the stable

phase (recorded during week 8 in the late time-point groups and week 7 for the early time point animals) in both sham and SNx cohorts. Notably, this was not accompanied by any significant change in SBP within either of the sham control (ES or LS) groups. This effect appears to be the result of acclimatisation to the experimental and handling procedures. Although the magnitude of these changes was small (maximal change in group mean from first recording: LS; - 2.4 % in week 8 and LN; - 4.4 % in week 22) the reduction persisted for the remainder of the experiment making the difference significant over time. Consequently while the change is statistically significant it will not be discussed further as it is not likely to represent a (patho)physiologically relevant change in HR.

Minor increases in SBP were noted in the SNx cohort during the initial phase of the study; as described previously by various research groups these changes increased in magnitude as the study progressed. SBP was significantly higher in the LN group (156.7 ± 2.5) after just 12 weeks (LS 132.0 ± 2.2 mmHg). This increase in SBP associated with the model was progressive, an effect which was not seen within the sham cohort with no change in SBP over the course of the study.

The progressive increase in SBP in the SNx cohort is consistent with previous reports in this model. The Advani group used adult rats undergoing the 5/6th SNx (infarction method) procedure to develop imaging methods capable of detecting changes in the glomerular vasculature. These rats developed hypertension by week 12 (SNx 182 ± 8 mmHg, and sham 134 ± 8), and whilst the sham data in this current study are highly comparable (132.0 ± 2.2 mmHg) the increase in SBP within the SNx group in this study is much less marked (156.7 ± 2.5 mmHg) at the same time-point.¹⁷⁷ Since the animals in the Advani group study were culled at 12 weeks it is impossible to determine whether SBP would continue to increase as was seen in this current work (172.5 ± 4.2 , in week 22) or whether SBP would then plateau. There is also evidence that the purely surgical method of nephrectomy used in this current work is associated with milder elevations in SBP and ACR than infarction methodologies.^{175,328} This progressive increase in systolic blood pressure is a hallmark of the 5/6th SNx model and in this aspect the model represents CKD well in both the progressive nature and heterogeneity within the SNx cohort.

SBP increased progressively in the SNx groups and was not accompanied by any increase in HR, suggesting that the resulting increase in SBP is most likely associated with increased total peripheral resistance (TPR) rather than changes in cardiac output (CO). A reduction cardiac output has been reported as a co-factor in

patients with CKD, particularly those in renal failure; however despite this finding a direct causative role appears to be absent.³⁴⁹ In contrast around 1 in 6 young (< 20 years of age) CKD2 - CKD4 patients have some degree of left-ventricular hypertrophy (LVH).³⁵⁰ While the extent of LVH within this sub-population does positively correlate with both CO and stroke volume and mean-arterial pressure (MAP), HR was not significantly different between patients with LVH and those without leading to belief that in these patients increased total blood volume and cardiac preload could play a role in the development of LVH in these younger patients.³⁵⁰ Elevated HR rate is rarely reported in CKD which is in stark contrast to blood pressure which is elevated in the majority of patients and considered causative in almost 1/3rd of CKD cases.⁶⁵

4.2.3 Renal function by albumin - creatinine ratio

In the SNx cohort ACR continued to increase as the study progressed, peaking 17 weeks after completion of the SNx procedure. However, individual ACR values peaked over a wide time frame (15 - 28 weeks). Generally, rats with higher ACR measurement early in the stable phase seem to reach the decline phase more rapidly: the relationship between physiological parameters and survival are discussed more completely in [Section 4.5](#) below. Where time points (weeks) are discussed data are taken as is and no attempt is made to differentiate the rapidly progressing individuals; where period averages (mean) are presented the stable period represents weeks 7 to 19 (sham) or week 7 onwards, excluding the final 2 'decline' data points (SNx).

uACR tended to be higher in the sham cohort during the stable phase (week 8 -19 period average: 0.036 ± 0.080 mg/ μ mol or 320.4 ± 706.6 mg/g, n = 62) than in the initial period (week 1 - 7, 0.009 ± 0.002 mg/ μ mol or 82.9 ± 14.2 mg/g, n = 62) with considerable inter-subject variation. There was clear biological variation within the sham cohort.

ACR was 10 fold higher in the SNx cohort, compared to time-matched controls 7 weeks post-surgery. This difference between the groups represents only a modest increase in ACR when taken in context with the remaining stable phase data: the group median continued to increase throughout the stable phase peaking at 2.042: 1.164 - 5.351 mg/ μ mol in week 17. The overall period average (1.537 ± 0.334 mg/ μ mol or 13587.3 ± 2950.1 mg/g) was considerably greater than that of the initial period (0.142 ± 0.045 mg/ μ mol or 1251.0 ± 399.1 mg/g) and is approaching severe

albuminuria (Table 4.3). This could indicate that the GFB is no longer functioning efficiently and suggests that podocyte function is severely impaired. Severe albuminuria has been associated with disruption of podocyte adhesion, retraction of foot processes that form the highly selective slit diaphragms and markers of podocyte death.¹¹⁸ *In vitro*, podocytes have been shown to be sensitive to mechanical flow stress like those proposed to occur with persistent hyperfiltration. Interactions between the capillary GEnCs and podocytes are vital in the maintenance of GBM composition and thickness which, in turn, is key to podocyte adhesion via interaction of $\alpha_3\beta_1$ integrin and Laminin-521, for example.^{14,15,101,125} A role in podocyte detachment has also be attributed to FGF-2-driven hypertrophy of endothelial and mesangial cells by physical disruption *in vitro*.³⁵¹ This would be further exacerbated by a reduction in the number of functioning glomeruli resulting from extension of the glomerulosclerotic lesions identified in histological samples after just 7 weeks; the remaining functional glomeruli would be subject to a greater functional load.^{124,125}

As ACR increased during the stable period the variability within the cohort increased which is inherent to the heterogeneous nature of progression rates. It appears that the inherent biological variation is amplified by the variations in disease progression such as increased SBP and renal function impairment.

4.2.4 Summary of the stable phase

During the stable phase the rats continued to gain weight and express typical behaviours. This is despite obvious changes in renal function and physiology such as substantially elevated ACR and marked increases in systolic blood pressure on top of the elevated plasma creatinine and BUN, indicative of renal impairment. The lack of obvious outward behavioural signs of impending decline required vigilant monitoring practices as well as detailed knowledge of the normal behaviour of the rats. As described previously the duration of this stable phase was variable and the (patho)physiology of the SNx cohort remained highly heterogeneous throughout this period.¹⁸⁰ Consequently it is difficult to define the end of the stable phase and beginning of the decline phase and so some generalisations are applied when describing the data and these are explained below (Section 4.3).

4.3 Decline phase

Time to renal function decline in the long term SNx group was variable, as previously described, with half of the cohort ($n = 7$) reaching the defined endpoint by week 30, and the 8th in week 31 (SNx survival: 30.3 ± 9.4 weeks (mean \pm SD). This is comparable with previous median survival times of 6 months, or 26 weeks.¹⁷⁹ For the purposes of clarity, due to variations in progression, the decline phase is discussed in terms of the last available monitoring measurements (pre-terminal sample collections) for each of the long term SNx and shams for SBP and HR; for ACR data the decline phase is the final 2 sampling points. For body weight the last 14 days of data are considered. Terminal data are discussed separately as there were procedural variations pertaining to the collection of these data.

4.3.1 Survival, body weight, appearance and behaviour

Previous studies using the 5/6th SNx model indicate that mean/median survival would typically be around 6 months and that decline may be rapid following a variable stable phase (Section 4.2).^{179,180} As such, more intense monitoring was employed based upon risk markers such as increased ACR, elevated SBP, weight loss, changes in appearance or subtle behavioural changes. Reduced activity levels, increased porphyrin deposition and paling of the eyes commonly accompanied gradual weight loss, and changes in appetite were monitored by challenge with a favoured food (soaked pellets).

4.3.1.1 Survival

Studies with the 5/6th SNx model have described a variable-length stable phase and consequently variable survival times. Similar variability was also seen in the current work with a range of survival from 16 (3.7) to 45 (10.3) weeks (months). Although average survival was not different from previous studies; the survival time (30.9 ± 8.5 weeks, mean \pm SD) was slightly greater than the 6 month (26 weeks) survival time that is generally associated with the 5/6th SNx model.¹⁷⁹ This may be the result of a smaller renal mass reduction (73.6 % compared to 83.3 % for a true 5/6th reduction), although in cases where renal mass reduction was greater there were cases of acute renal failure (2 cases of ARF in cohort with renal mass reductions of 75.5 and 85 %). Nonetheless, renal mass reduction alone was not a good predictor of survival over the narrow range achieved in this work ($R = 0.296$, adj. $R^2 = 0.18$, $p = 0.284$).

Despite this difference in renal mass reduction the animals in the LN group represent (near) renal failure ([Section 4.3.4](#)).

In an attempt to standardise the degree of renal dysfunction at the end point of experiments other groups have used a pre-determined marker of renal function such as serum creatinine > 2 mg/dL or 176.8 $\mu\text{mol/L}$ as described by Gretz et al.¹⁸⁰ However this approach would require increased blood sampling frequency which itself was associated with increased mortality rates in uraemic rats in the same study. The first major aim of the current work was to profile the progression of the CKD associated with the 5/6th SNx model, which was novel to the laboratory, and to describe expression of the urotensin II system, particularly in the late stage of CKD as this information is currently unavailable in animal models. To this end it was in the interest of the study to ensure long term survival of the later stage animals and as such more frequent blood sampling was avoided in favour of a terminal large-volume sample.

4.3.1.2 Body weight

Monitoring was regular and endpoints were based upon a constellation of factors including rapid or incremental weight loss, behavioural changes such as lethargy or social isolation and physiological symptoms such as unprovoked piloerection. The intense observation and weighing schedule allowed careful weight tracking and rapid identification of trends. This proved particularly useful in the identification of small and persistent reductions in weight which were cumulative in nature. Whilst a single rapid loss of weight was more inherently worrying these small additive changes tended to act as an early indicator, before any behavioural changes could be identified. Other indicators used to identify decline included paler eye colour and the build-up of porphyrin staining.

The adverse effects guidelines ([Section 2.3.1.2](#)) suggested that monitoring frequency should be increased when weight loss was 10 - 20 % compared to the previous measurement, with > 20 % loss indicating the recommended humane endpoint. In reality these guidelines were modified with persistent small reductions in body weight triggering the increased monitoring and termination typically occurring at a loss of 10 - 15 % (total weight loss from peak, average 10 % / maximal loss 18.6 %). This period of weight loss, or plateau, typically lasted between 7 and 21 days, and during the initial period rats showed interest when challenged with favoured foods and maintained social interactions.

Body weight in the SNx group was considerably lower than that of the shams during the latter part of the study (e.g. week 31, LN: 652.1 ± 33.7 , vs. LS: 740.4 ± 20.3 g); the growth curves of the two cohorts were not significantly different due to the substantial overlap during the early stages and due to a reduction in n numbers later in the study.

4.3.2 Systolic blood pressure and heart rate

Within the LN group systolic blood pressure continued to increase, reaching 172.5 ± 4.2 mmHg (n = 10) after 22 weeks, plateauing thereafter until week 31. This finding is of course complicated by variability in rate of disease progression within the LN cohort; however peak SBP (176.8 ± 4.2 mmHg) is comparable with the data from weeks 22, 28 and 31 suggesting that these data do in fact represent the expected plateau in SBP. This pattern was reflected in the sham cohort where SBP remained stable but lower than that of the SNx rats over weeks 22 to 31 (~ 142 mmHg). Throughout the later stages heart rate remained consistent and comparable over time and between the cohorts as described previously ([Section 4.2.2](#)).

There was variation in the individual peak SBPs which occurred at intervals between week 12 and week 28; the magnitude of the peaks was also variable (maximal SBP recorded in LN individuals: 150.1 - 204.7 mmHg). This peak SBP represents a substantial increase from baseline (max - min: 49.4 ± 3.8 mmHg) and an increase of 39 ± 3.2 %. Whilst the time frame for peak SBP appears wide the majority of individual peaks occurred in either week 22 (n = 6) or week 28 (n = 6). The nature of this variability is not unlike that seen within CKD patients; the data are continuous and normally distributed throughout. Hypertension is associated with a poorer prognosis in patients with recommended BP targets of < 138/85 mmHg used clinically; SBP > 200 mmHg was used as a measure of adverse events.^{81,128,154,352} Interestingly peak SBP is not a predictor of survival time (discussed in detail in [Section 4.5.1](#)). This makes logical sense when considering that the duration and extent of SBP elevation would be more likely to influence disease progression. Considering two theoretical individuals, subject A has a very high peak in SBP (> 200 mmHg) which occurs late in the study (20 weeks). Subject B where SBP peaks to a lesser degree (>190 mmHg) much earlier (12 weeks), subject B is symptomatic earlier (elevated SBP) which may be indicative of renal impairment occurring earlier in the study which is likely to lead to meeting the endpoint criteria earlier.

4.3.3 Renal function by albumin: creatinine ratio

As previously described the SNx cohort had significantly elevated uACR when compared to time matched controls ($p_{\text{SNx}} < 0.001$). This increase in uACR in the SNx cohort was progressive ($p_{\text{time}} < 0.001$, and $p_{\text{time} \times \text{SNx}} = 0.002$) and uACR was extremely high during the decline phase ($2.243 \pm 4.743 \text{ mg}/\mu\text{mol}$ or $19832.0 \pm 41928.5 \text{ mg/g}$, $n = 30$ data points from 15 individuals) and remained variable between individuals. The progressive drop out of cases resulted in reducing statistical power towards the end of the study. As a result although uACR was substantially higher in the SNx cohort than in time-matched sham controls at both 21 and 28 weeks post-surgery the difference was statistically significant in week 21 ($p = 0.009$) but not in week 28 ($p = 0.231$). It became clear that urinary albumin excretion in this model of CKD can reach exceptionally high levels with values reaching 1000 fold that of the shams. These exceptionally high albumin concentrations resulted in the need for serial dilution of samples in order to assay them. Samples from sham rats were typically diluted 1 in 1000 in accordance with the supplier's instructions; samples from SNx rats were typically diluted 1 in 10000 or 1 in 100000 or greater. In these cases it became standard to include the two most likely dilutions per sample. During dilution and prior to sample loading it was extremely important to ensure that samples were well mixed. In addition the sensitivity of the assay required careful and extensive washing between stages to ensure there was no sample carryover. The extreme quantities of albumin in the urine of SNx later towards the end of the study were indicative of severe disruption of the GFB along with gross renal structure. These changes are discussed more completely in [Section 4.3.5](#), along with accompanying histological changes.

During these later stages uACR also tended to be higher in the sham cohort (period average: $0.068 \pm 0.017 \text{ mg}/\mu\text{mol}$ or $602.34 \pm 137.9 \text{ mg/g}$, $p = 0.083$). While the extent of the change was not of the same magnitude as that seen in the SNx rats it represents a 7-fold change over the course of the experiment. This change in the control did not significantly affect the statistical outcomes as the changes seen in the SNx cohort were so extensive.

4.3.4 Terminal samples; kidney size and blood chemistry

As discussed previously ([Section 4.1.1](#)) the remnant kidney undergoes substantial hypertrophy in the weeks following surgery. The final mass of the remnant kidneys from the LN rats ($4.86 \pm 0.47 \text{ g}$) were substantially greater than those from the EN

group ($p < 0.001$); however during dissection it was clear that a significant proportion of this mass was retained fluid and large vacuous spaces were frequently seen in these samples (described in [Section 3.4](#)). It is not particularly useful to compare the renal mass of the remnant kidneys to the final single kidney weight of the time-matched sham control animals (2.47 ± 0.09 g) as the remnant kidney is only $\sim 1/3^{\text{rd}}$ the size of a normal kidney after the first surgical procedure. Instead it is more useful to compare the remnant mass to its own initial weight. This demonstrates that the remnant kidney increased in size substantially, gaining 320.4 ± 36.6 % in weight; this four-fold change is greatly underestimated when terminal renal mass is compared to that of the shams.

4.3.4.1 Serum analysis: blood urea nitrogen and plasma creatinine

For the late stage SNx animals the mean time to renal insufficiency was 30.3 ± 9.4 weeks (Mean \pm SD), with a steady decline in numbers seen from week 20 to week 45. There was substantial elevation of both BUN (66.19 ± 3.73 mmol/L) and plasma creatinine (351.3 ± 38.1 μ mol/L) concentration in the LN cohort which is indicative of severe renal dysfunction and associated uraemia. This represents a 4-fold (9.78 ± 1.18 mmol/L) and 7-fold (89.62 ± 6.68 μ mol/L) increase in these metabolic waste products compared to the time-matched sham controls, respectively. Ultimately all animals in the LN group reached a state of renal failure/end stage renal disease (plasma BUN > 200 mg/dL and/or plasma creatinine > 2.5 mg/dL), with the exception of two individuals where both these measures of renal function were markedly elevated but to levels below these limits. There was no overlap between individuals in the LN and EN groups for serum creatinine or BUN. Despite the severity of the renal impairment the terminal decline was short and rapid, careful assessment of experimental severity and animal welfare thus afforded sample collection to occur late in the disease timeline. The timing of this endpoint was particularly important as it allows appropriate alignment of these experimental samples to those from patients with late-stage CKD.

4.3.4.2 Terminal urine analysis

Terminal urine analyses are discussed separately from the time point data as the samples were collected as and when each individual reached the defined endpoints of the study rather than at pre-determined times; in addition the samples were collected directly from the bladder under anaesthesia rather than as a natural passage of urine whilst conscious.

Collectively these samples tended to have exceptionally high uACR (3.548: 1.548 - 6.130 mg/ μ mol or 31364.3: 13684.3 - 54189.2 mg/g) demonstrating that urinary albumin excretion becomes substantial in the later stages of the CKD associated with the 5/6th SNx model. The rats in this cohort suffered from severe albuminuria as the study progressed, and this was not seen in the time-matched sham controls (0.127: 0.049 - 0.281 mg/ μ mol or 1122.9: 433.2 - 2484.0 mg/g, n = 12, p < 0.001). In addition the extent of the albuminuria highlights the dampening of the uACR peak throughout the time course by varied progression rates within the LN cohort.

4.3.5 Renal histology

In line with previous studies using the 5/6th SNx model there were extensive changes in renal structure of the LN group rats. These were examined using a number of histological staining techniques. Sections stained with H & E showed the development of considerable lesions within the cortex of LN rats, with very little of the tissue appearing with any degree of normality. Tubules were recurrently enlarged often with the loss of the proximal tubule brush border structure and development of casts. There were also large voids (often > 100 μ m in diameter) present in the tissue, most likely resulting from redundant tubules downstream of closed (or ablated) glomeruli. The remaining glomeruli presented with extensive sclerosis and identification of the capillary loops was often impossible; however it was not uncommon to see occasional glomeruli that appeared almost entirely unaffected. There was substantial hypertrophy in the regions surrounding the tubules with extensive hyper-cellularity in these regions. PAS stain was more intense in the basement membranes of the remaining renal tubules in the LN group than the LS group ([Figure 3.13\(2\)](#)) and there was clear evidence of substantial glomerulosclerotic lesions (GSI score 3: 2 - 4, n = 150 glomeruli from 3 individuals) with increased PAS staining across the glomeruli with clear disruption of the glomerular structure. The images collected also suggest that the GBM is substantially thickened in the LN group; however it was not possible to quantify this change at the resolutions produced from standard light microscopy. Staining with MTC stain revealed that there were significant collagenous deposits within the glomeruli and within the surrounding areas of peritubular hyper-cellularity.

As discussed previously ([Section 4.2.3](#)), persistently increased hydrostatic pressure resulting from an increase in filtered load per glomerulus can result in (mal)adaptive responses to the increased fluid flow stress experienced by GEnCs and podocytes.¹²⁵ Communication between GEnCs and podocytes is vital to the

maintenance of the composition of the GMB.¹⁴ A persistent increase in hydrostatic pressure may result in compensatory deposition of ECM proteins by podocytes experiencing increased fluid flow stress, with consequent retraction of podocyte foot processes and ultimately detachment and death.^{4,124} The mechanisms by which these changes in GBM composition occur is not fully understood and are likely to depend upon the cause of the initial glomerular injury.^{15,52,175} The proteins involved in the regulation of ECM/GFB degradation would also be of particular interest as the ECM is a product of equilibrium between deposition and degradation. This is exemplified by Johnson et al. who report a substantial increase in collagen (type III and type IV) within the remnant kidneys of SNx rats, which is accompanied by increased expression of both MMPs (1 and 2) and their inhibitors, TIMPs (1, 2 and 3).¹²⁰ Although MMP proteins were abundant within the remnant kidneys, the overall proteolytic activity was lower.¹²⁰ The reason for this reduction in proteolytic activity in MMPs from SNx rats is not clear. Reduced GBM degradation is implicated in CKD/DN; in contrast in DN the reduction in GMB degradation is thought to result from excessive glycation of the substrates.^{102,105,353}

In the medulla the changes were less obvious; however it became increasingly difficult to accurately identify structures in this group as voids formed from tubular structures were common as were hyper-cellular areas which often coincided with the alanine blue component of the MTC stain for collagen. Whilst these changes did interfere with the identification of substructures of the renal medulla they tended to be less extensive than those seen in the cortex. Together these histological observations confirm that the rats in the LN group have severe changes in renal structure along with renal function impairment which is typical of late stage CKD.

4.3.6 Immunohistochemical analysis of collagen and laminin

The renal scarring within the LN group was severe: immunohistochemical staining of collagen IV and laminin- β was intense and widespread. Staining was no longer constrained to the basement membranes; fibrosis originally seen exclusively within focal lesions within the glomeruli (EN) was also seen in interstitial areas. This interstitial disruption was not homogenous and there was a stark contrast between areas surrounding glomeruli with a relatively normal appearance and those that were heavily sclerotic. This is consistent with the notion that fibrosis can be a consequence of functional nephron loss in that ECM deposition replaces the failed nephron.³⁵⁴ This complex process underlies the progression of CKD and DN and

since the kidney has a very limited capacity for re-generation, slowing or preventing renal fibrosis will be key in treating CKD.³⁵⁴

4.3.7 Immunohistochemical staining of urotensin II system components

Although immunohistochemical staining of UII reactive proteins and the UT receptor is not quantitative there are clear and consistent differences in the distribution and intensity of staining between the late SNx and late sham tissues and when comparing late SNx to early SNx.

4.3.7.1 UII and URP

The majority of antibody species used for the detection of UII demonstrate reactivity with all UII from all sources, including the homologue URP.²¹⁶ Methodologies reported more recently do allow for some differentiation of UII from URP in human plasma samples using luminescence-based antibody assays.²¹⁹ This is a result of increased affinity for the longer UII peptide over the shorter URP; however since there is still notable cross-reactivity antibodies alone do not provide sufficient specificity for assay purposes and further sample processing must occur to differentiate the two peptide fractions.²¹⁹ Further, even when an antibody with selectivity is used, when staining fixed tissue sections the kinetics of the system provide only qualitative data, since the antibody is allowed to reach equilibrium and is typically in excess hence the staining represents the detection of all reactive species.

In the cortex and medulla of late shams UII-immunoreactivity was comparable to that of the early shams, suggesting that time (ageing) alone has little impact on UII/URP protein expression. In the cortex staining was diffuse across the cells of the renal tubules though this tended to be slightly more intense than in the early shams, but less intense than in the early SNx. Staining for UII/URP in the medulla was faint and generally located in the collecting ducts which compared well with images from the early shams. In contrast staining patterns in the late SNx rats were substantially altered. In the cortex there was diffuse staining throughout areas of peritubular expansion and fibrosis along with high intensity staining in the renal tubules; in many cases the brush borders were indistinct and the tubular structure disrupted making anatomical identification much more difficult in these tissues. There was also evidence of staining in the glomeruli, a feature which was absent in all other groups.

In the medulla the changes in staining intensity were equally striking with strong staining in the collecting ducts and more diffuse staining in the surrounding tissues. The UII-reactive staining in these tissues was more widespread and more intense than in the time-matched shams and the earlier SNx group.

4.3.7.2 Urotensin II receptor

In the renal cortex of late sham rats positive staining is rarely seen for the UT receptor; this is consistent with sections from the early shams. This lack of cortical staining has been described previously in this laboratory.^{216,268} In contrast positive staining was seen in the medulla of the LS group and was typically localised to the cells of the collecting ducts, often presenting with a stippled or punctate pattern. Interestingly while the staining pattern appeared to be constrained within the cells of the collecting duct, not all cells of the collecting duct were positively stained for UT. Faint positive staining can also be seen in the thin limbs of the loop of Henle, a pattern which has been described in previous work.²¹⁶

There were obvious differences in the staining for UT in late SNx samples. This was true in both the cortex and medulla. The most obvious difference was visible in the cortex where positive staining was seen frequently, which is in stark contrast to the time-matched sham controls where staining for the UT receptor was rarely seen within cortical regions. This staining was generally within areas of peritubular expansion, the areas which appear fibrotic. Although the changes in the medulla were equally prominent this represented an increase in intensity rather than distribution. UT staining has been consistently reported in the IMCDs and thin limbs of healthy rats and this pattern was also seen in the late SNx tissues, albeit with substantially greater intensity. Of particular interest is the apical staining pattern which appears in close proximity to the apical membrane of the collecting duct epithelium. This could indicate increased surface expression of the receptor in these cells, or increased numbers of the receptor in vesicles near the apical membrane.

4.3.7.3 Summary of UII, URP and UT expression by immunohistochemistry

These findings add to profile of the UII system in the 5/6th SNx model of CKD beyond those that have been previously reported for UII/URP or the UT receptor. The increased intensity of staining for UII-reactive proteins in the late SNx group offers a point of comparison to clinical data where early time course data are unfortunately lacking. Increased concentrations of UII reactive peptides have been reported in the

urine of patients with renal failure and this observation is complemented by the increased UII reactive staining seen in the kidneys of late SNx rats.¹⁸²

UT receptor expression (protein) appears more intense and more widespread in the remnant kidneys of rats in (near) renal failure than in healthy rats (sham controls) or rats in the earlier stages of CKD. This is consistent with the increase in UT receptor (mRNA) expression previously reported by Mori et al.¹⁷⁸ in the early stages of experimental CKD and aligns more readily with clinical data which is generally from subjects in the later stages of DN including the substantial up-regulation of UT receptor (mRNA) expressions in diabetic nephropathy reported by Langham et al.²³³ These type II DM patients presented with severe glomerulosclerosis, despite the apparent short duration of diabetes. However this could stem from a period of unmonitored MetS with poor glycaemic control and subsequent improper management of renal disease.^{48,233}

The role of UT receptor signalling in CKD remains unknown; however the further increase in UII system peptides as CKD progresses raises questions over a potential role of UII in progressive renal scarring. Song et al. describe a reduction in eRBF and GFR in anaesthetised rats following UII administered as an i.v bolus of 6 pmol/100 g Bwt.²¹⁶ The dose was used as it had minimal effects on systemic blood pressure: this finding was replicated in further studies infusing UII at a similar concentration.²⁸⁴ Although the mechanisms behind these effects are largely speculative, the potential for UII to negatively regulate eRBF and GFR may provide some insight into the reasons why expression is increased in the 5/6th SNx model. Initial induction of the UII system may be a compensatory mechanism intended to counter the increases in GFR and intraglomerular pressure associated with a reduction in functional nephron number.³⁵⁵ UII-mediated constriction of afferent arterioles has been suggested as a potential mechanism behind UII-induced reductions in eRBF and GFR. UII-induced reductions in renal blood flow have also been demonstrated in immature kidneys of neonatal pigs, where surface expression of UT in has also been described in afferent arteriole-derived vSMCs.²⁸⁵ It remains to be seen whether these effects extend in to other species or mature kidneys. Excess UII could also result potentially from ineffective clearance of the reactive UII species, a mechanism which has been suggested previously.¹⁸² Evidence from other tissues suggests that UII may be a positive mediator of fibrosis. UT antagonist treatment improved outcomes in a rat model of congestive heart failure, and has been suggested to induce myocyte hypertrophy *in vitro*.^{276,279} UII has been tentatively linked to collagen synthesis with activation and proliferation of fibroblasts described

both *in vitro* and *in vivo*.^{181,184,278,356,357} Whether or not the process is initially compensatory, this state of elevated UII, URP and UT expression may play a role in the progression of glomerulosclerosis and tissue remodelling within the kidney in CKD.

Although this alone is not sufficient to determine any causal (or protective) role for UII, URP or the UT receptor in the development or progression of experimental CKD these results further the profile of UII/URP and the UT receptor in CKD where late-stage pre-clinical data were lacking, describing an increase in expression of the urotensin II receptor (UT) and its ligands UII/URP (at the level of the protein) in the kidneys of SNx rats in late stage CKD. The abundance of the UII/URP peptides and UT receptor in the kidneys of 5/6th SNx rats in the later stages of the disease is not only far greater than in time-matched sham controls, but also of a greater magnitude than the modest increase seen at earlier stages of CKD in the current work and by others.¹⁷⁸

4.3.8 Summary of the decline phase

The sham controls presented with age-related changes in renal function, particularly the development of mild albuminuria. Otherwise the physiological data from this group was comparable to previous work and the appropriate reference ranges for blood biochemistry.³⁰⁴ Thus the rats undergoing sham-surgery provided a stable and reliable control over the course of the study. The SNx cohort developed a severe renal profile and culminating in renal insufficiency and uraemia. The advanced kidney disease was characterised by extensive structural changes within both the cortex and medulla; particularly prominent were cortical scarring, glomerulosclerosis and loss of nephrons. UII, URP and UT receptor peptides were more highly expressed in the kidneys of SNx rats in (near) renal failure than in time-matched sham controls or SNx rats in early stages of disease.

4.4 Limitations of study design

The 5/6th model of CKD is by nature variable in the rate of disease progression, much like the clinical condition it represents. This variability remained despite consistent starting weights and highly reproducible resection of the renal poles (73.6 ± 3.5 %). This high degree of reproducibility is vital as the amount of tissue removed does ultimately have the potential to influence the rate of disease progression. Nonetheless there was no significant correlation between the mass of tissue

removed and survival over the range of renal mass reduction achieved in this study ($R = 0.410$, adjusted $R^2 = 0.104$, $p = 0.129$).

This issue was further complicated by variations in the time to peak: the peak ACR and SBP data were not aligned resulting in dampening of the mean/median values across a few time-points where individual peak values were localised. It is understandable that the worst affected individuals would experience a peak in these physiological parameters earlier in the study, and subsequently drop out earlier affecting the group mean/median. This also has an effect on the spread of data as some subjects present with severely elevated physiological parameters whilst others remained close to normal.

This persistent variability in survival substantially complicated the repeated-measures based statistical analysis of the data as whole cases (individuals) are excluded where no value is present for a single point over the time-course. This resulted in a significant drop in cases towards the end of the study, and the most obvious work-around involved analysing the data up to a specific time-point (week 28 for SBP, HR and ACR). While this did still result in some reduction of statistical power (reduced n-numbers from animals which reached the defined end points prior to these defined points) the effect was not as extreme as analysing to study completion where all but 2 SNx cases were effectively excluded by week 40 post-surgery. The remaining statistical power was great enough to detect differences between the groups, over time and at individual time-points in post-hoc testing, with the exception of ACR at week 28 which was confounded by reduced n numbers and measure variability along with a mild increase in sham ACR at this point (discussed in further detail in [Section 4.3.3](#)).

In order to maintain full power of analysis the data could be transformed to fit a standardised timeline, which would mean a smaller number of time-points were analysed to fit. This then raises additional questions of how to fit the data to such a timeline; would the point nearest the defined point be used and the remainder excluded or would the average of the points in a given period be more appropriate. Either method requires careful consideration; however there are not a great number of examples of such methods as in most biological settings time-points are pre-determined. Terminal data points were not affected by this matter as these were treated as a single point per subject within a 2 way factorial ANOVA.

4.5 Regression analysis - predicting survival

In a clinical setting aggressive management of albuminuria, hypertension and blood glucose (in diabetic patients) still prevail as the major therapeutic interventions in the treatment of CKD with the rationale that these factor contribute actively to the progression of CKD.^{48,51,54,61,313,358} With this in mind it is reasonable to examine whether elevated SBP or uACR can be used to predict survival time in the late SNx cohort.

4.5.1 Renal mass, peak SBP and peak ACR

Since the proportion of mass removed determines whether or not renal failure occurs it is important to consider variation in the remnant kidney as a source of variability in survival, regardless of the high degree of consistency achieved when performing the surgery.¹⁷⁹ As stated previously ([Section 4.3.1](#)) renal mass reduction ([Figure 4.1a](#)) was not a good predictor of survival alone ($R = 0.296$, adj. $R^2 = 0.18$, $p = 0.284$) or in conjunction with maximal uACR ([Figure 4.1b](#)) and maximal SBP ([Figure 4.1c](#)), $R = 0.230$, adj. $R^2 = -0.263$, $p = 0.916$); this is not particularly surprising as the time when the peak occurs is not considered.

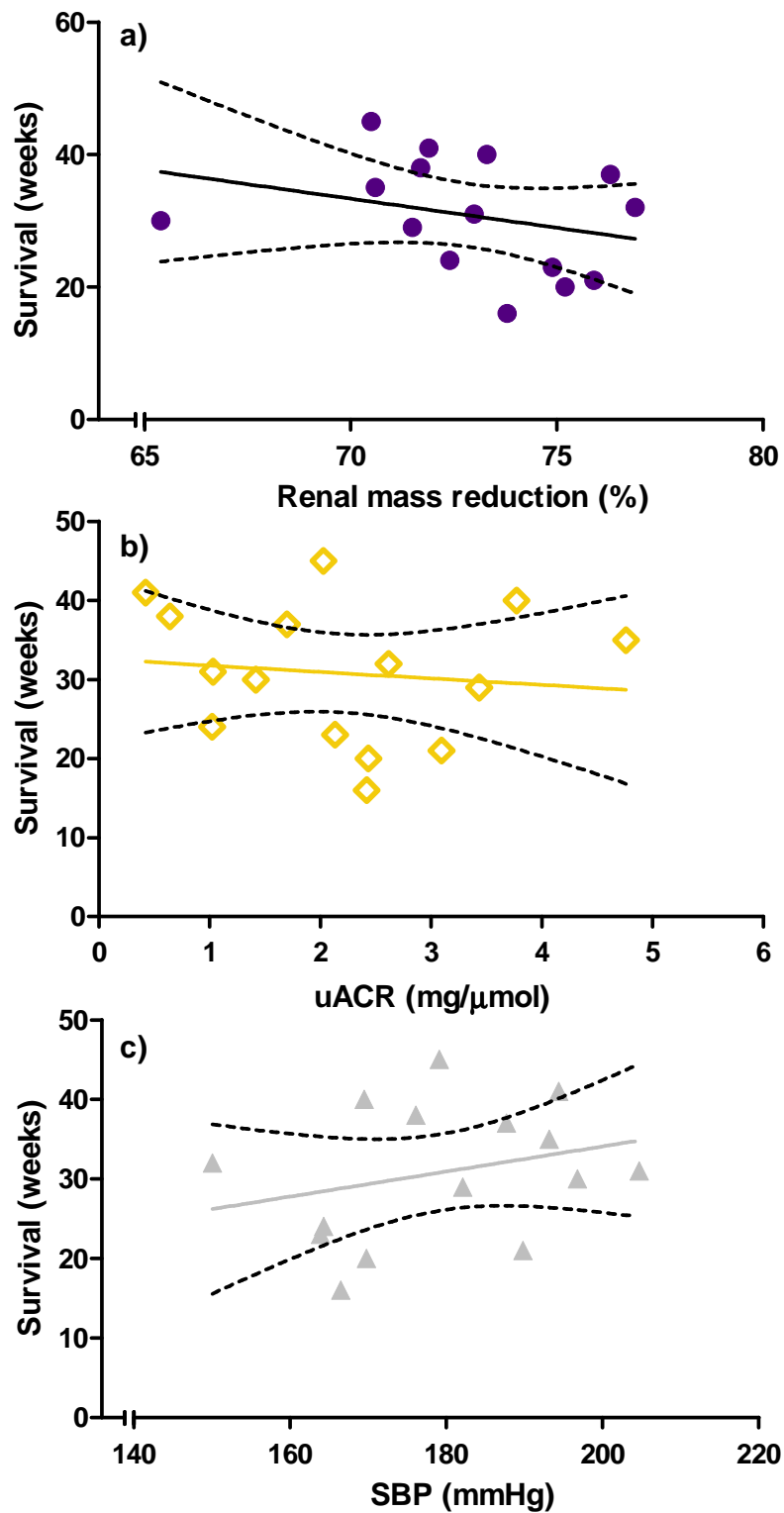


Figure 4.1 Renal mass reduction **(a)**, peak albumin:creatinine ratio **(b)** and peak systolic blood pressure **(c)** did not predict survival effectively ($R = 0.230$, adj. $R^2 = -0.263$, $p = 0.916$, multiple linear regression with three independent variables).

4.5.2 Model generation

Since peak values have no predictive power, renal mass reduction, SBP and uACR data from all time points were considered using as an automatic stepwise multiple linear regression in SPSS (IBM SPSS Statistics, version 22.0). Numerous variables were automatically rejected from model generation; rejection was based upon a lack of significant influence upon the dependent variable. These removed variables included: renal mass reduction, ACR at weeks 3, 5, 22, 28 and 30 and SBP at weeks 3, 12, 22, 28 and 31. The remaining values (ACR weeks 9 and 12 along with SBP at weeks 9 and 8) produced a model with an adjusted R^2 of 0.872 (Figure 4.2).

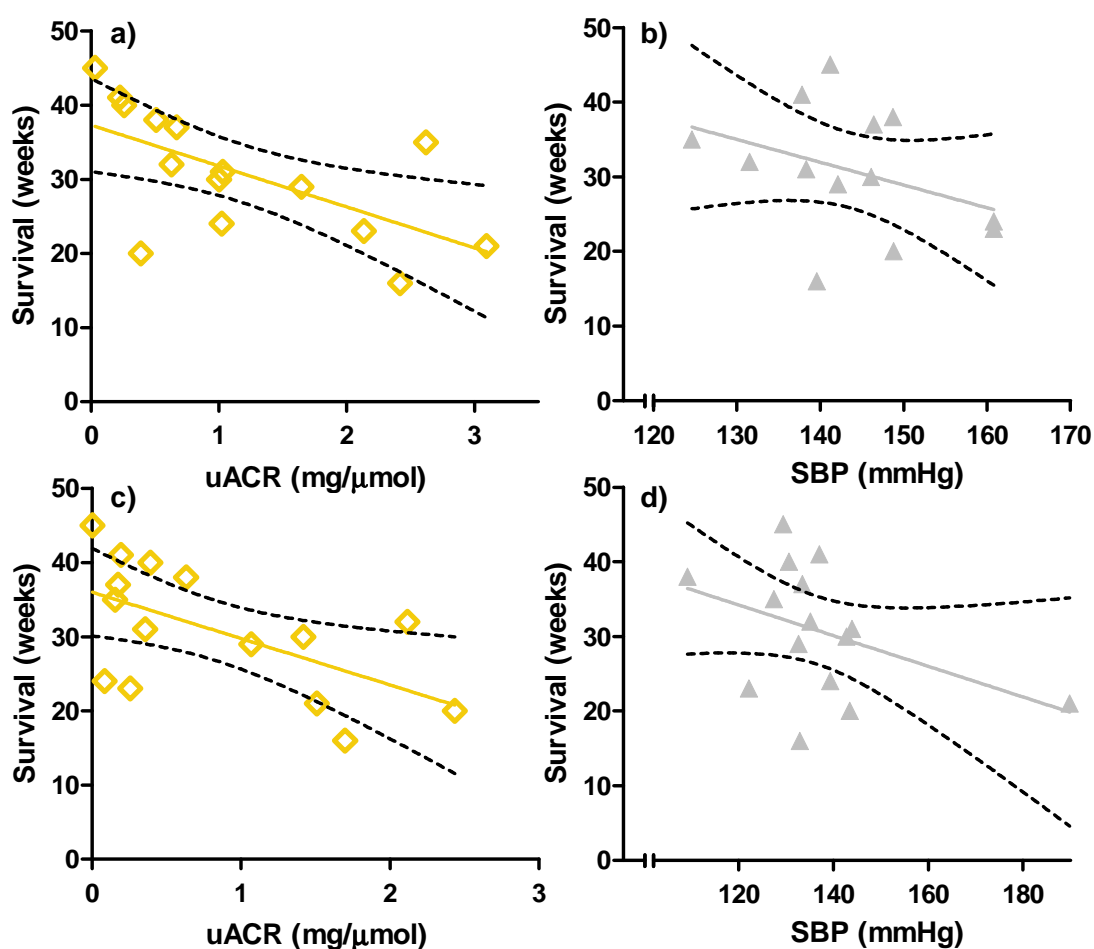


Figure 4.2 Final predictive variables included in the model, in order of importance, were: urinary albumin:creatinine ratio in **(a)** week 12 ($p < 0.001$), and **(c)** week 9 ($p = 0.001$) and systolic blood pressure in **(b)** week 8 ($p = 0.001$) and **(d)** week 6 ($p = 0.0038$). (Adj. $R^2 = 0.872$, $p < 0.001$, multiple linear regression, stepwise generation from 15 variables).

The model was statistically significant ($p < 0.001$) and the equation of the model (Equation 4.1) showed that all four included factors within the model act as inverse predictors of survival, which is consistent with advice pertaining to the management of CKD. That is, management of albuminuria and blood pressure is an important factor in disease progression.⁵⁵ These results require care in their interpretation as although the degree of co-linearity within the included variables was statistically acceptable (tolerance 0.873 - 0.959) by nature of being repeated measurements taken from the same sample these variables are not strictly independent.

$$\text{Survival} = 136.784 - (5.62 \times \text{ACR}_{12 \text{ weeks}}) - (0.433 \times \text{SBP}_{8 \text{ weeks}}) - (5.221 \times \text{ACR}_{9 \text{ weeks}}) - (0.236 \times \text{SBP}_{6 \text{ weeks}})$$

Equation 4.1

4.6 Conclusions

The 5/6th SNx model is a model of chronic kidney disease and presents with progressive albuminuria and hypertension. The surgical set-up is reproducible and reliable with minimal early mortality and the (patho)physiological profile of the disease is comparable to that of a number of previous studies. There is variation between the profile generated in this study and those previously reported; however there is noticeable variation between the previous studies from different laboratory groups arising from many causes including animal age, method of disease initiation, and other methodological variations in the disease monitoring processes.

Mild functional changes were evident during the initial phase with uACR elevated above that of the time-matched controls after just 7 weeks; this was accompanied by a small but significant increase in SBP. Terminal samples collected from early SNx rats (7 - 8 weeks) presented with visible changes in the renal tissue. These can be summarised as tubular dilation, mild glomerulosclerotic lesions and occasional small areas of peritubular expansion. Analysis of plasma samples for metabolites (urea and creatinine) removed via renal excretion revealed that the rats in the early SNx group had developed renal dysfunction. UII/URP and UT staining appeared more intense than in the time-matched sham control group which is consistent with previous work in this model and with data from CKD patients in later stages of the disease.^{178,182,233}

These functional changes progressed further during the stable phase of disease with continued increases in uACR and SBP but not HR. The SNx rats developed

substantial albuminuria; however there was little to indicate the underlying renal dysfunction during this phase of the disease. This period was of varied length which did complicate the statistical analysis later in the study.

Over the course of the study there were drifts in the baselines within the sham cohort for HR (reduction, acclimatisation) and uACR which increased slightly in a manner that is likely to be related to the age of the rats at this point (~ 1 year). Towards the end of the study the albuminuria in the SNx cohort was severe appearing almost limitless with uACR over 30-fold greater than in the sham controls during this period. SBP remained at an elevated plateau and analysis of terminal plasma samples revealed BUN and plasma creatinine concentrations indicative of renal failure. The extent of the renal damage was clear in histological samples which presented with substantial glomerulosclerosis, tubular dilatation with void formation, peritubular hypertrophy and extensive deposition of fibrotic components such as collagen throughout the cortex and medulla. The tissues from late SNx rats represent the lesions of late stage CKD (and particular DN) well; it is possible to produce renal failure following CKD in this model.

The immunohistochemical staining in this work suggests that both the peptides UII/URP and receptor (UT) are upregulated, at the protein level, in the CKD related renal failure associated with 5/6th model, not only relative to time-matched sham controls, but when compared to SNx rats 8 weeks after surgery. This extends previous work in this model where expression of UII, URP and UT has been described up to 8 weeks post-surgery. The continued increase in expression could suggest that UII signalling has a role in the progression of CKD, or conversely is upregulated in an adaptive manner. Changes in expression of the urotensin II system may be similar in this model of CKD to those in clinical CKD where increased UII/URP and UT expression (mRNA/protein) have been reported in (near) renal failure.¹⁸² However, clinical data from the early stages of CKD are currently not available and the (patho)physiological role of UII/URP and the UT receptor in the progression of CKD remains undefined both clinically and in experimental models. To understand this aspect further an interventional study was designed and the results are discussed in [Section 8](#).

5: Results of RT-qPCR for *Ywhaz*, *Uts2r*, *Uts2b* and *Uts2* over the course of CKD in 5/6th SNx model

Terminal renal cortex samples, collected as described in [Section 2.5.1](#), were treated with RNA/later-ICE ([Section 2.11.1.1](#)) before proceeding with RNA extraction, reverse transcription and qPCR.

As described previously ([Section 2.13](#)), SYBR Green qPCR was carried out on renal cortex tissue collected ([Section 2.5.1](#), enriched for cortex by macro dissection) from animals 8 weeks (early) and 30 ± 3 weeks (late) after the 5/6th SNx procedure ([Section 2.2](#)). At each time point tissue was also collected from age and time-matched sham controls (described previously, [Section 2.2.5](#)). The following terms are used throughout to denote the groups; ES (early sham, n = 6), EN (early SNx, n = 6), LS (late sham, n = 7) and LN (late SNx, n = 7), unless otherwise stated. For all qPCR data the n numbers in this section represent biological samples; each biological sample was comprised of two technical replicates.

Tissue samples were processed as described in [Section 2.11.1](#). Briefly; RNA was extracted and purified using the RNeasy[®] Plus mini kit (Qiagen) and a homogenisation drill (Powergen125, Fisher). RNA extracts were then quantified using a micro-volume spectrophotometer (Nanodrop 2000c, ThermoFisher) and quality verified by non-denaturing gel electrophoresis ([Section 2.11.1.5](#)) before reverse transcription into cDNA using QuantiTect[®] RT kit (Qiagen, [Section 2.11.1.2](#)).

5.1 RNA quantification and quality control

RNA extracts typically contained 212.3 ± 11.5 ng/μL ([Figure 5.1](#)), with A260/280 and A260/230 ratios of 2.07 ± 0.0 and 1.38 ± 0.1 respectively. This gives an indication that the samples were suitably concentrated and pure enough to progress with reverse transcription. Typical coefficient of variability (intra-sample) was 0.87 % (n = 2 replicate reads).

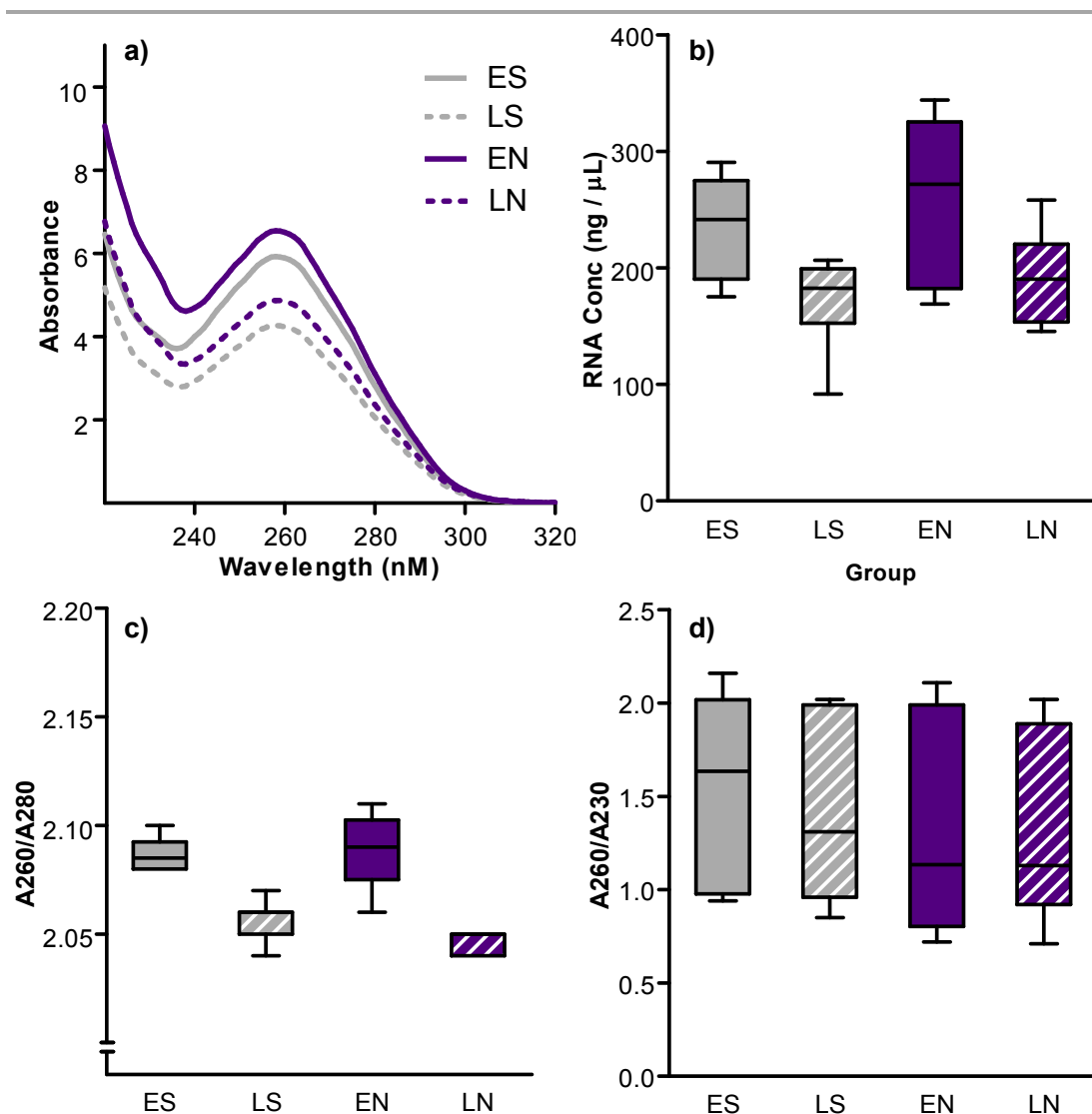


Figure 5.1 Micro-volume spectrophotometer analysis of RNA extracts produced **(a)** group mean absorbance spectra; all show the characteristic nucleotide peak at 260 nm, **(b)** this is converted (factor: 40 ng/μL for A260 = 1) to RNA concentration with **(c)** all samples producing an A260/280 ratio of 2.0 or greater. **(d)** The A260/230 ratio was more variable; all samples with ratios above 0.75 were included. n = 6 (ES and EN), or 7 (LS and LN).

To ensure that the RNA within the samples was of good quality samples were run on 1.5 % agarose gel in non-denaturing conditions ([Section 2.11.1.5](#)). All samples had two clear bands representative of the 18s and 28s ribosomal subunits, ([Figure 5.2, arrows](#)) with no apparent gDNA contamination (visible by the presence of high molecular weight banding or smear pattern towards the top of the gel). Similarly there were no clear indications of RNA degradation products (RNA fragments would result in banding or smearing towards the bottom of the gel) ([Figure 5.2](#)). Samples LS2 (lane 8, top panel) and LS8 (lane 14, top panel) had a lower RNA load due to a

decreased concentration (91.6 and 79.1 ng/ μ L, respectively) resulting in less intense banding.

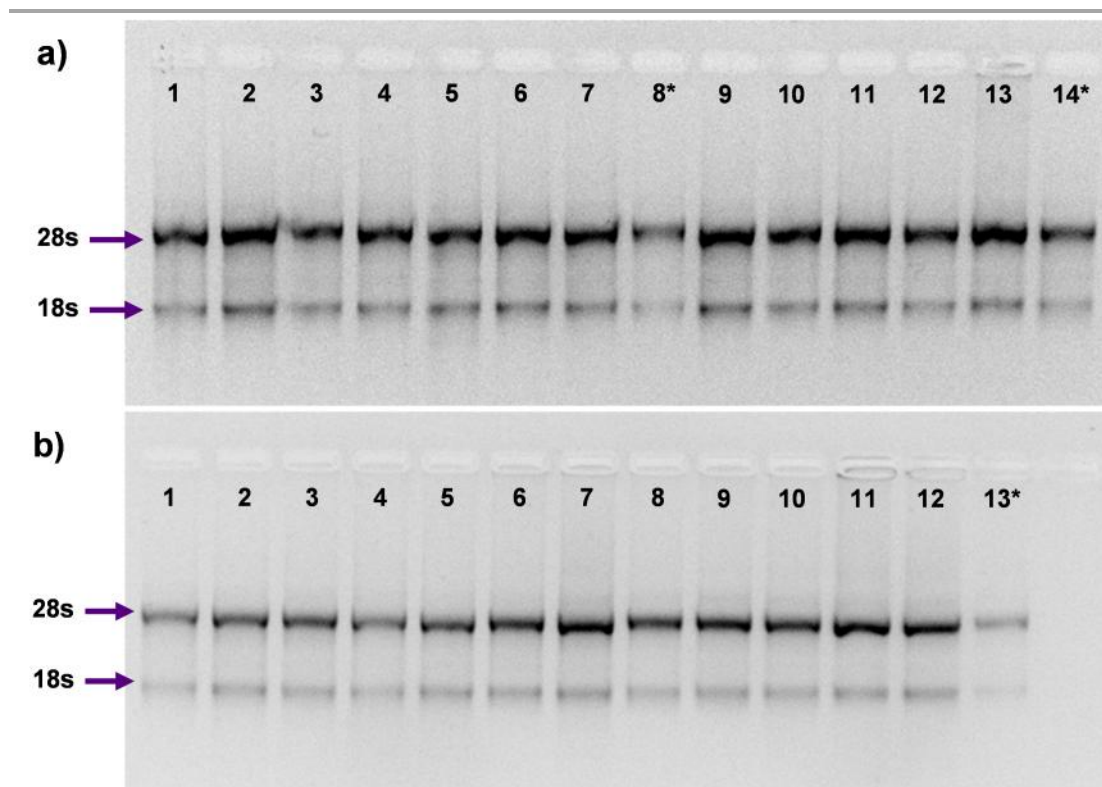


Figure 5.2 All RNA extracts showed intact 18s and 28s bands when examined by agarose gel electrophoresis. **(a)** Extracts from ES samples (lanes 1- 6) and LS samples (lanes 7 - 14) showed strong bands; the weaker bands in lanes 8 and 14 were the result of reduced RNA load (samples LS2 and LS8). **(b)** Extracts from EN samples (lanes 1- 6) and LS samples (lanes 7 - 13) showed strong bands. The LS sample in lane 13 had lower RNA content due to a lower RNA concentration.

5.2 *Ywhaz*

Following the protocol outlined in [Section 2.13.4](#) (40 cycles) the *Ywhaz* transcript was detectable in all standards and samples (diluted 1 in 100) amplifying within an appropriate C_t range (range 19.9-26.7 [Figure 5.3a](#)), and producing a single product peak on the dissociation curve (T_m =87.1 °C, [Figure 5.3b](#)). The assay had good reaction efficiency (104.0 %) and a well fitted standard curve ($R^2 = 0.998$, [Figure 5.3c](#)).

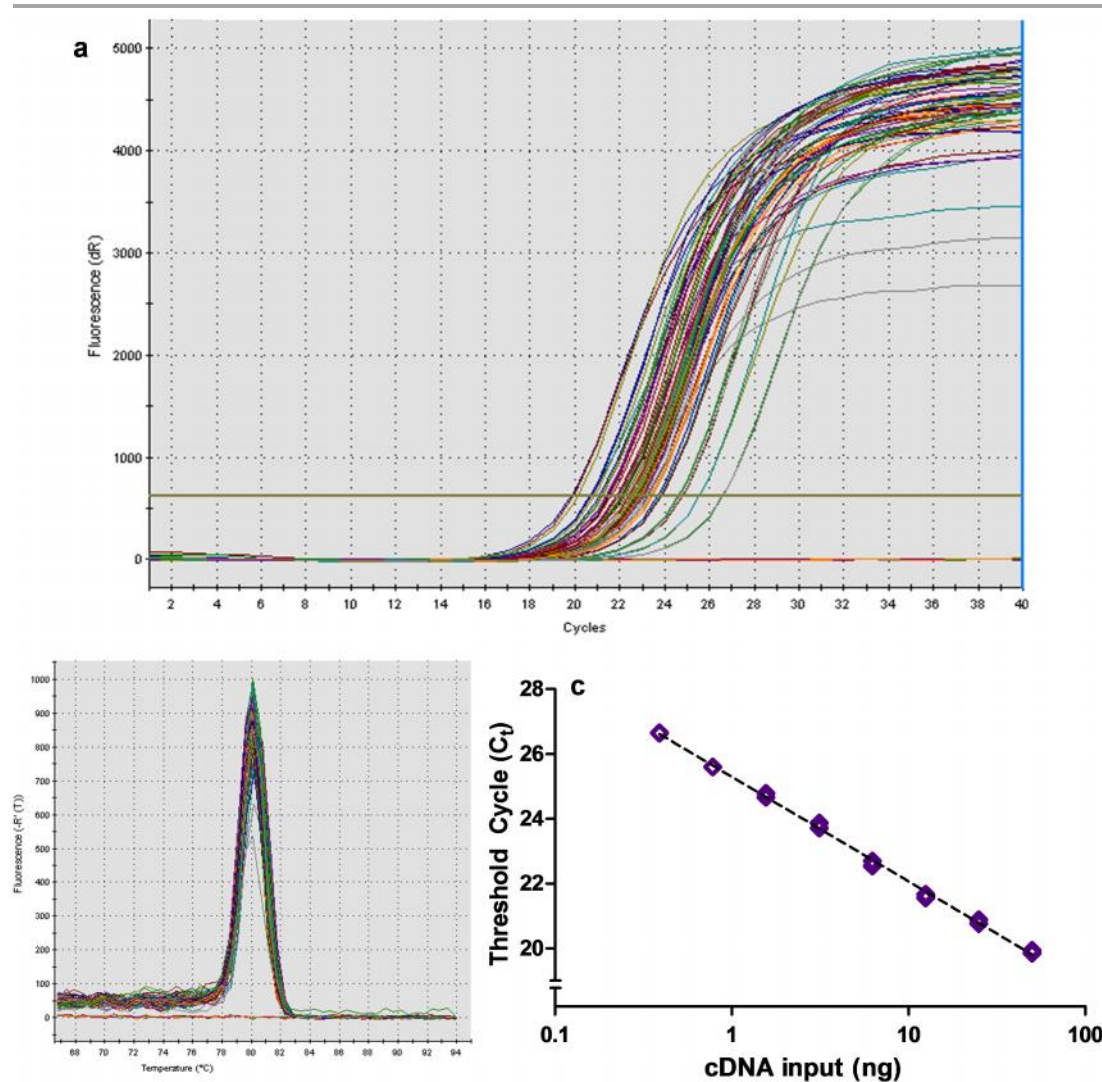


Figure 5.3 Results of qPCR for *Ywhaz* **(a)** sigmoidal plots showing consistent amplification. No amplification occurred in the no template, no reverse transcriptase or water controls. **(b)** A single peak in the dissociation curve. **(c)** log-linear standard curve with a slope of -3.229 and $R^2 = 0.998$ over 8 standards (50 - 0.391 ng).

Ywhaz amplified consistently across the experimental groups ($p_{\text{overall}} = 0.138$) with Ct values of 22.34 ± 0.19 (ES, $n = 6$), 22.89 ± 0.21 (LS, $n = 7$), 22.81 ± 0.20 (EN, $n = 6$) and 21.91 ± 0.35 (LN, $n = 7$, [Figure 5.4](#)). The placental control tissue also amplified within an appropriate range (22.95 , $n = 1$).

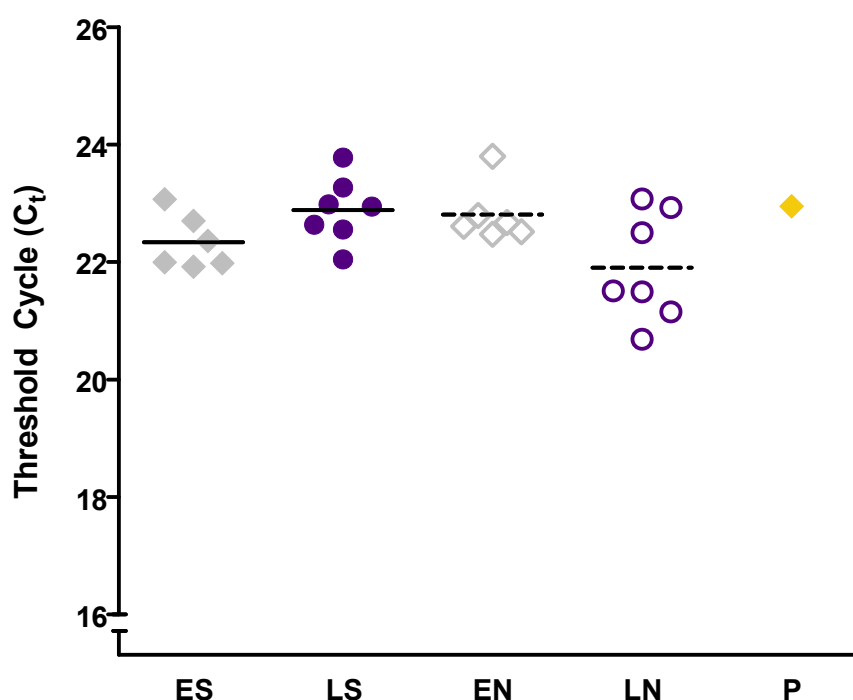


Figure 5.4 Ct values were not significantly different across the experimental groups ($p_{\text{overall}} = 0.138$). Two-way ANOVA on ranked data; placenta (P) was not included in the analysis and is included for reference only. ES, LS, EN and LN are early sham, late sham, early SNx and late SNx, respectively.

Two representative PCR reaction products from each experimental group (ES, LS, EN and LN) were examined ([Figure 5.5](#)) using 2.5% non-denaturing agarose gel as described in [Section 2.11.3.2](#) along with a high (50 ng, lane 2) and mid-range (3.125 ng, lane 3) standard. A single band was seen in all standards and samples (lanes 2 - 11) at around 100 bp consistent with the appearance of a single peak in the dissociation curve and with the predicted *Ywhaz* amplicon size (99 bp; [Table 2.7](#)). Representative NTC (lane 13), No RT (lane 14) and buffer (lane 15) negative controls were included and did not produce any visible bands; placenta (lane 12) produced a band at approximately 100bp. Hyperladders II (50 bp ladder, lane 1) and IV (100 bp ladder, lane 16) were included for reference.

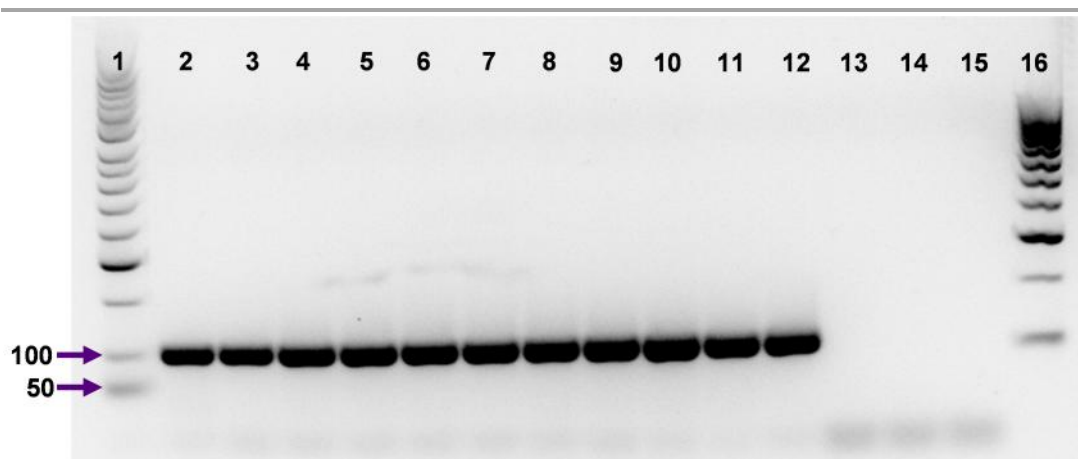


Figure 5.5 Strong bands were seen at approximately 100 bp in standards (lanes 2: 50 ng and 3: 3.125 ng), samples (lanes 4 to 11) and placenta (lane 12), consistent with the predicted *Ywhaz* amplicon size (99 bp). There were no bands in the no template (lane 13), no reverse transcriptase (lane 14) or water/buffer (lane 15) negative controls. Left to right: early sham (lanes 4 and 5), late sham (lanes 6 and 7), early SNx (lanes 8 and 9) and late SNx (lanes 10 and 11). Weight markers HyperLadder II (lane 1; 50 bp ladder) and HyperLadder IV (lane 16; 100 bp ladder) are included for reference.

5.3 *Uts2r*

Following the protocol outlined in [Section 2.13.5](#) (50 cycles and high cDNA load: 1 in 10) the *Uts2r* primer assay was generally successful, producing sigmoid-shaped amplification plots ([Figure 5.6a](#)) and a single peak in the dissociation curve ([Figure 5.6b](#)); detection (Ct) occurred at 30 - 38 cycles. Transcript was detectable in 6 of the 8 standards tested (tested range: 125 - 0.98 ng, detectable range: 125 - 3.91 ng), with good reaction efficiency (98.5 %, [Figure 5.6c](#)). The fit of the standard curve was reasonable but did not meet the assay acceptance criteria for full analysis ([Section 2.13.8](#)), however the *Uts2r* data here have been analysed as an example (see [Section 5.3.1](#) below).

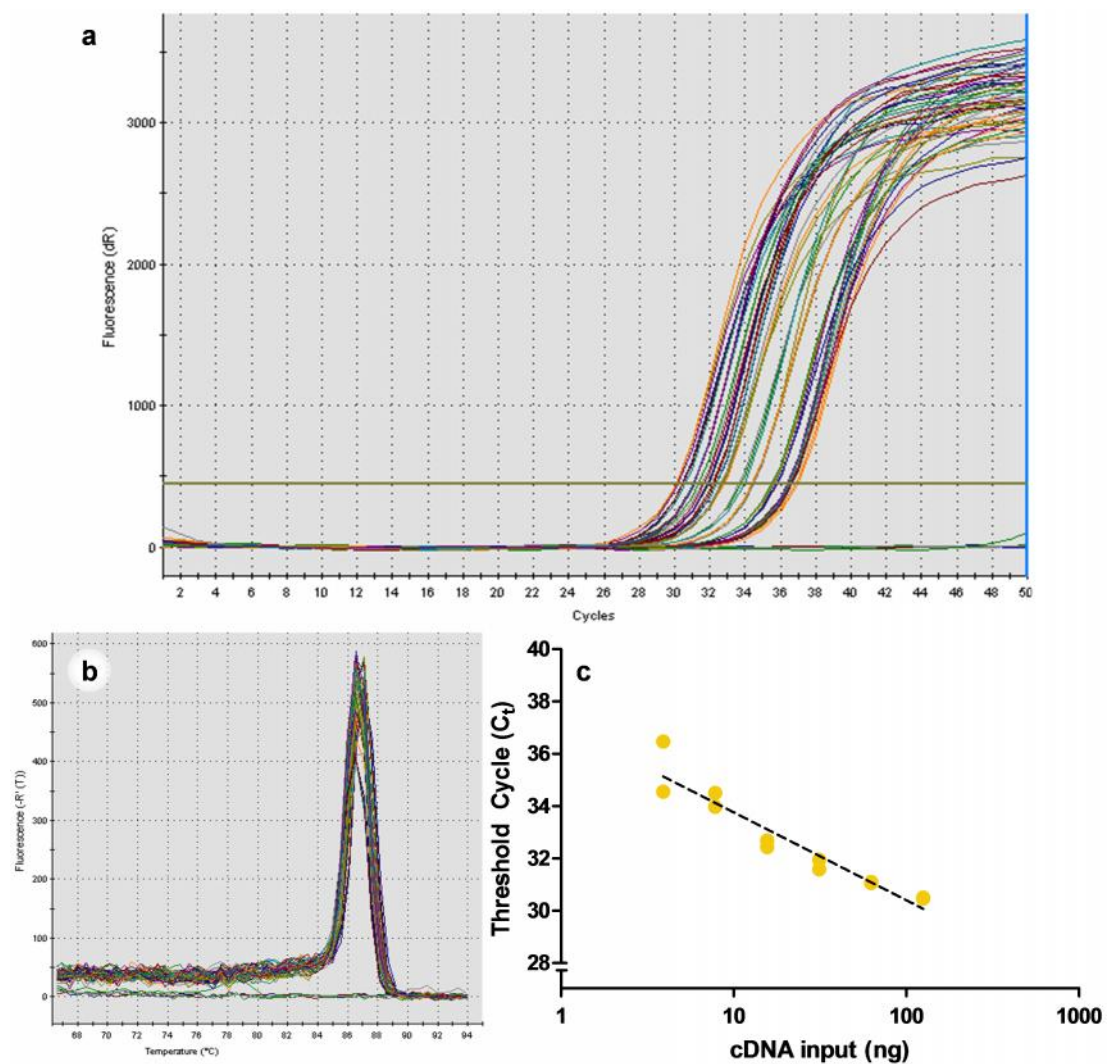


Figure 5.6 Results of qPCR assay for *Uts2r* **(a)** sigmoidal plots showing consistent amplification between 30 and 40 cycles. No amplification occurred in the no template, no reverse transcriptase or water controls. **(b)** A single peak in the dissociation curve. **(c)** log-linear standard curve with a slope of -3.359 and $R^2 = 0.909$ over 6 standards (125 - 3.91 ng).

Amplification viability varied from group to group; all samples in the LN group amplified ($n = 7$) whilst only 2 (out of 7) from the LS group amplified (Figure 5.7, individual points represent biological replicates). Amplification was also reliable in the placental sample (C_t : 30.16, $n = 1$) There was no amplification seen in the NTC, no RT or water negative controls.

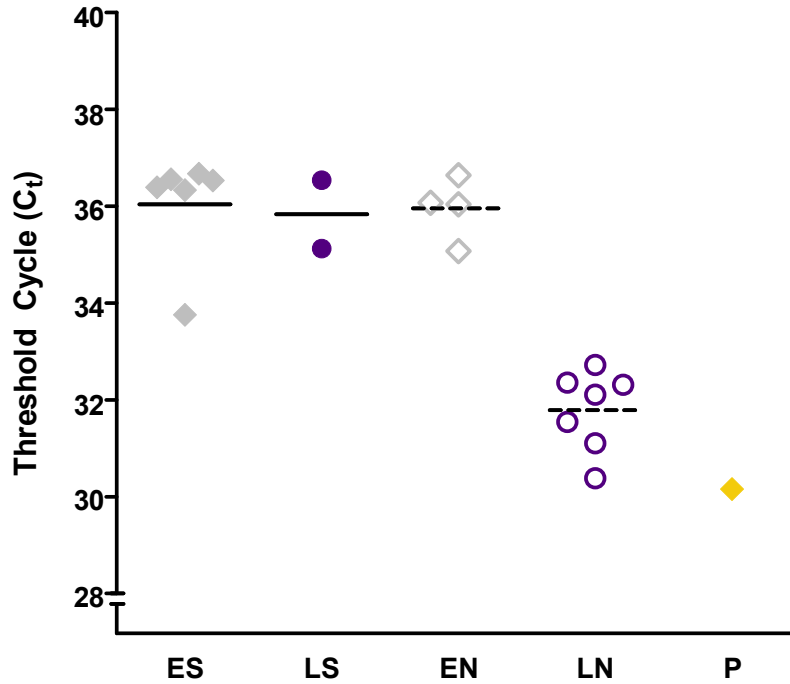


Figure 5.7 Ct values were significantly different across the experimental groups ($p_{\text{overall}} < 0.001$). Both fixed experimental factors had an effect on the Ct values reported, $p_{\text{SNx}} = 0.006$ and $p_{\text{time}} = 0.011$. Two-way ANOVA on ranked data, placenta (P) was not included in the analysis and is included for reference only. ES, LS, EN and LN are early sham, late sham, early SNx and late SNx, respectively.

Electrophoresis of final PCR reaction products produced prominent bands in all samples and standards which appeared slightly heavier than 100 bp in weight (Figure 5.8, lanes 2 - 12). This is consistent with the predicted *Uts2r* amplicon size (116 bp) and the presence of a single peak in the dissociation curve (Figure 5.6b); in addition the band was absent from the NTC, No RT and buffer negative controls, lanes 13, 14 and 15 respectively.

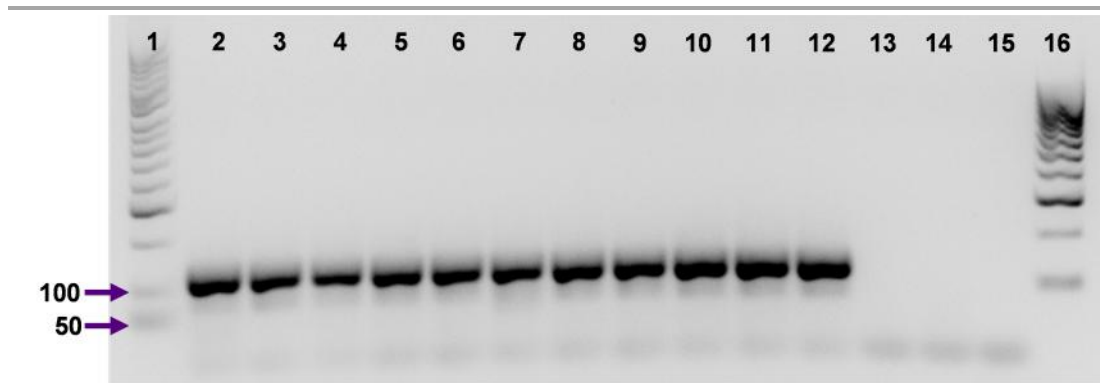


Figure 5.8 The *Uts2r* primer set produced an intense band above the 100 bp marker (predicted *Uts2r* amplicon size 116 bp) in all standards and samples. Lanes 2 and 3 contain standards (125 and 15.63 ng, respectively) with no bands seen in the negative controls; NTC, No RT and buffer loaded in lanes 13, 14 and 15, respectively. Samples are loaded as follows: lanes 4 and 5, early sham; 6 and 7, late sham; lanes 8 and 9, early SNx; lanes 10 and 11, late SNx; and lane 12, placenta. Weight markers HyperLadder II (lane 1; 50 bp ladder) and HyperLadder IV (lane 16; 100 bp ladder) are included for reference.

5.3.1 Example of further analysis of *Uts2r* expression

Example fold change expression (calibrator sample: placenta) analysis was carried out relative to internal control *Ywhaz* and taking into account variations in reaction efficiency according to the Pfaffl³¹¹ modification (as described in [Section 2.13.8](#), [Equation 2.7](#)). Relative *Uts2r* expression varied significantly between the groups ($p_{\text{overall}} = 0.001$, [Figure 5.9](#)). Notably, *Uts2r* expression was substantially higher in the LN group (1.084 ± 0.515 , $n = 7$) than in the ES (0.096 ± 0.062 , $n = 5$, $p = 0.001$) and EN groups (0.0672 ± 0.020 , $n = 4$, $p = 0.005$). Whilst relative *Uts2r* expression was also lower in the LS group (0.090 ± 0.020), compared to the LN group, this difference was not significant ($p = 0.138$); this was most likely the result of low n number in the LS group ($n = 2$). Data analysed by two-way ANOVA on ranks with a Tukey post-test.

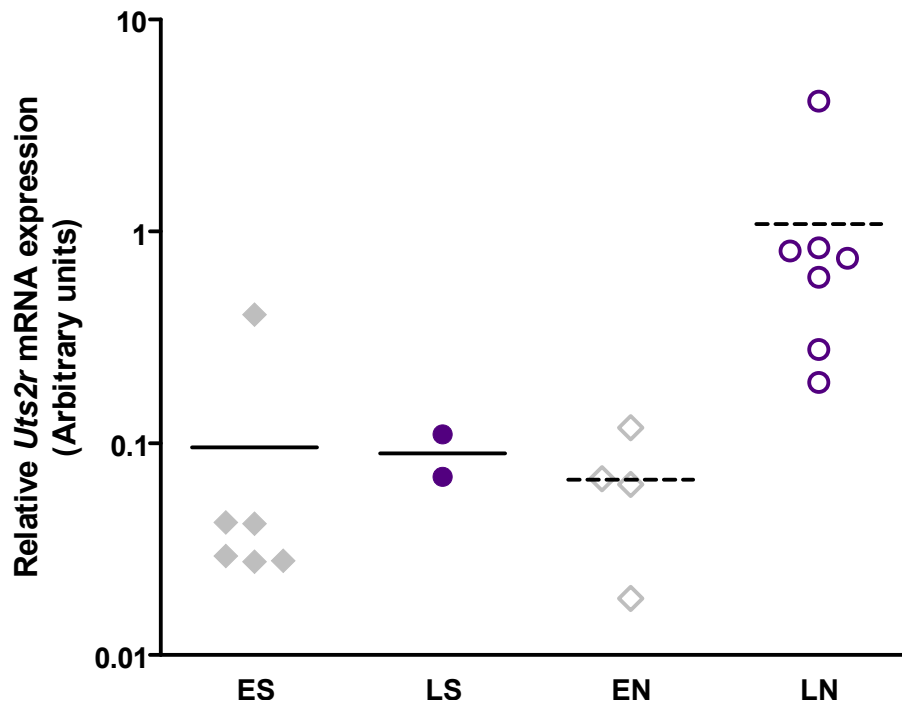


Figure 5.9 Relative expression of *Uts2r* was higher in the renal cortex of late SNx animals (LN, $n = 7$) than in early sham (ES, $n = 6$, $p = 0.001$) and early SNx (EN, $n = 4$, $p = 0.005$). There was no difference between LN and late sham (LS, $p = 0.138$) due to a reduction in n number ($n = 2$). Data are normalised to reference gene *Ywhaz* and expressed relative to calibrator sample (placenta). Calculation is adjusted for differences in reaction efficiency using the Pfaffl method.³¹¹ Data are analysed by two-way ANOVA on ranked data with a Tukey post-test, $p_{\text{overall}} = 0.001$.

5.4 *Uts2b*

Amplification of *Uts2b* (URP) occurred in most biological replicates; however amplification viability was not consistent across the technical replicates. In many samples only one replicate amplified successfully. This PCR assay was extended to 55 cycles (Figure 5.10a) and produced sigmoidal-shaped amplification plots in most samples (Ct typically 35-40). Amplification of *Uts2b* in the placental sample was sporadic and occurred only at high cycle numbers (Ct > 40); only reactions conforming to the single dissociation peak were included (Figure 5.10b). Amplification occurred in the top 4 standards; however both the fitting of the curve ($R^2 = 0.717$) and assay efficiency (184 %) were poor (Figure 5.10c); as such data are presented as raw Ct values.

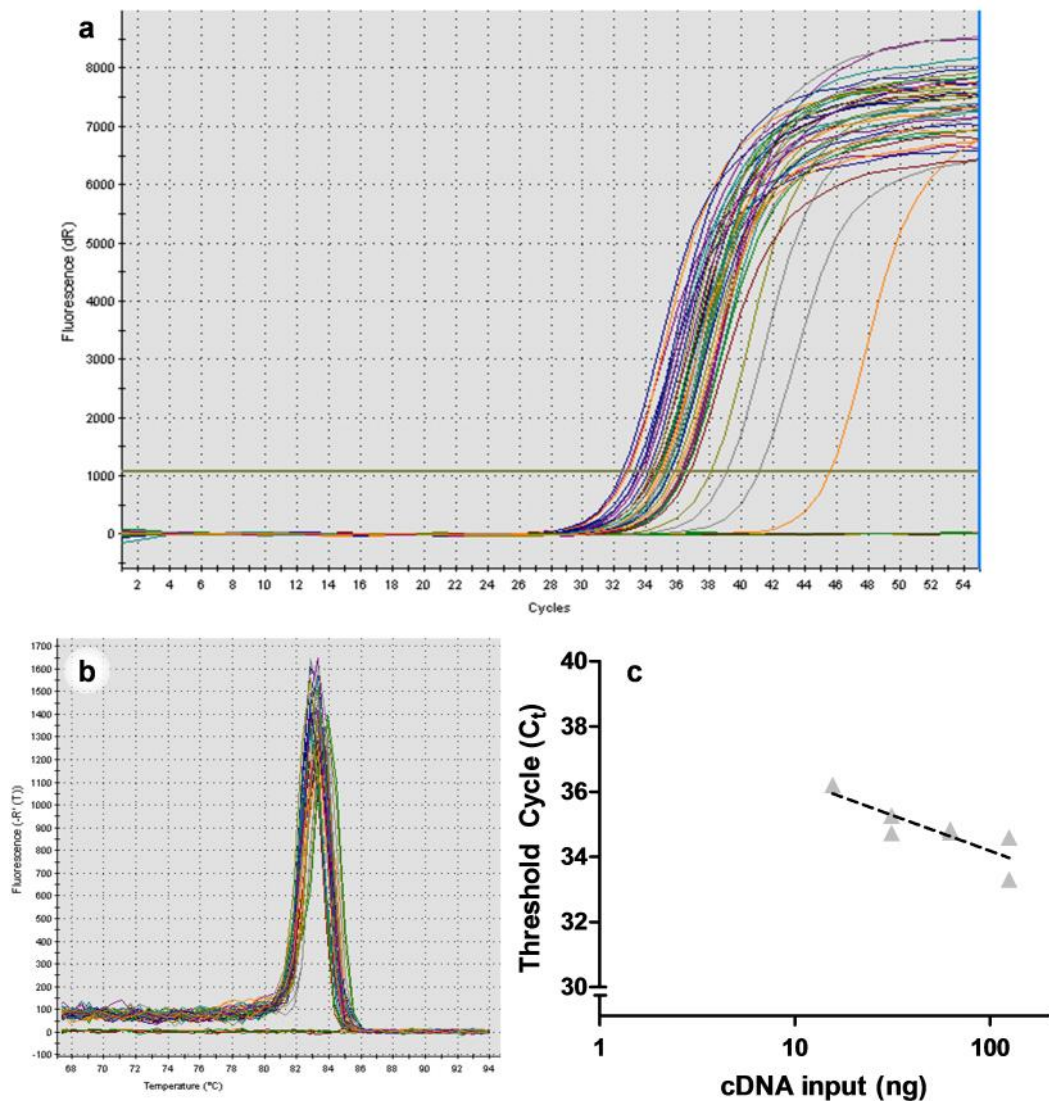


Figure 5.10 Results of qPCR assay for *Uts2b* **(a)** sigmoidal plots showing amplification in the range of 30 and 45 cycles. No amplification occurred in the no template, no-reverse transcriptase or water controls. **(b)** A single peak in the dissociation curve. **(c)** log-linear standard curve with a slope of -2.182 and $R^2 = 0.717$ over 4 standards (125 - 15.63 ng).

Amplification appeared to occur earlier in the SNx groups (EN: 35.29 ± 0.40 , $n = 6$ and LN: 33.94 ± 0.43 , $n = 7$) than in the shams (ES: 36.34 ± 0.68 , $n = 4$ and LS: 36.52 ± 0.46 , $n = 6$). Analysed by two-way ANOVA on ranks with Tukey post-test ($p_{\text{overall}} = 0.001$, $p_{\text{SNx}} = 0.001$ and $p_{\text{time}} = 0.345$, [Figure 5.11](#)), the LN group was different to both the ES ($p = 0.016$) and LS ($p = 0.002$) groups. It is disingenuous to suggest that this is indicative of altered expression as some samples produced additional bands in the PCR product gel ([Figure 5.12](#)) and the assay standard curve was stunted, with poor fit and provided an unreliable efficiency. However, there was no amplification seen in the NTC, no RT or water negative controls. In addition the

placental sample amplified extremely late in the assay ($C_t = 45.63$, one replicate from two amplified).

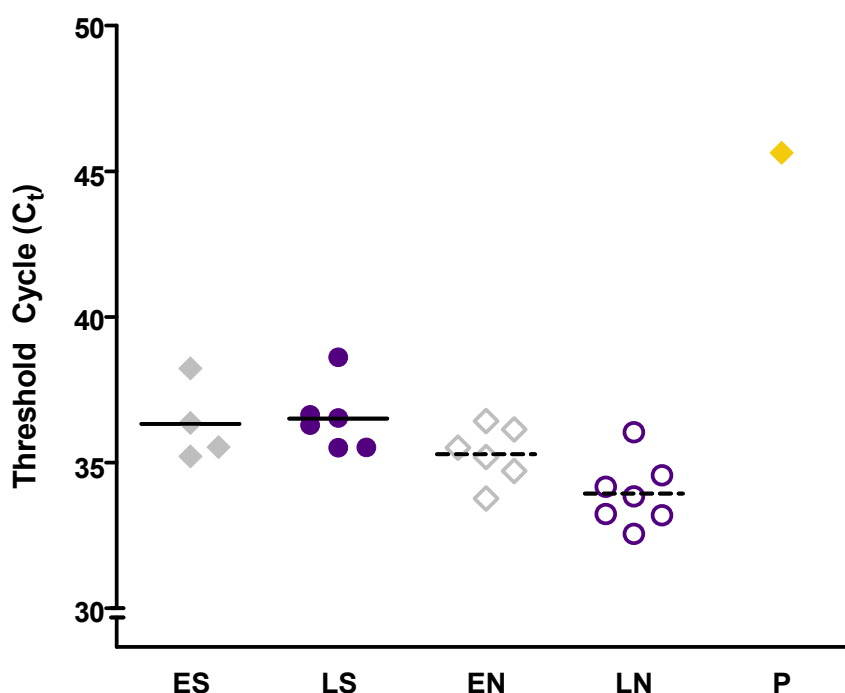


Figure 5.11 C_t values from the *Uts2b* assay were significantly different across the experimental groups ($p_{\text{overall}} = 0.002$). These effects predominantly arose from the effect of the SNx procedure ($p_{\text{SNx}} = 0.001$), whereas time alone was not significant ($p_{\text{time}} = 0.345$). Two-way ANOVA on ranked data, placenta (P) was not included in the analysis and is included for reference only. ES, LS, EN and LN are early sham, late sham, early SNx and late SNx, respectively.

The *Uts2b* primer set produced an intense band above the 100 bp marker (predicted *Uts2b* amplicon size 120 bp) in most standards and samples (**Figure 5.12**). Lanes 2 and 3 contain standards (125 and 15.63 ng, respectively) with no bands seen in the negative controls; NTC, No RT and buffer loaded in lanes 13, 14 and 15, respectively. Samples from the LS group (lanes 6 and 7) produced a single intense band in line with the band seen in the standards. A corresponding intense band was also seen in EN (lanes 8 and 9) and LN groups (lanes 10 and 11) and ES (lane 5). In some lanes (5, 8 and 10) this major band was accompanied by two faint bands with higher molecular weight (> 300 bp). In the placental sample (lane 12) the band appears to have migrated further. The anomalous band pattern in lane 4 corresponds, by weight, to the other lanes however the intensities are reversed. Weight markers HyperLadder II (lane 1; 50 bp ladder) and HyperLadder IV (lane 16; 100 bp ladder) are included for reference.

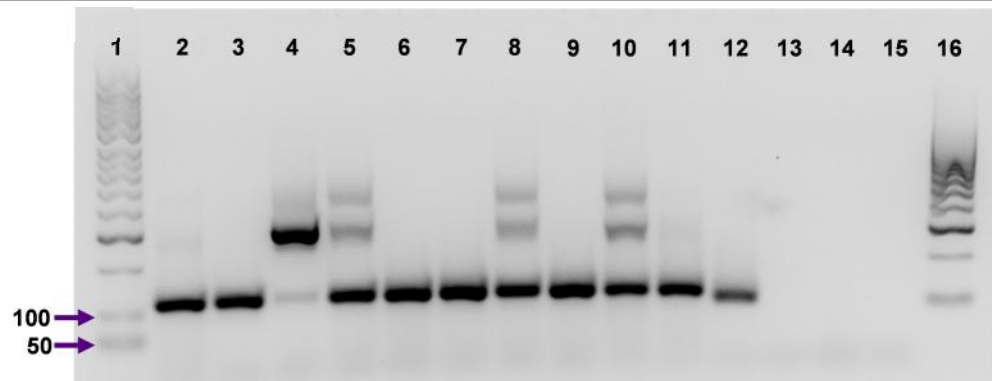


Figure 5.12 The *Uts2b* primer set produced an intense band above the 100 bp marker (predicted *Uts2b* amplicon size 120 bp) in most standards and samples. Lanes 2 and 3 contain standards (125 and 15.63 ng, respectively) with no bands seen in the negative controls; NTC, No RT and buffer loaded in lanes 13, 14 and 15, respectively. Samples are loaded as follows: lanes 4 and 5, early sham; 6 and 7, late sham; lanes 8 and 9, early SNx; lanes 10 and 11, late SNx; and lane 12, placenta. Weight markers HyperLadder II (lane 1; 50 bp ladder) and HyperLadder IV (lane 16; 100 bp ladder) are included for reference.

5.5 *Uts2*

Generally amplification of *Uts2* from the cortex of was not reliable in any experimental group. Initial examination of the amplification plots appeared promising, with appropriate curve shape. However amplification occurred very late, with a $C_t > 35$ in all wells (**Figure 5.13a**). This late stage amplification produced numerous peaks within the dissociation curve (**Figure 5.13b**) and amplification of standards was equally variable (**Figure 5.13c**). There was no clear standard curve ($R^2 = 0.101$) and the calculated reaction efficiency was incompatible with a successful qPCR assay (351.3 %). As a result there were no further findings to report from this assay.

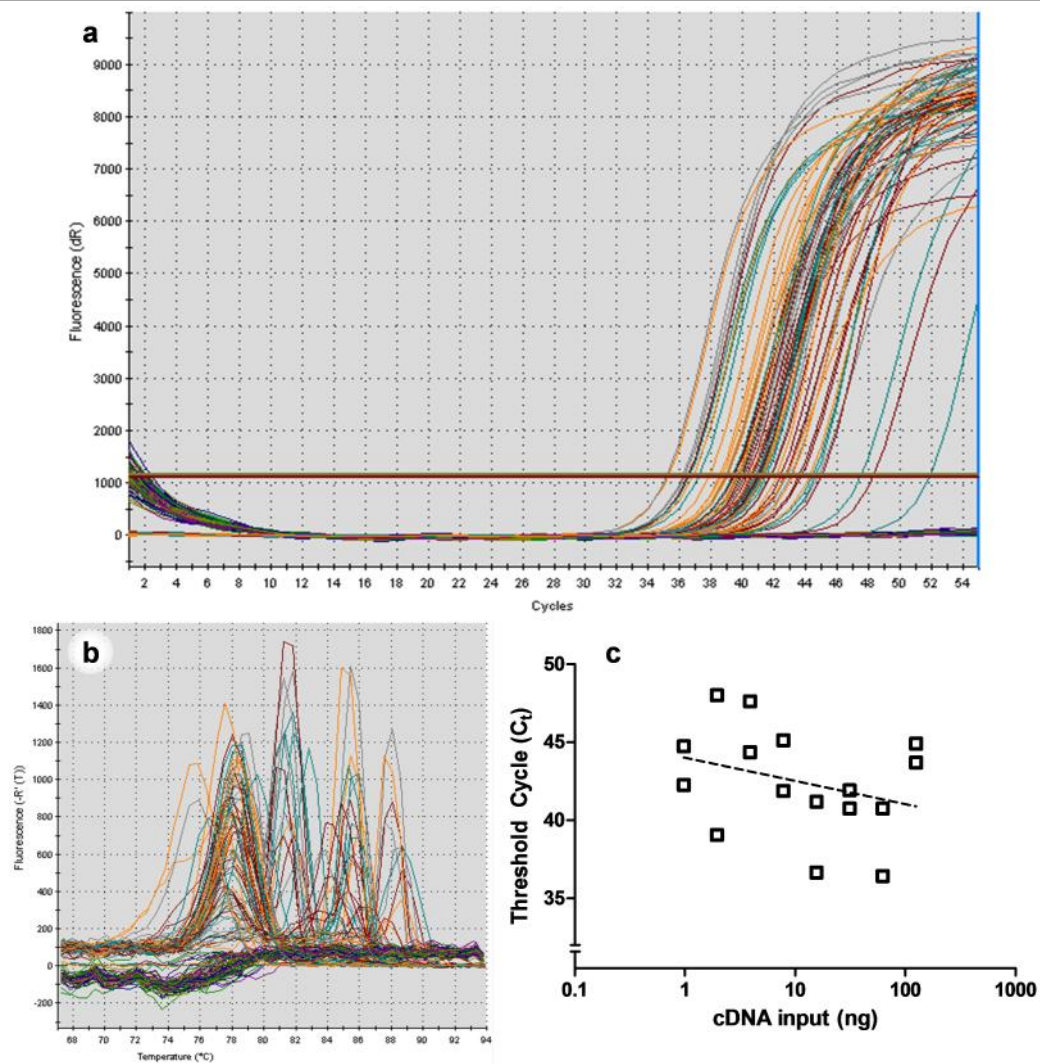


Figure 5.13 Results of qPCR assay for *Uts2* **(a)** sigmoidal plots showing amplification occurred late, $C_t > 35$. No amplification occurred in the no template, no-reverse transcriptase or water controls. **(b)** Multiple peaks in the dissociation curve, indicative of non-specific amplification. **(c)** There was no clear log-linear standard curve $R^2 = 0.101$ over the 8 tested standards (125 - 3.91 ng), slope = - 1.527; a slope of - 3.1 to - 3.6 is generally acceptable.

6: Discussion: Expression of *Uts2r*, *Uts2b* and *Uts2* by RT-qPCR in the SD rat following 5/6th SNx

The detection of urotensin II (UII) and urotensin II related peptide (URP) using antibody based methodologies has previously provided insight in to the tissue localisation of the peptides in a semi-quantitative manner or has been used to assay peptide concentrations in biological samples. However as discussed previously, when no separation process is applied the immuno-reactivity represents combined detection of UII, Pro-UII and URP: the peptides cannot be properly differentiated using antibodies alone due to significant sequence homology.²¹⁶ In contrast the genes and mRNAs encoding UII and URP expression are quite different and the loci are found on different chromosomes.^{359,360} Theoretically the differences between the mRNA sequences means that it is possible to examine the expression of UII and URP independently; however as will be discussed there were other technical hindrances associated with this process.

The initial experiments in this work demonstrated that RNeasy-Lysate was an effective method for the extraction of good quality RNA from previously frozen rat renal cortex samples ([Section 2.11](#)). From this the methods of reverse transcription (Qiagen Quantitect) and qPCR assay chemistry (Quantifast SYBR Green, Qiagen) were also validated using the *Ywhaz* target gene. Amplification of *Uts2r* (UT) was possible as was the amplification of *Uts2b* (URP). In contrast the assay for *Uts2* (UII) was exceptionally problematic. As such the results of these experiments should be interpreted with care.

6.1 mRNA extraction and quality controls

RNA is relatively unstable and as a result proper storage and handling is vital in preservation of sample integrity. Standard protocols generally call for rapid freezing (liquid nitrogen) and long-term storage at -70 °C or lower. The samples collected in this work were stored at -80 °C; storage duration was variable due to the nature of the long-term experiment. Snap frozen tissues present particular technical hurdles during mRNA extraction as the tissue must be pliable enough to homogenise completely for efficient extraction which often requires thawing. In addition heat is generated by the physical process of homogenisation, which is problematic as enzymatic mRNA degradation can occur before the homogenisation buffer penetrates the tissue completely. More recently the availability of storage solutions

(RNA/ater[®]) has reduced the potential for sample degradation during extraction; however these can only be used at the point of sample collection and not to treat previously frozen tissues retrospectively. Instead the samples in this work were treated with RNA/ater[®]-ICE prior to the RNA extraction procedure. Although the use of RNA/ater[®]-ICE was novel to this laboratory the reagent is well documented by the supplier as a reliable method of RNA extraction from previously frozen tissue.³⁶¹ This was supported by the results of the trial extractions ([Section 2.11.4](#)) where samples treated with RNA/ater[®]-ICE were indistinguishable from those treated with RNA/ater[®] in concentration, purity or amplification potential following reverse transcription.

6.1.1 RNA purity by absorbance

The standard accepted limits for RNA purity measured using a spectrophotometer-based method vary by source; however typical recommendations are that the A_{260}/A_{280} ratio should be around 2.0 and the $A_{260}/A_{230} > 2.0$. These ratios are used to determine contamination of the RNA samples and the limits on the A_{260}/A_{280} ratio have been firmly established with deterioration of amplification due to contaminant carry over. This can be particularly problematic in more dilute RNA samples due to increased carry-over in to the later stages of experiments. In contrast the limits for the A_{260}/A_{230} ratio are less well defined and samples with ratios as low as 0.43 have been shown to be of sufficient quality for qPCR reactions.^{310,362} This issue is complicated by the different guanidine salts used in lysis buffers; even small quantities of guanidine thiocyanate (as found in buffer RLT plus, Qiagen³⁶³) carried over during mRNA extraction have comparatively large effects on the A_{260}/A_{230} ratio whereas guanidine hydrochloride has a lesser effect on the absorbance at 230 nm.³⁰⁹ All RNA extracts used in this work were measured at $A_{260}/A_{280} \geq 2.0$ and $A_{260}/A_{230} > 0.5$.

The absorbance and ratios can be used to determine the concentration and purity of RNA extracts. These measures do not provide any insight into the quality (integrity) of any present RNA.³⁶⁴ To address this all RNA extracts were examined by gel electrophoresis for the presence of ribosomal RNA subunit bands (See example gels in [Figure 4.2](#)) and absence of both high molecular weight gDNA contamination and low molecular weight degradation products. Since this pilot study ([Section 2.11](#)) was carried out using freshly frozen or RNA/ater[®] treated tissue the potential for mRNA degradation resulting from storage temperature variation was minimal and the samples stored for the longer durations (EN, ES, LN and LS samples) all compared well with these qPCR pilot study samples and, as discussed below, the amplification

of a control gene (*Ywhaz*) was reliable which is indicative of RNA integrity and amplification potential.

6.2 Technical considerations of QuantiFast SYBR Green qPCR

The pre-prepared assay mastermix (QuantiFast SYBR Green PCR Master Mix, Qiagen) that was used is a proprietary reagent; as such the concentrations of Taq polymerase, dNTP, Mg^{2+} and ROX reference dye are not disclosed. Similarly the forward and reverse primers in primer assays (Quantitect primer assay, Qiagen) are provided pre-mixed and at undisclosed concentrations. A downside of this methodology is the inability to further optimise the assay conditions beyond cDNA input and cycling conditions. In contrast supplier-based optimisation removes the trial and error approach to assay optimisation within single laboratories and has the potential to standardise the assay set-up across both different genes and laboratories whilst also being highly reproducible across assays. This pre-optimisation does however present other issues; the primer sequences are not disclosed and are provided pre-mixed preventing sequencing of the amplification product and subsequent confirmation of the PCR product. This commercial protection of a product is understandable; however this makes it more difficult to conform to the minimum information for publication of quantitative real-time PCR experiments (MIQE) guidelines.^{364,365} It could be possible to design primers based upon the GeneGlobe specifications (provided in [Appendix A](#)^{307,308,366,367}) however since this is only a schematic location of the amplicon it would require trial and error type refinement so it is not practical given the limited availability of PCR product. To address these traceability issues a copy of the information about each primer assay has been included ([Appendix A](#)) and an electronic copy (PDF) of the webpage referenced has been retained.

6.2.1 Controls and sample selection

Selection of cortical tissue was based upon the premise that the majority of functional and structural changes that take place in CKD and the 5/6th SNx model are associated with the glomeruli and interstitial tissue of the renal cortex.^{294,301} It was this affected cortical tissue that presented the greatest potential for change over the course of disease and so efforts were initially focused on analysis of mRNA extracted from samples enriched for renal cortex. This did present other issues as

although UII/URP immunoreactivity has been consistently reported in the cortex UT is not routinely detected in these samples.^{178,268} In addition, qPCR analysis has shown previously that the mRNA expression of *Uts2*, *Uts2b* and *Uts2r* tends to be greater in the renal medulla.^{216,268}

Alongside the experimental samples a number of controls were included. Negative controls were included in each assay for the reverse transcription procedure (No RT and no template control) and for the qPCR assay reaction (No cDNA). Occasional amplification occurred in negative control samples at the extremes of the reaction and generally well above the amplification window of the positive samples. These instances will be discussed independently within the sections below in context of the assays. A secondary tissue type was included (placenta) for comparison to the renal samples and as a potential calibrator sample.

6.2.2 Reference gene: Tyrosine 3-monooxygenase/tryptophan 5-monooxygenase activation protein, zeta - *Ywhaz*

The *Ywhaz* gene is a commonly used reference gene with a reliable expression profile.^{368–370} *Ywhaz* has been identified as a suitable reference gene in multiple rat tissues including kidney. Furthermore, *Ywhaz* has been used as a reference gene in previous work in this laboratory (in combination with *Atp5b* and *Canx*) for expression analysis of renal tissue from SD rats (up to 4 weeks).^{232,306,371} Amplification of *Ywhaz* was consistent and reliable in all samples from cDNA prepared at a dilution of 1 in 100, producing regular sigmoidal plots with C_t values in the range of 20.69 - 23.80 (from mean of replicates, 2 per sample). In addition to the consistent amplification across the samples the assay produced a highly reliable standard curve ($E = 104.0\%$, $R^2 = 0.998$) which is in line with the general guidelines which suggest reaction efficiency should be between 90 and 110 % with a well fitted line through all standards ($R^2 \geq 0.985$). This amplification was reliable and served both as a control for amplification potential of the cDNA stocks and as an indicator of the reliability of the QuantiFast® SYBR green qPCR chemistry (Qiagen). Whether or not the primer sequences span exon:exon junctions is not indicated; however the supplier information for this primer assay indicates that the amplicon is located over two exons (Exons 2 and 3, Ensembl Transcript ID: ENSRNOT00000035628^{367,372}) separated by an intron and there is no suggestion that this primer pair would amplify

genomic DNA within the assay information.^{*2*} Analysis of the PCR products by gel electrophoresis indicated the presence of a single band consistent with the predicted amplicon size. If amplification of gDNA products did occur there would be a secondary, heavier weight, band seen in the gels. Overall the results of this assay indicated that, for well-expressed genes such as *Ywhaz*, the QuantiFast® qPCR technology was reliable and easy to implement.

6.3 Expression of urotensin II system components by RT-qPCR

Detection of UII/URP (*Uts2/Uts2b*) and UT (*Uts2r*) by immunohistochemical methods in rat kidney has proven largely reproducible; in contrast detection of mRNA transcripts has been more problematic.^{178,216,232,268} After the initial experiments it was clear that the UII system genes were expressed at a much lower level than *Ywhaz*. Sugo et al.²⁰⁰ were not able to detect *Uts2* or *Uts2b* transcripts in rat kidney using qPCR (TaqMan assay, cycle number was not disclosed) which is consistent with the earlier work of Coulouran et al.²⁰⁵; interestingly both groups detected transcripts in human kidney.^{196,200} Tal et al. describe an absence of mRNA for UT (*Uts2r*, referred to as SENR) by RT-PCR and Northern blot.³⁷³ However, successful amplification of these genes using the TaqMan methodology has been reported by Mori et al. although detection of *Uts2* in particular required a high cycle number which indicates that this was not a typical assay range and is consistent with the amplification of low copy number mRNAs (55 cycles).¹⁷⁸ When the RT-PCR and later RT-qPCR technologies were initially hypothesised and implemented there was an assumption that mRNA and protein expression would correlate; it is now known that this is not always the case and numerous factors affect the expression of both mRNA and protein and as a result this relationship is not simple or linear. Turnover rates of the peptide and mRNA (e.g. polyadenylation), translation efficiency (e.g. codon bias and mRNA folding), protein interaction and sequestration all affect the ratio between mRNA and protein.^{374–376}

6.3.1 Urotensin II receptor - *Uts2r*

Song et al. described UT immunostaining in a small number of glomerular capillaries and some distal tubule cells; beyond this UT is not routinely reported within the renal

^{*2*} Other non-spanning assays from this supplier include a warning regarding the potential to amplify genomic DNA. See [Appendix A](#)

cortex of adult rats.²¹⁶ In addition the mRNA transcript from the *Uts2r* gene has been detected by qPCR methodologies, but with poor consistency.^{216,268} Nonetheless Ull has been shown to have an effect on GFR in *in vivo* renal clearance studies implying that UT is present in the cortex.^{216,267,268,284} In the medulla there were clear differences in the staining intensity in the collecting ducts of late SNx rats compared to the other experimental groups which was accompanied by generalised staining within the cortex, so it was hoped that this difference would also be quantifiable at the mRNA level.

The *Uts2r* transcript is the product of a single exon therefore it is not possible to prevent amplification of gDNA products by primer design alone. However it is unlikely that sufficient gDNA remained within the samples to interfere with amplification as both the RNA extraction process (RNeasy® plus mini kit, Qiagen) and cDNA synthesis (QuantiTect® RT kit, Qiagen) included independent gDNA removal procedures.²³⁰ In addition to these gDNA removal processes a no RT control was included and this did not amplify during the qPCR assay.

Initial attempts to amplify *Uts2r* from cDNA at a 1 in 100 dilution were unsuccessful in all samples; it was however possible to consistently amplify a product from most samples using the cDNA at a 1 in 10 dilution. The UT receptor protein appears to have a clear distribution skew towards the medulla and so low expression was anticipated within the cortex. However UT staining was seen in the cortex of LN and to some extent within the EN rats; consistent with this observation the amplification of UT tended to occur earlier in the LN cohort.

Although the *Uts2r* assay did not meet the criteria for full analysis ($R^2 \geq 0.985$ and $90 \leq E \leq 110$ %) the data are analysed as an example and revealed a (potential) significant increase in *Uts2r* within the cortex of LN rats, a difference which would represent approximately a 10-fold increase in mRNA. Interestingly this is consistent with the previously reported mRNA analysis in SNx rats at 8 weeks post-surgery by Mori et al.¹⁷⁸. Further examination of the expression of *Uts2r* in the renal medulla of these experimental groups may be more successful as the expression of the receptor in these tissues is anticipated to be greater under normal conditions. If this assay was to be used in further work samples would be run in triplicate as this is more appropriate when working with low copy numbers since distribution of template copies between reactions tends not to follow a normal distribution.

6.3.2 Urotensin II related peptide - *Uts2b*

In contrast to immunohistochemical staining techniques it is possible to differentiate UII and URP using both PCR and RT-PCR methodologies as, despite the considerable sequence homology of the mature forms, the peptides are the product of different genes and there are pronounced differences in the mRNA transcripts.²⁰¹ *Uts2b* was also undetectable in cDNA from renal cortex when used at a 1 in 100 dilution; it was however detectable in a number of samples using the revised assay conditions. The *Uts2b* primer assay did not span an exon:exon junction as a result there is the potential to amplify gDNA product. However all cDNAs produced were subject to two separate gDNA removal steps. There appeared to be the presence of some generally minor larger products (~ 200 and 300 bp) in some samples which are unlikely to represent gDNA amplification as the amplicon size would be the same as that produced from cDNA as the primer binding sites are within the same exon. It is unclear what these additional bands represent and the dissociation curve for the wells included in the gel analysis produced a single peak.

For completion the data from the experiment were analysed by ranking data on the Ct values. This did suggest that *Uts2b* expression was greater in the SNx cohorts which is consistent with the total UII-immunoreactivity reported ([Section 3.6](#)) previously and with the increased mRNA expression described by Mori et al. in the remnant kidneys of SNx rats 8 weeks post-surgery, although it should not be over interpreted given the technical issues experienced.¹⁷⁸ UII-immunoreactive staining tended to be most intense in the LN cohort, with EN staining more intense than that of either sham control cohort. There is an indication that this same pattern is seen within the *Uts2b* assay; unfortunately despite extensive optimisation it was not possible to produce data with the appropriate properties for analysis within the remit of the QuantiFast[®] assay technology.

6.3.3 Urotensin II - *Uts2*

Increased expression of *Uts2* has been reported in the remnant kidneys of 5/6th SNx rats at 8, but not 2, weeks post-surgery.¹⁷⁸ Immunohistochemical staining of UII and URP (combined due to cross reactivity of the primary antibody) appeared more intense in the EN group than in the ES group, with even greater staining seen in the LN cohort. Unfortunately the *Uts2* primer assay did not consistently amplify a product in cDNA samples produced from the ES, EN, LS or LN groups in cDNA used at a 1 in 10 dilution (50 ng per reaction). The TaqMan assay conditions used by Mori et

al.¹⁷⁸ describe an increase in the number of PCR cycles to 55 compared to 34 for *Uts2r* and 36 for *Uts2b*. This could indicate that Ull was also difficult to amplify using the assays in their study.

6.4 Experimental limitation and further considerations

The findings in this portion of work were limited by the complications of low gene copy number even at the limits of optimisation. Had reliable amplification been possible final assay conditions would have undergone further refinement. In particular technical replicates would need to be increased to triplicate and the selection of additional reference genes using either GeNorm or NormFinder technologies to identify the most stable reference gene combination (typically 2 or 3 genes) over the experimental groups and calibrator sample. In addition selection of a reliable calibrator sample would allow proper analysis of relative expression; candidate calibrator samples include brain or spinal cord collected within the laboratory or purchased as mRNA extract or as a cDNA library. Care would have to be taken as primers for *Uts2r* cannot be designed to span exon boundaries as the mRNA is the product of one exon so prevention of gDNA contamination is paramount within the calibrator sample if purchased. The cDNA library created within this work included two separate gDNA treatment steps during the RNA extraction and reverse transcription processes.

Further qPCR analysis of ECM components collagen IV alpha 1 (*Col4a1*), laminin- β_1 (*lamb1*) and fibronectin 1 (*Fn1*) was carried out using the cDNA library (1 in 100) generated in this work (Appendix B, assays carried out by Tom Speight). All transcripts were amplified reliably at Ct < 35 cycles. The results of these assays support the suggestion that low copy number of the Ull system genes (*Uts2*, *Uts2b* and *Uts2r*) play a major role in the poor amplification of these genes.

6.5 Conclusions

Ywhaz was used as an amplification control and potential reference gene. It was reliably amplified in all samples, but not in any negative controls, producing a single peak in the dissociation curve and a single band in the PCR product gel. This band appeared to be the appropriate size which is indicative of a successful assay and provided proof of concept for both the RNA/ater[®]-ICE treatment and subsequent reverse transcription and qPCR. The interpretation and discussion of the *Uts2r*, *Uts2b* and particularly *Uts2* expression as assayed by QuantiFast[®] SYBR Green qPCR is

limited as despite substantial optimisation and approaching the cDNA load limit for the reaction conditions the assays had a variable degree of success. These hindrances appear to arise from low copy numbers of the Ull system components in the renal cortex of rats, a finding which is not unique to this work. Despite these difficulties there is a suggestion that the UT receptor (*Uts2r*) is upregulated in late SNx beyond the changes that have been described at 8 weeks. This difference was also noted in the immunohistochemical staining of both cortex and medulla ([Section 3.6](#)).

7: Intervention with UT receptor antagonist AZ13694621 (SB-611812)

Animals were monitored extensively for changes in health and renal function associated with CKD induced by the 5/6th SNx procedure and for adverse reaction to the UT-antagonist (UT-A) compound or dosing protocol.

Data are presented as mean \pm SEM, unless stated otherwise.

7.1 Acute renal failure incidence and survival

As described previously ([Section 2.2](#)) animals underwent a 5/6th SNx which was performed in two stages in order to reduce the risk of acute renal failure (ARF). Of the 24 animals in this study that underwent the 5/6th SNx, 1 went into ARF, an incidence rate of 4.2 %. The case of ARF occurred within 48 hours of the second surgical procedure and there were no post-surgery complications within the sham group (n = 6 per treatment regimen). As a result group numbers were as follows: Sham-vehicle (SV: n = 6), SNx-vehicle (NV, n = 11), Sham-UT-A (SA, n = 6) and SNx-UT-A (NA, n = 12). Over the course of the study there were 5 premature deaths (causes: complications of dosing x 2, renal complication x 1, unknown cause x 2) within the SNx cohort distributed evenly between the NV and NA groups, n = 3 and n = 2 respectively ([Figure 7.1](#)). There were no cases of premature mortality in the sham groups. There were no differences between the survival curves (p = 0.340).

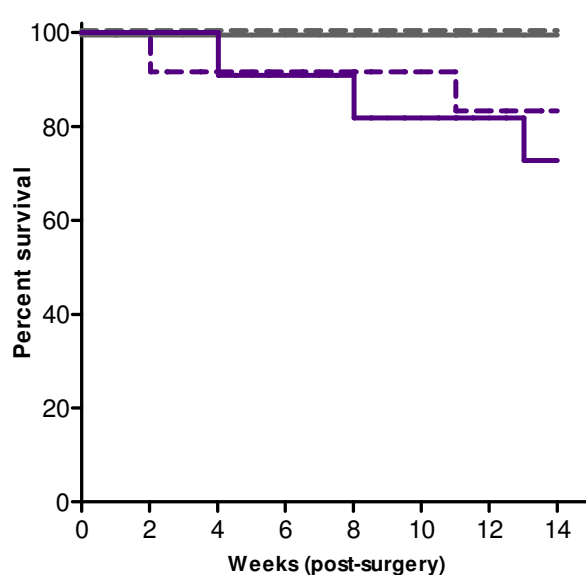


Figure 7.1 Kaplan-Meier survival analysis: the dosing procedure was well-tolerated in the sham groups (S, grey, vehicle (V): solid, UT receptor antagonist (A): dashed). Dosing was more problematic in the SNx (N, purple) groups, with 4 deaths in the NV group (one acute renal failure, solid) and 2 in the NA group (dashed). Initially n = 12 (NA), 11 (NV), 6 (SA) and 6 (SV). Survival was not significantly different between the groups (p = 0.340)

7.2 Physiological progression of CKD

Disease progression and treatment tolerance were monitored using a number of physiological parameters including changes in body weight ([Section 2.4.1](#)), systolic blood pressure ([Section 2.4.3](#)) and renal function by ACR in spot urine samples ([Section 2.4.2](#)).

7.2.1 Body weight

Initial weight was not different between the groups SV: 301.6 ± 5.9 g, $n = 6$, NV: 300.3 ± 4.4 g, $n = 12$, SA: 287.0 ± 4.9 g, $n = 6$ and NA: 286.0 ± 3.2 g, $n = 12$. Whilst rats in all of the groups gained weight throughout the study ($p_{\text{time}} < 0.001$) there was a visible divergence between the SNx groups and the matched-sham controls early (by week 1) in the study ($p_{\text{SNx}} = 0.002$). However, there were no differences between the UT-A groups and corresponding vehicle controls: the SV and SA group or NV and NA groups ($p_{\text{UT-A}} = 0.440$).

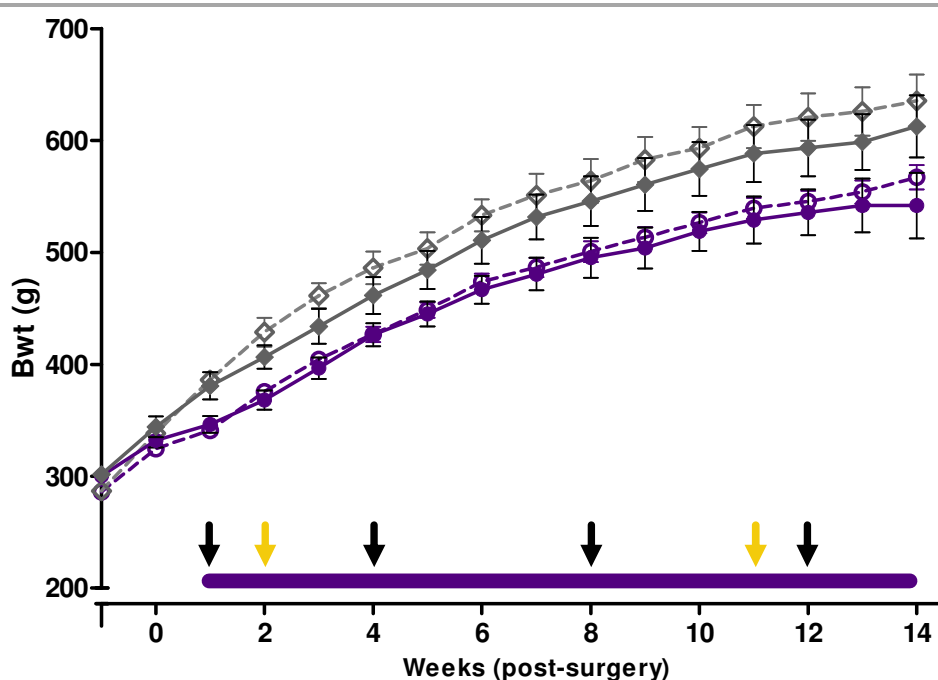


Figure 7.2 Growth curves for all groups demonstrate steady increases in body weight (bwt) up to approximately 600 g ($p_{\text{time}} < 0.001$), with no difference between animals receiving the UT receptor antagonist (A, dashed lines) or vehicle control (V, solid lines, $p_{\text{UT-A}} = 0.440$). However, both SNx (N) groups (purple, NV: solid, $n = 11$, and NA: dashed, $n = 12$) gained weight at a slower rate ($p_{\text{SNx}} = 0.002$) than the corresponding age-matched sham (S) groups (grey, SV: solid, $n = 6$ and SA: dashed, $n = 6$). Arrows represent mortality in the NV (black) and NA (yellow) groups, respectively. Analysed using a 3-way ANOVA with repeated measures (time).

7.2.2 Systolic blood pressure and heart rate

Time had a significant effect on SBP ($p_{\text{time}} < 0.001$) but SBP was comparable between the vehicle and UT-A treated shams (SV overall mean over study period: 136.9 ± 0.8 mmHg, compared to 137.2 ± 0.8 mmHg in the SA group) and remained consistent throughout the study period in both the SV ([Figure 7.3](#): solid grey line, $n = 6$, week 14: 135.1 ± 2.4 mmHg compared to week 2: 140.3 ± 4.3 mmHg,) and SA (dashed grey line, $n = 6$, week 14: 134.3 ± 3.2 mmHg compared to week 2: 142.5 ± 6.7 mmHg, [Figure 7.3](#)).

		Bwt	SBP	HR
Within Subject (RM)	Time	< 0.001	< 0.001	0.141
	Time * SNx	< 0.001	< 0.001	0.641
	Time * UT-A	0.001	0.697	0.331
	Time * SNx * UT-A	0.991	0.358	0.613
Between Subjects	SNx	0.002	< 0.001	0.420
	UT-A	0.440	0.032	0.180
	SNx * UT-A	0.649	0.050	0.883

[Table 7.1](#) Summary of results from 3-way analysis of variance (ANOVA) with repeated measures (RM, time, within subject) for physiological data. Probability values are shown for body weight (Bwt), systolic blood pressure (SBP) and heart rate (HR).

In contrast, rats within both of the SNx groups presented with a progressive ($p_{\text{time} \times \text{SNx}} < 0.001$) increase in SBP over the course of the study (purple lines, NV: solid and NA: dashed, [Figure 7.3](#)). Blood pressure was lower in the UT-A treated cohorts than in the vehicle treated controls ($p_{\text{UT-A}} = 0.032$); specifically the SNx rats within the UT-A treated group had lower SBP than those receiving the vehicle control by 6 mmHg (average difference in group mean: 5.9 ± 0.5 mmHg, $p_{\text{SNx} \times \text{UT-A}} = 0.050$). In the vehicle treated group the SBP was higher in the SNx group compared to the sham controls after 10 weeks (SNx: 154.4 ± 7.7 mmHg, $n = 9$ vs. sham: 137.1 ± 4.0 mmHg, $n = 6$, $p = 0.001$). Whilst in the UT-A treated group the SBP was not different between SNx (151.5 ± 11.0 mmHg, $n = 10$) and sham cohorts (134.8 ± 3.9 , $n = 6$) until week 12 ($p < 0.001$), representing a two week delay in the onset of an increase on SBP when compared to the SNx rats receiving the vehicle control. Once the SNx groups had diverged from the corresponding sham groups the difference between them persisted until the end of the study: in the vehicle treated group final SBP was

158.4 ± 6.8 mmHg (n = 8) in the SNx animals compared to SV: 135.1 ± 2.4 mmHg (n = 6) in the shams (p < 0.001). Similarly SBP was 151.8 ± 11.5 mmHg (n=10) in the UT-A treated SNx compared with 134.2 ± 3.2 mmHg (n = 6) in shams receiving UT-A. Final SBP tended to be lower in the SNx rats receiving UT-A compared to those receiving vehicle but this did not reach statistical significance.

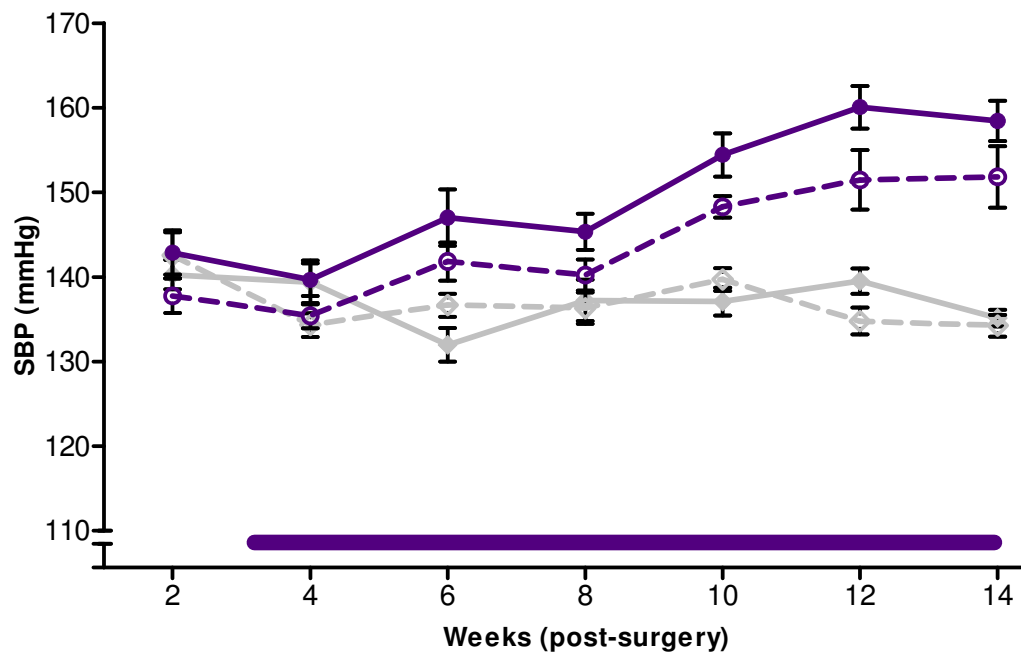


Figure 7.3 SNx rats developed progressive systolic hypertension over the course of the experiment ($p_{\text{time} \times \text{SNx}} < 0.001$). SBP deviated significantly from the treatment-matched sham controls in the vehicle treated SNx group (NV: purple solid line, 154.4 ± 7.7 vs. sham vehicle: grey solid line, 137.1 ± 4.0 mmHg, p = 0.001) and UT-A treated SNx group (NA: purple dashed line, 151.5 ± 11.1 vs. sham UT-A: grey dashed line, 134.8 ± 3.9 mmHg, p = 0.001) 10 and 12 weeks post-surgery, respectively. There was no significant change in blood pressure in the sham controls over the course of the experiment. 3-way analysis of variance (ANOVA) with repeated measures (RM, time, within subject)

In contrast, HR was not significantly different between any of the groups (**Figure 7.4**, p = 0.424). There was a modest increase in HR over the course of the study; however this was not significant (grand mean (all data) week 2: 427.2 ± 4.2 BPM, n = 34, rising to 438.1 ± 2.8 BPM in week 14, n = 30, $p_{\text{time}} = 0.141$).

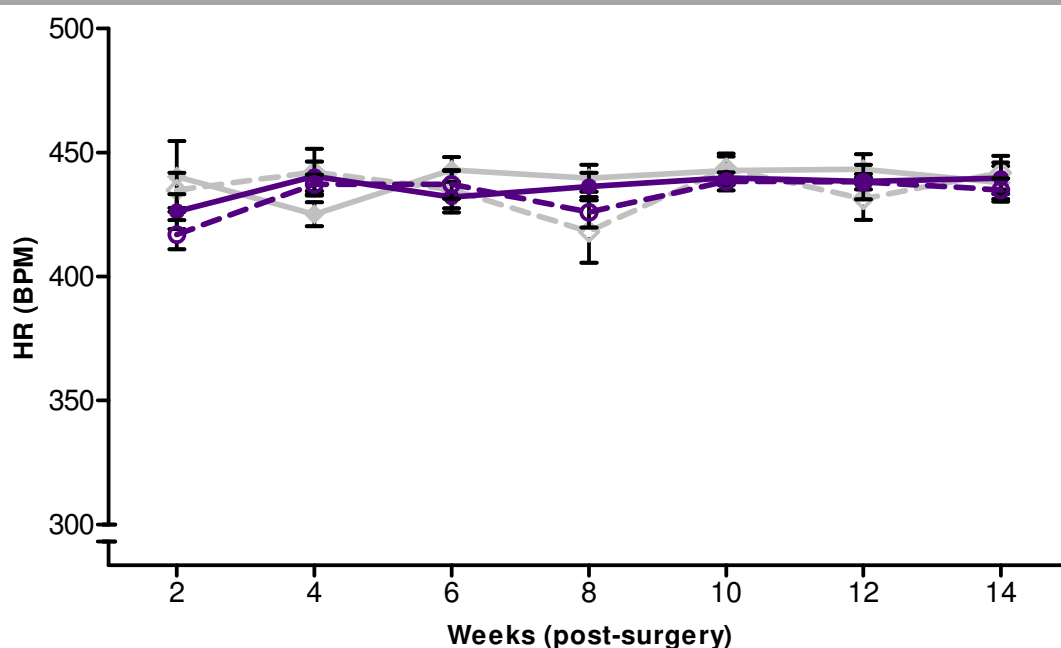


Figure 7.4 Heart rate (HR) was not different between the experimental groups ($p = 0.424$) and remained consistent over the course of the study ($p_{\text{time}} = 0.141$). Purple and grey lines denote SNx and sham groups, respectively. Similarly solid or dashed lines represent vehicle or urotensin II antagonist treatment, respectively. Data analysed by 3-way analysis of variance (ANOVA) with repeated measures (RM, time, within subject).

3.2.3 Renal function by ACR

ACR was calculated as described in [Section 2.6.3](#); the resulting raw ratio data were non-normally distributed, and as a result the values presented are median: IQR. Week 14 data points represent terminal urine samples collected under anaesthesia ($n = 5, 8, 4$ and 11 in the SV, NV, SA and NA groups, respectively).

Collectively the SNx rats developed albuminuria ($p < 0.001$) as the study progressed. ACR was significantly higher in the vehicle-treated SNx rats compared to the matched sham controls after 6 weeks (NV: $0.453: 0.036 - 1.515 \text{ mg}/\mu\text{mol}$, $n = 11$ compared to SV: $0.009: 0.006 - 0.011 \text{ mg}/\mu\text{mol}$, $n = 6$, $p = 0.013$). However the UT-A treated rats did not exhibit an increase in ACR until 8 weeks (NA: $1.445: 0.319 - 4.55 \text{ mg}/\mu\text{mol}$, $n = 10$ compared to SA: $0.009: 0.003 - 0.010 \text{ mg}/\mu\text{mol}$, $n = 5$, $p = 0.006$). After which ACR remained significantly elevated for the remainder of the study ([Figure 7.5](#)). Whilst ACR was elevated in both SNx groups (NV and NA) relative to the matched shams, ACR was not significantly different ($p = 0.473$) between the two SNx cohorts.

ACR in the UT-A treated shams ([Figure 7.5](#), open diamonds, SA, n = 6) was not significantly different from those receiving the vehicle control (filled diamonds, SV, n = 6, p = 0.963). In addition there was no time-dependent effects seen within either of the sham control groups over the course of the study; p = 1.000 and 0.890 for week 14 compared to week 2 in the vehicle (SV, n = 6) and UT-A (SA, n = 6) treated shams, respectively.

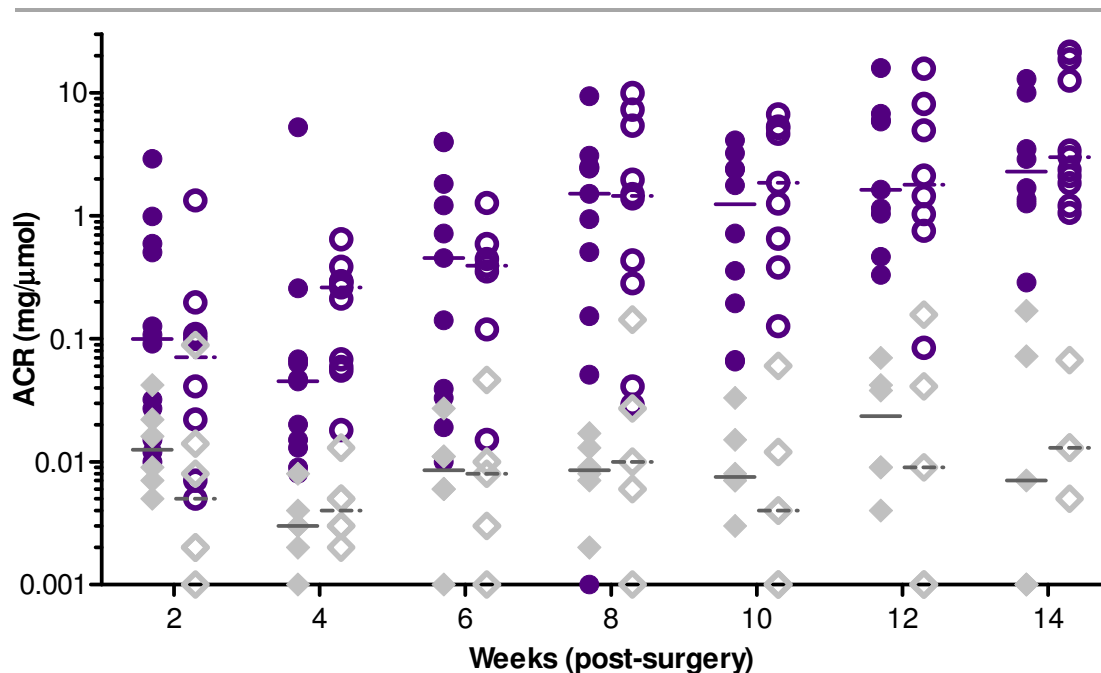


[Figure 7.5](#) SNx rats (purple) presented with progressively elevated albumin:creatinine ratio (ACR, p < 0.001). After 6 weeks ACR was significantly elevated in the vehicle treated SNx (NV, filled circles) compared to treatment-matched sham controls (SV, filled diamonds, p = 0.013). Whereas ACR was not significantly increased (relative to treatment-matched sham controls, SA, open diamonds) in the urotensin II antagonist treated SNx (NA, open circles) until 8 weeks post-surgery (p = 0.006). There was no difference in ACR between the NA and NV groups (p = 0.473, circles) or the SA and SV groups (p = 0.963, diamonds). SV: n = 6, SA: n = 5 - 6, NV: n = 12 - 9 and NA: n = 11 - 7) over the course of the study. Horizontal lines represent median. Log₁₀ transformed data analysed by 3-way ANOVA with repeated measures.

7.3 Terminal data

Terminal samples were collected as described in [Section 2.5](#). Terminal plasma samples were analysed for creatinine and blood urea nitrogen (BUN). BUN was significantly higher in the terminal plasma samples ([Figure 7.6a](#)) from SNx rats that

had received vehicle (NV, filled circles: 15.7 ± 3.5 mmol/L, $n = 6$) than in matched shams (SV, filled diamonds: 2.7 ± 0.9 mmol/L, $n = 4$, $p = 0.037$). BUN was similarly elevated (NA, open circles: 15.6 ± 2.9 mmol/L, $n = 9$) in SNx rats that received UT-A compared to UT-A treated shams (SA, open diamonds: 4.1 ± 0.8 mmol/L, $n = 6$, $p = 0.021$). UT-A treatment had no effect ($p = 0.881$) on BUN in shams ($p = 0.998$, compared to sham rats receiving vehicle) or SNx rats ($p = 1.000$, compared to vehicle control).

Whilst plasma creatinine concentration ([Figure 7.6b](#)) in the SNx groups (NV, filled circles: 72.6 ± 13.3 $\mu\text{mol/L}$, $n = 6$ and NA, open circles: 92.9 ± 24.4 $\mu\text{mol/L}$, $n = 9$) were approximately double that of the treatment-matched sham controls (SV, filled diamonds: group 29.9 ± 6.4 $\mu\text{mol/L}$, $n = 5$ and SA, open diamonds: 29.9 ± 7.5 $\mu\text{mol/L}$, $n = 6$), these differences were not significant ($p = 0.471$ and $p = 0.087$ in rats receiving vehicle or UT-A, respectively). The modest difference between the SNx rats receiving UT antagonist and vehicle control was not significant ($p = 0.853$) and there was no difference between the shams receiving UT-A compared to those receiving vehicle control ($p = 1.000$).

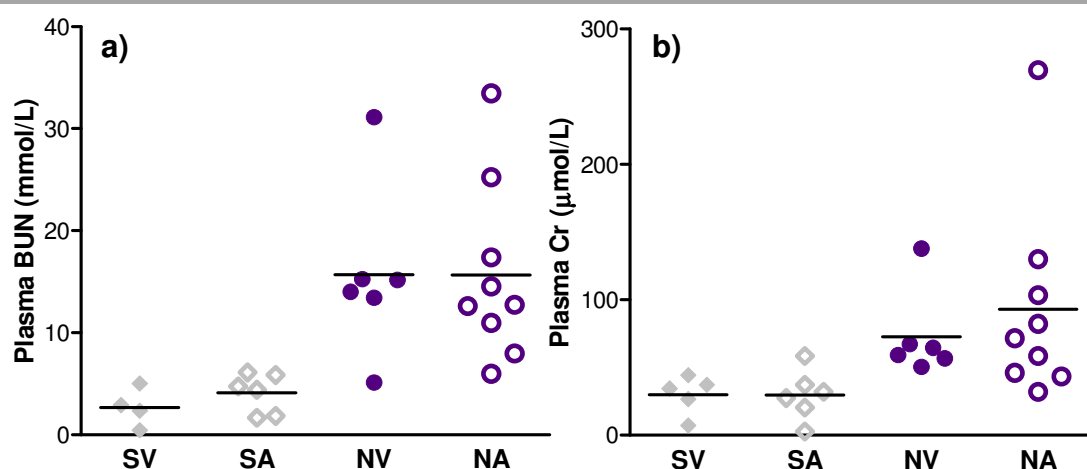


Figure 7.6 **a)** Terminal blood Urea Nitrogen (BUN) was not significantly different in SNx rats receiving a urotensin II receptor (UT) antagonist (NA, $n = 9$) from SNx rats receiving vehicle control (NV, $n = 6$, $p = 1.000$). However, BUN was elevated in both SNx cohorts (NA and NV) relative to the respective treatment-matched sham controls; sham vehicle (SV, $n = 4$, $p = 0.037$) and sham UT-antagonist (SA, $n = 6$, $p = 0.021$). **b)** Although terminal plasma creatinine tended to be higher in the NV group ($n = 5$) compared with the SV group ($n = 6$) and in the NA group ($n = 9$) compared to the SA group ($n = 6$) these differences were not significant ($p = 0.471$ and 0.087 , respectively). The modest difference between the SNx rats receiving UT antagonist and vehicle control was not significant ($p = 0.853$).

The mass of the remnant kidneys, as determined at post mortem after 14 weeks of treatment, of the SNx rats increased substantially ([Figure 7.7a](#)) in both the vehicle (NV, + 179.5 ± 25.8 %, n = 6) and UT-A treated groups (NA, + 208.9 ± 24.1 %, n = 5). The degree of change was similar in both groups (p = 0.434). Initial kidney weight was calculated as right kidney weight minus weight of the removed (left kidney) poles. There was no difference (p = 0.296) in the estimated starting weight of the kidneys from NV (0.98 ± 0.05 g, n = 6) compared to NA rats (0.90 ± 0.05 g, n = 5). Final kidney weights are based on weight of tissue prior to freezing; fixed tissues were excluded as the infiltration of paraformaldehyde increased tissue mass.

In contrast there were no differences in final kidney weight between the sham vehicle (3.19 ± 0.25 g/Kg, n = 6) and sham UT-A groups (3.01 ± 0.15 g/Kg, n = 5, p = 0.998) or between UT-A treated SNx (4.85 ± 0.53 g/Kg, n = 5) and those SNx rats receiving vehicle (5.18 ± 0.56 g/Kg, n = 6, p = 0.999). Terminal individual kidney mass was higher in the SNx cohort than in the sham controls (p = 0.013 and 0.018 in the vehicle and UT-A treated groups, respectively).

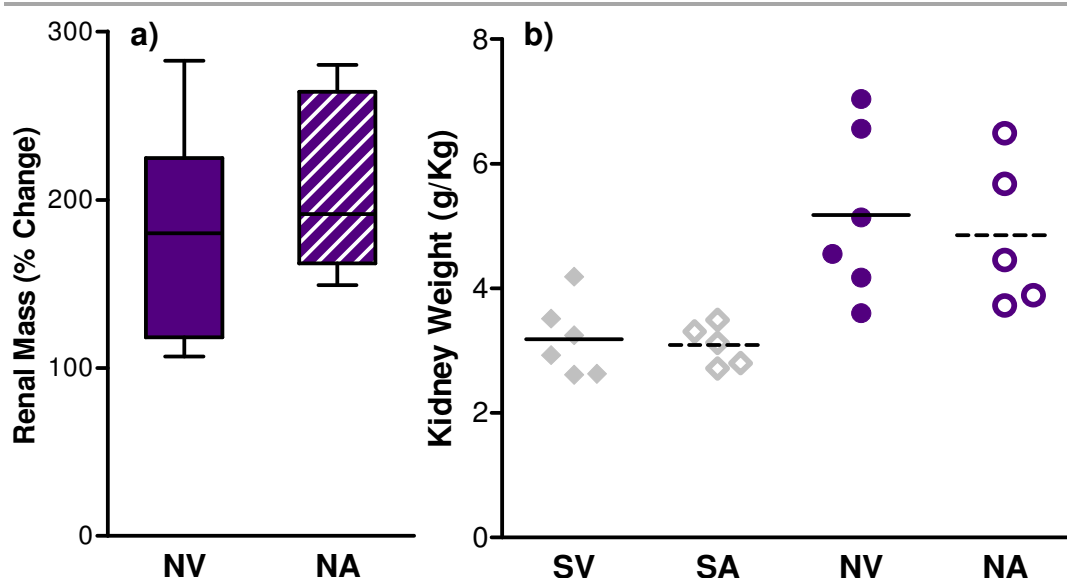


Figure 7.7 **a)** Remnant kidney increased by a similar amount (p = 0.434) in SNx rats in the vehicle treated group (NV, solid bar, n = 6) and urotensin II receptor (UT) antagonist treated group (NA, dashed bar, n = 5). **b)** Terminal single kidney weight (g/Kg) was higher in SNx rats receiving vehicle (NV, filled circles, n = 6) compared to matched shams (SV, filled diamonds, n = 6, p = 0.013). Left kidney was also higher in SNx rats receiving UT antagonist (NA, open circles, n = 5) compared to treatment-matched shams (SA, open circles, n = 5, p = 0.018).

7.4 Histology

PFA fixed, paraffin embedded renal tissue samples were stained with a variety of histological agents in order to examine the structure of both cortical and medullary regions. Haematoxylin and eosin (H&E) staining allowed visual inspection of general structure, Periodic acid Schiff (PAS) stained cortical sections allowed analysis of the glomerular basement membrane and any associated glomerulosclerosis. Similarly Masson's trichrome (MTC) stained sections were used to visualise glomerulosclerosis and fibrosis derived from collagen deposition.

H&E staining of cortical sections ([Figure 7.8](#)) from sham rats receiving (a) vehicle or (b) UT-A revealed glomeruli surrounded by tightly packed tubules. Where tubules were sectioned in a perpendicular plane the lumen were round and uniformly sized. Proximal convoluted tubules (P) can be identified by relatively thick walls and the presence of a brush border. There were mild to moderate changes seen within the cortices from the SNX rats with no definitive way to differentiate between those receiving vehicle (NV, [Figure 7.8c](#)) or UT receptor antagonist (NA, [Figure 7.8d](#)). Tubular dilatation was common in the cortex of SNx rats (black star) as was the presence of peritubular hyper-cellularity (arrowhead) and enlarged glomeruli. Images in [Figure 7.8](#) are representative of the group medians; there was variation in the extent of cortical lesions and examples of more extensive lesions are shown in [Figure 7.10a](#).

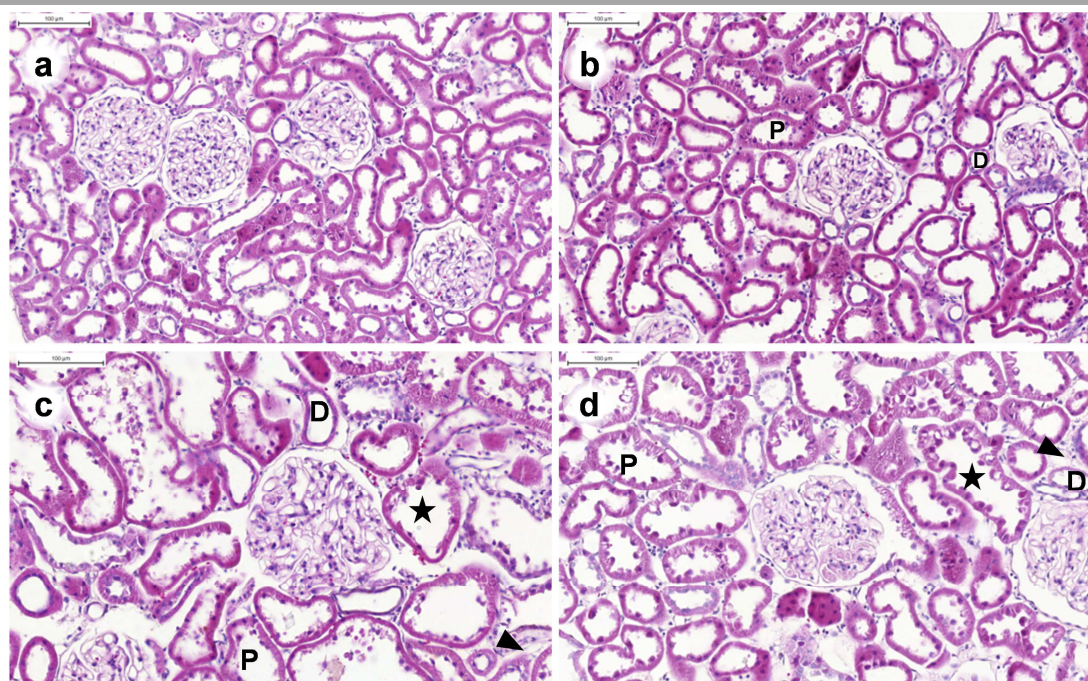


Figure 7.8 Haematoxylin and eosin stained cortical sections from **(a)** sham rats receiving vehicle (SV) or **(b)** urotensin II receptor antagonist (SA) both present with well-defined glomeruli, and densely packed proximal (P) and distal (D) convoluted tubules which are clearly visible. Glomeruli in the vehicle **(c)** and UT-A **(d)** treated SNx rats were visibly larger with evidence of tubular dilatation (stars) and areas of hyper-cellularity (arrowheads). Images captured at x20 magnification, 100 μm scale bar.

Representative sections of medulla (longitudinal orientation) highlighted that the nephrectomy-related changes were less extensive than those seen in the cortex (**Figure 7.9c** and **d**). Generally, these changes were limited to tubular casts (arrows) and small areas of proliferation although larger areas of expansion and disruption were occasionally seen in both SNx cohorts (**Figure 7.10b**).

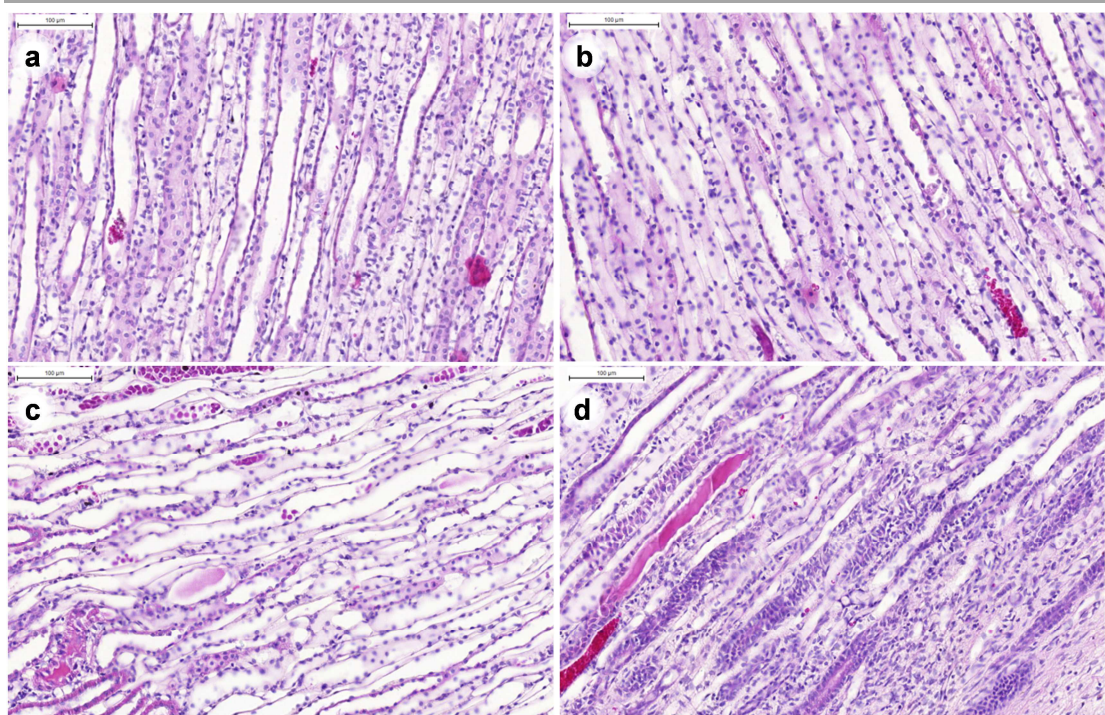


Figure 7.9 Medullary sections from **(a)** sham rats receiving vehicle (SV) or **(b)** urotensin II receptor antagonist (SA) show uniform collecting tubule/duct structure. Some minor abnormalities such as casts can be seen in sections of medulla from vehicle **(c)** and UT-A **(d)** treated SNx rats. Images captured at x20 magnification, 100 µm scale bar.

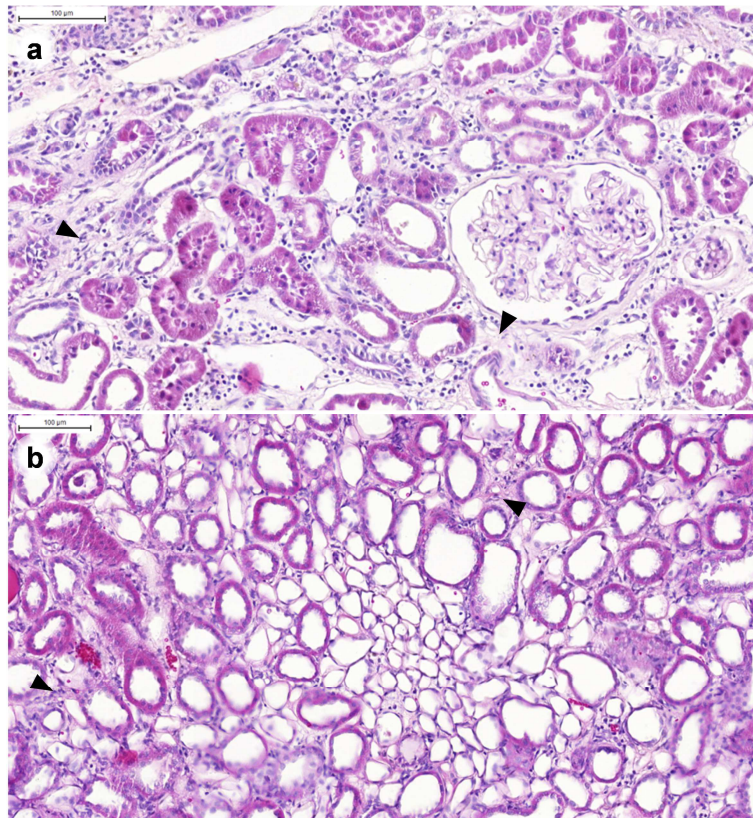


Figure 7.10 Examples of abnormal peritubular hyper-cellular expansion (arrowheads) within the **(a)** cortex and **(b)** medulla of UT receptor antagonist treated SNx rats. Images captured at x20 magnification with 100 µm scale bar.

7.4.1 Periodic acid Schiff

Glomeruli stained with periodic acid Schiff (PAS) were scored on a glomerulosclerosis index (GSI, 0 - 4, as described in [Section 2.8.3](#)) with results presented as median: IQR ([Figure 7.11](#)). There were no differences ($p = 1.000$) between the GSI scores of sham rats treated with UT-A ([Figure 7.12\(1\)](#), panel **(b)**, 0: 0 - 0, $n = 250$) and those from sham rats receiving the vehicle control ([Figure 7.12\(1\)](#), panel **(a)**, 0: 0 - 0, $n = 250$). Similarly GSI scores from SNx rats receiving UT-A ([Figure 7.12\(2\)](#), panel **(b)**, 1: 0 - 2, $n = 225$) were not different ($p = 1.000$) from those of SNx rats receiving vehicle ([Figure 7.12\(2\)](#), panel **(a)**, 1: 0 - 2, $n = 250$). Comparisons between SNx and treatment-matched sham control rats receiving UT-A, or vehicle control, highlighted mild to moderate increases in GSI scores in the SNx groups; both $p < 0.001$.

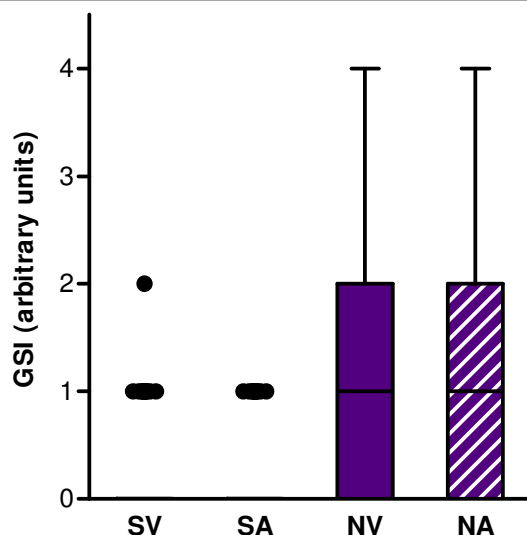


Figure 7.11 Glomerulosclerosis index (GSI) scores were higher in SNx rats receiving UT-A (NA, 1: 0 - 2, n = 225) or vehicle (NV: 1: 0 - 2, n = 250) than in treatment-matched shams (UT-A, SA: 0: 0 - 0, n = 250, $p < 0.001$) and (Veh, SV: 0: 0 - 0, n = 250, $p < 0.001$). Box represents IQR with a line at the median.

Fine staining of the glomerular basement membrane (deep pink, black arrowheads) is clearly visible within the glomeruli of SV ([Figure 7.12\(1\)a](#)) and SN rats ([Figure 7.12\(1\)b](#)). This staining remains visible in rats from both the NV ([Figure 7.12\(2\)a](#)) and NA groups ([Figure 7.12\(2\)a](#)); however in sections from these groups the staining pattern was less well defined and replaced by patches of PAS-positive focal glomerulosclerosis ([Figure 7.12\(2\)a and b](#), white arrows), representative sections shown.

Further structural changes were noticeable in the surrounding cortical structure. The renal tubules (proximal convoluted tubule, PCT) were densely packed with very little space between them in both sham groups ([Figure 7.12\(1\) Vehicle \(a\)](#) and [UT-A \(b\)](#)). In addition, the brush border on the apical surface of the PCT cells (luminal surface) stained pink (SV: [Figure 7.12\(1\)a](#) and SA: [Figure 7.12\(1\)b](#) fuzzy stain pattern, black arrow) as did the basement membrane of the tubules (basal surface, fine staining, not labelled). In contrast, in sections from the SNx groups ([Figure 7.12\(2\)](#), SV ([a](#)) and SA ([b](#))) there were clear morphological changes; the tubules were dilated (black asterisk) and brush border staining in the proximal convoluted tubules (labelled PCT, luminal surface) was less defined. Areas of peritubular hyper-cellularity were visible (white stars), disrupting the normally dense packing of the tubules. There was no clear difference in the extent of cortical damage between the NV and NA groups.

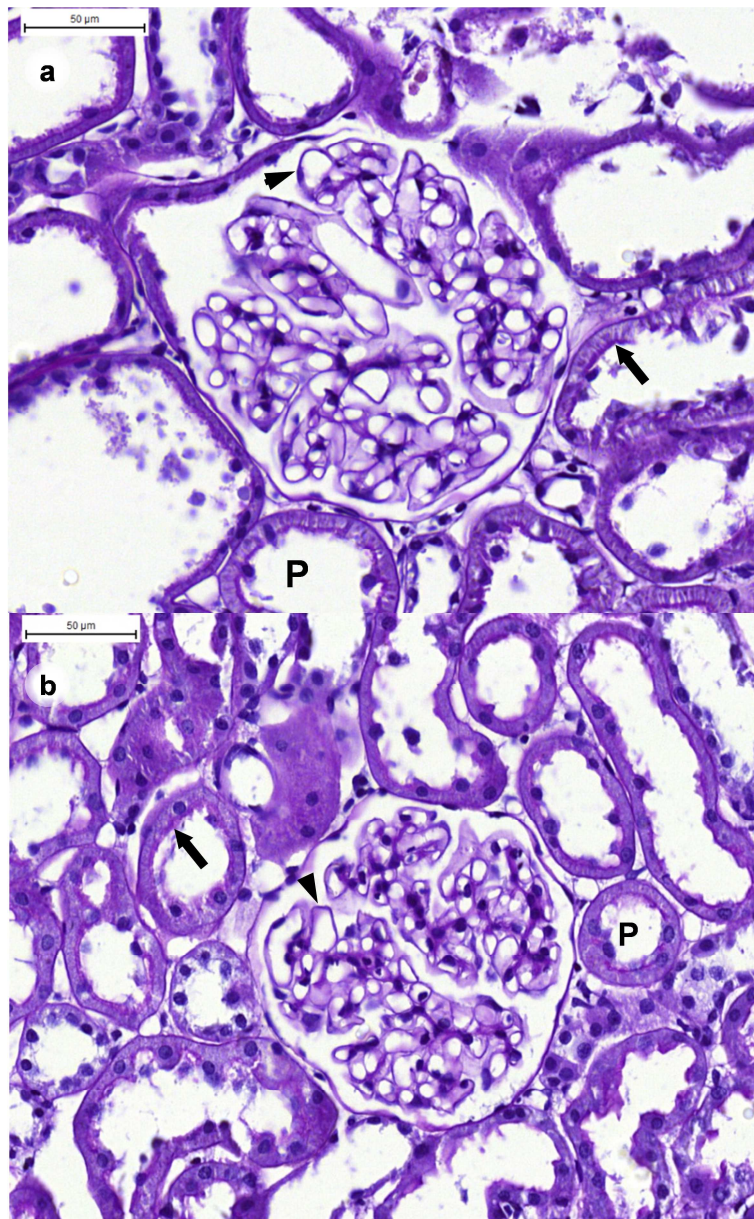


Figure 7.12(1) PAS stained glomeruli from sham controls receiving **(a)** vehicle (SV) and **(b)** urotensin II receptor antagonist (SA). Both SV **(a)** and SA **(b)** rats present with well-defined intraglomerular structure including fine staining of the glomerular basement membrane (black arrowheads). Outside the glomeruli, proximal convoluted tubules (PCT, with apical brush border, black arrows) are clearly visible and the tubules are densely packed with no evidence of abnormal dilatation. Images captured at x20 magnification, 50 µm scale bar

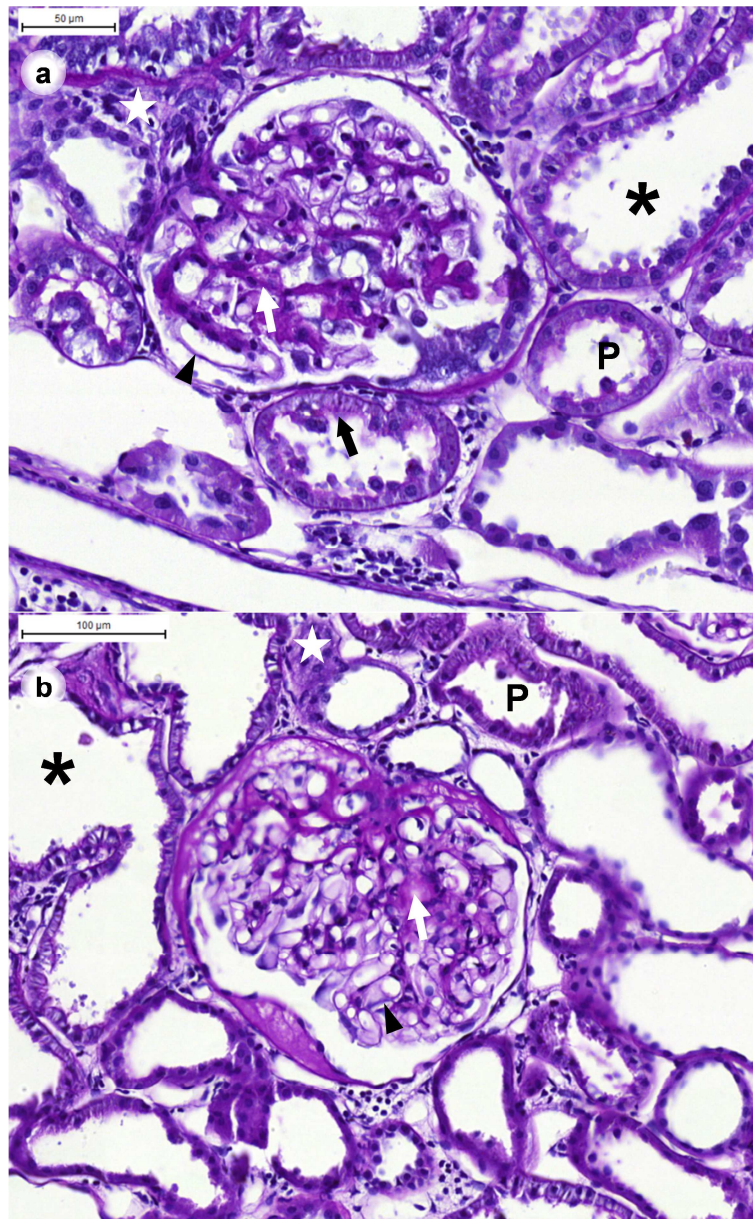
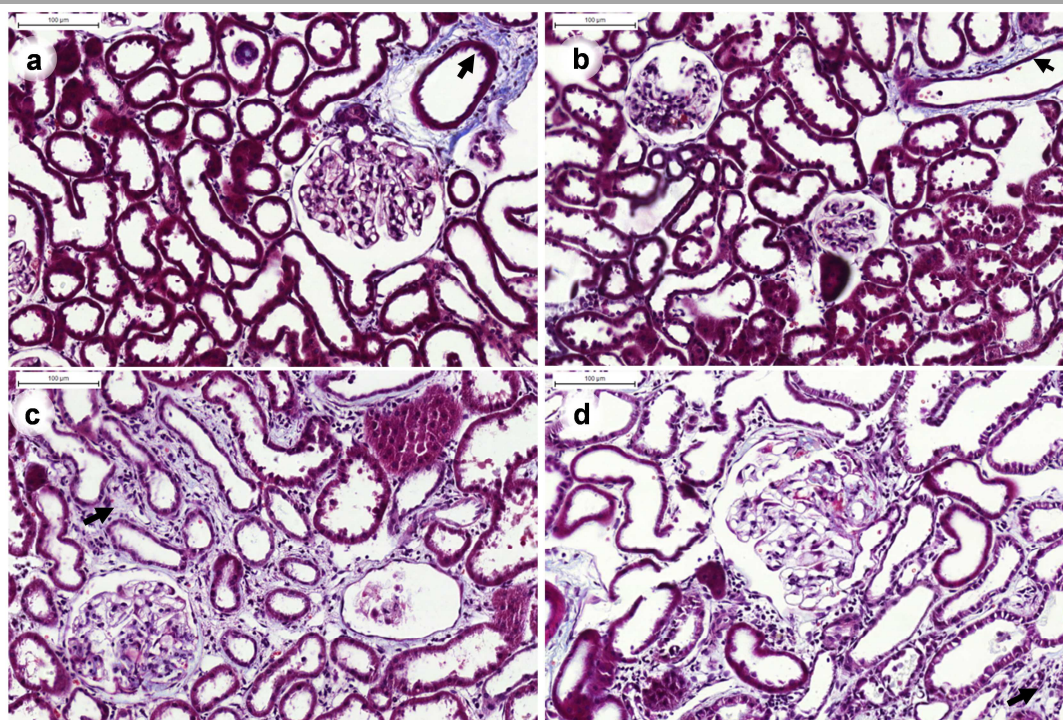


Figure 7.12(2) PAS stained glomeruli from SNx rats receiving **(a)** vehicle (NV) and **(b)** urotensin II receptor antagonist (NA). Fine staining of the glomerular basement membrane (black arrowheads) is visible within glomeruli from both NA **(a)** and NV **(b)** rats. Apical brush border staining was generally visible in the proximal convoluted tubules (PCT) in both groups). However, dilatation of the tubules (asterisks), peritubular hyper-cellularity (white stars) and focal glomerulosclerotic lesions (white arrows) were clearly visible in both groups. Images captured at x20 magnification. 50 µm and 100 µm scale bars in **(a)** and **(b)**, respectively.

7.4.2 Masson's Trichrome stain for collagen

Masson's trichrome staining for collagen revealed minimal staining in the cortex of sham controls, whether receiving **(a)** vehicle or **(b)** UT antagonist ([Figure 7.13](#)). Strong blue staining of collagen was limited to areas surrounding arterioles and venules (arrows, [Figure 7.13a](#) and **b**). There was diffuse blue staining throughout cortical regions of peritubular hyper-cellularity from both vehicle **(c)** and UT-A **(d)** treated SNx which was not seen in the shams.



[Figure 7.13](#) Masson's trichrome stained sections of cortex from sham rats receiving **(a)** vehicle (SV) or **(b)** urotensin II antagonist (UT-A, SA) showed minimal blue collagen staining, localised to renal arterioles and venules. In contrast both **(c)** vehicle (NV) and **(d)** UT-A (NA) treated SNx rats presented with diffuse collagen staining within the cortex and glomeruli. All images captured at x20 magnification with 100 µm scale bar.

In the medulla ([Figure 7.14](#)) there was little evidence of collagen staining in the vehicle **(a)** and UTA **(b)** treated shams, although collecting duct epithelial cells (arrow panel **a**) and erythrocytes (in vasa recta, arrow, panel **b**) stained strongly with the red Biebrich scarlet-acid fuchsin dye. Where cortical changes were common in the SNx cohort, changes in the medulla were less extensive. Vehicle **(c)** and UT-A **(d)** treated SNx rats tended to present with intact collecting ducts (arrows); however there was evidence of dilatation.

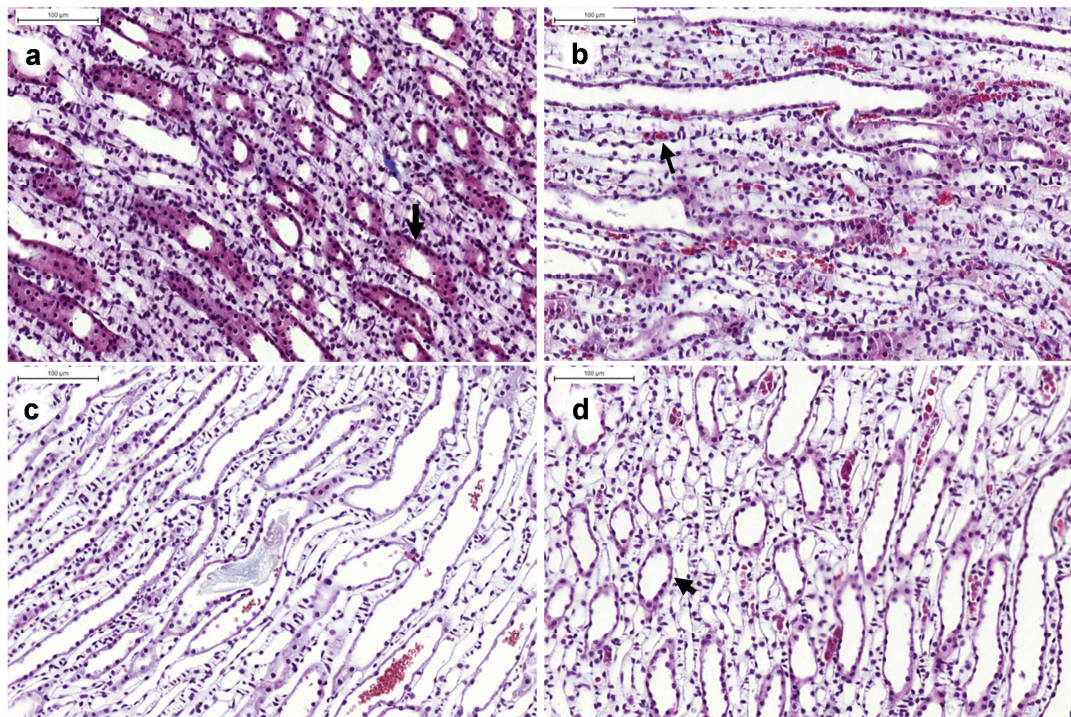


Figure 7.14 Masson's trichrome stained sections of medulla from sham rats receiving **(a)** vehicle (SV) or **(b)** urotensin II antagonist (UT-A, SA) showed minimal blue collagen staining, similarly **(c)** vehicle (NV) and **(d)** UT-A (NA) treated SNx rats presented with intact structure and minimal collagen staining. Erythrocytes within the vasa recta stained strongly red (panel **b**, arrow). All images captured at x20 magnification with 100 µm scale bar.

7.5 Immunohistochemical staining of basement membrane components

In addition to MTC staining for collagen, antibodies were used to allow the specific staining of basement membrane components; collagen (IV) and laminin- β . Within the cortex ([Figure 7.15](#)) of the vehicle **(a)** and UT-A treated **(b)** shams collagen staining was most prominent in the basement membranes of the proximal and distal tubules, the glomerular capsule and glomerular basement membrane (GBM). The staining pattern was similar for laminin- β ([Figure 7.16](#)) with linear staining of the tubule basement membranes and glomerular capsule; staining of the GBM was less pronounced. Collagen staining in the SNx rats was of a similar intensity to that of the shams, irrespective of whether they received vehicle **(c)** or UT-A **(d)**. However, areas of peritubular expansion (arrows) and focal lesions within the glomeruli (arrowheads) stained positive for collagen.

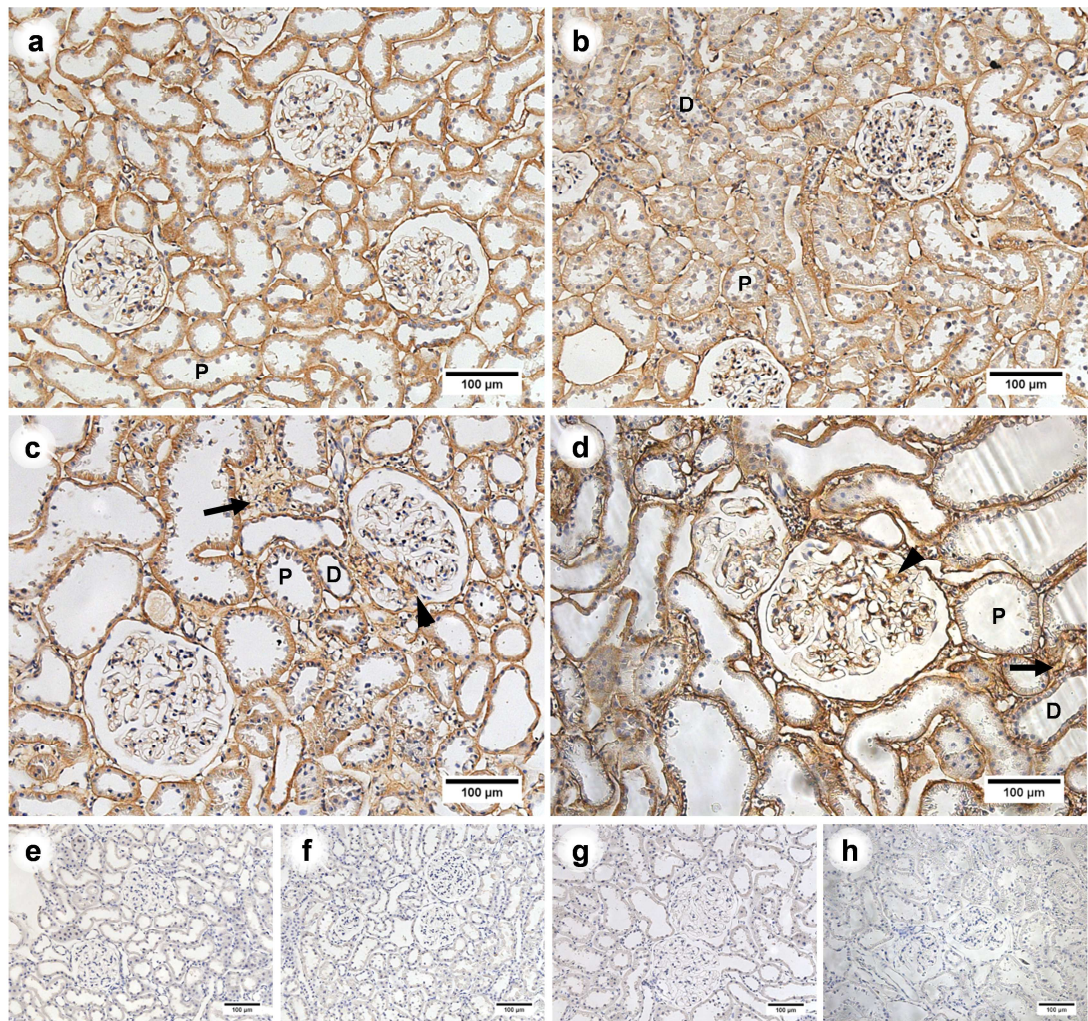


Figure 7.15 Immunohistochemical staining of collagen IV in the cortex of sham rats receiving **(a)** vehicle (SV) or **(b)** urotensin-II antagonist (UT-A, SA) was localised to the basement membranes of the proximal (P) and distal (D) tubules and glomeruli. The glomerular capsule also stained positive for collagen IV. The staining was similar in SNx rats treated with vehicle (NV) **(c)** or UT-A (NA) **(d)** with additional staining seen in areas of peritubular expansion (arrows) and focal lesions within the glomeruli (arrowheads). In both SNx groups changes in general structure of the tissue were evident. **(e - h)** Representative negative controls (primary antibody omitted) from SV, SA, NV and NA, respectively. All images captured at x20 magnification with 100 μ m scale bar.

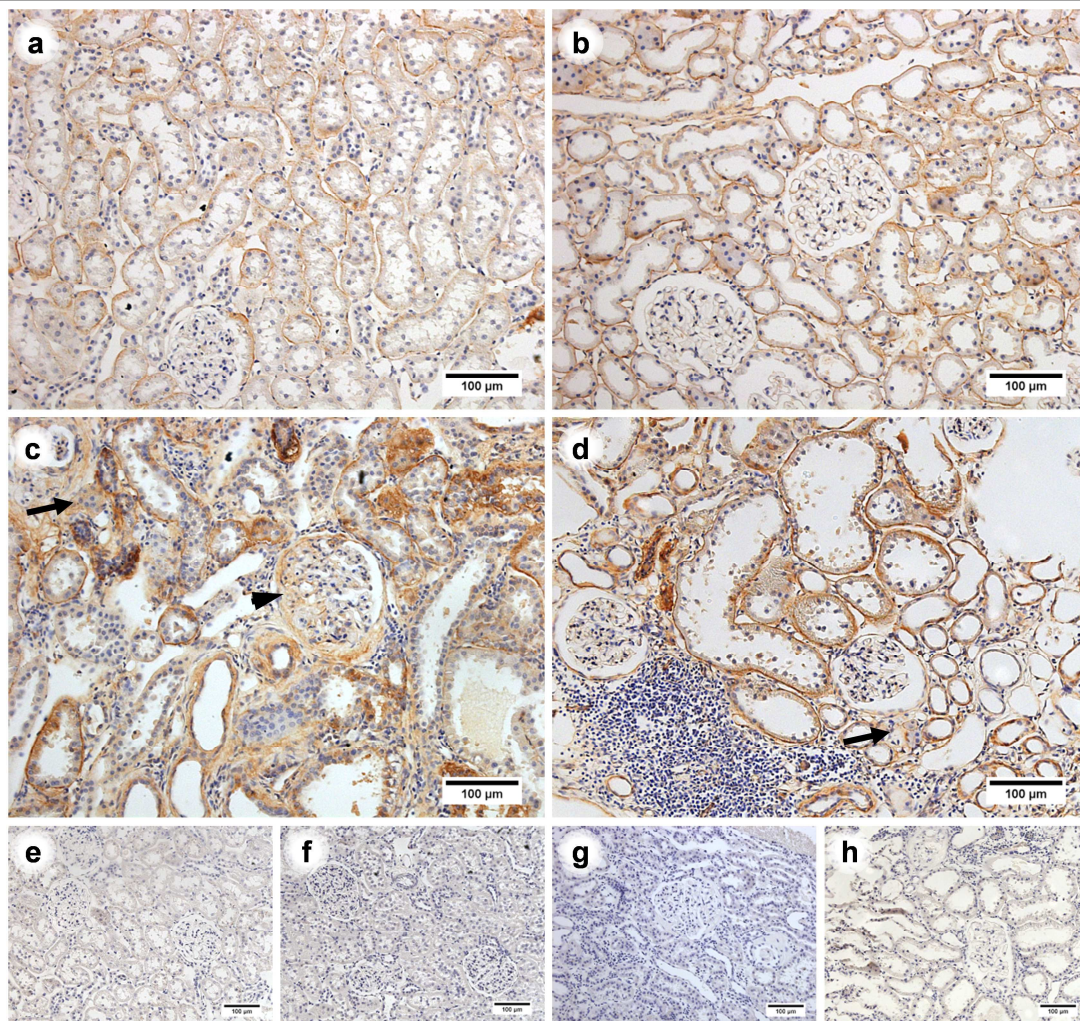


Figure 7.16 Immunohistochemical staining of laminin- β in the cortex of sham rats receiving **(a)** vehicle (SV) or **(b)** urotensin-II antagonist (UT-A, SA) was localised to the basement membranes of the glomerular capsule, proximal (P) tubules and distal (D) tubules. The staining tended to be more intense in SNx rats treated with vehicle (NV) **(c)** or UT-A (NA) **(d)**; additional staining was seen in areas of peritubular expansion (arrows) and focal lesions within the glomeruli (arrowheads). In both SNx groups changes in general structure of the tissue were evident. **(e - h)** Representative negative controls (primary antibody omitted) from SV, SA, NV and NA, respectively. All images captured at x20 magnification with 100 μ m scale bar.

In the medulla, collagen IV staining in sham rats receiving vehicle ([Figure 7.17a](#)) or UT-A ([Figure 7.22b](#)) was limited to the basement membranes of tubular structures including the collecting tubules, vasa recta and loops of Henle. The staining for laminin- β was similarly localised to the basement membranes ([Figure 7.18](#)). Staining tended to be more intense within the medulla of SNx rats when stained for collagen IV ([Figure 7.17](#)) or laminin- β ([Figure 7.18](#)) when compared to treatment-matched

controls; staining patterns within the NV and NA rats appeared comparable in intensity and distribution. Areas of hypercellular expansion stained more intensely for collagen IV that the surrounding tissue, whilst also staining positive for laminin- β .

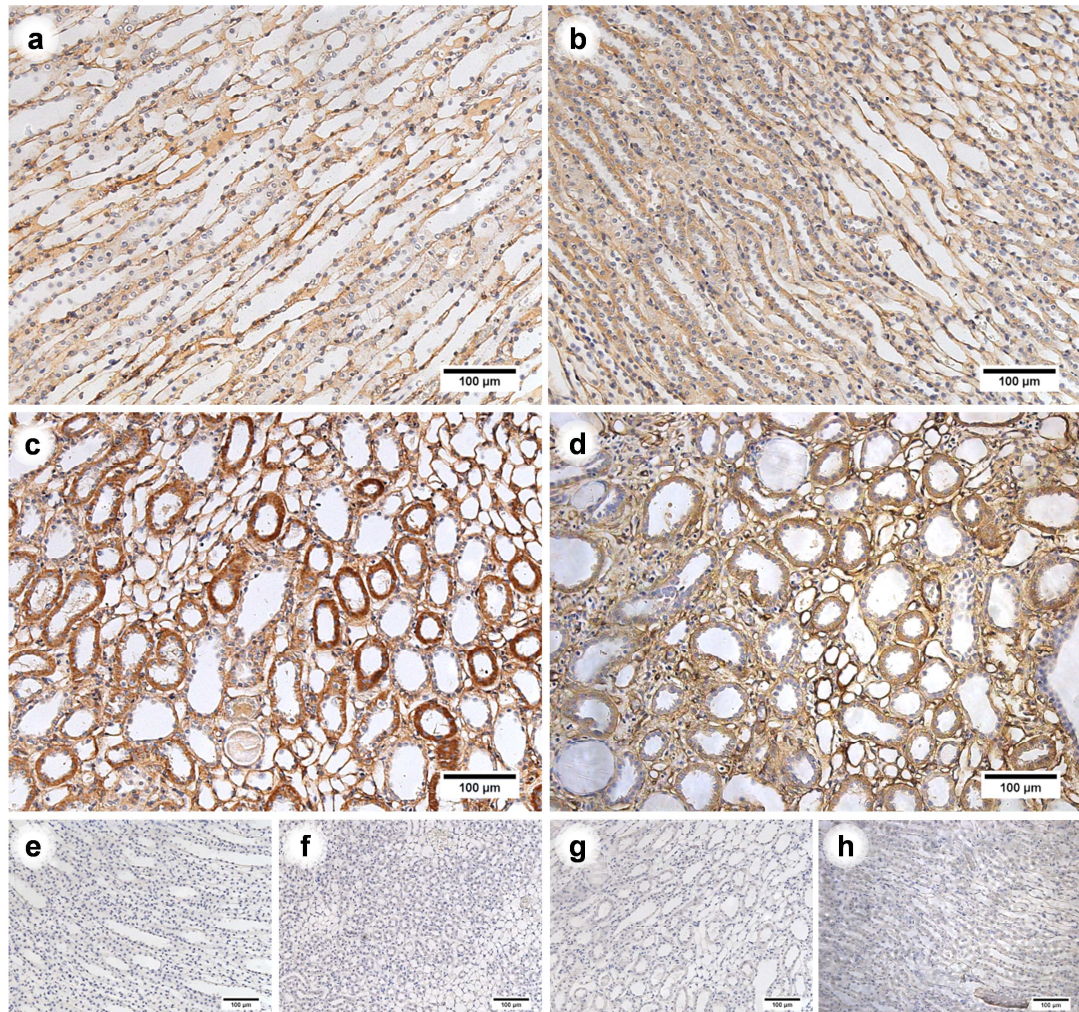


Figure 7.17 Immunohistochemical staining of collagen IV in the medulla of sham rats receiving **(a)** vehicle (SV) or **(b)** urotensin-II antagonist (UT-A, SA) was localised to the basement membranes of the collecting tubules, loops of Henle and vasa recta. The staining was more intense and widespread in SNx rats treated with vehicle (NV) **(c)** or UT-A (NA) **(d)**, with additional staining seen in areas of peritubular expansion (arrows). In both SNx groups changes in general disruption of tissue structure was evident. **(e - h)** Representative negative controls (primary antibody omitted) from SV, SA, NV and NA, respectively. All images captured at x20 magnification with 100 μ m scale bar.

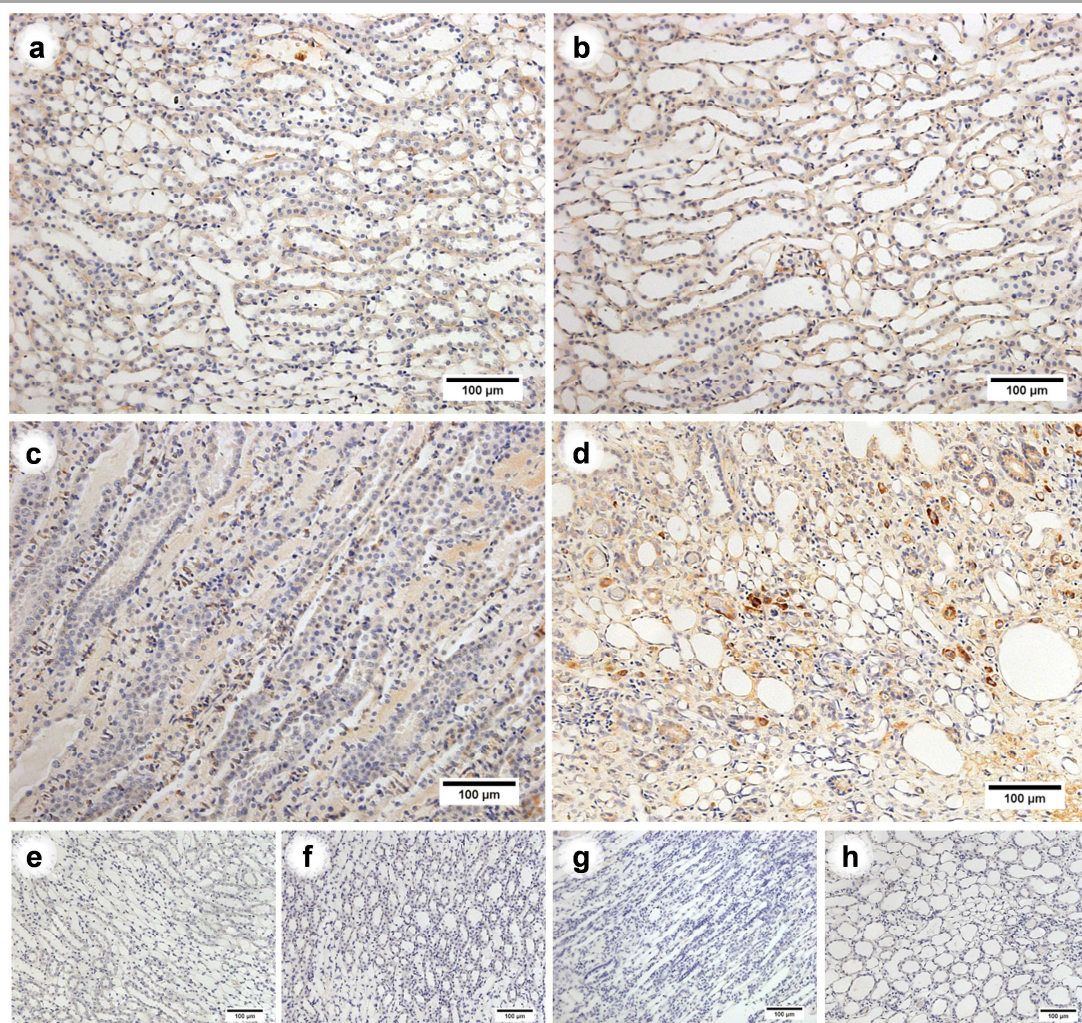


Figure 7.18 Immunohistochemical staining of laminin- β in the medulla of sham rats receiving **(a)** vehicle (SV) or **(b)** urotensin-II antagonist (UT-A, SA) was localised to the basement membranes of the collecting tubules, loops of Henle and vasa recta. The staining in SNx rats treated with vehicle (NV) **(c)** or UT-A (NA) **(d)** was more widespread and less specific to the basement membranes. Tissue samples from both SNx groups presented with general disruption in the gross structure. **(e - h)** Representative negative controls (primary antibody omitted) from SV, SA, NV and NA, respectively. All images captured at x20 magnification with 100 μ m scale bar.

7.6 Immunohistochemical analysis of UII, URP and UT

UII-immunoreactivity encompasses the mature UII and URP peptides as staining was carried out using an antibody raised against the conserved cyclic region of flounder UII, which is common to both peptides; the antibody has also been shown to detect pro-UII. The high degree of structural homology between UII and URP (all species) means that it is not possible to differentiate between the two peptides with this, or any commercially available antibody.²¹⁶

7.6.1 UII-immunoreactive staining

Staining for UII immuno-reactive peptides (UII, URP and pro-UII) was typically localised in a diffuse manner throughout the renal cortex ([Figure 7.19](#)). In the sham animals (panels **a** and **b**) staining was feint and spread throughout the renal tubules, with greater staining intensity seen in the proximal tubules. Comparison to a negative control section (panels **e** and **f**) highlights the widespread nature of staining. A similar staining pattern is evident in sections from SNx receiving (**c**) vehicle or (**d**) UT-A. Whilst the staining pattern remained generally within the tubular epithelial cells the intensity tended to be greater than in the sham controls. Staining appeared less intense in the UT-A treated SNx when compared with those receiving vehicle.

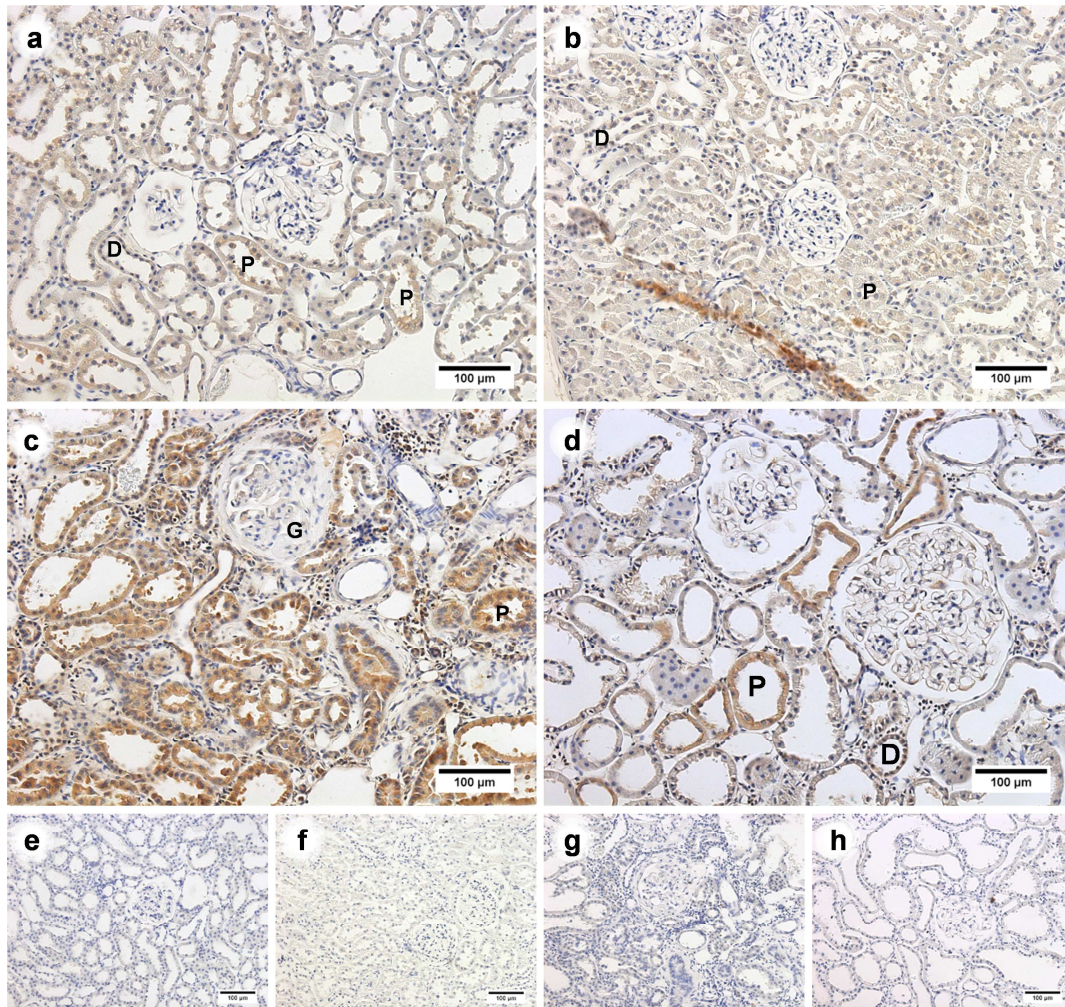


Figure 7.19 Immunohistochemical staining for urotensin II in the cortex of sham rats receiving **(a)** vehicle (SV) or **(b)** urotensin II antagonist (UT-A, SA) was diffuse across the whole section, with the most prominent staining localised to the proximal tubules (P). Staining was also diffuse but tended to be more intense in SNx rats receiving **(c)** vehicle (NV) or **(d)** UT-A (NA), with greatest intensity seen in the proximal tubules. **(e - h)** Representative negative controls (primary antibody omitted) from SV, SA, NV and NA, respectively. All images captured at x20 magnification with 100 μm scale bar.

In the medulla (**Figure 7.20**) staining was most intense within collecting duct epithelial cells (arrows, all panels). The staining intensity in these cells appeared consistent across the groups, although staining of the surrounding tissues tended to be more intense in the SNx groups, compared to the treatment-matched sham controls.

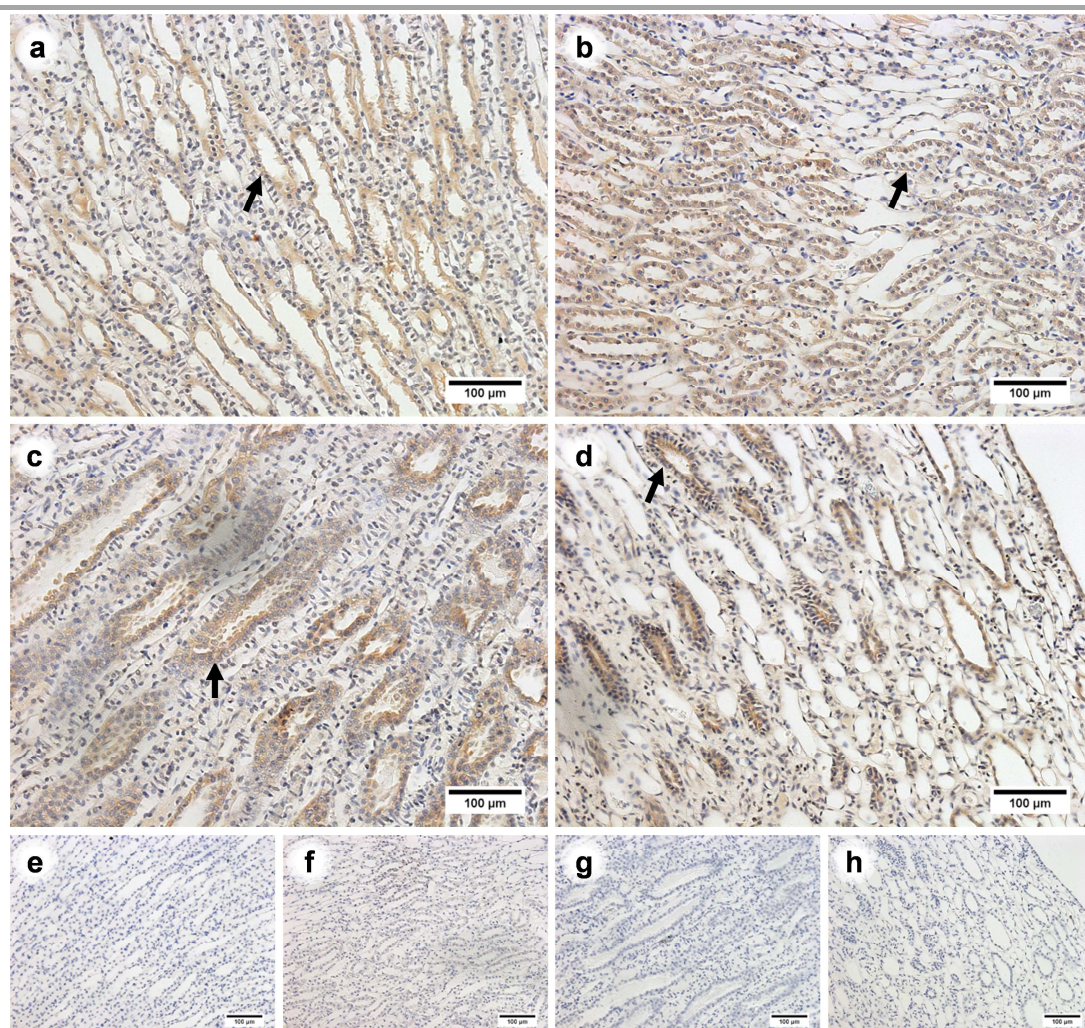


Figure 7.20 In the medulla of sham rats receiving **(a)** vehicle (SV) or **(b)** urotensin II antagonist (UT-A, SA) immunohistochemical staining for urotensin II was primarily localised within the collecting duct epithelium. This pattern was also seen in SNx rats receiving **(c)** vehicle (NV) or **(d)** UT-A (NA), with less intense staining seen in the surrounding cells. **(e - h)** Representative negative controls (primary antibody omitted) from SV, SA, NV and NA, respectively. All images captured at x20 magnification with 100 µm scale bar.

7.6.2 Immunohistochemistry for the UT receptor

In contrast to Ull there was little evidence of staining for the UT receptor in the cortex ([Figure 7.21](#)) of sham rats treated with UT-A (SA, panel **b**) or the vehicle controls (SV, panel **a**). Similarly there was little UT staining seen in normal structures of the cortex of SNx rats treated with UT-A (NA, panel **d**) or vehicle (NV, panel **c**). However there was UT staining associated with areas of peritubular expansion (arrowheads, panels **c** and **d**), and occasionally in the parietal layer of the Bowman's capsule (panels **c** and **d**, arrows).

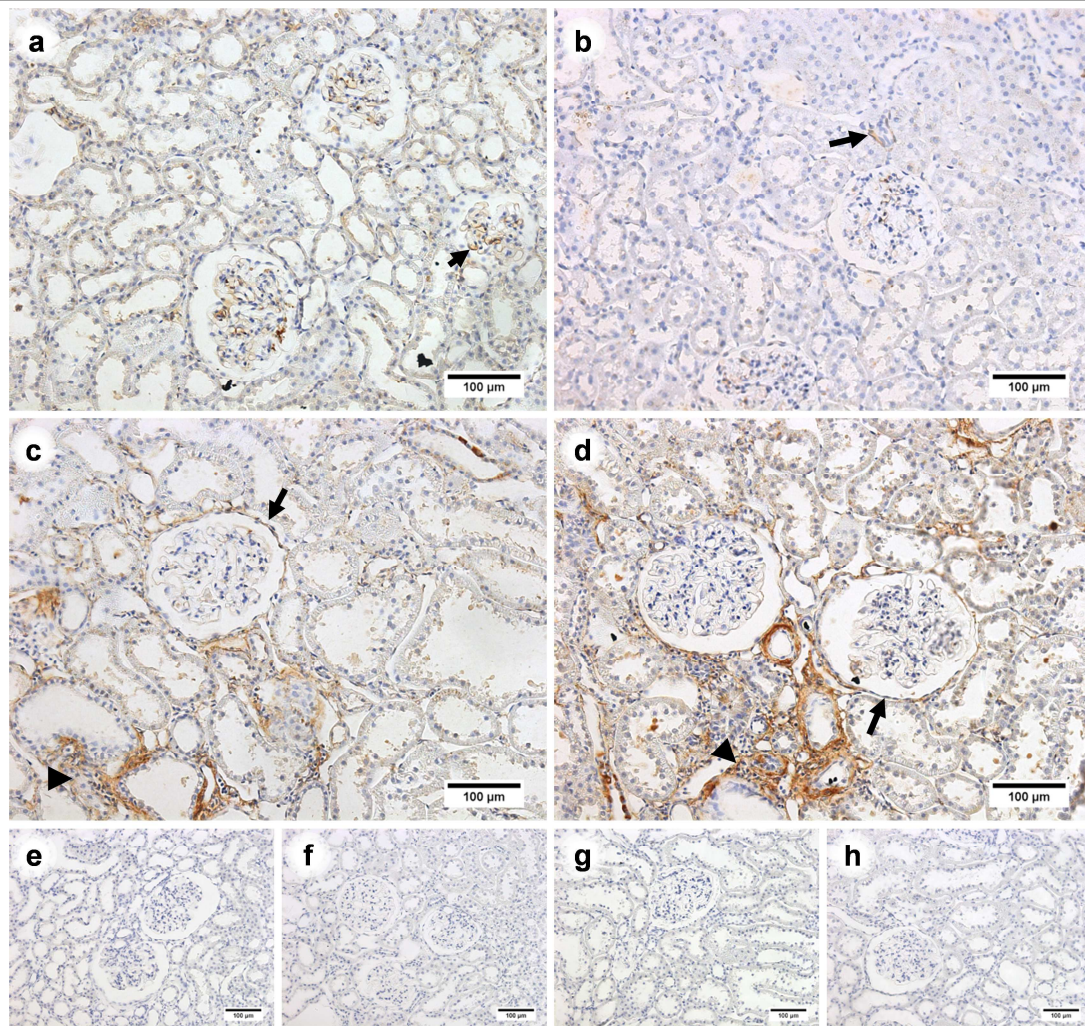


Figure 7.21 Urotensin II receptor (UT) staining was limited in cortical sections from sham rats receiving **(a)** vehicle (SV) or **(b)** urotensin II antagonist (UT-A, SA). This pattern was also seen in SNX rats receiving **(c)** vehicle (NV) or **(d)** UT-A (NA) with staining primarily seen within areas of hyper-cellular expansion (arrowheads) rather than within intact cortical structure; some additional staining was seen in the parietal layer (arrows). **(e - h)** Representative negative controls (primary antibody omitted) from SV, SA, NV and NA, respectively. All images captured at x20 magnification with 100 µm scale bar

Staining for UT was noticeably more prominent in the medulla (**Figure 7.22**). Staining was most intense within the epithelial cells of the collecting duct system; collecting tubules, collecting ducts and inner medullary collecting ducts all stained strongly for UT (arrowheads, all panels). UT staining was also seen in some thin limb cells (arrows, panels **a** and **d**), with more intense staining in these structures seen in the SNx rats (panel **d**) than shams (panel **a**). In the SNx groups (panels **c** and **d**) UT staining was also seen within the surrounding cellular areas (hyper-cellular

expansion) in the cortex ([Figure 7.21c](#) and [d](#)) and medulla ([Figure 7.23b](#)). Interestingly there is a clear association of staining in proximity to the apical (luminal) membrane which is particularly noticeable in the collecting ducts of the inner medulla (stars, [Figure 7.23](#), panels [a](#) and [b](#)). UT staining does not appear in all epithelial cells (representative example of staining voids marked with arrowheads, [Figure 7.23](#), panels [c](#), [d](#) and [e](#)), and often appears in a stippled pattern (arrows, panel [d](#) and [e](#), [Figure 7.23](#)) where staining is less intense.

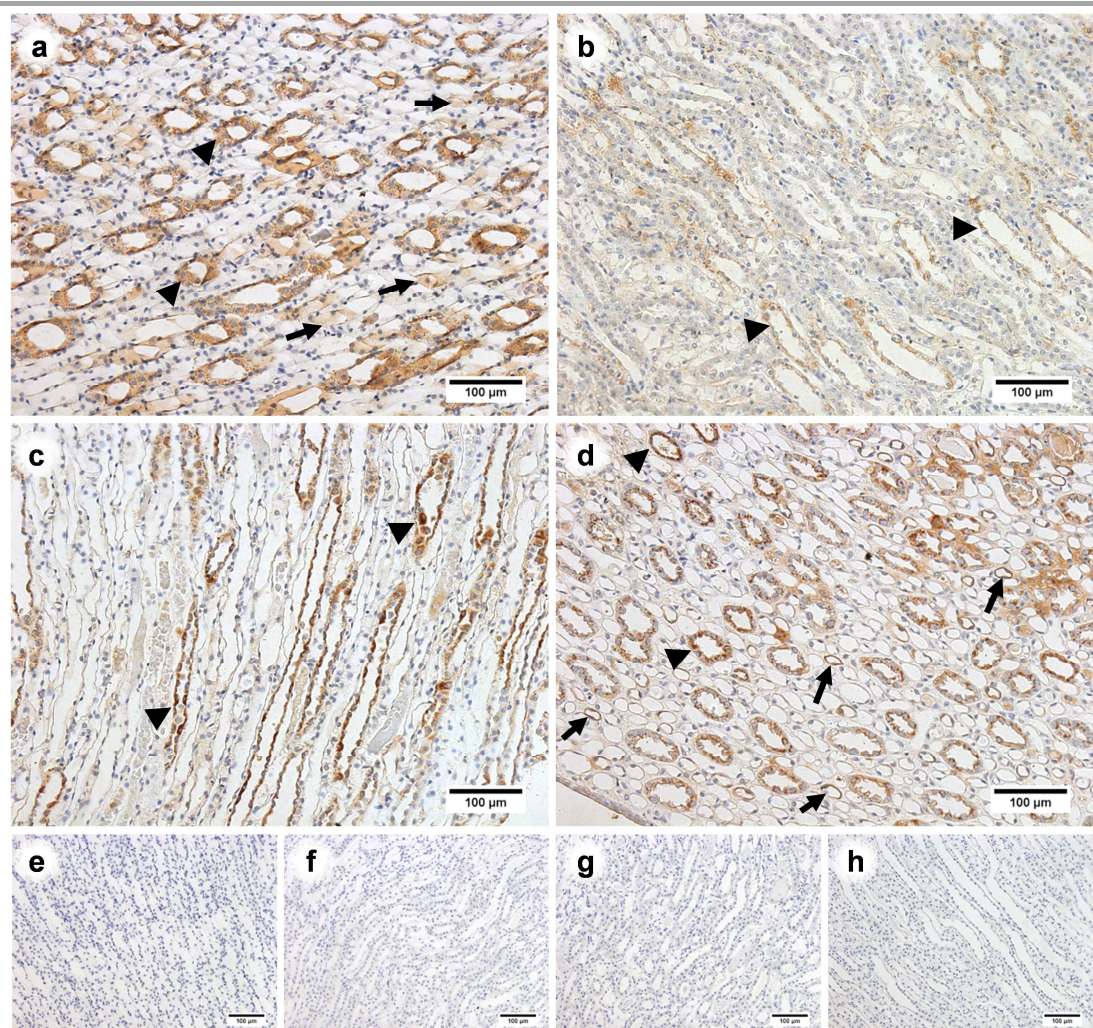


Figure 7.22 Detection of the urotensin II receptor by immunohistochemical staining showed consistent expression in the medulla of sham rats receiving **(a)** vehicle (SV) or **(b)** urotensin II antagonist (UT-A, SA) and SNx rats receiving **(c)** vehicle (NV) or **(d)** UT-A (NA). Staining was most intense in the collecting ducts (arrowheads, all panels), staining was also seen in the thin limbs of the loop of Henle (arrows, panels **a** and **d**) **(e - h)** Representative negative controls (primary antibody omitted) from SV, SA, NV and NA, respectively. All images captured at x20 magnification with 100 µm scale bar

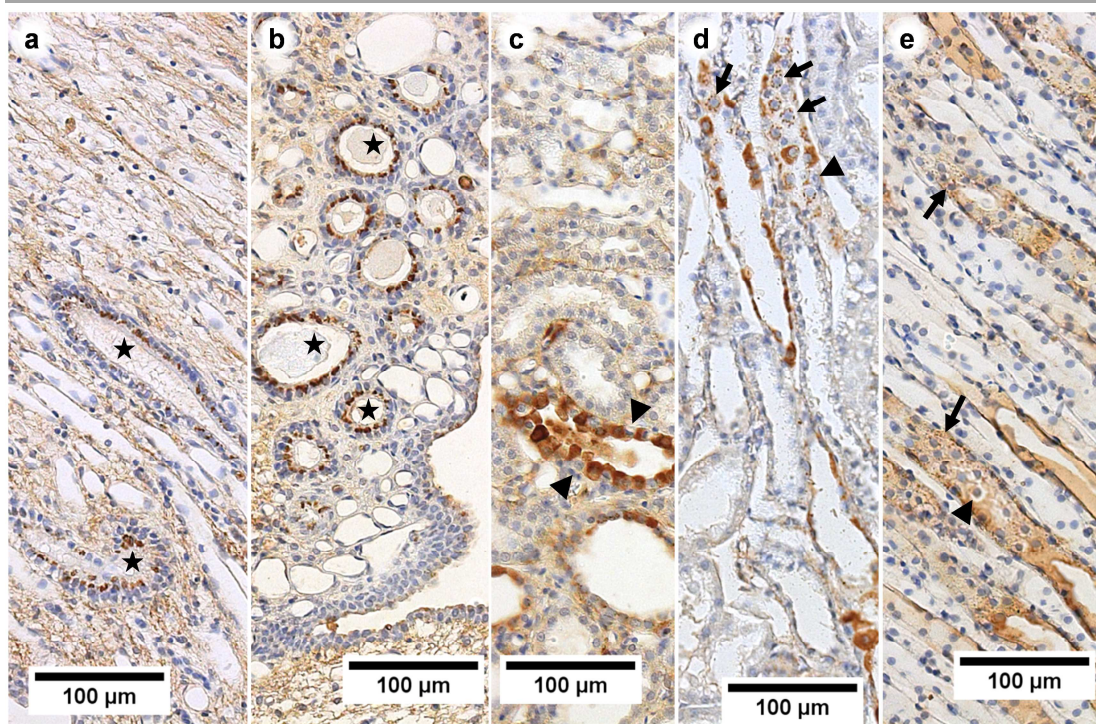


Figure 7.23 Examples of urotensin II receptor (UT) staining patterns within the medulla. Staining was often associated with the apical membrane (**a** and **b**) in the collecting ducts of the inner medulla. Staining intensity was not consistent within all collecting duct epithelial cells (arrows and arrowheads, **c**, **d** and **e**) or across individual cells (**d** and **e**), proteinaceous casts were common (black stars). Representative sections of staining patterns are from SNx receiving UT-antagonist (**a - c**), SNx receiving vehicle (**d**) and sham rats receiving vehicle (**e**). All images captured at x20 magnification with 100 µm scale bar

7.7 qPCR analysis of renal cortex samples

Renal cortex tissue collected from rats 14 weeks after undergoing the 5/6th SNx procedure, or sham control and receiving either U1I receptor antagonist (UT-A) or vehicle control ([Section 2.3.2](#)) were processed as described in [Section 2.5.1](#), before extraction of RNA, reverse transcription and qPCR analysis for U1I (*Uts2*), URP (*Uts2b*) and UT (*Uts2r*) along with the reference gene YWHAZ (*Ywhaz*) as detailed in ([Section 2.13](#)).

7.7.1 RNA quantification and quality control

RNA extracts typically contained 275.4 ± 20.9 ng/ μ L ([Figure 7.24a](#)), with A260/280 and A260/230 ratios of 2.06 ± 0.0 and 1.92 ± 0.07 respectively. This gives an indication that the samples were suitably concentrated and pure enough to progress with reverse transcription. Typical coefficient of variability (intra-sample) was 1.5 % (n = 3 samples with 2 - 4 replicates per sample).

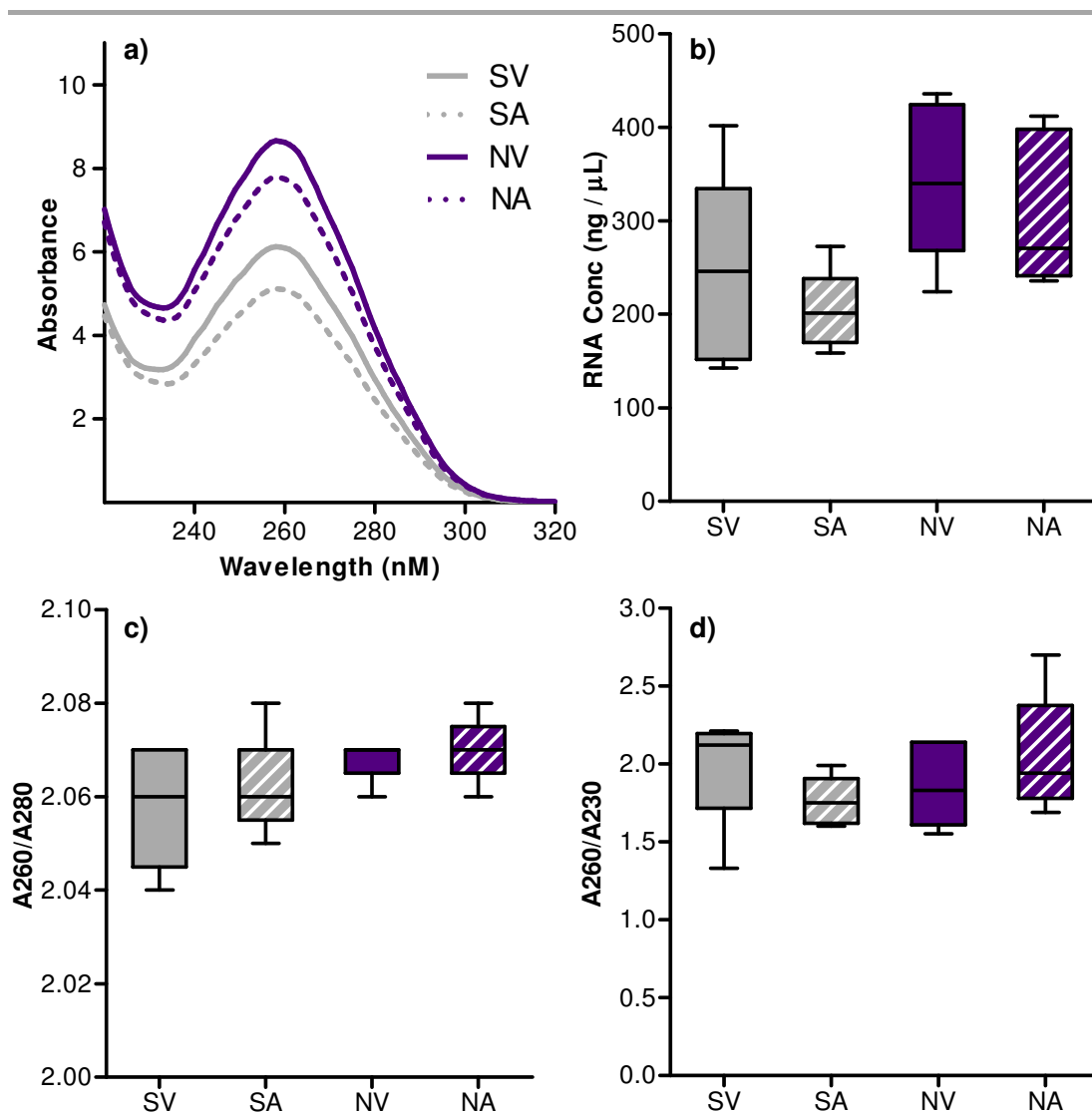


Figure 7.24 Micro-volume spectrophotometer analysis of RNA extracts from the renal cortex of vehicle treated (SV) or urotensin II antagonist (UT-A, SA) sham and SNx rats treated with vehicle (NV) or UT-A (NA) produced **(a)** group mean absorbance spectra which all show the characteristic nucleotide peak at 260 nm, **(b)** this is converted (factor: 40 ng/ μ L for A260 = 1) to RNA concentration with **(c)** all samples producing an A260/280 ratio of 2.0 or greater. **(d)** The A260/230 ratio was more variable, all samples with ratios above 0.75 were included. n = 5 in all groups.

To ensure that the RNA within the samples was of good quality samples were run on a 1.5 % agarose gel in non-denaturing conditions ([Section 2.11.1.5](#)). All samples had two clear bands representative of the 18s and 28s ribosomal subunits ([Figure 7.25](#), arrows), and there were no clear indications of RNA degradation products (RNA fragments would result in banding or smearing towards the bottom of the gel). Similarly there was no apparent gDNA contamination (visible by the presence of high molecular weight banding or smear pattern towards the top of the gel) in any NV

(Figure 7.25, panel **a** lanes 10-14), SA or NA groups (Figure 7.25, panel **b**, lanes 1 - 5 and 10 - 14, respectively). The extracts from SV rats (Figure 7.25, panel **a**, lanes 1 - 5) showed weaker, but present 18s and 28s bands with faint heavy bands also seen in some lanes; the bottom of the lanes were clear, (Figure 7.25a).

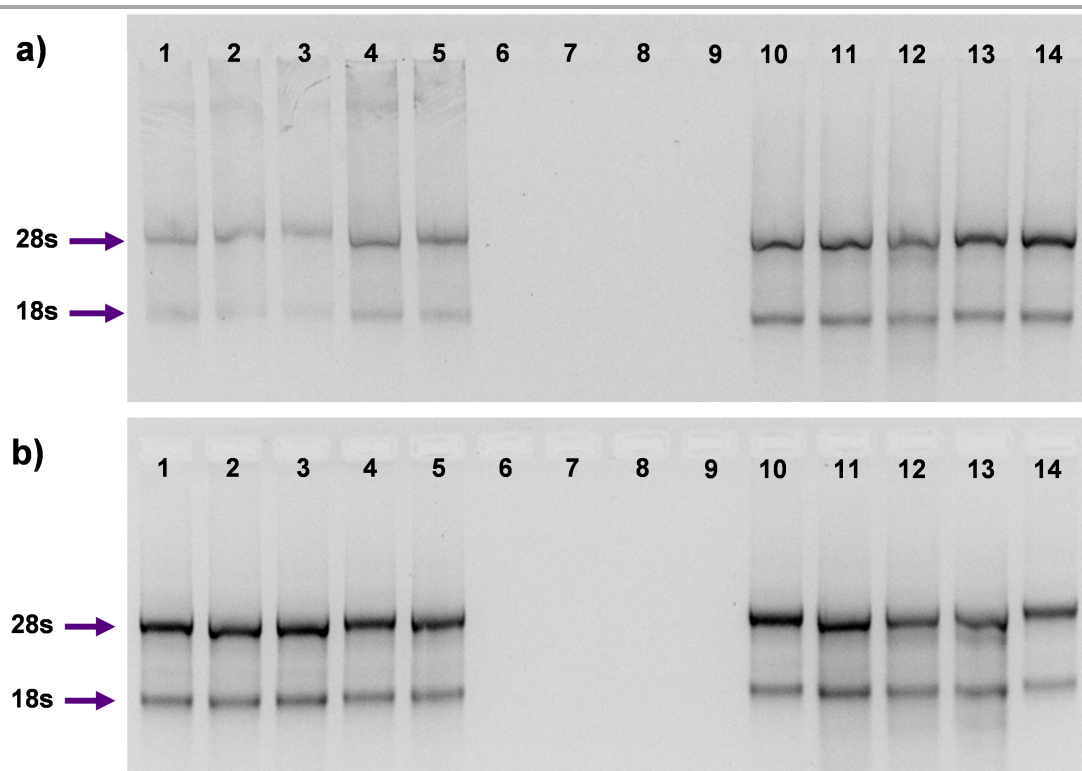


Figure 7.25 RNA extracts showed intact 18s and 28s bands when examined by agarose gel electrophoresis. RNA banding patterns of extracts from the renal cortex of **(a)** vehicle-treated shams (lanes 1- 5) and SNx (lanes 10 - 14) and **(b)** U1I receptor antagonist treated SNx (lanes 10 - 14) and shams (lanes 1 - 5). Lanes 6 - 9 were intentional left blank.

7.7.2 *Ywhaz*

Amplification occurred from C_t 20.19 - 26.82 in the standards and 20.89 - 25.91 in samples ($n = 2$ per sample or standard, Figure 7.26a), producing a single peak at 80.1 °C in the melt curve (Figure 7.26b). The assay standard curve was reasonably well fitted ($R^2 = 0.964$) with good efficiency (105.4 %, Figure 7.26c).

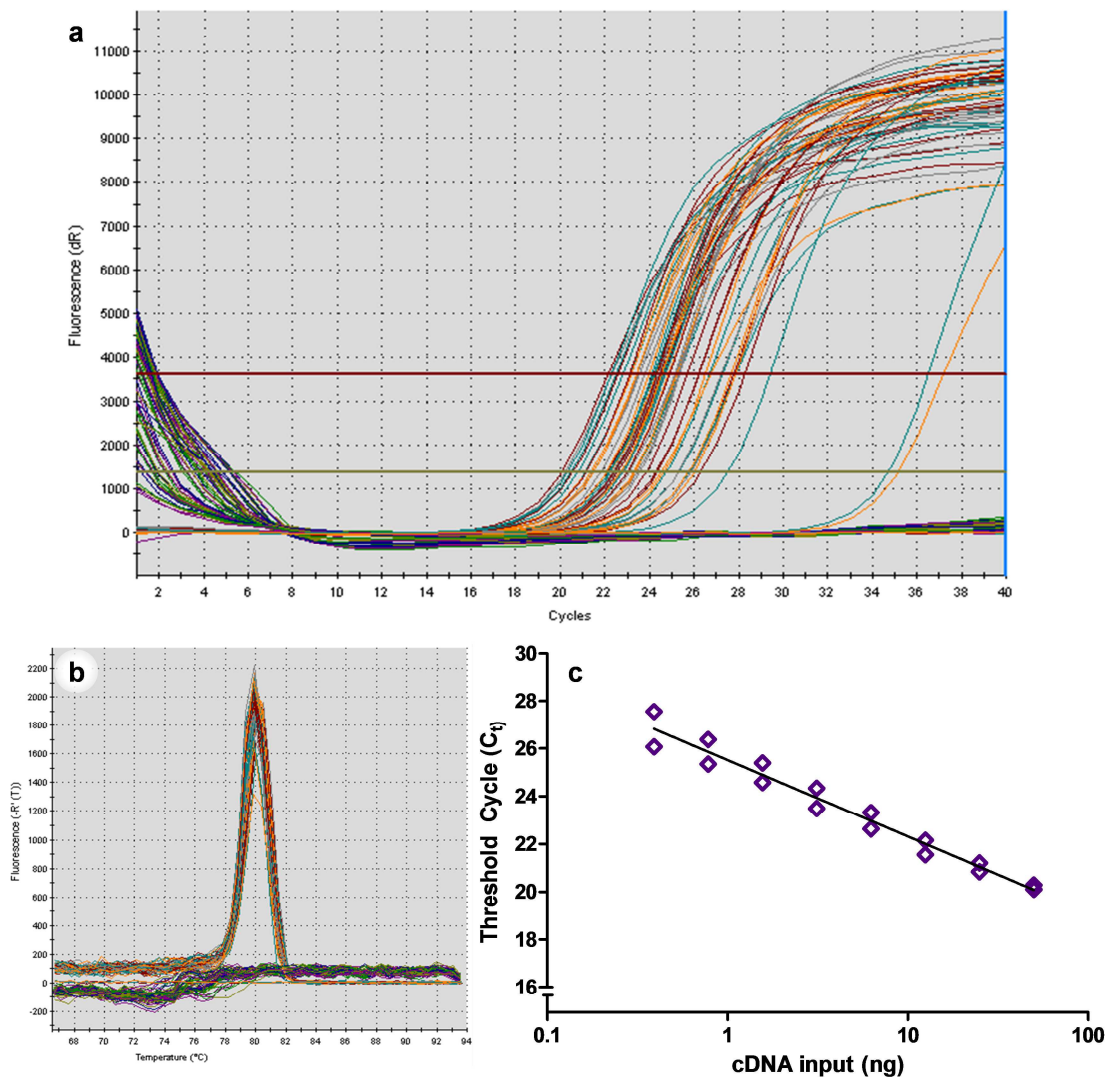


Figure 7.26 Results of qPCR for *Ywhaz* **(a)** sigmoidal plots showing consistent amplification, with trace amplification > 35 cycle in the no template control. No amplification occurred in the no-reverse transcriptase or water controls. **(b)** A single peak in the dissociation curve. **(c)** log-linear standard curve with a slope of -3.198 and $R^2 = 0.964$ over 8 standards (50 - 0.391 ng).

Replicates ($n = 2$) are averaged and plotted; horizontal line represents group mean (Figure 7.27). Analysis of rank-transformed Ct values by two-way ANOVA (treatment; vehicle or UT-A and nephrectomy: sham or SNx) revealed significant variability between the treatment groups ($p_{\text{overall}} = 0.007$) with Ct highest in UT-A treated SNx (NA: 24.53 ± 0.66 , mean \pm SEM, $n = 5$). The remaining group averages were: SV, 21.75 ± 0.45 , $n = 5$; NV, 22.42 ± 0.46 , $n = 5$ and SA, 22.69 ± 0.10 , $n = 5$. Placenta (P) was included as positive control tissue and amplified well, Ct = 23.08.

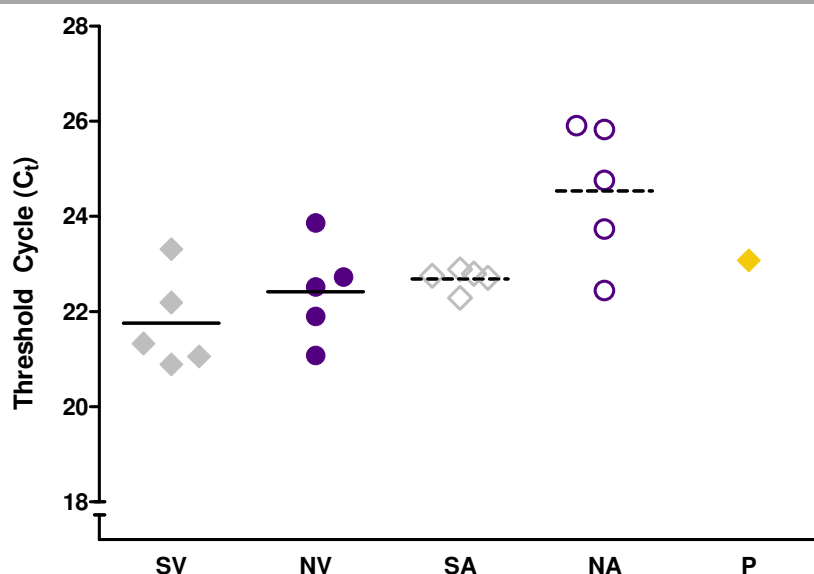


Figure 7.27 The *Ywhaz* primer set produced consistent amplification in all samples of cDNA produced from the renal cortex of shams receiving vehicle (SV) or urotensin-II antagonist (SA) and SNz rats treated with urotensin II antagonist (NA) or vehicle control (NV). Ct was different across the groups ($p_{\text{overall}} = 0.007$), being noticeably delayed in the NA group. Lines represent group mean, points represent mean of two replicates, analysed by two-way ANOVA on ranks.

Two representative PCR reaction products from each experimental group were examined ([Figure 7.28](#)) using 2.5% non-denaturing agarose gel as described in [Section 2.13.9](#) along with a high (50 ng, lane 2) and middle (3.125 ng, lane 3) standard. Representative NTC (lane 13), No RT (lane 14) and buffer (lane 15) negative controls were included along with the positive control (placenta, lane 12). Single bands were seen in lanes 2 - 12 at around 100 bp consistent with the single dissociation peak and predicted *Ywhaz* amplicon size (99 bp; [Table 2.7](#)). Hyperladders II (50 bp ladder, lane 1) and IV (100 bp ladder, lane 16) were included for reference.

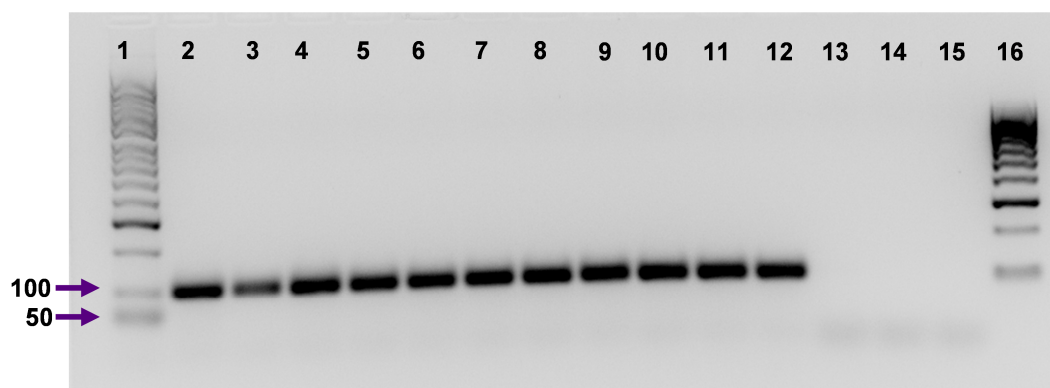


Figure 7.28 The *Ywhaz* primer set produced a single band at approximately 100 bp (predicted *Ywhaz* amplicon size 99 bp) in all standards and samples. Lanes 2 and 3 contain standards (50 and 3.125 ng, respectively) with negative controls (NTC, No RT and buffer) in lanes 13, 14 and 15 respectively. Lanes 4 and 5 contain PCR product from vehicle treated sham, 6 and 7 contain vehicle treated SNx, 8 and 9 contain urotensin II antagonist (UT-A) treated sham and 10 and 11 contain SNx receiving UT-A. HyperLadder II (lane 1; 50 bp ladder) and HyperLadder IV (lane 16; 100 bp ladder).

7.7.3 *Uts2r*

Amplification using the *Uts2r* primers occurred in a much higher Ct range ([Figure 7.29a](#)) than for *Ywhaz* despite increased cDNA input (details in [Section 2.13.5](#)) in both samples and standards (Ct range of replicate means (n = 2) for samples: 28.46 - 36.20 and standards: 28.54 - 33.18). There was no amplification in any of the NTC, no RT or buffer negative controls; in contrast amplification in the positive control (placenta) occurred at Ct = 28.47 (mean of n = 2 replicates). A six point standard curve (125 - 3.91 ng, [Figure 7.29c](#)) had good fit ($R^2 = 0.972$) and calculated reaction efficiency of 115.0 %.

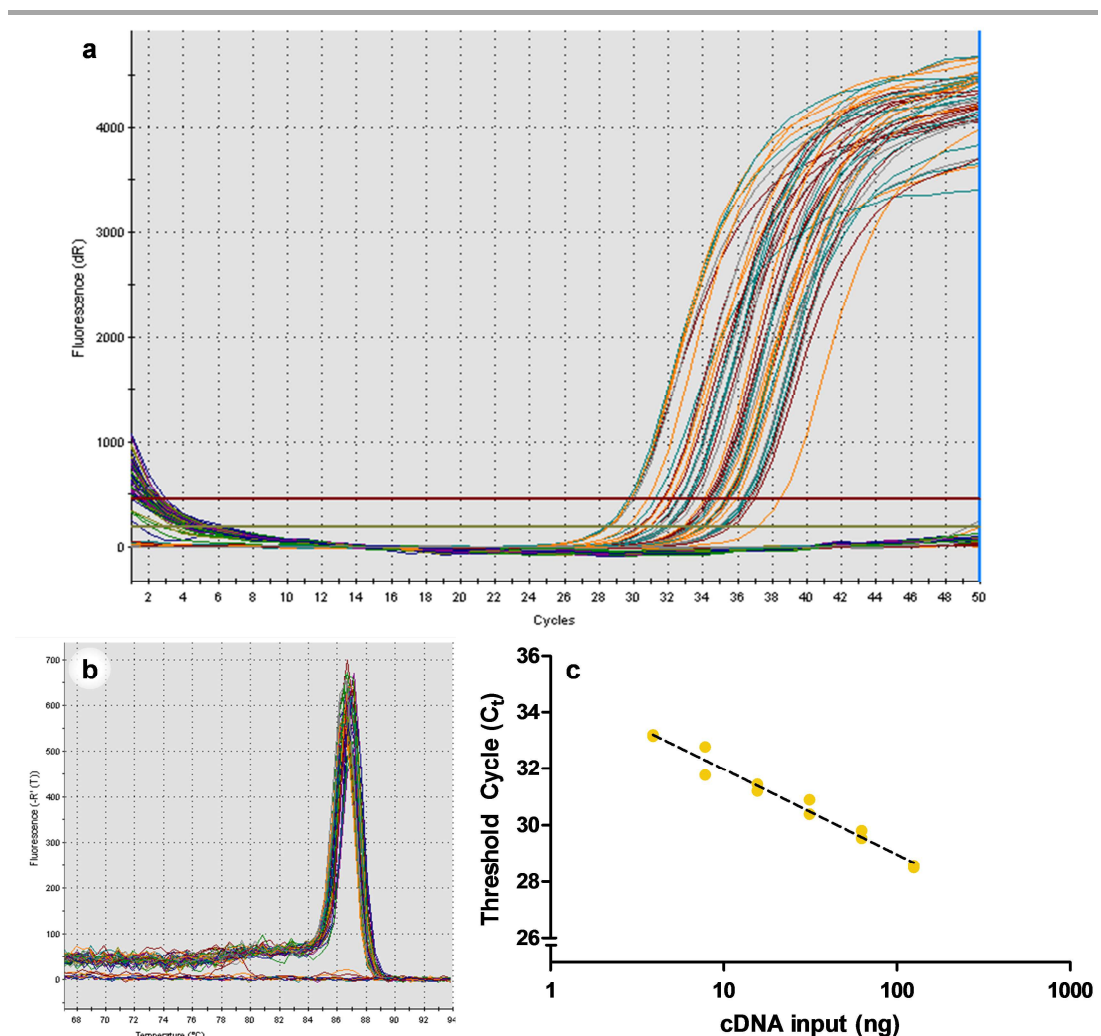


Figure 7.29 Results of qPCR for *Uts2r* **(a)** sigmoidal plots showing consistent amplification, with amplification occurring 25 - 40 cycles. No amplification occurred in the no template control, no-reverse transcriptase or water controls. **(b)** A single peak in the dissociation curve. **(c)** log-linear standard curve with a slope of -3.008 and $R^2 = 0.972$ over 6 standards (125 - 3.91 ng).

Amplification occurred in most samples and standards. There were 5 biological replicates per treatment group; amplification occurred in samples from 5 (NV and SV) or 4 (NA and SA) individuals producing a single peak within the dissociation curve. Raw Ct values appeared lower in the placental sample (Ct 28.47, $n = 1$) compared to shams receiving vehicle (SV: 33.77 ± 0.83 , $n = 5$) or UT-A (SA: 34.16 ± 0.18 , $n = 4$) and compared to SNx treated with UT-A (NA: 33.04 ± 0.46 , $n = 4$) and those receiving vehicle control (NV: 32.37 ± 1.09 , $n = 5$, [Figure 7.30](#)). This difference was not tested statistically as the single sample only served as a positive test sample and calibrator; however there was no difference in Ct values between the SV, NV, SA or NA groups ($p_{\text{overall}} = 0.474$, two-way ANOVA on ranks).

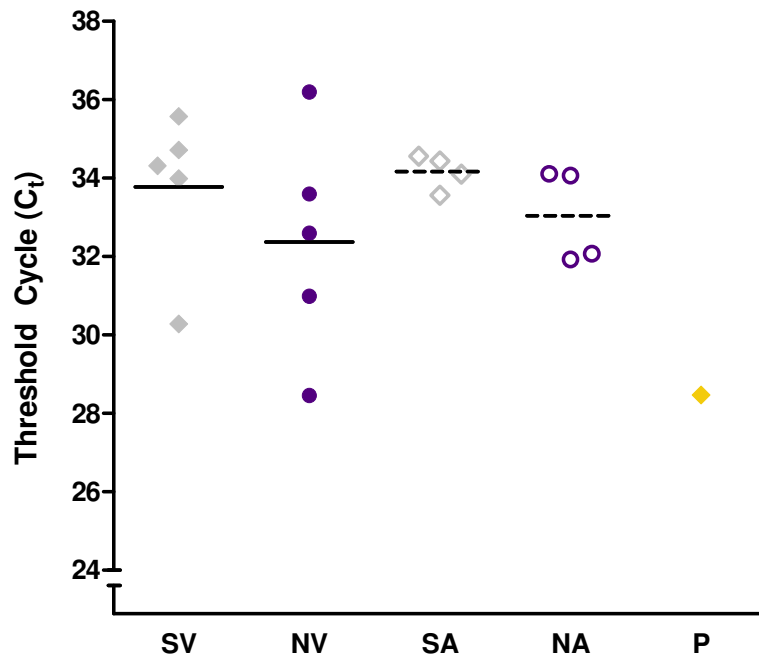


Figure 7.30 The *Uts2r* primer set produced amplification in most samples of cDNA produced from the renal cortex of shams receiving vehicle (SV, n = 5) or urotensin-II antagonist (SA, n = 4) and SNx rats treated with urotensin II antagonist (NA, n = 4) or vehicle control (NV, n = 5). Samples from placenta (P) amplified and reached the threshold (Ct) at an earlier cycle. Lines represent group mean, points represent mean of two technical replicates, and each point is a biological replicate.

Electrophoresis of final PCR reaction products produced prominent bands in all samples and standards which appeared slightly heavier than 100 bp in weight ([Figure 7.31](#), lanes 2 - 12). This is consistent with the predicted *Uts2r* amplicon size (116 bp) and the band was absent from the NTC, No RT and buffer negative controls, lanes 13, 14 and 15 respectively.

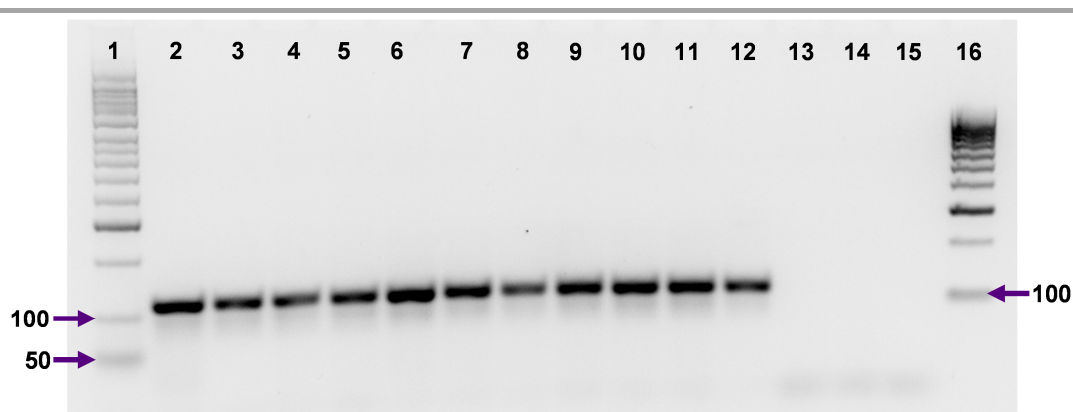


Figure 7.31 The *Uts2r* primer set produced a single band above the 100 bp marker (predicted *Uts2r* amplicon size 116 bp) in all standards and samples. Lanes 2 and 3 contain standards (125 and 7.813 ng, respectively) with no bands seen in the negative controls; NTC, No RT and buffer loaded in lanes 13, 14 and 15, respectively. Samples are loaded as follows: lanes 4 and 5, vehicle treated sham; 6 and 7, sham receiving urotensin II receptor; lanes 8 and 9, SNx receiving vehicle; lanes 10 and 11, SNx receiving urotensin II antagonist; and lane 12, placenta. HyperLadder II (lane 1; 50 bp ladder) and HyperLadder IV (lane 16; 100 bp ladder).

7.7.3.1 Example of further analysis of *Uts2r* expression

Example fold change expression (calibrator: placenta) analysis is carried out relative to internal control *Ywhaz* and taking into account variations in reaction efficiency according to the Pfaffl¹ modification (as described in [Section 2.13.8](#), [Equation 2.7](#)). This revealed ([Figure 7.32](#)) that relative *Uts2r* expression tended to be higher in SNx rats whether receiving UT-A (0.094 ± 0.043) or vehicle control (0.114 ± 0.081) than in in shams treated with UT-A (0.010 ± 0.002) or vehicle (0.0134 ± 0.010 , two-way ANOVA on ranks: $p_{\text{overall}} = 0.068$, $p_{\text{SNx}} = 0.021$ and $p_{\text{UT-A}} = 0.171$). However UT-A treatment did not affect *Uts2r* expression compared to vehicle in either sham or SNx animals.

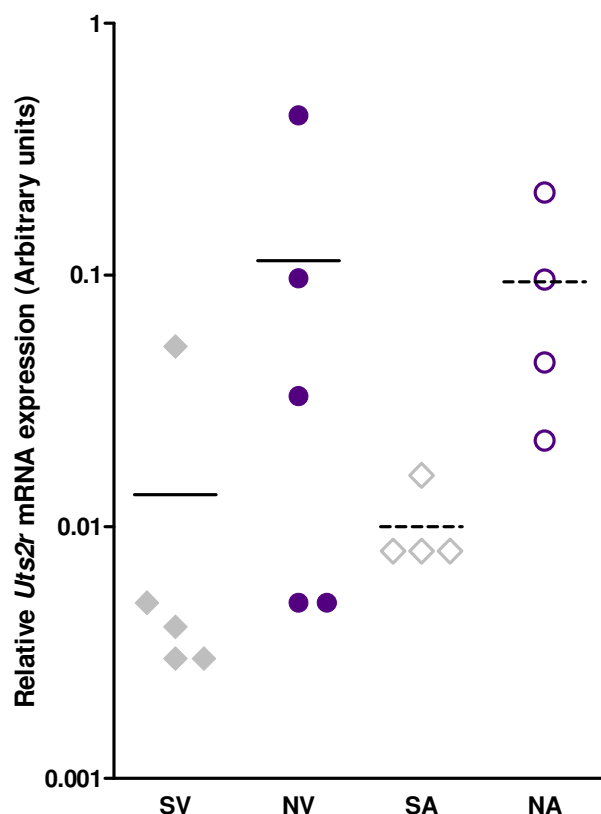


Figure 7.32 Relative *Uts2r* mRNA expression normalised to internal reference *Ywhaz*. *Uts2r* tended to be higher in SNx rats receiving vehicle (NV, n = 5, filled circles) or urotensin II receptor antagonist treatment (NA, n = 4, open circles) than in treatment matched shams (SV, n = 5 and SA, n = 4, respectively). All data are presented relative to calibrator placenta. Two-way ANOVA on ranks: $p_{\text{overall}} = 0.068$, $p_{\text{SNx}} = 0.021$ and $p_{\text{UT-A}} = 0.171$, line at group mean.

7.7.4 *Uts2b*

Amplification using the *Uts2b* primers also occurred in a much higher Ct range (Figure 7.33a) than for *Ywhaz* despite increased cDNA input (Section 2.13.6) in both samples and standards (Ct range of replicate means (n = 2) for samples: 33.83 - 38.79 and standards: 34.10 - 36.72). There was no amplification in any of the NTC, no RT or buffer negative controls. Amplification was also poor in the control tissue, placenta, with only one replicate amplifying successfully (Ct = 35.79) from 2 replicates at a 1 in 10 cDNA dilution; there was no amplification at either a 1 in 20 or 1 in 40 dilution. Only four (125 - 15.63 ng) of the eight standards amplified and the standard curve was not fitted adequately for any further analysis (Figure 7.33c, $R^2 = 0.858$); the calculated reaction efficiency was 106.4 %.

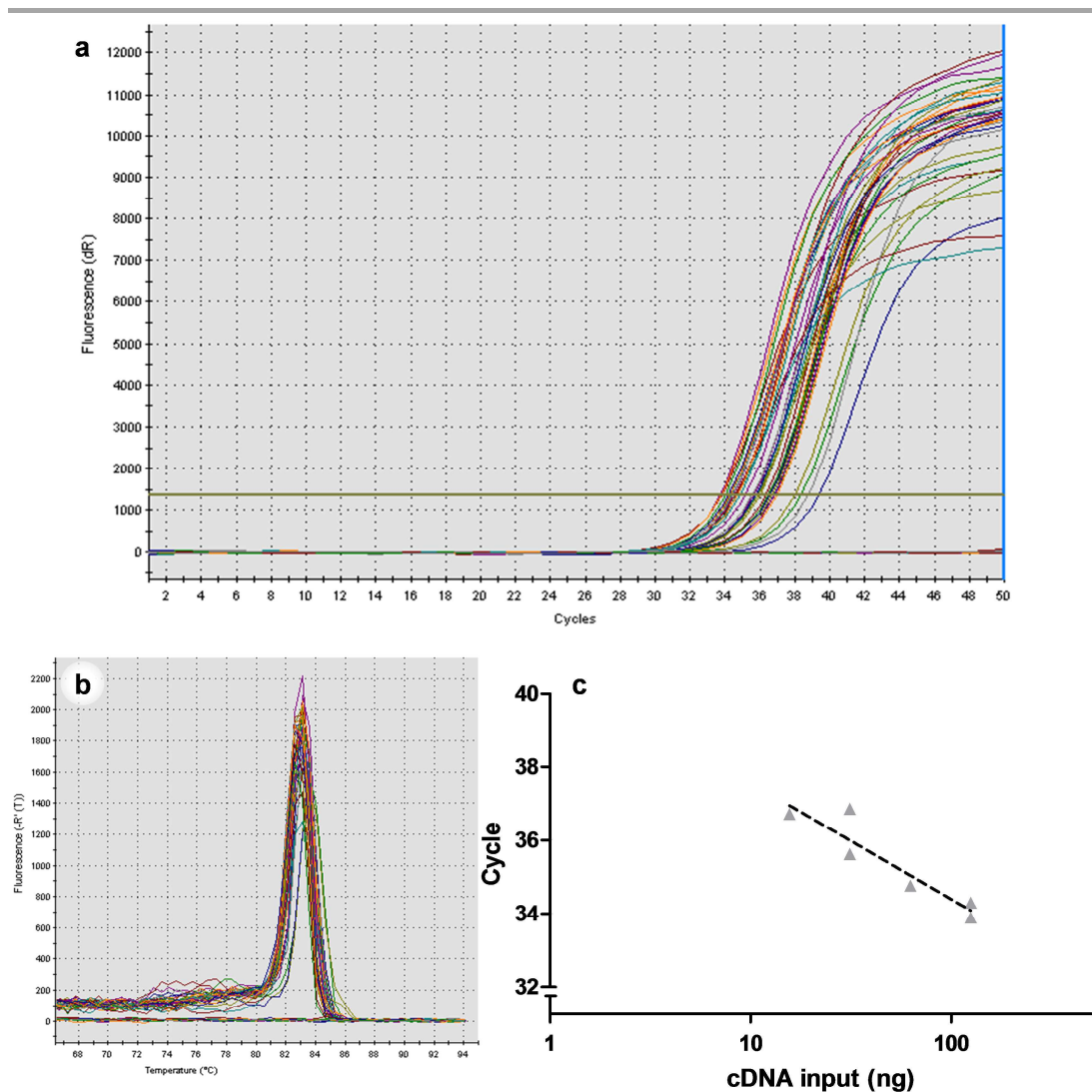


Figure 7.33 Results of qPCR for *Uts2b* **(a)** sigmoidal plots showing consistent amplification, with amplification occurring 30 - 40 cycles. No amplification occurred in the no template control, no reverse transcriptase or water controls. **(b)** A single peak in the dissociation curve. **(c)** log-linear standard curve with a slope of -3.177 and $R^2 = 0.858$ over 4 standards (125 - 15.63 ng).

Amplification occurred in at least one replicate from most samples and standards. There were 5 biological replicates per treatment group; amplification occurred in samples from 5 (SA) or 4 (SV, NV and NA) individuals producing a single peak within the dissociation curve. Where amplification occurred raw Ct values were comparable ($p = 0.068$, two-way ANOVA on ranks) across all groups, shams receiving vehicle (SV: 36.07 ± 0.65 , $n = 4$) or UT-A (SA: 35.86 ± 0.46 , $n = 5$), and SNx treated with UT-A (NA: 37.52 ± 0.73 , $n = 4$) or those receiving vehicle control (NV: 35.16 ± 0.44 , $n = 4$, [Figure 7.34](#)). The Ct value was also similarly high in the placental sample (Ct 35.79, $n = 1$).

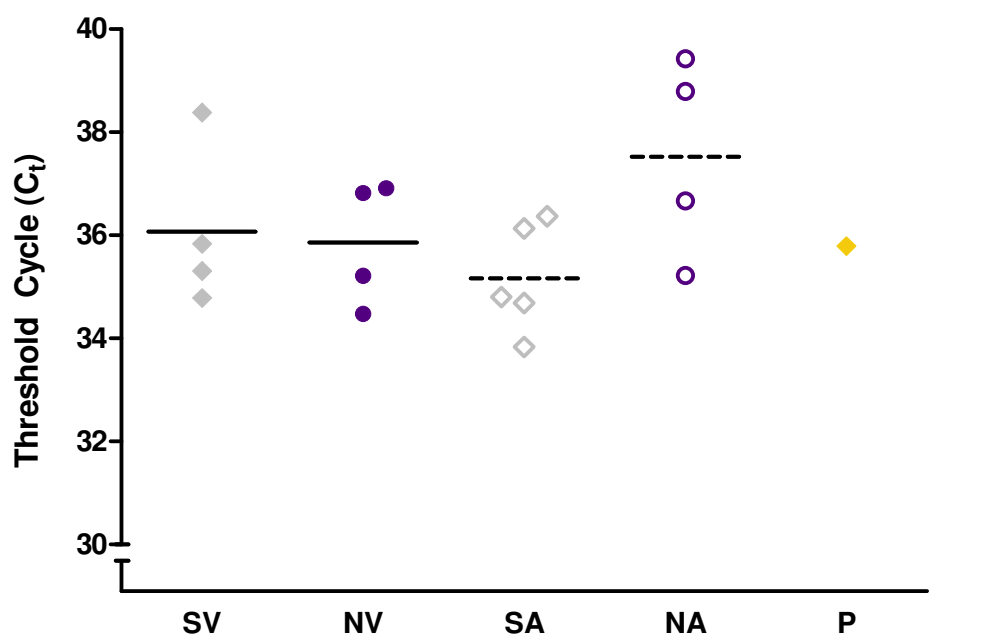


Figure 7.34 The *Uts2b* primers produced amplification in most samples of cDNA produced from the renal cortex of shams receiving vehicle (SV, n = 5) or urotensin-II antagonist (SA, n = 4) and SNx rats treated with urotensin II antagonist (NA, n = 4) or vehicle control (NV, n = 5). Samples from placenta (P) amplified and reached the threshold (Ct) at an earlier cycle. Lines represent group mean, points represent mean of two technical replicates, and each point is a biological replicate.

Electrophoresis of final PCR reaction products (as per [Section 2.13.9](#)) produced prominent bands in all samples and standards which appeared slightly heavier than 100 bp in weight ([Figure 7.35](#), lanes 2 - 12). This is consistent with the predicted *Uts2b* amplicon size (120 bp) and the band was absent from the NTC, No RT and buffer negative controls, lanes 13, 14 and 15 respectively. There were additional less intense heavier bands (250 - 450 bp) seen in lane 4 (SV) and lane 7 (NV); lane 8 (SA) had an additional band slightly heavier than the major product.

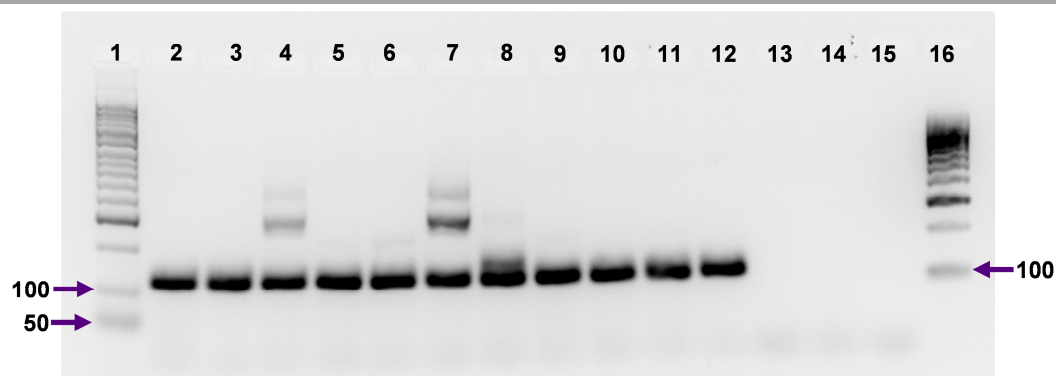


Figure 7.35 Gel electrophoretic examination of final PCR reaction products produced a major band which was slightly heavier than 100 bp (predicted *Uts2b* amplicon size 120 bp) in all standards (125 ng, lane 2 and 62.5 ng, lane 3) and samples. There were no visible bands in the negative controls; no template control (lane 13), no reverse transcriptase control (lane 14) and water control (lane 15). Samples are loaded as follows: lanes 4 and 5, vehicle treated sham; 6 and 7, sham receiving urotensin II receptor; lanes 8 and 9, SNx receiving vehicle; lanes 10 and 11, SNx receiving urotensin II antagonist; and lane 12, placenta. Weight markers HyperLadder II (lane 1; 50 bp ladder) and HyperLadder IV (lane 16; 100 bp ladder) are included for reference.

7.7.5 *Uts2*

Amplification of *Uts2* was problematic despite extensive troubleshooting; increased cDNA load, rightward shift applied to the standard curve (125 ng, top standard), which was produced from a SNx enriched cDNA pool and increased cycle number did not produce reliable or reproducible amplification plots. Amplification occurred only at $C_t > 35$ ([Figure 7.36a](#)). The dissociation curve had multiple peaks ([Figure 7.36b](#)), however placental samples amplifying before 38 - 40 cycles produced a single dissociation peak ([Figure 7.36c](#)). The standards did not amplify well, producing mixed dissociation peaks and no useable standard curve ([Figure 7.36d](#)).

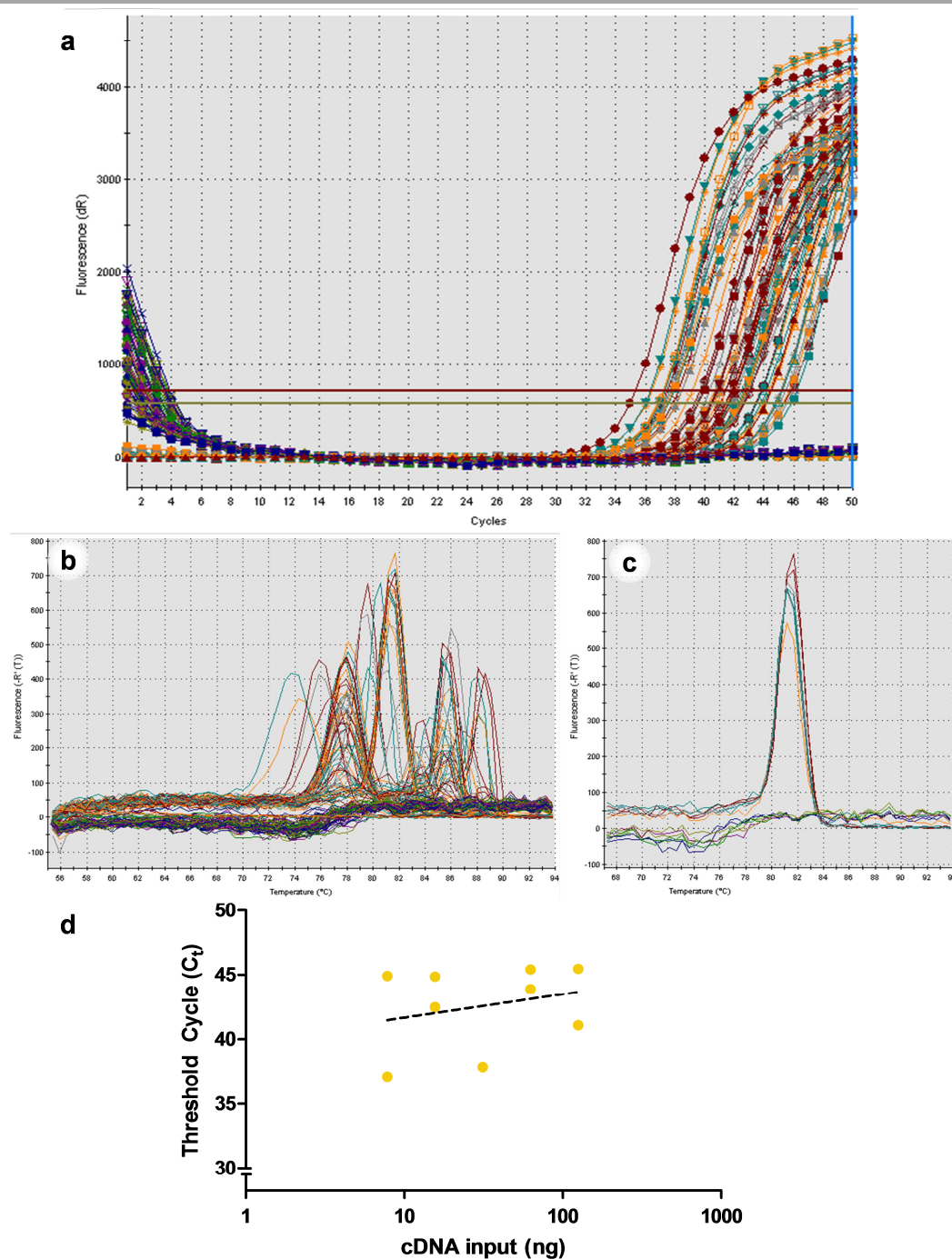
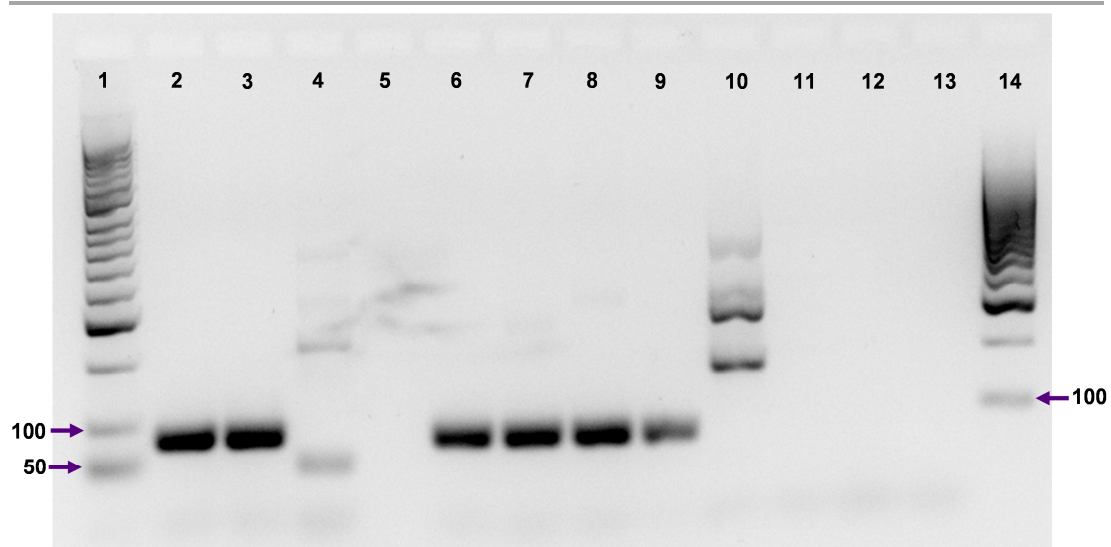


Figure 7.36 Results of qPCR for *Uts2* **(a)** sigmoidal plots showing amplification at very high cycle numbers. No amplification occurred in the no template control, no-reverse transcriptase or water controls. **(b)** Multiple peaks in the dissociation curve across all wells **(c)** with a single peak seen in most placental samples. **(d)** There was no clear standard curve over the 8 standards used (125 - 3.91 ng), fit: $R^2 = 0.072$ and slope 1.814.

Electrophoresis of final PCR products from placental samples (see [Section 2.13.9](#)). Most of these samples produced a single band between 50 and 100bp which is consistent with the predicted *Uts2* amplicon size (82 bp). There were no visible bands in lanes containing NTC (lane 11), No RT (lane 12) or buffer (lane 13) negative controls ([Figure 7.37](#)).



[Figure 7.37](#) Final PCR reaction products from placenta tended to produce a major band near to 100 bp in size (predicted *Uts2* amplicon size 82 bp) when examined by gel electrophoresis (lane 1 - 10). There were no visible bands in the negative controls; no template control (lane 11), no reverse transcriptase control (lane 12) and water control (lane 13). Weight markers HyperLadder II (lane 1; 50 bp ladder) and HyperLadder IV (lane 14; 100 bp ladder) are included for reference.

8: Discussion - Effect of urotensin-II receptor antagonist AZ13694621 on progression of chronic kidney disease in the 5/6th SNx rat

The 5/6th SNx is a previously validated model of renal dysfunction, culminating in renal failure.^{177,266} Using this model (established as described in [Section 2.3.2](#)), and data from the initial characterisation study, the effect of intervention using a non-peptide urotensin-II receptor antagonist (UT-A: AZ13694621, also known as SB-611812 / SB-657510A)^{302,356,377} was explored.

8.1 Dosing regimen and tolerance

Following recovery from procedure two there were no incidences of post-operative complications and the rate of acute renal failure (ARF) was extremely low (2.8 %). In this study dosing was started one week after completion of the second surgical procedure and while this does not represent the typical clinical situation, it afforded the best opportunity to determine whether intervention with a UT-A would be beneficial in this experimental model of CKD. In the first two months after the 5/6th SNx procedure the effectiveness of intervention may be complicated by the concurrent recovery from (near) ARF and the following hypertrophic response; however, in this study the dosing period was extended substantially beyond this initial period (1 week recovery followed by 13 weeks dosing). In addition attempting to randomise subjects later in the disease profile has been described previously to provide ineffective matching due to the variability in disease progression.¹⁸⁰ Thus while this approach does not match the potential clinical application of a UT-A, it does allow the demonstration of proof of principle.

8.1.1 Compound selection and administration

While a number of compounds with UT antagonist activity exist, a large proportion, including the highly potent urantide,²³⁵ were produced by systematic modification of the minimally active fragment of human UII peptide (hUll₄₋₁₁). Although urantide has been shown to be a potent full antagonist in isolated rat aorta the peptide ligand has some residual agonist activity in CHO cells expressing hUT.²⁴⁹ As a result of its peptide nature the experimental and clinical use of urantide and related compounds is limited since it cannot be effectively administered orally as the peptide structures would be digested by the numerous peptidase enzymes in the stomach. The first

broadly documented non-peptide UT-A compound, palosuran (ACT-058362) produced variable results showing greater potency at hUT than rUT in membrane preparations, with further variation reported when whole cell systems were considered.²⁵¹ This variability is also evident *in vivo*; palosuran improved the metabolic profile of diabetic rats but had no discernible effects in patients with diabetic nephropathy and hypertension.^{297,299}

The UT-A compound selection criteria employed in the current study was for a potent non-peptide antagonist of the UT receptor. Initially this lead to AZ13631437 and AZ13631439, the L and S enantiomers of a compound published in an aminomethylpiperazine compound series.²⁴⁶ This compound was reported to show favourable properties in an aortic ring assay for UT antagonism; however, when synthesised (by AstraZeneca) and tested in an *in vivo* pharmacokinetic (PK) study the compound did not have a favourable clearance profile and so was unsuitable for daily oral dosing. Following this a secondary compound was identified (AZ13694621 or SB-611812).^{302,356} AZ13694621 is less potent than AZ13631437/AZ13631439, but there are published studies describing *in vivo* efficacy of AZ13694621 (SB-611812) following oral dosing in rats, and the PK profile was favourable in Sprague-Dawley (SD) rats ([Section 2.3.2.1](#)).

After confirming the bioavailability in the SD rat using a standard PK protocol ([Section 2.3.2.1](#)) dosing was carried out by daily oral gavage in a commonly used suspension vehicle (0.5 % HPMC with 0.1 % Tween20 in water) at a previously published effective dose (30 mg.Kg⁻¹.day⁻¹).^{276,356} The PK data showed sufficient compound concentrations within the blood over the course of the 24 hour monitoring period. Nonetheless it should be noted that the compound is highly (95 - 98 %)³⁷⁸ protein bound in human blood although corresponding rat data are not readily available. However, previous studies using this particular non-peptide UT-A have shown that this dosing regimen is effective, at least in some rat models of cardiovascular disease.^{276,302,356} While the vehicle used herein is not identical to that in other studies, the role of cellulose is purely to increase viscosity, thereby reducing the rate of suspension settling and ensuring more reliable dosing. In previous studies this compound was also delivered in a cellulose-based suspension, in water (0.1% - 1 % methylcellulose, grades not provided). The use of a suspension vehicle was the result of poor water solubility. However it seemed most appropriate to proceed with a dosing method which has been shown previously to be effective with this particular compound. Further PK studies would be necessary to demonstrate bioavailability via diet-based administration if longer study periods were required in future. However, it

is important to consider that there could be periods of reduced appetite later in the study in the SNx cohort which could affect the dosing accuracy.

8.1.1.2 Dosing period

Dosing was continued for 13 weeks, until week 14 after the second surgical procedure ([Figure 2.5](#)), as from the previous work (Chapter 3 and discussed in Chapter 6) this time frame represented a period of measurable change; the physiological status of the SNx rats diverged from time-matched controls in uACR, SBP, plasma biochemistry and renal histology. Weight gain following surgery was similar across all groups and consistent with the characterisation study. During these initial 6 - 8 weeks there were no notable changes in the rats' behaviour whilst physiological data showed only minor deviation from that of the sham controls. Towards the end of the study period the SNx groups presented with moderate increases in SBP along with evidence of renal function impairment such as marked elevation of uACR, plasma creatinine and plasma urea. Final kidney weight was also significantly increased relative to the sham controls and the tissues showed evidence of cortical fibrosis and glomerulosclerosis. This time point also represented a void between the previous report of up-regulation of UT, URP and UII mRNA by Mori et al.¹⁷⁸ and supporting 8 week (early) time point within the characterisation study ([Section 3.6](#)) and the substantial over expression described within the immunohistochemical staining in the late SNx cohort. Hence this experiment afforded the opportunity to examine tissues from a mid-point for both CKD progression and UII system expression.

8.1.2 Growth curves and survival

The rats in this study were well matched for age and weight at the start of the study, and the study length of 14 weeks (3.5 months) occurred almost entirely within the normal growth period, approaching the plateau phase at around week 12 post-surgery. Unlike the initial study ([Section 3.2.1](#)) there was an early and significant divergence between the SNx and sham rats ($p_{\text{SNx}} = 0.002$), which persisted until the end of the study. This difference was not seen in the previous study where SNx and sham cohorts did not visibly diverge until 15 - 20 weeks post-surgery. This suggests that the SNx rats may have had a lower tolerance to the stress of the dosing procedure than the sham controls; the treatment group had no effect. This effect was also seen in the survival curves where 5 SNx rats reached humane end points before the end of the dosing period compared to none in the sham groups, although

overall survival was not significantly different between the groups ($p = 0.340$). It is worth noting that only 1 subject in the previous study reached the defined endpoint within 14 weeks, and this was a secondary complication.

8.2 Physiological profile of intervention

Using the (patho)physiological profile from the characterisation study (results in [Section 3](#)) as guidance the SNx rats receiving UT-A (NA) or vehicle control (NV) were monitored for disease progression as described ([Section 2.4](#)) along with treatment-matched sham controls.

8.2.1 Systolic blood pressure and heart rate

Increasing (systolic) blood pressure (SBP) is considered to be both a complication and a causative factor in the progression of CKD; as such it provides a target for therapeutic intervention and point of monitoring.

There was a progressive increase in SBP within the SNx cohorts as the study progressed ($p_{\text{time} \times \text{SNx}} < 0.001$) which is consistent and comparable to findings in the previous experiment (discussed in [Section 6](#)). Interestingly blood pressure was lower in the UT-A treated cohort than in those receiving vehicle ($p_{\text{UT-A}} = 0.032$) and there is an apparent delay in the onset of significant elevation of SBP in the UT-A treated SNx cohort. The SBP in the UT-A treated SNx is not significantly elevated (compared to the treatment-matched shams) until week 12; in the SNx rats receiving vehicle the increase in SBP was significant two weeks earlier, in week 10. There was a small and non-significant difference in the SBP of the two groups in week 2; all four groups (SV, NV, SA and NA) were clustered between 137.8 and 142.9 mmHg. It is possible that the NA group had naturally lower blood pressure, but taking this in to consideration the difference between the NV and NA group tended to be greater towards the end of the study. It would be interesting to find out whether the extent of this increase in SBP in the UT-A treated SNx would reach that of the vehicle group in the later period of the disease. Would SBP reach the 170 - 200 mmHg range seen in the characterisation study? Given the intensity of the dosing schedule it would have been more appropriate to administer the antagonist in the diet of the animals if longer term dosing was required, a route by which the compound would have needed further pharmacokinetic validation.

These increases in SBP was not accompanied by any change in heart rate which remained consistent throughout the 14 weeks of the study ($p_{\text{time}} = 0.141$) and comparable across the groups ($p = 0.424$). The range within the HR data is consistent with the findings in the characterisation experiment ([Section 3](#)).

8.2.2 Renal function

It has long been established that the presence of persistent albuminuria is an important marker of disease progression in CKD as it indicates dysfunction at the glomerular filtration barrier. However, more recent studies have shown that albuminuria is not just a marker, but an important therapeutic target in the management of CKD.³⁵⁸ It has been suggested that it is active peptide fractions (eg. TGB- β) within the measured albuminuria/proteinuria, and not albumin per se, that are responsible for this effect.¹³⁵

Over the course of the study renal function was monitored by measuring urinary albumin-creatinine ratio (uACR, mg/ μ mol); this surrogate marker provided insight in to the underlying glomerular damage and renal function decline. A terminal blood sample was analysed for the metabolic waste products creatinine and urea nitrogen (BUN). These metabolic waste products accumulate when renal function is impaired and reduced renal function affects BUN more readily than plasma creatinine. This difference is in part a result of active secretion of creatinine into the renal tubules which is largely unaffected by the formation of glomerulosclerotic lesions. It has been highlighted that this active transport of creatinine can lead to an overestimation of renal function (eGFR) in the clinical setting where calculations are based upon creatinine clearance alone. This issue is particularly evident in the lower ranges of renal function.³⁵ This issue also impacts upon the uACR measurement method. Ideally renal function would be measured using a molecule which is cleared at the glomerulus alone (inulin, for example); however this methodology was not practical in the context of the current study. Protocols for accurate renal clearance and GFR calculation are available; one commonly used and validated method³⁰⁶ is carried out under terminal anaesthesia over a period of 2 - 6 hours, and so does not lend itself to repeated measurements or in application to animals with underlying complications (CKD). Considering practicality, stressor effects, reliability and accuracy the surrogate uACR method with blood plasma profile (creatinine and BUN) provides sufficient insight into renal function with significantly reduced procedural stresses.

8.2.2.1 Urinary albumin: creatinine ratio

The timeline of progression in this experiment was consistent with the characterisation study (described in [Section 6](#)). The sham rats provided a consistent baseline throughout the study and data were comparable between the sham rats receiving the UT-A and vehicle. ACR was significantly higher in SNx rats receiving vehicle (than in treatment-matched controls) after 6 weeks. In the SNx rats receiving UT-A deviation from the treatment-matched shams occurred in week 8. This is a small difference and it mirrors the delay seen in the SBP data. Unlike the SBP data, the extent of ACR elevation towards the end of the study was comparable between the groups.

8.2.2.2 Creatinine and urea in blood plasma

By the end of the study (week 14) plasma BUN, but not creatinine, was significantly higher in the SNx groups. The extent of this elevation was similar in both the vehicle and UT-A treated SNx, although there appeared to be greater variability in the UT-A treated cohort. The cause of this variation is unclear; it could be an artefact of increased samples number or potentially indicate a heterogeneous response to the UT-A treatment.

8.3 Histology: Renal mass, structure and fibrosis

Kidneys (expressed as g per Kg of body weight, g/Kg) from the NV and NA groups were significantly heavier than the treatment-matched shams. With an estimated increase of + 200 %, the weight of the kidneys at collection was comparable between the NV and NA groups ($p = 0.434$). The hypertrophic response following the 5/6th SNx procedure is well documented and is considered important to sufficient recovery for the avoidance of ARF.

When examined by light microscopy the kidneys of SNx rats, from both groups, presented with structural abnormalities associated with CKD. H and E staining highlighted enlargement of the glomeruli, dilatation of the renal tubules and peritubular expansion within the cortex. The structure of the medulla was typically intact although some areas of hypercellular expansion were present. Within the glomeruli PAS staining showed that focal sclerotic lesions were common (GSI scores NV: 1: 0 - 2, $n = 250$ and NA: 1: 0 - 2, $n = 225$) and the brush border within the proximal tubules tended to be less pronounced, features which are clearly visible

upon comparison to the treatment-matched controls. Around the tubules the blue component of the MTC stain showed that there was evidence of fibrosis, which was corroborated with increased immunohistochemical staining for the extracellular matrix components collagen IV and laminin- β relative to treatment-matched sham controls. All of these changes were observed to a comparable extent in both the UT-A and vehicle treated SNx cohorts suggesting that UT antagonism with AZ13694621 at 30 mg.Kg⁻¹.day⁻¹ p.o. did not alter the final histological profile of CKD at 14 weeks (post-surgery).

Further analysis of the mRNA expression of *Col4a1*, *Lamb1* and *Fn1* (carried out by Tom Speight on the 1:100 cDNA stocks produced in [Section 2.13.4](#), see [Appendix C](#)) revealed that amplification tended to occur later in the SNx rats receiving UT-A relative to those receiving vehicle, suggesting that mRNA expression of *Col4a1*, *Lamb1* and *Fn1* is lower in this group. However, only *Col4a1* and *Fn1* appear to amplify at an earlier cycle in the vehicle-treated SNx cohort relative to the treatment matched shams. Although the mRNA for the proteins appears to be less abundant in the cortex of SNx rats receiving UT-A the immunohistochemical staining appears comparable between the groups. Numerous groups have shown that although protein and mRNA concentrations often correlate this cannot be assumed and the correlation between the expression levels of mRNA and that of the protein produced can be weak or indistinct; the relationship between transcription and translation is not linear and not simple.^{375,376} Within the context of this work there are a number of reasons for the differences in the expression of mRNA and protein such as the increased sensitivity of qPCR based methodologies relative to the qualitative/semi-quantitative immunohistochemical stains. There is increased specificity associated with qPCR analysis, as each primer set detects only one variant (in this case collagen IV, alpha-1 and laminin- β_1) whereas the antibody staining represents the cumulative total of multiple isoforms of the peptides, which may not be expressed in equal quantities and these proportions can be altered in the course of disease. This effect is further complicated by the nature of ECM turnover which is the net result of the rate of synthesis and rate of degradation by matrix metalloproteases, for example.³⁷⁹

8.4 Expression of Ull system components

Consistent with the expression pattern described previously ([Section 3.6](#)), and published reports, Ull-reactive staining was diffuse and faint in the renal cortex tissue of sham rats (receiving UT-A or vehicle). Staining was localised to cells of the

proximal and distal tubules with no staining generally seen within the glomeruli.^{178,216} In the SNx rats the staining was similarly localised to the renal tubule epithelial cells, but there was an increase in the intensity of staining relative to the sham controls. In the UT-A treated SNx rats this staining was seen to a lesser extent than in the vehicle treated SNx, with the most intense staining observed in the proximal tubules. In the medulla UII staining appeared comparable within the cells of the collecting ducts, although there was additional staining in the surrounding tissue in the SNx cohorts which was not seen in the sham groups. This immunoreactivity represents both UII and URP. It was not possible to amplify a reliable UII (*Uts2*) transcript (For detailed discussion of this see [Section 4](#)) and although the assay for URP (*Uts2b*) was more successful the data produced were not subject to full analysis as the reaction efficiency was poor.^{311,364,380,381} The Ct values suggest that *Uts2b* mRNA may be less abundant in the samples from SNx rats receiving vehicle; however without normalising to reference genes it is not possible to determine whether this is a real difference in mRNA abundance or whether it is the result of a difference in the sample affecting all transcripts. There is a suggestion within this data as a whole that total UII-reactive peptides (UII and URP) may be reduced in the renal cortex of 5/6th SNx receiving UT-A compared to the SNx rats receiving vehicle control. However without developing more sensitive methods for the detection of these problematic transcripts it will be difficult to answer the question fully.

The UT receptor was largely absent from cortical regions in all groups, which is in line with the staining reported previously and with that seen in the sham groups in the previous experiment. There were small areas of positive staining associated with areas of peritubular expansion and fibrosis in the SNx groups. This visible increase in UT staining within cortical tissues was also seen in the mRNA expression analysis where relative expression was approximately 10-fold higher in both SNx groups. This qPCR analysis is purely exploratory for reasons discussed in [Section 4](#); however it is consistent with the increase in mRNA expression reported at 8 weeks by Mori et al.¹⁷⁸

8.5 Conclusions

Urotensin-II receptor antagonism with AZ13694621 does not appear to slow the progression of the non-diabetic chronic kidney disease associated with the 5/6th SNx model in rat over the initial and early stable phase of the disease. There are small delays in the development of elevated SBP and albuminuria within the UT-A cohort, and delays in these parameters could be indicative of slower disease progression,

but without further investigation it is not possible to know whether these effects are physiologically relevant to the overall progression of the disease.

General renal structure was clearly altered in both SNx groups when compared to the sham controls and these changes appeared to be of a similar magnitude in SNx rats receiving UT-A or vehicle and were most prominent within the renal cortex with less extensive changes in the medulla. Accumulation of extracellular matrix (ECM) components was seen in the SNx cohorts, particularly within the cortex. There is some evidence of an onset delay in some physiological measures of disease progression in the SNx cohort receiving the UT-A when compared to the vehicle control; however this did not translate into preservation of renal structure or reduced fibrosis in this experiment.

Although AZ13694621 administered at a dose of 30mg/kg/day is not likely to be a useful therapeutic intervention in this model of non-diabetic CKD, the data in this work suggest that UT-antagonism in CKD is worth further study. The previously published conflicting data in clinical and pre-clinical studies highlight the importance of dose, timing and compound. In addition the results of this work also provide a novel insight into expression of UT and UII during the established stable phase (14 weeks post-surgery) of CKD in the 5/6th SNx and bridging the gap between the literature (8 weeks on the cusp of the stable phase) and the study described in [Section 3](#). The pattern of disease progression and extensive glomerulosclerotic lesions developed by the 5/6th SNx rat closely resemble those seen in DN however there is no diabetic/hyperglycaemic drive. The lack of diabetic symptoms subverts the role that hyperglycaemia, and by extension AGEs, have been repeatedly shown to play in the development and progression of DN. As a result of this distinction and differential pathophysiological drive the combination of these results with those from a complementary diabetic model could prove useful in disentangling the potential therapeutic value of UT receptor antagonists in diabetic and non-diabetic renal disease.

9: General Discussion

The 5/6th SNx is a previously validated model of renal dysfunction, culminating in renal failure.^{177,266} Using this model (established as described in [Section 2.3.2](#)), and data from the initial characterisation study, the effect of intervention using a non-peptide urotensin-II receptor antagonist (UT-A: AZ13694621, also known as SB-611812 / SB-657510A)^{302,356,377} was explored.

The UII system was identified 30 years ago; since then a vast array of tissues have been shown to respond to this small cyclic peptide and the related URP.^{193,194,269} UII remains the most potent endogenous vasoconstrictor identified and has been described as a cardio-renal mediator.^{207,214} Expression of UII, URP and UT is disrupted in a number of disease states including CKD, DN, diabetes mellitus and essential hypertension.^{182,183,272,273,287} Despite the differences between populations the role of UII in these diseases remains unanswered, in part due to the use of peptide-based pharmacological agents such as urantide.^{235,382} The emergence of potent non-peptide UT ligands, such as AZ13694621, has been important in furthering the UII research field.^{246,383}

Increased circulating and urinary concentrations of UII have been reported in patients with CKD; however these reports are limited to patients in CKD-associated renal failure.^{178,182,183} In contrast, Mori et al. describe an increased expression of UT and its ligands, UII and URP, in SNx rats 8 weeks post-operatively.¹⁷⁸ Thus there is disparity between the time-frame of data from human subjects with CKD and that collected from CKD models *in vivo*. Hence the first study described within the current work aimed to address this gap. The results of the current work suggest that the apparent up-regulation of UII/URP and UT in the 5/6th SNx model of CKD go far beyond those reported by Mori et al. at 8 weeks post-surgery.¹⁷⁸ Although the (patho)physiological role of the UII system in CKD remains undefined UT inhibition has shown promise; Clozel et al. report a reduction of albuminuria and improved metabolic profile in the STZ model of DN when treated with UT antagonist palosuran *in vivo*.²⁹⁷ The second major aim of the current work was to extend Clozel's study in the 5/6th SNx model. This aspect of the study was partially successful: there was a short delay in the development of albuminuria and onset of SBP increase in response to the UT antagonist AZ13694621. Unfortunately this difference was not reflected in the terminal data. Nonetheless, these data suggest that further exploration of UT-antagonist intervention in CKD is warranted.

9.1 RT-qPCR for Urotensin II system components in the renal medulla

Within the current work samples of renal cortex were assayed by RT-qPCR for UII system components UII (*Uts2*), URP (*Uts2b*) and UT (*Uts2r*), a process which proved problematic as a result of low copy number.²⁰⁰ The focus was placed upon cortical, rather than medullary, samples based upon the glomeruli representing a major site of change in CKD. This is mirrored by SNx rats which develop substantial glomerulosclerosis over the course of the induced CKD.^{121,294} Unfortunately expression of UII system components has been shown to be less intense in the cortex than in the medulla and this was reflected in the results with difficulty detecting the transcripts, particularly in the control groups.^{216,268} Therefore it would be worthwhile following up the original RT-qPCR with analysis of the same targets in tissues enriched for medulla, with the hope of quantifying this expression. This would also be of interest as it may reproduce the results of Mori et al. describing the increased expression of *Uts2*, *Uts2b* and *Uts2r* mRNAs in the remnant kidneys of SNx rats 8 weeks post-surgery.¹⁷⁸

9.2 (Mal)adaption of the glomerular basement membrane

The combination of staining techniques used through the current work provides a qualitative overview of the distribution of ECM proteins throughout the renal cortex. In addition, PAS staining provides semi-quantitative assessment of glomerulosclerosis. This highlighted a substantial increase in the deposition of ECM throughout the cortex of late SNx rats. The staining produced by standard antibody methodologies, such as those used here, cannot differentiate the type IV collagen α chains and so represent total collagen IV. Similarly, laminin- β staining represents all four laminin- β isoforms. Consequently it would be beneficial to follow up the current work with a RT-qPCR-based study examining the specifics of these changes in the SNx rats following dosing with UT-A compound. GBM specific components type IV collagen α_3 (*Col4a3*) and laminin- β_2 (*Lamb2*) could provide a starting point with further consideration of the collagen IV α_4 (*Col4a4*) and α_5 (*Col4a3*) chains and laminin- α_5 (*Lama5*) and γ_2 (*Lamc1*).¹⁶ Although increased expression of collagen III and IV has been reported in the remnant kidneys of SNx rats the proportional composition has not been fully explored. Since the heterotrimeric type IV collagen $\alpha_3\alpha_4\alpha_5$ is vital to proper GBM function an isoform switch could impact negatively upon function without affecting total expression (by pan immunological methods).^{14,16,120}

Similarly, disruption of the laminin-521 network is associated with podocyte adhesion and survival and ultimately GFB functionality.^{4,15}

9.3 Scope for further intervention studies

The dosing regimen used in the current work was a reflection of the one used in previous studies by Bousette et al. reporting efficacy in rat models of cardiac failure.^{276,356} Despite the reported efficacy the dose used may not have been optimal for the current work; it is not uncommon for a clinical drug to be used at differing doses in the treatment of different conditions. The compound was poorly soluble and p.o. administration by gavage is not particularly suited to longer term dosing, particularly in the later stages of CKD. Ideally AZ13694621, or an alternative antagonist, would be milled into standard chow to allow longer term dosing without the additional stresses associated with the gavage procedure. Interpretation of the potential therapeutic use of AZ13694621 in CKD is dependent upon a number of further considerations. Although the compound was produced for AstraZeneca by a commercial supplier, the chemical structure and purity of the batch of AZ13694621 used in the current study should be confirmed. The dose of AZ13694621 employed in this study was based on that used in a previous study in which *in vivo* efficacy was demonstrated;³⁰² nonetheless the circulating free concentration of AZ13694621 achieved during the stable phase of the SNx model should be established. Finally evidence of successful inhibition of UT receptor signalling by AZ13694621 *in vivo*, for example expression of a downstream marker or UT receptor phosphorylation, should be undertaken.

In designing a follow up study there are two major experimental designs to consider: either starting the dosing period immediately post-recovery in order to achieve the largest potential impact or using a more physiologically and clinically relevant regimen and dosing from ~8 weeks, until renal failure. Hopefully this longer period of intervention could provide some insight into whether intervention with a UT-antagonist has the potential to increase survival time or physiological condition in this SNx model of CKD. In contrast, dosing to renal failure will impact upon terminal samples effectively masking any potential improvement in histological and immunological markers. Subsequently these terminal samples could reveal less about the effects of the treatment as all rats would theoretically reach the (near) renal failure endpoint, regardless of whether one group reaches the pre-determined endpoint earlier than the other. Selection of an alternative longer term period of dosing would be complex due the variable rate of disease progression. This would

likely require the use of an earlier intervention period in order to administer the UT-antagonist for a significant duration.

Further, it is worth considering that while the 5/6th SNx model represents the histological lesions of secondary focal segmental glomerulosclerosis well; abnormalities in UII signalling have been described most widely in relation to diabetes, particularly type II diabetes and MetS.^{175,233,264,290,292} As such the use of an additional diabetic model would complement the robust but non-diabetic 5/6th SNx. Diabetes is the leading single cause of CKD (DN) and the prevalence is increasing; subsequently it would be of benefit to explore the potential of UT-antagonism here. Particularly, Clozel et al. have reported that a UT antagonist, palosuran, has shown promise in a model of DN.^{297,384} The model used was a model of DN in type I diabetes and relies on the toxicity of STZ to destroy pancreatic β -cells, thus limiting insulin production. The vast majority of DN patients have type II diabetes and often present with other confounding factors.^{48,100} In addition blood glucose is often poorly controlled in type II individuals due to the silent nature of the condition during the earlier stages.⁹⁸ Due to the increased size of the type II DN population and the reported association of UII abnormalities within this population it would be worth investigating the expression of UT/UII/URP and the effect of intervention in a model of this condition. The uninephrectomised STZ model allows the diabetic condition to precede the renal injury, but there can be non-specific nephrotoxicity associated with STZ administration which could potentially confound the renal profile.^{169,172} In contrast, in models of inheritable type II diabetes there is a period of pre-diabetes of variable length. Similar to the standalone STZ model the extent of glomerulosclerosis is typically mild; consequently uninephrectomy on a diabetic rat or mouse background may best represent the lesions of DN in a model with type II diabetes as strains tend to present with only mild glomerulosclerotic lesions during the natural disease course.^{159,385} It could be particularly interesting to study the effects of UT antagonism in the non-diabetic 5/6th SNx and a diabetic strain (with or without uninephrectomy) concurrently in order to compare the profiles and responses in these different chronic kidney diseases.

9.4 Conclusion

Prior to the current study there was little overlap between available *in vivo* data in pre-clinical models and clinical data describing the expression of UII, URP or UT in CKD. The results of the current work present a novel insight into the pattern of UII/URP and UT receptor expression over the course of CKD progression in the 5/6th SNx model. They show that UII system components are up-regulated from the earliest stages of the disease and that expression levels increase as renal function deteriorates towards end stage failure. The intervention study did not yield clear-cut evidence that UT antagonism can slow or prevent progression of CKD: more refined studies are necessary to establish definitively whether this is a potentially useful therapeutic approach. Nonetheless the results were encouraging and suggest that the role of UT-inhibition in CKD is worth pursuing.

References

1. Edwards, A., (2010) Modeling transport in the kidney: investigating function and dysfunction., *Am. J. Physiol. Renal Physiol.* **298** F475–F484.
2. Sturm, G., Kollerits, B., Neyer, U., Ritz, E. and Kronenberg, F., (2008) Uric acid as a risk factor for progression of non-diabetic chronic kidney disease? The Mild to Moderate Kidney Disease (MMKD) Study., *Exp. Gerontol.* **43** 347–52.
3. Bertram, J. F., Douglas-Denton, R. N., Diouf, B., Hughson, M. D. and Hoy, W. E., (2011) Human nephron number: Implications for health and disease, *Pediatr. Nephrol.* **26** 1529–1533.
4. Pavenstädt, H., Kriz, W. and Kretzler, M., (2003) Cell biology of the glomerular podocyte., *Physiol. Rev.* **83** 253–307.
5. Miner, J. H., (2012) The glomerular basement membrane., *Exp. Cell Res.* **318** 973–978.
6. Patrakka, J. and Tryggvason, K., (2010) Molecular make-up of the glomerular filtration barrier., *Biochem. Biophys. Res. Commun.* **396** 164–169.
7. Tryggvason, K. and Wartiovaara, J., (2005) How does the kidney filter plasma?, *Physiology* **20** 96–101.
8. Haraldsson, B., Nyström, J. and Deen, W. M., (2008) Properties of the glomerular barrier and mechanisms of proteinuria., *Physiol. Rev.* **88** 451–487.
9. Obeidat, M., Obeidat, M. and Ballermann, B. J., (2012) Glomerular endothelium: a porous sieve and formidable barrier., *Exp. Cell Res.* **318** 964–72.
10. Rostgaard, J. and Qvortrup, K., (1997) Electron microscopic demonstrations of filamentous molecular sieve plugs in capillary fenestrae., *Microvasc. Res.* **53** 1–13.
11. Hjalmarsson, C., Johansson, B. R. and Haraldsson, B., (2004) Electron microscopic evaluation of the endothelial surface layer of glomerular capillaries, *Microvasc. Res.* **67** 9–17.
12. Stan, R. V, Tse, D., Deharvengt, S. J., Smits, N. C., Xu, Y., Luciano, M. R., McGarry, C. L., Buitendijk, M., Nemani, K. V, Elgueta, R., Kobayashi, T., Shipman, S. L., Moodie, K. L., Daghljan, C. P., Ernst, P. A., Lee, H.-K., Suriawinata, A. A., Schned, A. R., Longnecker, D. S., Fiering, S. N., Noelle, R. J., Gimi, B., Shworak, N. W. and Carrière, C., (2012) The diaphragms of fenestrated endothelia: gatekeepers of vascular permeability and blood composition., *Dev. Cell* **23** 1203–18.
13. Ballermann, B. J. and Stan, R. V, (2007) Resolved: capillary endothelium is a major contributor to the glomerular filtration barrier., *J. Am. Soc. Nephrol.* **18** 2432–2438.

14. Byron, A., Randles, M. J., Humphries, J. D., Mironov, A., Hamidi, H., Harris, S., Mathieson, P. W., Saleem, M. a, Satchell, S. C., Zent, R., Humphries, M. J. and Lennon, R., (2014) Glomerular Cell Cross-Talk Influences Composition and Assembly of Extracellular Matrix., *J. Am. Soc. Nephrol.* 1–14.
15. Lennon, R., Randles, M. J. and Humphries, M. J., (2014) The Importance of Podocyte Adhesion for a Healthy Glomerulus, *Front. Endocrinol. (Lausanne)*. **5** 1–17.
16. Lennon, R., Byron, A., Humphries, J. D., Randles, M. J., Carisey, A., Murphy, S., Knight, D., Brenchley, P. E., Zent, R. and Humphries, M. J., (2014) Global Analysis Reveals the Complexity of the Human Glomerular Extracellular Matrix., *J. Am. Soc. Nephrol.* **25** 939–951.
17. Naito, I., Nomura, S., Inoue, S., Kagawa, M., Kawai, S., Gunshin, Y., Joh, K., Tsukidate, C., Sado, Y. and Osawa, G., (1997), *Normal distribution of collagen IV in renal basement membranes in Epstein's syndrome.*
18. Finne, K., Vethe, H., Skogstrand, T., Leh, S., Dahl, T. D., Tenstad, O., Berven, F. S., Reed, R. K. and Vikse, B. E., (2014) Proteomic analysis of formalin-fixed paraffin-embedded glomeruli suggests depletion of glomerular filtration barrier proteins in two-kidney, one-clip hypertensive rats, *Nephrol. Dial. Transplant.* **29** 2217–2227.
19. Rodin, S., Antonsson, L., Hovatta, O. and Tryggvason, K., (2014) Monolayer culturing and cloning of human pluripotent stem cells on laminin-521–based matrices under xeno-free and chemically defined conditions, *Nat. Protoc.* **9** 2354–2368.
20. Sarrazin, S., Lamanna, W. C. and Esko, J. D., (2011) Heparan sulfate proteoglycans., *Cold Spring Harb. Perspect. bBiology* **3** 1–33.
21. Hamano, Y., Grunkemeyer, J. a, Sudhakar, A., Zeisberg, M., Cosgrove, D., Morello, R., Lee, B., Sugimoto, H. and Kalluri, R., (2002) Determinants of vascular permeability in the kidney glomerulus., *J. Biol. Chem.* **277** 31154–62.
22. Ruotsalainen, V., Ljungberg, P., Wartiovaara, J., Lenkkeri, U., Kestilä, M., Jalanko, H., Holmberg, C. and Tryggvason, K., (1999) Nephrin is specifically located at the slit diaphragm of glomerular podocytes., *Proc. Natl. Acad. Sci. U. S. A.* **96** 7962–7.
23. Rask-Madsen, C. and King, G. L., (2010) Podocytes lose their footing, *Nat. Res.* **468** 42–44.
24. Reiser, J. and Sever, S., (2013) Podocyte biology and pathogenesis of kidney disease., *Annu. Rev. Med.* **64** 357–366.
25. Putaala, H., Soininen, R., Kilpeläinen, P., Wartiovaara, J. and Tryggvason, K., (2001) The murine nephrin gene is specifically expressed in kidney, brain and pancreas: inactivation of the gene leads to massive proteinuria and neonatal death., *Hum. Mol. Genet.* **10** 1–8.
26. Sands, J. M. and Layton, H. E., (2009) The Physiology of Urinary Concentration: An Update, *Semin. Nephrol.* **29** 178–195.

27. Miles, B. E., Paton, A. and De Wardener, H. E., (1954) Maximum urine concentration., *Br. Med. J.* **2** 901–905.
28. Delanaye, P., Radermecker, R. P., Rorive, M., Depas, G. and Krzesinski, J. M., (2005) Indexing glomerular filtration rate for body surface area in obese patients is misleading: concept and example., *Nephrol. Dial. Transplant.* **20** 2024–2028.
29. U.S. National Library of Medicine and National Institutes of Health, (2014), Glomerular filtration rate, *Medline Medical Encyclopedia*. Available at: <http://www.nlm.nih.gov/medlineplus/ency/article/007305.htm>. [Accessed: 14-Sep-2014].
30. Traynor, J., Mactier, R., Geddes, C. C. and Fox, J. G., (2006) How to measure renal function in clinical practice., *BMJ* **333** 733–737.
31. Sambataro, M., Thomaseth, K., Pacini, G., Robaudo, C., Carraro, A., Bruseghin, M., Brocco, E., Abaterusso, C., DeFerrari, G., Fioretto, P., Maioli, M., Tonolo, G. C., Crepaldi, G. and Nosadini, R., (1996) Plasma clearance rate of ⁵¹Cr-EDTA provides a precise and convenient technique for measurement of glomerular filtration rate in diabetic humans., *J. Am. Soc. Nephrol.* **7** 118–127.
32. De Santo, N. G., Anastasio, P., Cirillo, M., Santoro, D., Spitali, L., Mansi, L., Celentano, L., Capodicasa, D., Cirillo, E., Del Vecchio, E., Pascale, C. and Capasso, G., (1999) Measurement of Glomerular Filtration Rate by the ^{99m}Tc-DTPA Renogram Is Less Precise than Measured and Predicted Creatinine Clearance, *Nephron* **81** 136–140.
33. Levey, A. S. and Stevens, L., (2009) A new equation to estimate glomerular filtration rate, *Ann. Intern. Med.* **150** 604–612.
34. Reubi, F. C., (1953) Glomerular filtration rate, renal blood flow and blood viscosity during and after diabetic coma., *Circ. Res.* **1** 410–413.
35. Helal, I., Fick-Brosnahan, G. M., Reed-Gitomer, B. and Schrier, R. W., (2012) Glomerular hyperfiltration: definitions, mechanisms and clinical implications., *Nat. Rev. Nephrol.* **8** 293–300.
36. Coffman, T. M. and Crowley, S. D., (2008) Kidney in hypertension: guyton redux., *Hypertension* **51** 811–816.
37. Guyton, a C., (1991) Blood pressure control--special role of the kidneys and body fluids., *Science* **252** 1813–6.
38. Hilgers, K. F. and Mann, J. F. E., (2002) ACE inhibitors versus AT(1) receptor antagonists in patients with chronic renal disease., *J. Am. Soc. Nephrol.* **13** 1100–1108.
39. Li, M., Liu, K., Michalicek, J., Angus, J. a., Hunt, J. E., Dell'Italia, L. J., Feneley, M. P., Graham, R. M. and Husain, A., (2004) Involvement of chymase-mediated angiotensin II generation in blood pressure regulation, *J. Clin. Invest.* **114** 112–120.

40. Crowley, S. D. and Coffman, T. M., (2012) Recent advances involving the renin-angiotensin system, *Exp. Cell Res.* **318** 1049–1056.
41. Nguyen Dinh Cat, A. and Touyz, R. M., (2011) A new look at the renin-angiotensin system—Focusing on the vascular system, *Peptides* **32** 2141–2150.
42. Ferrão, F. M., (2014) Renin-angiotensin system in the kidney: What is new?, *World J. Nephrol.* **3** 64.
43. Santos, R. a S., Ferreira, A. J., Verano-Braga, T. and Bader, M., (2013) Angiotensin-converting enzyme 2, angiotensin-(1-7) and Mas: New players of the renin-angiotensin system, *J. Endocrinol.* **216**.
44. Kanaide, H., Ichiki, T., Nishimura, J. and Hirano, K., (2003) Cellular mechanism of vasoconstriction induced by angiotensin II: it remains to be determined., *Circ. Res.* **93** 1015–1017.
45. Dunn, F. L., Brennan, T. J., Nelson, A. E. and Robertson, G. L., (1973) The Role of Blood Osmolality and Volume, *J. Clin. Invest.* **52** 3212–3219.
46. Pecly, I. M. D., Genelhu, V. and Francischetti, E. A., (2006) Renal functional reserve in obesity hypertension., *Int. J. Clin. Pract.* **60** 1198–203.
47. Palatini, P., (2012) Glomerular hyperfiltration: a marker of early renal damage in pre-diabetes and pre-hypertension., *Nephrol. Dial. Transplant.* **27** 1708–1714.
48. Levey, A. S., Coresh, J., Balk, E., Kausz, A. T., Levin, A., Steffes, M. W., Hogg, R. J., Perrone, R. D., Lau, J. and Eknoyan, G., (2003) National Kidney Foundation practice guidelines for chronic kidney disease: evaluation, classification, and stratification, *Ann. Intern. Med.* **139** 137–149.
49. The National Collaborating Centre for Chronic Conditions, (2008), *Chronic kidney disease: national clinical guideline for early identification and management in adults in primary and secondary care* (Royal College of Physicians).
50. NHS Kidney Care, (2010), Kidney Disease: Key Facts and Figures. Available at: www.healthcheck.nhs.uk/document.php?o=81. [Accessed: 08-Sep-2014].
51. National Institute for Health and Care Excellence, (2014), Chronic kidney disease: early identification and management of chronic kidney disease in adults in primary and secondary care., *NICE clinical guideline 182*. Available at: guidance.nice.org.uk/cg182. [Accessed: 08-Sep-2014].
52. Levey, A. S., Atkins, R., Coresh, J., Cohen, E. P., Collins, A. J., Eckardt, K.-U., Nahas, M. E., Jaber, B. L., Jadoul, M., Levin, A., Powe, N. R., Rossert, J., Wheeler, D. C., Lameire, N. and Eknoyan, G., (2007) Chronic kidney disease as a global public health problem: approaches and initiatives - a position statement from Kidney Disease Improving Global Outcomes., *Kidney Int.* **72** 247–259.

53. World Health Organization, (2011) Burden: mortality , morbidity and risk factors, in *Global Status Report on Noncommunicable Diseases 2010*, ed. World Health Organization (WHO Press, Geneva), pp. 9–31.
54. Levey, A. S., Andreoli, S. P., DuBose, T., Provenzano, R. and Collins, A. J., (2007) Chronic kidney disease: common, harmful and treatable--World Kidney Day 2007., *Am. J. Nephrol.* **27** 108–112.
55. Stevens, P. E., O'Donoghue, D. J., de Lusignan, S., Van Vlymen, J., Klebe, B., Middleton, R., Hague, N., New, J. and Farmer, C. K. T., (2007) Chronic kidney disease management in the United Kingdom: NEOERICA project results., *Kidney Int.* **72** 92–99.
56. Nugent, R. a, Fathima, S. F., Feigl, A. B. and Chyung, D., (2011) The Burden of Chronic Kidney Disease on Developing Nations: A 21st Century Challenge in Global Health., *Nephron. Clin. Pract.* **118** c269–c277.
57. International Society for Nephrology and International Federation of Kidney Foundations, (2014), World Kidney Day. Available at: <http://www.worldkidneyday.org/>. [Accessed: 05-Sep-2014].
58. Merkin, S. S., Diez Roux, A. V, Coresh, J., Fried, L. F., Jackson, S. a and Powe, N. R., (2007) Individual and neighborhood socioeconomic status and progressive chronic kidney disease in an elderly population: The Cardiovascular Health Study., *Soc. Sci. Med.* **65** 809–21.
59. Patzer, R. E. and McClellan, W. M., (2012) Influence of race, ethnicity and socioeconomic status on kidney disease., *Nat. Rev. Nephrol.* **8** 533–41.
60. Merkin, S. S., Coresh, J., Diez Roux, A. V, Taylor, H. A. and Powe, N. R., (2005) Area socioeconomic status and progressive CKD: the Atherosclerosis Risk in Communities (ARIC) Study., *Am. J. Kidney Dis.* **46** 203–213.
61. Johnson, C. A., Levey, A. S., Coresh, J., Levin, A., Lau, J. and Eknoyan, G., (2004) Clinical practice guidelines for chronic kidney disease in adults: Part I. Definition, disease stages, evaluation, treatment, and risk factors., *Am. Fam. Physician* **70** 869–876.
62. National Kidney Foundation, (2014), About Chronic Kidney Disease. Available at: <http://www.kidney.org/kidneydisease/aboutckd>. [Accessed: 13-Sep-2014].
63. Levey, A. S. and Coresh, J., (2012) Chronic kidney disease., *Lancet* **379** 165–180.
64. Gilg, J., Rao, A. and Fogarty, D., (2013) UK Renal Registry 16th annual report: chapter 1 UK renal replacement therapy incidence in 2012: national and centre-specific analyses., *Nephron. Clin. Pract.* **125** 1–27.
65. National Institutes of Health and National Institute of Diabetes and Digestive and Kidney Diseases, (2012) An introduction to ESRD in the U.S., in *USRDS 2013 Annual Data Report: Atlas of Chronic Kidney Disease and End-Stage Renal Disease in the United States* pp. 154–168.

66. Biesenbach, G., (2001) Prognosis of Patients with Diabetic Nephropathy, in *Diabetic Nephropathy*, ed. C. Hasslacher (Wiley), pp. 297–304.
67. Hostetter, T. H., (2003) Prevention of the Development and Progression of Renal Disease, *J. Am. Soc. Nephrol.* **14** 144S–147.
68. American Diabetes Association, (2004) Nephropathy in Diabetes, *Diabetes Care* **27** S79–S83.
69. Marshall, S. M., (2004) Recent advances in diabetic nephropathy., *Postgrad. Med. J.* **80** 624–33.
70. National Kidney Foundation, (2012) KDOQI Clinical Practice Guideline for Diabetes and CKD: 2012 Update., *Am. J. Kidney Dis.* **60** 850–886.
71. Wolf, G., Chen, S. and Ziyadeh, F. N., (2005) From the periphery of the glomerular capillary wall toward the center of disease, *Diabetes* **54** 1626 – 1634.
72. Fornoni, A., (2010) Proteinuria, the Podocyte, and Insulin Resistance., *N. Engl. J. Med.* **363** 2068.
73. Laville, M. and Nazare, J., (2009) Diabetes, insulin resistance and sugars., *Obes. Rev.* **10 Suppl 1** 24–33.
74. Langin, D., (2001) Diabetes, insulin secretion, and the pancreatic beta-cell mitochondrion., *N. Engl. J. Med.* **345** 1772–1774.
75. Ruggerenti, P., Fassi, A., Ilieva, A. P., Bruno, S., Iliev, I. P., Brusegan, V., Rubis, N., Gherardi, G., Arnoldi, F. and Ganeva, M., (2004) Preventing microalbuminuria in type 2 diabetes, *N. Engl. J. Med.* **351** 1941–1951.
76. Heine, R. J., (1999) Diabetes in the next century: challenges and opportunities., *Neth. J. Med.* **55** 265–70.
77. Wild, S., Roglic, G., Green, A., Sicree, R. and King, H., (2004) Global prevalence of diabetes estimates for the year 2000 and projections for 2030, *Diabetes Care* **27** 1047–1053.
78. Danaei, G., Finucane, M. M., Lu, Y., Singh, G. M., Cowan, M. J., Paciorek, C. J., Lin, J. K., Farzadfar, F., Khang, Y.-H., Stevens, G. a, Rao, M., Ali, M. K., Riley, L. M., Robinson, C. a and Ezzati, M., (2011) National, regional, and global trends in fasting plasma glucose and diabetes prevalence since 1980: systematic analysis of health examination surveys and epidemiological studies with 370 country-years and 2·7 million participants., *Lancet* **378** 31–40.
79. Chilton, R., Wyatt, J., Nandish, S., Oliveros, R. and Lujan, M., (2011) Cardiovascular comorbidities of type 2 diabetes mellitus: defining the potential of glucagonlike peptide-1-based therapies., *Am. J. Med.* **124** S35–53.
80. Diabetes UK, (2014), Blood Glucose. Available at: <http://www.diabetes.org.uk/Guide-to-diabetes/Monitoring/Testing/#glucose>. [Accessed: 10-Sep-2014].

81. National Institute for Health and Care Excellence, (2011), Hypertension: Clinical management of primary hypertension in adults, *NICE clinical guideline* 127. Available at: <http://www.nice.org.uk/guidance/cg127>.
82. Whitworth, J. a, (2003) 2003 World Health Organization (WHO)/International Society of Hypertension (ISH) statement on management of hypertension., *J. Hypertens.* **21** 1983–92.
83. National High Blood Pressure Education Program, (2004) The seventh report of the Joint National Committee on prevention, detection, evaluation, and treatment of high blood pressure,.
84. American Heart Association, (2014), Understanding Blood Pressure Readings. Available at: http://www.heart.org/HEARTORG/Conditions/HighBloodPressure/AboutHighBloodPressure/Understanding-Blood-Pressure-Readings_UCM_301764_Article.jsp. [Accessed: 10-Sep-2014].
85. Kearney, P. M., Whelton, M., Reynolds, K., Muntner, P., Whelton, P. K. and He, J., (2005) Global burden of hypertension: analysis of worldwide data., *Lancet* **365** 217–223.
86. World Health Organization, (2014), Raised blood pressure. Available at: http://www.who.int/gho/ncd/risk_factors/blood_pressure_prevalence_text/en/#. [Accessed: 10-Sep-2014].
87. Chawla, L. S., (2011) Acute kidney injury leading to chronic kidney disease and long-term outcomes of acute kidney injury: the best opportunity to mitigate acute kidney injury?, *Contrib. Nephrol.* **174** 182–190.
88. Rifkin, D. E., Coca, S. G. and Kalantar-Zadeh, K., (2012) Does AKI truly lead to CKD?, *J. Am. Soc. Nephrol.* **23** 979–84.
89. Chawla, L. S. and Kimmel, P. L., (2012) Acute kidney injury and chronic kidney disease: an integrated clinical syndrome., *Kidney Int.* **82** 516–524.
90. Hsu, C., (2012) Yes, AKI truly leads to CKD., *J. Am. Soc. Nephrol.* **23** 967–9.
91. Chawla, L. S., Eggers, P. W., Star, R. a and Kimmel, P. L., (2014) Acute kidney injury and chronic kidney disease as interconnected syndromes., *N. Engl. J. Med.* **371** 58–66.
92. National Institutes of Health and U.S. National Library of Medicine, (2014), Acute kidney failure: MedlinePlus Medical Encyclopedia, *Medline Medical Encyclopedia*. Available at: <http://www.nlm.nih.gov/medlineplus/ency/article/000501.htm>. [Accessed: 13-Sep-2014].
93. Hilton, R., (2006) Acute renal failure., *BMJ* **333** 786–790.
94. Ishani, A., Xue, J. L., Himmelfarb, J., Eggers, P. W., Kimmel, P. L., Molitoris, B. a and Collins, A. J., (2009) Acute kidney injury increases risk of ESRD among elderly., *J. Am. Soc. Nephrol.* **20** 223–8.

95. Lo, L. J., Go, A. S., Chertow, G. M., McCulloch, C. E., Fan, D., Ordoñez, J. D. and Hsu, C., (2009) Dialysis-requiring acute renal failure increases the risk of progressive chronic kidney disease., *Kidney Int.* **76** 893–899.
96. Wald, R., Quinn, R. R., Luo, J., Li, P., Scales, D. C., Mamdani, M. M. and Ray, J. G., (2009) Chronic dialysis and death among survivors of acute kidney injury requiring dialysis., *JAMA* **302** 1179–85.
97. Bergström, J., Ahlberg, M. and Alvestrand, A., (1985) Influence of protein intake on renal hemodynamics and plasma hormone concentrations in normal subjects., *Acta Med. Scand.* **217** 189–96.
98. Hasslacher, C., (2001) Natural course of diabetic nephropathy, in *Diabetic Nephropathy* (Wiley Online Library), pp. 19–32.
99. Bilo, H. J. G., Ter Wee, P. M. and Gans, R. O. B., (2001) Pathogenesis of Diabetic Nephropathy: Haemodynamic Alterations, in *Diabetic Nephropathy*, ed. C. Hasslacher (Wiley Online Library), pp. 59–68.
100. Ritz, E. and Rychlik, I., (2001) Natural Course - the Size of the Problem, in *Diabetic Nephropathy* pp. 4–17.
101. Anderson, S. and Vora, J. P., (1995) Current concepts of renal hemodynamics in diabetes., *J. Diabetes Complications* **9** 304–307.
102. Goldin, A., Beckman, J. a, Schmidt, A. M. and Creager, M. a, (2006) Advanced glycation end products: sparking the development of diabetic vascular injury., *Circulation* **114** 597–605.
103. Mahajan, N. and Dhawan, V., (2013) Receptor for advanced glycation end products (RAGE) in vascular and inflammatory diseases, *Int. J. Cardiol.* **168** 1788–1794.
104. Xie, J., Méndez, J. D., Méndez-Valenzuela, V. and Aguilar-Hernández, M. M., (2013) Cellular signalling of the receptor for advanced glycation end products (RAGE), *Cell. Signal.* **25** 2185–2197.
105. Mott, J. D., Khalifah, R. G., Nagase, H., Shield, C. F., Hudson, J. K. and Hudson, B. G., (1997) Nonenzymatic glycation of type IV collagen and matrix metalloproteinase susceptibility., *Kidney Int.* **52** 1302–1312.
106. Melsom, T., Mathisen, U. D., Ingebretsen, O. C., Jenssen, T. G., Njølstad, I., Solbu, M. D., Toft, I. and Eriksen, B. O., (2011) Impaired fasting glucose is associated with renal hyperfiltration in the general population., *Diabetes Care* **34** 1546–1551.
107. Sun, F., Tao, Q. and Zhan, S., (2010) Metabolic syndrome and the development of chronic kidney disease among 118 924 non-diabetic Taiwanese in a retrospective cohort., *Nephrology (Carlton)*. **15** 84–92.
108. Brenner, B. M., Lawler, E. V and Mackenzie, H. S., (1996) The hyperfiltration theory: a paradigm shift in nephrology., *Kidney Int.* **49** 1774–1777.

109. Neuringer, J. and Brenner, B., (1992) Glomerular hypertension: cause and consequence of renal injury, *J. Hypertens.* **10** 91–97.
110. Anderson, S. E. and Brenner, B. M., (1986) The role of intraglomerular pressure in the initiation and progression of renal disease., *J. Hypertens.* **4** S236–8.
111. Kambham, N., Markowitz, G. S., Valeri, A. M., Lin, J. and D'Agati, V. D., (2001) Obesity-related glomerulopathy: an emerging epidemic., *Kidney Int.* **59** 1498–1509.
112. Darouich, S., Goucha, R., Jaafoura, M. H., Zekri, S., Ben Maiz, H. and Kheder, A., (2011) Clinicopathological characteristics of obesity-associated focal segmental glomerulosclerosis., *Ultrastruct. Pathol.* **35** 176–182.
113. Glasscock, R. J., (2011) The aging kidney: more pieces to the puzzle., *Mayo Clin. Proc.* **86** 271–272.
114. Ravera, M., Re, M., Deferrari, L., Vettoretti, S. and Deferrari, G., (2006) Importance of blood pressure control in chronic kidney disease., *J. Am. Soc. Nephrol.* **17** S98–S103.
115. Kato, S., Nazneen, A., Nakashima, Y., Razzaque, M. S., Nishino, T., Furusu, A., Yorioka, N. and Taguchi, T., (2009) Pathological influence of obesity on renal structural changes in chronic kidney disease., *Clin. Exp. Nephrol.* **13** 332–340.
116. Navar, L. G., (2009) Glomerular permeability: a never-ending saga., *Am. J. Physiol. Renal Physiol.* **296** F1266–F1268.
117. Badr, K. F., (2005) Filtration function in glomerulonephritis., *Kidney Int.* **68** 1905–1919.
118. Shankland, S., (2006) The podocyte's response to injury: role in proteinuria and glomerulosclerosis, *Kidney Int.* **69** 2131–2147.
119. Bendayan, M., (1985) Alteration in the distribution of type IV collagen in glomerular basal laminae in diabetic rats as revealed by immunocytochemistry and morphometrical approach., *Diabetologia* **28** 373–8.
120. Johnson, T. S., Haylor, J. L., Thomas, G. L., Fisher, M. and El Nahas, A. M., (2002) Matrix Metalloproteinases and Their Inhibitions in Experimental Renal Scarring, *Exp. Nephrol.* **10** 182–195.
121. Zelmanovitz, T., Gerchman, F., Balthazar, A. P., Thomazelli, F. C., Matos, J. D. and Canani, L. H., (2009) Diabetic nephropathy., *Diabetol. Metab. Syndr.* **1** 10.
122. Chen, Y. M., Kikkawa, Y. and Miner, J. H., (2011) A missense LAMB2 mutation causes congenital nephrotic syndrome by impairing laminin secretion., *J. Am. Soc. Nephrol.* **22** 849–858.

123. Chen, H.-M., Liu, Z.-H., Zeng, C.-H., Li, S.-J., Wang, Q.-W. and Li, L.-S., (2006) Podocyte lesions in patients with obesity-related glomerulopathy., *Am. J. Kidney Dis.* **48** 772–779.
124. Endlich, N., Kress, K. R., Reiser, J., Uttenweiler, D., Kriz, W., Mundel, P. and Endlich, K., (2001) Podocytes respond to mechanical stress in vitro., *J. Am. Soc. Nephrol.* **12** 413–22.
125. Srivastava, T., Celsi, G. E., Sharma, M., Dai, H., McCarthy, E. T., Ruiz, M., Cudmore, P. a, Alon, U. S., Sharma, R. and Savin, V. a, (2014) Fluid flow shear stress over podocytes is increased in the solitary kidney., *Nephrol. Dial. Transplant* **29** 65–72.
126. Ravid, M., (2009) Dual blockade of the renin-angiotensin system in diabetic nephropathy., *Diabetes Care* **32 Suppl 2** S410–S413.
127. Hunsicker, L. G., (2004) Emerging trends for prevention and treatment of diabetic nephropathy: blockade of the RAAS and BP control., *J. Manag. Care Pharm.* **10** S12–7.
128. Ritz, E., Schmieder, R. E. and Pollock, C. A., (2010) Renal protection in diabetes : lessons from ONTARGET ®, *Cardiovasc. Diabetol.* 1–10.
129. Nakamura, K., Yamagishi, S.-I., Nakamura, Y., Takenaka, K., Matsui, T., Jinnouchi, Y. and Imaizumi, T., (2005) Telmisartan inhibits expression of a receptor for advanced glycation end products (RAGE) in angiotensin-II-exposed endothelial cells and decreases serum levels of soluble RAGE in patients with essential hypertension., *Microvasc. Res.* **70** 137–41.
130. Yamagishi, S.-I., Takeuchi, M., Matsui, T., Nakamura, K., Imaizumi, T. and Inoue, H., (2005) Angiotensin II augments advanced glycation end product-induced pericyte apoptosis through RAGE overexpression., *FEBS Lett.* **579** 4265–4270.
131. Abbate, M., Zoja, C. and Remuzzi, G., (2006) How does proteinuria cause progressive renal damage?, *J. Am. Soc. Nephrol.* **17** 2974–2984.
132. Jafar, T. H., Stark, P. C., Schmid, C. H., Landa, M., Maschio, G., Marcantoni, C., de Jong, P. E., de Zeeuw, D., Shahinfar, S., Ruggenenti, P., Remuzzi, G. and Levey, A. S., (2001) Proteinuria as a modifiable risk factor for the progression of non-diabetic renal disease., *Kidney Int.* **60** 1131–1140.
133. Lawrence, T., (2009) The nuclear factor NF-kappa β pathway in inflammation., *Cold Spring Harb. Perspect. Biol.* **1** a001–a016.
134. Gomez-Garre, D., Largo, R., Tejera, N., Fortes, J., Manzarbeitia, F. and Egido, J., (2001) Activation of NF- B in Tubular Epithelial Cells of Rats With Intense Proteinuria : Role of Angiotensin II and Endothelin-1, *Hypertension* **37** 1171–1178.
135. Hirschberg, R. and Wang, S., (2005) Proteinuria and growth factors in the development of tubulointerstitial injury and scarring in kidney disease., *Curr. Opin. Nephrol. Hypertens.* **14** 43–52.

136. Witasap, a, Carrero, J. J., Heimbürger, O., Lindholm, B., Hammarqvist, F., Stenvinkel, P. and Nordfors, L., (2011) Increased expression of pro-inflammatory genes in abdominal subcutaneous fat in advanced chronic kidney disease patients., *J. Intern. Med.* **269** 410–9.
137. Colombo, P. C., Ganda, A., Lin, J., Onat, D., Harxhi, A., Iyasere, J. E., Uriel, N. and Cotter, G., (2012) Inflammatory activation: cardiac, renal, and cardio-renal interactions in patients with the cardiorenal syndrome., *Heart Fail. Rev.* **17** 177–90.
138. Cheung, W. W., Paik, K. H. and Mak, R. H., (2010) Inflammation and cachexia in chronic kidney disease., *Pediatr. Nephrol.* **25** 711–24.
139. Kato, S., Chmielewski, M., Honda, H., Pecoits-Filho, R., Matsuo, S., Yuzawa, Y., Tranaeus, A., Stenvinkel, P. and Lindholm, B., (2008) Aspects of immune dysfunction in end-stage renal disease., *Clin. J. Am. Soc. Nephrol.* **3** 1526–33.
140. Barreto, D. V, Barreto, F. C., Liabeuf, S., Temmar, M., Lemke, H.-D., Tribouilloy, C., Choukroun, G., Vanholder, R. and Massy, Z. a, (2010) Plasma interleukin-6 is independently associated with mortality in both hemodialysis and pre-dialysis patients with chronic kidney disease., *Kidney Int.* **77** 550–556.
141. National Institute for Health and Care Excellence, (2014), Type 2 diabetes: the management of type 2 diabetes, *NICE clinical guideline 87*. Available at: guidance.nice.org.uk/cg87.
142. Ruzicka, M., Burns, K. D., Culleton, B. and Tobe, S., (2007) Treatment of hypertension in patients with nondiabetic chronic kidney disease, *Can. J. Cardiol.* **23** 595–601.
143. Toto, R. D., (2005) Treatment of hypertension in chronic kidney disease., *Semin. Nephrol.* **25** 435–439.
144. National Kidney Foundation, (2012) KDIGO Clinical Practice Guideline for the Management of Blood Pressure in Chronic Kidney Disease, *Kidney Int. Supp*:**2** 337–414.
145. Parving, H.-H., Brenner, B. M., McMurray, J. J. V, de Zeeuw, D., Haffner, S. M., Solomon, S. D., Chaturvedi, N., Persson, F., Desai, A. S., Nicolaidis, M., Richard, A., Xiang, Z., Brunel, P. and Pfeffer, M. a, (2012) Cardiorenal end points in a trial of aliskiren for type 2 diabetes., *N. Engl. J. Med.* **367** 2204–13.
146. Ruggenenti, P., Perna, A., Loriga, G., Ganeva, M., Ene-Iordache, B., Turturro, M., Lesti, M., Perticucci, E., Chakarski, I. N., Leonardis, D., Garini, G., Sessa, A., Basile, C., Alpa, M., Scanziani, R., Sorba, G., Zoccali, C. and Remuzzi, G., (2005) Blood-pressure control for renoprotection in patients with non-diabetic chronic renal disease (REIN-2): multicentre, randomised controlled trial., *Lancet* **365** 939–946.
147. Peterson, J. C., Adler, S., Burkart, J. M., Greene, T., Hebert, L. A., Hunsicker, L. G., King, A. J., Klahr, S., Massry, S. G. and Seifter, J. L., (1995) Blood pressure control, proteinuria, and the progression of renal disease. The Modification of Diet in Renal Disease Study., *Ann. Intern. Med.* **123** 754–762.

148. Ruggenenti, P., Perna, A., Gherardi, G., Garini, G., Zoccali, C., Salvadori, M., Scolari, F., Schena, F. P. and Remuzzi, G., (1999) Renoprotective properties of ACE-inhibition in non-diabetic nephropathies with non-nephrotic proteinuria., *Lancet* **354** 359–364.
149. GISEN, (1997) Randomised placebo-controlled trial of effect of ramipril on decline in glomerular filtration rate and risk of terminal renal failure in proteinuric, non-diabetic nephropathy. The GISEN Group (Gruppo Italiano di Studi Epidemiologici in Nefrologia), *Lancet* **349** 1857–1863.
150. Lewis, E. J., Hunsicker, L. G., Bain, R. P. and Rohde, R., (1993) The effect of angiotensin-converting-enzyme inhibition on diabetic nephropathy. The Collaborative Study Group., *N. Engl. J. Med.* **329** 1456–62.
151. Björck, S., Mulec, H., Johnsen, S. a, Nordén, G. and Aurell, M., (1992) Renal protective effect of enalapril in diabetic nephropathy., *BMJ* **304** 339–343.
152. Kunz, R., Friedrich, C., Wolbers, M. and Mann, J. F. E., (2008) Meta-analysis: effect of monotherapy and combination therapy with inhibitors of the renin angiotensin system on proteinuria in renal disease., *Ann. Intern. Med.* **148** 30–48.
153. Berl, T., (2009) Review: renal protection by inhibition of the renin-angiotensin-aldosterone system., *J. Renin. Angiotensin. Aldosterone. Syst.* **10** 1–8.
154. Lewis, E. J., Hunsicker, L. G., Clarke, W. R., Berl, T., Pohl, M. A., Lewis, J. B., Ritz, E., Atkins, R. C., Rohde, R. and Raz, I., (2001) Renoprotective effect of the angiotensin-receptor antagonist irbesartan in patients with nephropathy due to type 2 diabetes, *N. Engl. J. Med.* **345** 851–860.
155. Khan, U. a, Garg, A. X., Parikh, C. R. and Coca, S. G., (2013) Prevention of chronic kidney disease and subsequent effect on mortality: a systematic review and meta-analysis., *PLoS One* **8** e71784.
156. Advani, A., (2014) The End of the Road for Dual Renin Angiotensin System Blockade in Diabetic Nephropathy: Which Way Now?, *Can. J. Diabetes* **38** 292–295.
157. Becker, G. J. and Hewitson, T. D., (2013) Animal models of chronic kidney disease: useful but not perfect., *Nephrol. Dial. Transplant.* **28** 2432–2438.
158. Susztak, K., Bitzer, M., Meyer, T. W. and Hostetter, T. H., (2008) Animal models of renal disease., *Kidney Int.* **73** 526–528.
159. Rees, D. a and Alcolado, J. C., (2005) Animal models of diabetes mellitus., *Diabet. Med.* **22** 359–370.
160. Gretz, N. and Strauch, M., (1988) Animal models to induce renal failure: a historical survey, in *Contributions to Nephrology: International Workshop on Animal Models for the Assessment of the Effects of Conservative Treatment in Chronic Renal Failure, Heidelberg, January 1987*, eds. N. Gretz and M. Strauch (Karger Publishers, Mannheim), pp. 1–8.

161. Bortell, R. and Yang, C., (2012) The BB rat as a model of human type 1 diabetes., *Methods Mol. Biol.* **933** 31–44.
162. Kawano, K., Hirashima, T., Mori, S. and Natori, T., (1994) OLETF (Otsuka Long-Evans Tokushima fatty) rat: A new NIDDM rat strain, *Diabetes Res. Clin. Pract.* **24**.
163. Chen, H., Charlat, O., Tartaglia, L. a, Woolf, E. a, Weng, X., Ellis, S. J., Lakey, N. D., Culpepper, J., Moore, K. J., Breitbart, R. E., Duyk, G. M., Tepper, R. I. and Morgenstern, J. P., (1996) Evidence that the diabetes gene encodes the leptin receptor: Identification of a mutatioan in the leptin receptor gene in db/db mice, *Cell* **84** 491–495.
164. Sharma, K., McCue, P. and Dunn, S. R. S. R., (2003) Diabetic kidney disease in the db/db mouse, *Am. J. Physiol. Renal Physiol.* **284** F1138.
165. Marsh, S. a, Powell, P. C., Agarwal, A., Italia, L. J. D. and Chatham, J. C., (2007) Cardiovascular dysfunction in Zucker obese and Zucker diabetic fatty rats: role of hydronephrosis, *Am. J. Physiol. Heart Circ. Physiol.* **0005** 292–298.
166. Baynes, J. and Murray, D. B., (2009) Cardiac and renal function are progressively impaired with aging in Zucker diabetic fatty type II diabetic rats., *Oxid. Med. Cell. Longev.* **2** 328–34.
167. The Jackson Laboratory, (2014), Jax mice database: BKS.Cg-Dock7m +/+ Leprdb/J. Available at: <http://jaxmice.jax.org/strain/000642.html>. [Accessed: 22-Nov-2014].
168. Belke, D. D. and Severson, D. L., (2012) Diabetes in mice with monogenic obesity: The db/db mouse and its use in the study of cardiac consequences, *Methods Mol. Biol.* **933** 47–57.
169. Breyer, M. D., Böttinger, E., Brosius, F. C., Coffman, T. M., Harris, R. C., Heilig, C. W. and Sharma, K., (2005) Mouse models of diabetic nephropathy., *J. Am. Soc. Nephrol.* **16** 27–45.
170. Chang, J. H. and Gurley, S. B., (2012) Assessment of diabetic nephropathy in the Akita mouse, *Methods Mol. Biol.* **933** 17–29.
171. Shiao, M. S., Liao, B. Y., Long, M. and Yu, H. T., (2008) Adaptive evolution of the insulin two-gene system in mouse, *Genetics* **178** 1683–1691.
172. Brosius, F. C., Alpers, C. E., Bottinger, E. P., Breyer, M. D., Coffman, T. M., Gurley, S. B., Harris, R. C., Kakoki, M., Kretzler, M., Leiter, E. H., Levi, M., McIndoe, R. a, Sharma, K., Smithies, O., Susztak, K., Takahashi, N. and Takahashi, T., (2009) Mouse models of diabetic nephropathy., *J. Am. Soc. Nephrol.* **20** 2503–2512.
173. Bradford, J. R., (1899) The results following partial Nephrectomy and the influence of the Kidney on Metabolism., *J. Physiol.* **23** 415–496.
174. Giacomini, K. M., Roberts, S. M. and Levy, G., (1981) Evaluation of methods for producing renal dysfunction in rats, *J. Pharm. Sci.* **70** 117–121.

175. Yang, H.-C., Zuo, Y. and Fogo, A. B., (2010) Models of chronic kidney disease, *Drug Discov. Today Dis. Model.* **7** 13–19.
176. Ma, L. J. and Fogo, A. B., (2003) Model of robust induction of glomerulosclerosis in mice: Importance of genetic background, *Kidney Int.* **64** 350–355.
177. Advani, A., Connelly, K. A., Yuen, D. A., Zhang, Y., Advani, S. L., Trogadis, J., Kabir, M. G., Shachar, E., Kuliszewski, M. A., Leong-Poi, H., Stewart, D. J. and Gilbert, R. E., (2011) Fluorescent microangiography is a novel and widely applicable technique for delineating the renal microvasculature., *PLoS One* **6** e24695.
178. Mori, N., Hirose, T., Nakayama, T., Ito, O., Kanazawa, M., Imai, Y., Kohzuki, M., Takahashi, K. and Totsune, K., (2009) Increased expression of urotensin II-related peptide and its receptor in kidney with hypertension or renal failure., *Peptides* **30** 400–408.
179. Gretz, N., Waldherr, R. and Strauch, M., (1993) The remnant kidney model, in *Experimental and Genetic Rat Models of Chronic Renal Failure*, eds. N. Gretz and M. Strauch (Karger Publishers), pp. 1–28.
180. Gretz, N., Meisinger, E. and Strauch, M., (1988) Partial nephrectomy and chronic renal failure: the “mature” rat model, in *Contributions to Nephrology: International Workshop on Animal Models for the Assessment of the Effects of Conservative Treatment in Chronic Renal Failure, Heidelberg, January 1987*, eds. N. Gretz and M. Strauch (Karger Publishers, Mannheim), pp. 46–55.
181. Kemp, W., Kompa, A., Phrommintikul, A., Herath, C., Zhiyuan, J., Angus, P., McLean, C., Roberts, S. and Krum, H., (2009) Urotensin II modulates hepatic fibrosis and portal hemodynamic alterations in rats., *Am. J. Physiol. Gastrointest. Liver Physiol.* **297** G762–767.
182. Totsune, K., Takahashi, K., Arihara, Z., Sone, M., Satoh, F., Ito, S., Kimura, Y., Sasano, H. and Murakami, O., (2001) Role of urotensin II in patients on dialysis, *Lancet* **358** 810–811.
183. Totsune, K., Takahashi, K., Arihara, Z., Sone, M., Murakami, O., Ito, S., Kikuya, M., Ohkubo, T., Hashimoto, J. and Imai, Y., (2004) Elevated plasma levels of immunoreactive urotensin II and its increased urinary excretion in patients with Type 2 diabetes mellitus: association with progress of diabetic nephropathy, *Peptides* **25** 1809–1814.
184. Zhang, Y.-G., Li, Y.-G., Liu, B.-G., Wei, R.-H., Wang, D.-M., Tan, X.-R., Bu, D.-F., Pang, Y.-Z. and Tang, C.-S., (2007) Urotensin II accelerates cardiac fibrosis and hypertrophy of rats induced by isoproterenol., *Acta Pharmacol. Sin.* **28** 36–43.
185. Choi, C. U., Park, C. G., Cha, D. R., Kim, S. H., Shin, S. Y., Kim, Y. K., Na, J. O., Kim, J. W., Lim, H. E., Kim, E. J., Rha, S., Seo, H. S. and Oh, D. J., (2010) Effects of Angiotensin II Type 2 Receptor on the Fibrosis of Diabetic Heart in the Otsuka Long-Evans Tokushima Fatty (OLETF) Rat, *J. Korean Hypertens.* **16** 19–29.

186. Bern, H. A., (1985) The Elusive Urophysis—Twenty-five Years in Pursuit of Caudal Neurohormones, *Integr. Comp. Biol.* **25** 763–770.
187. McCrohan, C. R., Lu, W., Brierley, M. J., Dow, L. and Balment, R. J., (2007) Fish caudal neurosecretory system: A model for the study of neuroendocrine secretion, *Gen. Comp. Endocrinol.* **153** 243–250.
188. Moore, G., Burford, G. and Lederis, K., (1975) Properties of urophysial proteins from the white sucker, CATOSTOMUS COMMERSONI*, *Mol. Cell. Endocrinol.* **3** 297–307.
189. Pearson, D., Shively, J. E., Clark, B. R., Geschwind, I. I., Barkley, M., Nishioka, R. S. and Bern, H. a, (1980) Urotensin II: a somatostatin-like peptide in the caudal neurosecretory system of fishes., *Proc. Natl. Acad. Sci. U. S. A.* **77** 5021–5024.
190. Zelnik, P. R. and Lederis, K., (1973) Chromatographic separation of urotensins., *Gen. Comp. Endocrinol.* **20** 392–400.
191. Conlon, J. M., Yano, K., Waugh, D. and Hazon, N., (1996) Distribution and molecular forms of urotensin II and its role in cardiovascular regulation in vertebrates., *J. Exp. Zool.* **275** 226–38.
192. Ohsako, S., Ishida, I., Ichikawa, T. and Deguchi, T., (1986) Cloning and sequence analysis of cDNAs encoding precursors of urotensin II-alpha and -gamma., *J. Neurosci.* **6** 2730–5.
193. Gibson, A., Bern, H. A., Ginsburg, M. and Botting, J. H., (1984) Neuropeptide-induced contraction and relaxation of the mouse anococcygeus muscle, *Proc. Natl. Acad. Sci.* **81** 625–629.
194. Gibson, A., (1987) Complex effects of Gillichthys urotensin II on rat aortic strips., *Br. J. Pharmacol.* **91** 205–212.
195. Conlon, J. M., (2008) Liberation of urotensin II from the teleost urophysis: an historical overview., *Peptides* **29** 651–7.
196. Coulouarn, Y., Lihrmann, I., Jegou, S., Anouar, Y., Tostivint, H., Beauvillain, J.-C., Conlon, J. M., Bern, H. A. and Vaudry, H., (1998) Cloning of the cDNA encoding the urotensin II precursor in frog and human reveals intense expression of the urotensin II gene in motoneurons of the spinal cord., *Proc. Natl. Acad. Sci. U. S. A.* **95** 15803–15808.
197. Vaudry, H., Do Rego, J.-C., Le Mevel, J.-C., Chatenet, D., Tostivint, H., Fournier, A., Tonon, M.-C., Pelletier, G., Conlon, J. M. and Leprince, J., (2010) Urotensin II, from fish to human., *Ann. N. Y. Acad. Sci.* **1200** 53–66.
198. Gibson, A., Wallace, P. and Bern, H. A., (1986) Cardiovascular effects of urotensin II in anesthetized and pithed rats., *Gen. Comp. Endocrinol.* **64** 435–9.
199. Itoh, H., McMaster, D. and Lederis, K., (1988) Functional receptors for fish neuropeptide urotensin II in major rat arteries., *Eur. J. Pharmacol.* **149** 61–66.

200. Sugo, T., Murakami, Y., Shimomura, Y., Harada, M., Abe, M., Ishibashi, Y., Kitada, C., Miyajima, N., Suzuki, N., Mori, M. and Fujino, M., (2003) Identification of urotensin II-related peptide as the urotensin II-immunoreactive molecule in the rat brain, *Biochem. Biophys. Res. Commun.* **310** 860–868.
201. Sugo, T. and Mori, M., (2008) Another ligand fishing for G protein-coupled receptor 14. Discovery of urotensin II-related peptide in the rat brain., *Peptides* **29** 809–12.
202. Chatenet, D., Dubessy, C., Leprince, J., Boullaran, C., Carlier, L., Ségalas-Milazzo, I., Guilhaudis, L., Oulyadi, H., Davoust, D., Scalbert, E., Pfeiffer, B., Renard, P., Tonon, M.-C., Lihmann, I., Pacaud, P. and Vaudry, H., (2004) Structure-activity relationships and structural conformation of a novel urotensin II-related peptide., *Peptides* **25** 1819–30.
203. Grieco, P., Carotenuto, A., Campiglia, P., Marinelli, L., Lama, T., Patacchini, R., Santicoli, P., Maggi, C. a, Rovero, P. and Novellino, E., (2005) Urotensin-II receptor ligands. From agonist to antagonist activity., *J. Med. Chem.* **48** 7290–7297.
204. Russell, F. D., Meyers, D., Galbraith, A. J., Bett, N., Toth, I., Kearns, P. and Molenaar, P., (2003) Elevated plasma levels of human urotensin-II immunoreactivity in congestive heart failure., *Am. J. Physiol. Heart Circ. Physiol.* **285** H1576–H1581.
205. Coulouarn, Y., Jégou, S. and Tostivint, H., (1999) Cloning, sequence analysis and tissue distribution of the mouse and rat urotensin II precursors, *FEBS Lett.* **457** 28–32.
206. Mori, M., Sugo, T., Abe, M., Shimomura, Y., Kurihara, M., Kitada, C., Kikuchi, K., Shintani, Y., Kurokawa, T., Onda, H., Nishimura, O. and Fujino, M., (1999) Urotensin II is the endogenous ligand of a G-protein-coupled orphan receptor, SENR (GPR14)., *Biochem. Biophys. Res. Commun.* **265** 123–129.
207. Ames, R. S., Sarau, H. M., Chambers, J. K., Willette, R. N., Aiyar, N. V., Romanic, A. M., Loudon, C. S., Foley, J. J., Sauermelch, C. F., Coatney, R. W., Ao, Z., Disa, J., Holmes, S. D., Stadel, J. M., Martin, J. D., Liu, W.-S., Glover, G. I., Wilson, S., McNulty, D. E., Ellis, C. E., Elshourbagy, N. A., Shabon, U., Trill, J. J., Hay, D. W. P., Ohlstein, E. H., Bergsma, D. J. and Douglas, S. A., (1999) Human urotensin-II is a potent vasoconstrictor and agonist for the orphan receptor GPR14., *Nature* **401** 282–286.
208. Chartrel, N., Leprince, J., Dujardin, C., Chatenet, D., Tollemer, H., Baroncini, M., Balment, R. J., Beauvillain, J.-C. and Vaudry, H., (2004) Biochemical characterization and immunohistochemical localization of urotensin II in the human brainstem and spinal cord., *J. Neurochem.* **91** 110–8.
209. Dubessy, C., Cartier, D., Lectez, B., Bucharles, C., Chartrel, N., Montero-Hadjadje, M., Bizet, P., Chatenet, D., Tostivint, H., Scalbert, E., Leprince, J., Vaudry, H., Jégou, S. and Lihmann, I., (2008) Characterization of urotensin II, distribution of urotensin II, urotensin II-related peptide and UT receptor mRNAs in mouse: evidence of urotensin II at the neuromuscular junction., *J. Neurochem.* **107** 361–74.

210. Russell, F. D., Kearns, P., Toth, I. and Molenaar, P., (2004) Urotensin-II-converting enzyme activity of furin and trypsin in human cells in vitro, *J. Pharmacol. Exp. Ther.* **310** 209.
211. Bilodeau, J., Désilets, A., McDuff, F.-O., St-Pierre, C., Barbar, E., Leduc, R. and Lavigne, P., (2011) Influence of Ca²⁺ and pH on the folding of the prourotesin II precursor., *FEBS Lett.* **585** 1910–1914.
212. Charles, C. J., Rademaker, M. T., Richards, A. M. and Yandle, T. G., (2005) Urotensin II: evidence for cardiac, hepatic and renal production., *Peptides* **26** 2211–4.
213. Ashton, N., (2006) Renal and vascular actions of urotensin II., *Kidney Int.* **70** 624–629.
214. Douglas, S. A., Dhanak, D. and Johns, D. G., (2004) From “gills to pills”: urotensin-II as a regulator of mammalian cardiorenal function., *Trends Pharmacol. Sci.* **25** 76–85.
215. Zoccali, C. and Mallamaci, F., (2008) Urotensin II: a cardiovascular and renal update., *Curr. Opin. Nephrol. Hypertens.* **17** 199.
216. Song, W., Abdel-Razik, A. E. S., Lu, W., Ao, Z., Johns, D. G., Douglas, S. A., Balment, R. J. and Ashton, N., (2006) Urotensin II and renal function in the rat., *Kidney Int.* **69** 1360–1368.
217. Matsushita, M., Shichiri, M., Imai, T., Iwashina, M., Tanaka, H., Takasu, N. and Hirata, Y., (2001) Co-expression of urotensin II and its receptor (GPR14) in human cardiovascular and renal tissues., *J. Hypertens.* **19** 2185–90.
218. Elshourbagy, N. A., Douglas, S. A., Shabon, U., Harrison, S. M., Duddy, G., Sechler, J. L., Ao, Z., Maleeff, B. E., Naselsky, D., Disa, J. and Aiyar, N. V., (2002) Molecular and pharmacological characterization of genes encoding urotensin-II peptides and their cognate G-protein-coupled receptors from the mouse and monkey., *Br. J. Clin. Pharmacol.* **136** 9–22.
219. Jani, P. P., Narayan, H. and Ng, L. L., (2013) The differential extraction and immunoluminometric assay of Urotensin II and Urotensin-related peptide in heart failure., *Peptides* **40** 72–6.
220. Nothacker, H. P., Wang, Z., McNeill, a M., Saito, Y., Merten, S., O'Dowd, B., Duckles, S. P. and Civelli, O., (1999) Identification of the natural ligand of an orphan G-protein-coupled receptor involved in the regulation of vasoconstriction., *Nat. Cell Biol.* **1** 383–5.
221. Douglas, S. A. and Ohlstein, E. H., (2000) Urotensin receptors, in *The IUPHAR Receptor Compendium of Receptor Characterization and Classification*, ed. D. Girdlestone (IUPHAR Media Ltd., London), pp. 365–372.
222. Lu, W., Abdel-Razik, A. E. S., Ashton, N. and Balment, R. J., (2008) Urotensin II: lessons from comparative studies for general endocrinology., *Gen. Comp. Endocrinol.* **157** 14–20.

223. Aiyar, N. V, Johns, D. G., Ao, Z., Disa, J., Behm, D. J., Foley, J. J., Buckley, P. T., Sarau, H. M., Van-der-Keyl, H. K., Elshourbagy, N. A. and Douglas, S. A., (2005) Cloning and pharmacological characterization of the cat urotensin-II receptor (UT)., *Biochem. Pharmacol.* **69** 1069–1079.
224. Larkin, M. A., Blackshields, G., Brown, N. P., Chenna, R., McGettigan, P. A., McWilliam, H., Valentin, F., Wallace, I. M., Wilm, A., Lopez, R., Thompson, J. D., Gibson, T. J. and Higgins, D. G., (2007) Clustal W and Clustal X version 2.0., *Bioinformatics* **23** 2947–2948.
225. McWilliam, H., Li, W., Uludag, M., Squizzato, S., Park, Y. M., Buso, N., Cowley, A. P. and Lopez, R., (2013) Analysis Tool Web Services from the EMBL-EBI., *Nucleic Acids Res.* **41** W597–600.
226. Reche, P., (2013), Sequence Identities and Similarities. Available at: <http://imed.med.ucm.es/Tools/sias.html>. [Accessed: 22-Nov-2014].
227. Boivin, S., Ségalas-Milazzo, I., Guilhaudis, L., Oulyadi, H., Fournier, A. and Davoust, D., (2008) Solution structure of urotensin-II receptor extracellular loop III and characterization of its interaction with urotensin-II., *Peptides* **29** 700–10.
228. Boivin, S., Guilhaudis, L., Milazzo, I., Oulyadi, H., Davoust, D. and Fournier, A., (2006) Characterization of urotensin-II receptor structural domains involved in the recognition of U-II, URP, and urantide., *Biochemistry* **45** 5993–6002.
229. Boucard, A. A., Sauvé, S. S., Guillemette, G., Escher, E. and Leduc, R., (2003) Photolabelling the rat urotensin II/GPR14 receptor identifies a ligand-binding site in the fourth transmembrane domain., *Biochem. J.* **370** 829 –838.
230. European Bioinformatics Institute, European Molecular Biology Laboratory and The Wellcome Trust, (2014), Ensemble Genome - Uts2r, *Ensembl* (release 78). Available at: http://dec2014.archive.ensembl.org/Rattus_norvegicus/Gene/Summary?db=core;g=ENSRNOG00000036669;r=10:109951008-109952168;t=ENSRNOT00000054926. [Accessed: 05-Mar-2015].
231. Tölle, M. and van der Giet, M., (2008) Cardioresnovascular effects of urotensin II and the relevance of the UT receptor., *Peptides* **29** 743–63.
232. Forty, E. J. and Ashton, N., (2012) Ontogeny of the renal urotensin II system in the rat., *Exp. Physiol.* **97** 785–795.
233. Langham, R. G., Kelly, D. J., Gow, R. M., Zhang, Y., Dowling, J. K., Thomson, N. M., Gilbert, R. E. and Gitbert, R. E., (2004) Increased expression of urotensin II and urotensin II receptor in human diabetic nephropathy, *Am. J. Kidney Dis.* **44** 826–831.
234. Leprince, J., Chatenet, D., Dubessy, C., Fournier, A., Pfeiffer, B., Scalbert, E., Renard, P., Pacaud, P., Oulyadi, H., Ségalas-Milazzo, I., Guilhaudis, L., Davoust, D., Tonon, M.-C. and Vaudry, H., (2008) Structure-activity relationships of urotensin II and URP., *Peptides* **29** 658–73.

235. Patacchini, R., Santicoli, P., Giuliani, S., Grieco, P., Novellino, E., Rovero, P. and Maggi, C. A., (2003) Urantide: an ultrapotent urotensin II antagonist peptide in the rat aorta., *Br. J. Pharmacol.* **140** 1155–1158.
236. Grieco, P., Carotenuto, A., Campiglia, P., Zampelli, E., Patacchini, R., Maggi, C. a., Novellino, E. and Rovero, P., (2002) A new, potent urotensin II receptor peptide agonist containing a Pen residue at the disulfide bridge, *J. Med. Chem.* **45** 4391–4394.
237. Douglas, S. A., (2003) Human urotensin-II as a novel cardiovascular target: “heart” of the matter or simply a fishy “tail”?, *Curr. Opin. Pharmacol.* **3** 159–167.
238. Labarrère, P., Chatenet, D., Leprince, J., Marionneau, C., Loirand, G., Tonon, M.-C., Dubessy, C., Scalbert, E., Pfeiffer, B., Renard, P., Calas, B., Pacaud, P. and Vaudry, H., (2003) Structure-activity relationships of human urotensin II and related analogues on rat aortic ring contraction., *J. Enzyme Inhib. Med. Chem.* **18** 77–88.
239. Proulx, C. D., Holleran, B. J., Lavigne, P., Escher, E., Guillemette, G. and Leduc, R., (2008) Biological properties and functional determinants of the urotensin II receptor, *Peptides* **29** 691–699.
240. Holleran, B. J., Beaulieu, M.-E., Proulx, C. D., Lavigne, P., Escher, E. and Leduc, R., (2007) Photolabelling the urotensin II receptor reveals distinct agonist- and partial-agonist-binding sites., *Biochem. J.* **402** 51–61.
241. Giebing, G., Tolle, M., Jürgensen, J., Eichhorst, J., Furkert, J., Beyermann, M., Neuschäfer-Rube, F., Rosenthal, W., Zidek, W., Van Der Giet, M. and Oksche, A., (2005) Arrestin-independent internalization and recycling of the urotensin receptor contribute to long-lasting urotensin II-mediated vasoconstriction, *Circ. Res.* **97** 707–715.
242. Song, W., McDonald, J., Camarda, V., Calo, G., Guerrini, R., Marzola, E., Thompson, J. P., Rowbotham, D. J. and Lambert, D. G., (2006) Cell and tissue responses of a range of Urotensin II analogs at cloned and native urotensin II receptors. Evidence for coupling promiscuity., *Naunyn. Schmiedebergs. Arch. Pharmacol.* **373** 148–57.
243. Opgaard, O. S., Nothacker, H.-P., Ehlert, F. J. and Krause, D. N., (2000) Human urotensin II mediates vasoconstriction via an increase in inositol phosphates, *Eur. J. Pharmacol.* **406** 265–271.
244. McDonald, J., Batuwangala, M. and Lambert, D. G., (2007) Role of urotensin II and its receptor in health and disease., *J. Anesth.* **21** 378–89.
245. Rodríguez-Moyano, M., Díaz, I., Dionisio, N., Zhang, X., Avila-Medina, J., Calderón-Sánchez, E., Trebak, M., Rosado, J. A., Ordóñez, A. and Smani, T., (2013) Urotensin-II promotes vascular smooth muscle cell proliferation through store-operated calcium entry and EGFR transactivation., *Cardiovasc. Res.* **100** 297–306.
246. Hilfiker, M. a, Zhang, D., Dowdell, S. E., Goodman, K. B., McAtee, J. J., Dodson, J. W., Viet, A. Q., Wang, G. Z., Sehon, C. A., Behm, D. J., Wu, Z.,

- Carballo, L. H., Douglas, S. A. and Neeb, M. J., (2008) Aminomethylpiperazines as selective urotensin antagonists., *Bioorg. Med. Chem. Lett.* **18** 4470–4473.
247. Flohr, S., Kurz, M., Kostenis, E., Brkovich, A., Fournier, A. and Klabunde, T., (2002) Identification of nonpeptidic urotensin II receptor antagonists by virtual screening based on a pharmacophore model derived from structure-activity relationships and nuclear magnetic resonance studies on urotensin II., *J. Med. Chem.* **45** 1799–805.
248. Grieco, P., Carotenuto, A., Campiglia, P., Gomez-Monterrey, I., Auriemma, L., Sala, M., Marcozzi, C., d'Emmanuele di Villa Bianca, R., Brancaccio, D., Rovero, P., Santicioli, P., Meini, S., Maggi, C. a and Novellino, E., (2009) New insight into the binding mode of peptide ligands at Urotensin-II receptor: structure-activity relationships study on P5U and urantide., *J. Med. Chem.* **52** 3927–40.
249. Camarda, V., Song, W., Marzola, E., Spagnol, M., Guerrini, R., Salvadori, S., Regoli, D., Thompson, J. P., Rowbotham, D. J., Behm, D. J., Douglas, S. A., Calo', G. and Lambert, D. G., (2004) Urantide mimics urotensin-II induced calcium release in cells expressing recombinant UT receptors., *Eur. J. Pharmacol.* **498** 83–86.
250. Behm, D. J., Stankus, G., Doe, C. P. A., Willette, R. N., Sarau, H. M., Foley, J. J., Schmidt, D. B., Nuthulaganti, P., Fornwald, J. A., Ames, R. S., Lambert, D. G., Calo', G., Camarda, V., Aiyar, N. V and Douglas, S. A., (2006) The peptidic urotensin-II receptor ligand GSK248451 possesses less intrinsic activity than the low-efficacy partial agonists SB-710411 and urantide in native mammalian tissues and recombinant cell systems., *Br. J. Pharmacol.* **148** 173–190.
251. Clozel, M., Binkert, C., Birker-Robaczewska, M., Boukhadra, C., Ding, S., Fischli, W., Hess, P., Mathys, B., Morrison, K., Müller, C. C., Müller, C. C., Naylor, O., Qiu, C., Rey, M., Scherz, M. W., Velker, J., Weller, T., Xi, J. and Ziltener, P., (2004) Pharmacology of the urotensin-II receptor antagonist palosuran (ACT-058362; 1-[2-(4-benzyl-4-hydroxy-piperidin-1-yl)-ethyl]-3-(2-methyl-quinolin-4-yl)-urea sulfate salt): first demonstration of a pathophysiological role of the urotensin System., *J. Pharmacol. Exp. Ther.* **311** 204–212.
252. Behm, D. J., McAtee, J. J., Dodson, J. W., Neeb, M. J., Fries, H. E., Evans, C. A., Hernandez, R. R., Hoffman, K. D., Harrison, S. M., Lai, J. M., Wu, C., Aiyar, N. V, Ohlstein, E. H. and Douglas, S. A., (2008) Palosuran inhibits binding to primate UT receptors in cell membranes but demonstrates differential activity in intact cells and vascular tissues., *Br. J. Pharmacol.* **155** 374–386.
253. Maryanoff, B. E. and Kinney, W. a, (2010) Urotensin-II receptor modulators as potential drugs., *J. Med. Chem.* **53** 2695–708.
254. Douglas, S. A., Sulpizio, A. C., Piercy, V., Sarau, H. M., Ames, R. S., Aiyar, N. V, Ohlstein, E. H. and Willette, R. N., (2000) Differential vasoconstrictor activity of human urotensin-II in vascular tissue isolated from the rat, mouse,

- dog, pig, marmoset and cynomolgus monkey., *Br. J. Pharmacol.* **131** 1262–1274.
255. Stirrat, A. and Gallagher, M., (2001) Potent vasodilator responses to human urotensin-II in human pulmonary and abdominal resistance arteries, *Am. J. Physiol. Heart Circ. Physiol.* **280** H925 – H928.
 256. Bottrill, F. E., Douglas, S. A., Hiley, C. R. and White, R., (2000) Human urotensin-II is an endothelium-dependent vasodilator in rat small arteries., *Br. J. Pharmacol.* **130** 1865–70.
 257. Camarda, V., Rizzi, A., Calò, G., Gendron, G., Perron, S. I., Kostenis, E., Zamboni, P., Mascoli, F. and Regoli, D., (2002) Effects of human urotensin II in isolated vessels of various species; comparison with other vasoactive agents., *Naunyn. Schmiedeberg's Arch. Pharmacol.* **365** 141–9.
 258. Cheung, B. M., Leung, R., Man, Y. B. and Wong, L. Y. F., (2004) Plasma concentration of urotensin II is raised in hypertension, *J. Hypertens.* **22** 1341–1344.
 259. Suguro, T., Watanabe, T., Ban, Y., Kodate, S., Misaki, A., Hirano, T., Miyazaki, A. and Adachi, M., (2007) Increased human urotensin II levels are correlated with carotid atherosclerosis in essential hypertension., *Am. J. Hypertens.* **20** 211–217.
 260. Suzuki, S., Wenyi, Z., Hirai, M., Hinokio, Y., Suzuki, C., Yamada, T., Yoshizumi, S., Suzuki, M., Tanizawa, Y., Matsutani, A. and Oka, Y., (2004) Genetic variations at urotensin II and urotensin II receptor genes and risk of type 2 diabetes mellitus in Japanese., *Peptides* **25** 1803–8.
 261. Okumus, S., Igci, Y. Z., Taskin, T., Oztuzcu, S., Gurler, B., Eslik, Z., Gogebakan, B., Coskun, E., Erbagci, I., Demiryurek, S., Cengiz, B. and Demiryurek, A. T., (2012) Association between Thr21Met and Ser89Asn polymorphisms of the urotensin-II (UTS2) gene, diabetes mellitus, and diabetic retinopathy., *Curr. Eye Res.* **37** 921–9.
 262. Ong, K. L., Wong, L. Y. F., Man, Y. B., Leung, R. Y. H., Song, Y.-Q., Lam, K. S. L. and Cheung, B. M. Y., (2006) Haplotypes in the urotensin II gene and urotensin II receptor gene are associated with insulin resistance and impaired glucose tolerance., *Peptides* **27** 1659–67.
 263. Ong, K. L., Wong, L. Y. F. and Cheung, B. M. Y., (2008) The role of urotensin II in the metabolic syndrome., *Peptides* **29** 859–67.
 264. Barrette, P.-O. and Schwertani, A. G., (2012) A closer look at the role of urotensin II in the metabolic syndrome., *Front. Endocrinol. (Lausanne)*. **3** 165.
 265. Watanabe, T., Suguro, T., Kanome, T., Sakamoto, Y.-I., Kodate, S., Hagiwara, T., Hongo, S., Hirano, T., Adachi, M. and Miyazaki, A., (2005) Human urotensin II accelerates foam cell formation in human monocyte-derived macrophages., *Hypertension* **46** 738–744.
 266. Hirose, T., Takahashi, K., Mori, N., Nakayama, T., Kikuya, M., Ohkubo, T., Kohzaki, M., Totsune, K. and Imai, Y., (2009) Increased expression of

urotensin II, urotensin II-related peptide and urotensin II receptor mRNAs in the cardiovascular organs of hypertensive rats: comparison with endothelin-1., *Peptides* **30** 1124–9.

267. Forty, E. J. and Ashton, N., (2013) The urotensin system is up-regulated in the pre-hypertensive spontaneously hypertensive rat., *PLoS One* **8** e83317.
268. Abdel-Razik, A. E. S., Balment, R. J. and Ashton, N., (2008) Enhanced renal sensitivity of the spontaneously hypertensive rat to urotensin II., *Am. J. Physiol. Renal Physiol.* **295** F1239–F1247.
269. Balat, A. and Büyükçelik, M., (2012) Urotensin-II: More Than a Mediator for Kidney., *Int. J. Nephrol.* **2012** 249790.
270. Lin, Y., Tsuchihashi, T., Matsumura, K., Abe, I. and Iida, M., (2003) Central cardiovascular action of urotensin II in conscious rats., *J. Hypertens.* **21** 159–65.
271. Watanabe, T., Kanome, T., Miyazaki, A. and Katagiri, T., (2006) Human urotensin II as a link between hypertension and coronary artery disease., *Hypertens. Res.* **29** 375–387.
272. Peng, H., Zhang, M., Cai, X., Olofindayo, J., Tan, A. and Zhang, Y., (2013) Association between human urotensin II and essential hypertension--a 1:1 matched case-control study., *PLoS One* **8** e81764.
273. Gruson, D., Rousseau, M. F., Ahn, S. A., van Linden, F. and Ketelslegers, J. M., (2006) Circulating urotensin II levels in moderate to severe congestive heart failure: its relations with myocardial function and well established neurohormonal markers., *Peptides* **27** 1527–31.
274. You, Z., Al Kindi, H., Abdul-Karim, A., Barrette, P.-O. and Schwertani, A., (2014) Blocking the urotensin II receptor pathway ameliorates the metabolic syndrome and improves cardiac function in obese mice., *FASEB J.* **28** 1210–20.
275. Gao, S., Oh, Y.-B., Shah, A., Park, W. H., Chung, M. J., Lee, Y.-H. and Kim, S. H., (2010) Urotensin II receptor antagonist attenuates monocrotaline-induced cardiac hypertrophy in rats., *Am. J. Physiol. Heart Circ. Physiol.* **299** H1782–H1789.
276. Bousette, N., Hu, F., Ohlstein, E. H., Dhanak, D., Douglas, S. A. and Giaid, A., (2006) Urotensin-II blockade with SB-611812 attenuates cardiac dysfunction in a rat model of coronary artery ligation., *J. Mol. Cell. Cardiol.* **41** 285–95.
277. Zhang, Y.-G., Hu, Y., Mao, Y., Wei, R.-H., Bao, S. and Wu, L., (2010) Transforming growth factor- β 1 involved in urotensin II-induced phenotypic differentiation of adventitial fibroblasts from rat aorta, *Chinese Med. J. ...* **123** 3634–3639.
278. Zhang, Y.-G., Li, J., Li, Y.-G. and Wei, R.-H., (2008) Urotensin II induces phenotypic differentiation, migration, and collagen synthesis of adventitial fibroblasts from rat aorta, *J. Hypertens.* **26** 1119.

279. Onan, D., Pipolo, L., Yang, E., Hannan, R. D. and Thomas, W. G., (2004) Urotensin II promotes hypertrophy of cardiac myocytes via mitogen-activated protein kinases., *Mol. Endocrinol.* **18** 2344–54.
280. Bousette, N., Patel, L., Douglas, S. A., Ohlstein, E. H. and Giaid, A., (2004) Increased expression of urotensin II and its cognate receptor GPR14 in atherosclerotic lesions of the human aorta., *Atherosclerosis* **176** 117–523.
281. Behm, D. J., Harrison, S. M., Ao, Z., Maniscalco, K., Pickering, S. J., Grau, E. V, Woods, T. N., Coatney, R. W., Doe, C. P. a, Willette, R. N., Johns, D. G. and Douglas, S. A., (2003) Deletion of the UT receptor gene results in the selective loss of urotensin-II contractile activity in aortae isolated from UT receptor knockout mice., *Br. J. Pharmacol.* **139** 464–472.
282. Papadopoulos, P., Bousette, N. and Giaid, A., (2008) Urotensin-II and cardiovascular remodeling., *Peptides* **29** 764–9.
283. Zhang, A. Y., Chen, Y.-F., Zhang, D. X., Yi, F.-X., Qi, J., Andrade-Gordon, P., de Garavilla, L., Li, P.-L. and Zou, A.-P., (2003) Urotensin II is a nitric oxide-dependent vasodilator and natriuretic peptide in the rat kidney, *Am. J. Physiol. Renal Physiol.* **285** F792.
284. Abdel-Razik, A. E. S., Forty, E. J., Balment, R. J. and Ashton, N., (2008) Renal haemodynamic and tubular actions of urotensin II in the rat., *J. Endocrinol.* **198** 617–624.
285. Soni, H. and Adebisi, A., (2013) Pressor and renal regional hemodynamic effects of urotensin II in neonatal pigs, *J. Endocrinol.* **217** 317–326.
286. Mosenkis, A., Kallem, R. R., Danoff, T. M., Aiyar, N. V, Bazeley, J. and Townsend, R. R., (2011) Renal impairment, hypertension and plasma urotensin II., *Nephrol. Dial. Transplant* **26** 609–614.
287. Zoccali, C., Mallamaci, F., Tripepi, G., Cutrupi, S., Pizzini, P. and Malatino, L., (2006) Urotensin II is an inverse predictor of incident cardiovascular events in end-stage renal disease., *Kidney Int.* **69** 1253–1258.
288. Ravani, P., Tripepi, G., Pecchini, P., Mallamaci, F., Malberti, F. and Zoccali, C., (2008) Urotensin II is an inverse predictor of death and fatal cardiovascular events in chronic kidney disease., *Kidney Int.* **73** 95–101.
289. Mallamaci, F., Cutrupi, S., Pizzini, P., Tripepi, G. and Zoccali, C., (2006) Urotensin II and biomarkers of endothelial activation and atherosclerosis in end-stage renal disease., *Am. J. Hypertens.* **19** 505–510.
290. Gruson, D., Rousseau, M. F., Ketelslegers, J.-M. and Hermans, M. P., (2010) Raised plasma urotensin II in type 2 diabetes patients is associated with the metabolic syndrome phenotype., *J. Clin. Hypertens. (Greenwich)*. **12** 653–60.
291. Jiang, Z., Michal, J. J., Tobey, D. J., Wang, Z., Macneil, M. D. and Magnuson, N. S., (2008) Comparative understanding of UTS2 and UTS2R genes for their involvement in type 2 diabetes mellitus., *Int. J. Biol. Sci.* **4** 96–102.

292. Sáez, M. E., Smani, T., Ramírez-Lorca, R., Díaz, I., Serrano-Ríos, M., Ruiz, A. and Ordoñez, A., (2011) Association Analysis of Urotensin II Gene (UTS2) and Flanking Regions with Biochemical Parameters Related to Insulin Resistance., *PLoS One* **6** e19327.
293. Wenyi, Z., Suzuki, S., Hirai, M., Hinokio, Y., Tanizawa, Y., Matsutani, a, Satoh, J. and Oka, Y., (2003) Role of urotensin II gene in genetic susceptibility to Type 2 diabetes mellitus in Japanese subjects., *Diabetologia* **46** 972–6.
294. Waldherr, R. and Gretz, N., (1988) Natural course and the development of histological lesions after 5/6 nephrectomy, in *Contributions to Nephrology: International Workshop on Animal Models for the Assessment of the Effects of Conservative Treatment in Chronic Renal Failure, Heidelberg, January 1987*, eds. N. Gretz and M. Strauch (Mannheim), pp. 64–72.
295. Boos, C. J. and Lip, G. Y. H., (2006) Urotensin and cardiovascular risk among patients with end-stage renal disease: fact or fiction?, *Am. J. Hypertens.* **19** 511–512.
296. Trebicka, J., Leifeld, L., Hennenberg, M., Biecker, E., Eckhardt, A., Fischer, N., Pröbsting, A. S., Clemens, C., Lammert, F., Sauerbruch, T. and Heller, J., (2008) Hemodynamic effects of urotensin II and its specific receptor antagonist palosuran in cirrhotic rats., *Hepatology* **47** 1264–76.
297. Clozel, M., Hess, P., Qiu, C., Ding, S. and Rey, M., (2006) The urotensin-II receptor antagonist palosuran improves pancreatic and renal function in diabetic rats., *J. Pharmacol. Exp. Ther.* **316** 1115–1121.
298. Sidharta, P. N., van Giersbergen, P. L. M. and Dingemanse, J., (2009) Pharmacokinetics and pharmacodynamics of the urotensin-II receptor antagonist palosuran in healthy male subjects., *J. Clin. Pharmacol.* **49** 1168–75.
299. Vogt, L., Chiurchiu, C., Chadha-Boreham, H., Danaietash, P., Dingemanse, J., Hadjadj, S., Krum, H., Navis, G., Neuhart, E. and Parvanova, A. I., (2010) Effect of the Urotensin Receptor Antagonist Palosuran in Hypertensive Patients With Type 2 Diabetic Nephropathy, *Hypertension* **55** 1206–1209.
300. Sidharta, P. N., Wagner, F. D., Bohnemeier, H., Jungnik, A., Halabi, A., Krähenbühl, S., Chadha-Boreham, H. and Dingemanse, J., (2006) Pharmacodynamics and pharmacokinetics of the urotensin II receptor antagonist palosuran in macroalbuminuric, diabetic patients., *Clin. Pharmacol. Ther.* **80** 246–256.
301. Gretz, N., Meisinger, E., Waldherr, R. and Strauch, M., (1988) Acute renal failure after 5/6 nephrectomy: histological and functional changes, in *Contributions to Nephrology: International Workshop on Animal Models for the Assessment of the Effects of Conservative Treatment in Chronic Renal Failure, Heidelberg, January 1987*, eds. N. Gretz and M. Strauch (Karger Publishers, Mannheim), pp. 56–63.
302. Rakowski, E., Hassan, G. S., Dhanak, D., Ohlstein, E. H., Douglas, S. A. and Gaiad, A., (2005) A role for urotensin II in restenosis following balloon

angioplasty: use of a selective UT receptor blocker., *J. Mol. Cell. Cardiol.* **39** 785–91.

303. Kurien, B. T., Everds, N. E. and Scofield, R. H., (2004) Experimental animal urine collection: a review., *Lab. Anim.* **38** 333–61.
304. Johnson-Delaney, C., (2008), *Exotic Companion Medicine Handbook for Veterinarians* (Zoological Education Network).
305. Ropero-Miller, J. D., Paget-Wilkes, H., Doering, P. L. and Goldberger, B. A., (2000) Effect of oral creatine supplementation on random urine creatinine, pH, and specific gravity measurements, *Clin. Chem.* **46** 295–297.
306. Forty, E. J., Role of urotensin II in the developing kidney during the onset of hypertension (2011).
307. Qiagen, (2014), GeneGlobe Specification for Rn_Uts2r_1_SG QuantiTect Primer Assay (QT01082690). Available at: <http://www.qiagen.com/products/catalog/assay-technologies/real-time-pcr-and-rt-pcr-reagents/quantitect-primer-assays?catno=QT01082690#geneglobe>. [Accessed: 15-Jul-2014].
308. Qiagen, (2014), GeneGlobe Specification for Rn_Uts2b_1_SG QuantiTect Primer Assay (QT00438767). Available at: <http://www.qiagen.com/products/catalog/assay-technologies/real-time-pcr-and-rt-pcr-reagents/quantitect-primer-assays?catno=QT00438767#geneglobe>. [Accessed: 15-Jul-2014].
309. Qiagen, (2010) Effects of low A260/A230 ratios in RNA preparations on downstream applications, *Qiagen Newsl.* **15** A7–8.
310. Cicinnati, V. R., Shen, Q., Sotiropoulos, G. C., Radtke, A., Gerken, G. and Beckebaum, S., (2008) Validation of putative reference genes for gene expression studies in human hepatocellular carcinoma using real-time quantitative RT-PCR., *BMC Cancer* **8** 350.
311. Pfaffl, M. W., (2001) A new mathematical model for relative quantification in real-time RT-PCR., *Nucleic Acids Res.* **29** e45.
312. Pfaffl, M. W., (2004) Quantification strategies in real-time PCR, in *A-Z of Quantitative PCR*, ed. S. a Bustin pp. 87–112.
313. Johnson, C. A., Levey, A. S., Coresh, J., Levin, A., Lau, J. and Eknoyan, G., (2004) Clinical practice guidelines for chronic kidney disease in adults: Part II. Glomerular filtration rate, proteinuria, and other markers., *Am. Fam. Physician* **70** 1091–7.
314. Oldroyd, S. D., Miyamoto, Y., Moir, A., Johnson, T. S., El Nahas, A. M. and Haylor, J. L., (2006) An IGF-I antagonist does not inhibit renal fibrosis in the rat following subtotal nephrectomy., *Am. J. Physiol. Ren. Physiol.* **290** F695–F702.

315. Nutter, F., Khwaja, A. and Haylor, J. L., (2012) Seliciclib inhibits renal hypertrophy but not fibrosis in the rat following subtotal nephrectomy., *Nephron. Exp. Nephrol.* **122** 114–22.
316. Eliahou, H. E., Cohen, D., Herzog, D., Shechter, P., Serban, I., Kapuler, S., Schiby, G. and Gavendo, S., (1988) The control of hypertension and its effect on renal function in rat remnant kidney., *Nephrol. Dial. Transplant* **3** 38–44.
317. Charles River, (2014), *Charles River research models and services*.
318. Harlan, (2008), Sprague Dawley® Outbred Rat. Available at: http://www.harlan.com/products_and_services/research_models_and_services/research_models/sprague_dawley_outbred_rat.hi.
319. Charles River, (2014), Sprague Dawley® Rat, *Sprague Dawley Rat*. Available at: <http://www.criver.com/products-services/basic-research/find-a-model/sprague-dawley-rat>.
320. Alemaan, C. L., Mas, R. M., Rodeiro, I., Noa, M., Hernandez, C., Menendez, R. and Gamez, R., (1998) Reference database of the main physiological parameters in Sprague-Dawley rats from 6 to 32 months, *Lab. Anim.* **32** 457–466.
321. Onyeausi, B. I., Adeniyi, A. A., Onyeausi, C. G., Ayo, J. O. and Ibe, C. S., (2009) A Study of the Kidney of the Wistar Rat in Northern / Guinea Savannah Zone: the Morphometric Aspect, *Pakistan J. Nutr.* **8** 1040–1042.
322. Kanerva, R. L., Lefever, F. R. and Alden, C. L., (1983) Comparison of Fresh and Fixed Organ Weights of Rats, *Toxicol. Pathol.* **11** 129–131.
323. Griffin, K. and Picken, M., (2000) Functional and structural correlates of glomerulosclerosis after renal mass reduction in the rat, *J. Am. Soc. Nephrol.* 497–506.
324. Feld, L. G., Van Liew, J. B., Galaske, R. G. and Boylan, J. W., (1977) Selectivity of renal injury and proteinuria in the spontaneously hypertensive rat., *Kidney Int.* **12** 332–343.
325. Yin, F. C., Spurgeon, H. A., Rakusan, K., Weisfeldt, M. L. and Lakatta, E. G., (1982) Use of tibial length to quantify cardiac hypertrophy: application in the aging rat., *Am. J. Physiol.* **243** H941–H947.
326. Lu, M.-H., Chao, C.-F., Chin, Y.-H., Yu, K.-R. and Pai, L., (1998) The correlation of blood pressure, age and endothelin-1 binding sites in aortic smooth muscle cells of rats., *Jpn. Circ. J.* **62** 532–6.
327. D'Angelo, G., Elmarakby, A. A., Pollock, D. M. and Stepp, D. W., (2005) Fructose feeding increases insulin resistance but not blood pressure in Sprague-Dawley rats., *Hypertension* **46** 806–811.
328. Griffin, K. A., Picken, M. and Bidani, A. K., (1994) Method of renal mass reduction is a critical modulator of subsequent hypertension and glomerular injury., *J. Am. Soc. Nephrol.* **4** 2023–31.

329. Lemmer, B., Mattes, A., Bohm, M. and Ganten, D., (1993) Circadian blood pressure variation in transgenic hypertensive rats, *Hypertension* **22** 97–101.
330. Smithies, O., (2003) Why the kidney glomerulus does not clog: a gel permeation/diffusion hypothesis of renal function., *Proc. Natl. Acad. Sci. U. S. A.* **100** 4108–13.
331. Deen, W. M., (2006) Cellular contributions to glomerular size-selectivity., *Kidney Int.* **69** 1295–1297.
332. Sapan, C. V, Lundblad, R. L. and Price, N. C., (1999) Colorimetric protein assay techniques., *Biotechnol. Appl. Biochem.* **29 (Pt 2)** 99–108.
333. Noble, J. E. and Bailey, M. J. a, (2009), *Quantitation of protein.*, 1st ed. (Elsevier Inc.).
334. Moody, W. E., Chue, C. D., Inston, N. G., Edwards, N. C., Steeds, R. P., Ferro, C. J. and Townend, J. N., (2012) Understanding the effects of chronic kidney disease on cardiovascular risk: are there lessons to be learnt from healthy kidney donors?, *J. Hum. Hypertens.* **26** 141–148.
335. Chavan, V. U., Sayyed, A. K., Durgawale, P. P., Sontakke, A. V and Nilakhe, S. D., (2011) Practical Aspects of Calculation, Expression and Interpretation Of Urine Albumin Measurement, *Natl. J. Integr. Res. Med.* **2** 29 – 34.
336. So, B. I., Song, Y. S., Fang, C. H., Park, J. Y., Lee, Y., Shin, J. H., Kim, H. and Kim, K. S., (2013) G-CSF Prevents Progression of Diabetic Nephropathy in Rat, *PLoS One* **8** 1–10.
337. Han, S.-Y., So, G.-A., Jee, Y.-H., Han, K.-H., Kang, Y.-S., Kim, H.-K., Kang, S.-W., Han, D.-S., Han, J.-Y. and Cha, D.-R., (2004) Effect of retinoic acid in experimental diabetic nephropathy., *Immunol. Cell Biol.* **82** 568–76.
338. Fu, J., Li, Y., Wang, L., Gao, B., Zhang, N. and Ji, Q., (2009) Paeoniflorin prevents diabetic nephropathy in rats., *Comp. Med.* **59** 557–566.
339. Sung, J. K., Koh, J. H., Lee, M. Y., Kim, B. H., Nam, S. M., Kim, J. H., Yoo, J. H., Kim, S. H., Hong, S. W., Lee, E. Y., Choi, R. and Chung, C. H., (2010) Aldose reductase inhibitor ameliorates renal vascular endothelial growth factor expression in streptozotocin-induced diabetic rats, *Yonsei Med. J.* **51** 385–391.
340. Roy, A., Neuhaus, O. and Harmison, C., (1966) Preparation and characterization of a sex-dependent rat urinary protein☆, *Biochim. Biophys. Acta - Gen. Subj.* **127** 72–81.
341. McCarthy, F. P., Drewlo, S., Kingdom, J., Johns, E. J., Walsh, S. K. and Kenny, L. C., (2011) Peroxisome proliferator-activated receptor-γ as a potential therapeutic target in the treatment of preeclampsia, *Hypertension* **58** 280–286.
342. Ahmed, A. K., Haylor, J. L., El Nahas, A. M. and Johnson, T. S., (2007) Localization of matrix metalloproteinases and their inhibitors in experimental progressive kidney scarring., *Kidney Int.* **71** 755–763.

343. The National Kidney Disease Education Program and National Institutes of Health, (2010), Urine Albumin-to-Creatinine Ratio (UACR), *NIH Publications*. Available at: nkdep.nih.gov/resources/quick-reference-uacr-gfr-508.pdf. [Accessed: 05-Jun-2011].
344. Roemer, I., Vogel, T., Otto, A., Fichtner, I. and Klose, J., (2001) Proteins of rat serum, urine, and cerebrospinal fluid: VI. Further protein identifications and interstrain comparison, *Electrophoresis* **22** 3043–3052.
345. Remuzzi, A., Puntorieri, S., Alfano, M., Macconi, D., Abbate, M., Bertani, T. and Remuzzi, G., (1992) [Abstract] Pathophysiologic implications of proteinuria in a rat model of progressive glomerular injury., *Lab. Invest.* **67** 572–579.
346. Zhu, D., Kim, Y., Steffes, M. W., Groppoli, T. J., Butkowski, R. J. and Mauer, S. M., (1994) Glomerular distribution of type IV collagen in diabetes by high resolution quantitative immunochemistry., *Kidney Int.* **45** 425–433.
347. Dalla Vestra, M., (2003) Diabetic nephropathy: renal structural studies in type 1 and type 2 diabetic patients, *Int. Congr. Ser.* **1253** 163–169.
348. Yard, B. A., van Det, N. F. and van der Woude, F. J., (2001) Pathogenesis of Diabetic Nephropathy: Biochemical and Functional Alterations of Glomerular Basement Membrane and Mesangium, in *Diabetic Nephropathy* (Wiley Online Library), pp. 39–52.
349. Schetz, M., (2009) Cardiorenal syndrome., *F1000 Med. Rep.* **1** 1–5.
350. Weaver, D. J., Kimball, T. R., Koury, P. R. and Mitsniefes, M. M., (2009) Cardiac output and associated left ventricular hypertrophy in pediatric chronic kidney disease., *Pediatr. Nephrol.* **24** 565–70.
351. Kriz, W., Hahnel, B., Hosser, H., Rosener, S. and Waldherr, R., (2014) Structural Analysis of How Podocytes Detach from the Glomerular Basement Membrane Under Hypertrophic Stress, *Front. Endocrinol. (Lausanne)*. **5** 1–10.
352. Bakris, G. L., (2005) Protecting renal function in the hypertensive patient: clinical guidelines., *Am. J. Hypertens.* **18** 112S–119S.
353. Vlassara, H., Striker, L. J., Teichberg, S., Fuh, H., Li, Y. M. and Steffes, M., (1994) Advanced glycation end products induce glomerular sclerosis and albuminuria in normal rats., *Proc. Natl. Acad. Sci. U. S. A.* **91** 11704–11708.
354. Hewitson, T. D., (2012) Fibrosis in the kidney: is a problem shared a problem halved?, *Fibrogenesis Tissue Repair* **5** S14.
355. Hoy, W. E., Hughson, M. D., Bertram, J. F., Douglas-Denton, R. and Amann, K., (2005) Nephron number, hypertension, renal disease, and renal failure., *J. Am. Soc. Nephrol.* **16** 2557–2564.
356. Bousette, N., Pottinger, J., Ramli, W., Ohlstein, E. H., Dhanak, D., Douglas, S. A. and Giaid, A., (2006) Urotensin-II receptor blockade with SB-611812 attenuates cardiac remodeling in experimental ischemic heart disease., *Peptides* **27** 2919–2926.

357. Dai, H., He, T., Li, X., Xu, W. and Ge, Z., (2010) Urotensin-2 promotes collagen synthesis via ERK1/2-dependent and ERK1/2-independent TGF- β 1 in neonatal cardiac fibroblasts, *Cell Biol. Int.* **35** 93–98.
358. Karalliedde, J. and Viberti, G., (2010) Proteinuria in diabetes: bystander or pathway to cardiorenal disease?, *J. Am. Soc. Nephrol.* **21** 2020–7.
359. European Bioinformatics Institute, European Molecular Biology Laboratory and The Wellcome Trust, (2014), Ensembl Genome - Uts2, *Ensembl* (release 78). Available at: http://dec2014.archive.ensembl.org/Rattus_norvegicus/Gene/Summary?db=core;g=ENSRNOG00000018393;r=5:171655843-171661230;t=ENSRNOT00000024798. [Accessed: 05-Mar-2015].
360. European Bioinformatics Institute, European Molecular Biology Laboratory and The Wellcome Trust, (2014), Ensembl Genome - Uts2b, *Ensembl* (release 78). Available at: http://dec2014.archive.ensembl.org/Rattus_norvegicus/Gene/Summary?db=core;g=ENSRNOG00000038512;r=11:83876035-83890793;t=ENSRNOT00000042650. [Accessed: 05-Mar-2015].
361. Ambion, (2014), RNAlater®-ICE tissue transition solution user guide. Available at: https://tools.lifetechnologies.com/content/sfs/manuals/cms_057306.pdf. [Accessed: 01-May-2014].
362. Luebbehusen, H., (2004), The Significance of the 260/230 Ratio in Determining Nucleic Acid Purity, *Baylor College of Medicine*. Available at: <https://www.bcm.edu/mcfweb/?PMID=3100>. [Accessed: 03-Mar-2015].
363. Qiagen, (2013), Safety data sheet - Buffer RLT Plus. Available at: <http://www.qiagen.com/gb/support/qa-qc-safety-data/safety-data-sheets?MSDSCountryID=GB&CatNo=1053393>. [Accessed: 03-Mar-2015].
364. Taylor, S., Wakem, M., Dijkman, G., Alsarraj, M. and Nguyen, M., (2010) A practical approach to RT-qPCR-Publishing data that conform to the MIQE guidelines., *Methods* **50** S1–5.
365. Bustin, S. a, Benes, V., Garson, J. a, Hellemans, J., Huggett, J., Kubista, M., Mueller, R., Nolan, T., Pfaffl, M. W., Shipley, G. L., Vandesompele, J. and Wittwer, C. T., (2009) The MIQE guidelines: minimum information for publication of quantitative real-time PCR experiments., *Clin. Chem.* **55** 611–622.
366. Qiagen, (2014), GeneGlobe Specification for Rn_Uts2_1_SG QuantiTect Primer Assay (QT00193018). Available at: <http://www.qiagen.com/products/catalog/assay-technologies/real-time-pcr-and-rt-pcr-reagents/quantitect-primer-assays?catno=QT00193018#geneglobe>. [Accessed: 15-Jul-2014].
367. Qiagen, (2014), GeneGlobe Specification for Rn_Ywhaz_3_SG QuantiTect Primer Assay (QT02382184). Available at: <http://www.qiagen.com/products/catalog/assay-technologies/real-time-pcr-and-rt-pcr-reagents/quantitect-primer-assays?catno=QT02382184#geneglobe>. [Accessed: 15-Jul-2014].

368. Solanky, N., Requena Jimenez, A., D'Souza, S. W., Sibley, C. P. and Glazier, J. D., (2010) Expression of folate transporters in human placenta and implications for homocysteine metabolism, *Placenta* **31** 134–143.
369. Bagés, S., Estany, J., Tor, M. and Pena, R. N., (2015) Investigating reference genes for quantitative real-time PCR analysis across four chicken tissues, *Gene* **561** 82–87.
370. Park, S.-J., Kwon, S. G., Hwang, J. H., Park, D. H., Kim, T. W. and Kim, C. W., (2015) Selection of appropriate reference genes for RT-qPCR analysis in Berkshire, Duroc, Landrace, and Yorkshire pigs, *Gene* **558** 152–158.
371. Kim, H. J., Na, J. I., Min, B. W., Na, J. Y., Lee, K. H., Lee, J. H., Lee, Y. J., Kim, H. S. and Park, J. T., (2014) Evaluation of protein expression in housekeeping genes across multiple tissues in rats, *Korean J. Pathol.* **48** 193–200.
372. European Bioinformatics Institute, European Molecular Biology Laboratory and The Wellcome Trust, (2014), Ensembl Genome - Ywhaz, *Ensembl* (release 78). Available at: http://dec2014.archive.ensembl.org/Rattus_norvegicus/Gene/Summary?db=core;g=ENSRNOG00000008195;r=7:75721286-75743714;t=ENSRNOT000000035628. [Accessed: 05-Mar-2015].
373. Tal, M., Ammar, D. A., Karpuj, M., Krizhanovsky, V., Naim, M. and Thompson, D. A., (1995) A novel putative neuropeptide receptor expressed in neural tissue, including sensory epithelia., *Biochem. Biophys. Res. Commun.* **209** 752–759.
374. Tuller, T., Waldman, Y. Y., Kupiec, M. and Ruppin, E., (2010) Translation efficiency is determined by both codon bias and folding energy., *Proc. Natl. Acad. Sci. U. S. A.* **107** 3645–3650.
375. Maier, T., Güell, M. and Serrano, L., (2009) Correlation of mRNA and protein in complex biological samples, *FEBS Lett.* **583** 3966–3973.
376. Vogel, C. and Marcotte, E. M., (2012) Insights into the regulation of protein abundance from proteomic and transcriptomic analyses, *Nat. Rev. Genet.* **13** 227–232.
377. You, Z., Genest, J., Barrette, P. O., Hafiane, A., Behm, D. J., D'Orleans-Juste, P. and Schwertani, A. G., (2012) Genetic and pharmacological manipulation of urotensin II ameliorate the metabolic and atherosclerosis sequelae in mice, *Arterioscler. Thromb. Vasc. Biol.* **32** 1809–1816.
378. Smith, D. and Ashton, N., (2013) Personal Communication,.
379. Wang, H., Mehta, J. L., Chen, K., Zhang, X. and Li, D., (2004) Human urotensin II modulates collagen synthesis and the expression of MMP-1 in human endothelial cells., *J. Cardiovasc. Pharmacol.* **44** 577–81.

380. Livak, K. J. and Schmittgen, T. D., (2001) Analysis of relative gene expression data using real-time quantitative PCR and the 2(-Delta Delta C(T)) Method., *Methods* **25** 402–8.
381. Schmittgen, T. D. and Livak, K. J., (2008) Analyzing real-time PCR data by the comparative CT method, *Nat. Protoc.* **3** 1101–1108.
382. Chatenet, D., Dubessy, C., Boularan, C., Scalbert, E., Pfeiffer, B., Renard, P., Lihrmann, I., Pacaud, P., Tonon, M.-C., Vaudry, H. and Leprince, J., (2006) Structure-activity relationships of a novel series of urotensin II analogues: identification of a urotensin II antagonist., *J. Med. Chem.* **49** 7234–7238.
383. Lehmann, F., Currier, E. a, Clemons, B., Hansen, L. K., Olsson, R., Hacksell, U. and Luthman, K., (2009) Novel and potent small-molecule urotensin II receptor agonists., *Bioorg. Med. Chem.* **17** 4657–4665.
384. Chen, J., (2012) Diabetic Nephropathy: Scope of the Problem, in *Diabetes and Kidney Disease*, eds. E. V Lerma and V. Batuman (Springer, New York), pp. 9–14.
385. Nakamura, S., Makita, Z., Ishikawa, S., Yasumura, K., Fujii, W., Yanagisawa, K., Kawata, T. and Koike, T., (1997) Progression of nephropathy in spontaneous diabetic rats is prevented by OPB-9195, a novel inhibitor of advanced glycation, *Diabetes* **46** 895–899.
386. Qiagen, (2015), GeneGlobe specification for Rn_Col4a1_1_SG QuantiTect Primer Assay (QT01620073). Available at: <http://www.qiagen.com/gb/products/catalog/assay-technologies/real-time-pcr-and-rt-pcr-reagents/quantitect-primer-assays?catno=QT01620073#geneglobe>. [Accessed: 03-Mar-2015].
387. Qiagen, (2015), GeneGlobe specification for Rn_Lamb1_1_SG QuantiTect Primer Assay (QT01574531). Available at: <http://www.qiagen.com/gb/products/catalog/assay-technologies/real-time-pcr-and-rt-pcr-reagents/quantitect-primer-assays?catno=QT01574531#geneglobe>. [Accessed: 03-Mar-2015].
388. Qiagen, (2015), Geneglobe specification for Rn_Fn1_1_SG QuantiTect Primer Assay (QT00179333). Available at: <http://www.qiagen.com/gb/products/catalog/assay-technologies/real-time-pcr-and-rt-pcr-reagents/quantitect-primer-assays?catno=QT00179333#geneglobe>. [Accessed: 03-Mar-2015].
389. Ross, B., McKendy, K. and Giaid, A., (2010) Role of urotensin II in health and disease., *Am. J. Physiol. Regul. Integr. Comp. Physiol.* **298** R1156–R1172.

A: Properties of QuantiTect® primer assays

Commercial primer assays were used for the RT-qPCR work carried out in this project; as a result the primer sequences are not publically available. For the purpose of traceability the full properties the primers used can be found below.

A.1 Ywhaz primer assay

The Ywhaz assay used (Qiagen, QT02382184) spanned an exon:exon junction preventing the amplification of gDNA transcripts. The properties of this primer assay can be found in [Table A.1](#), along with the approximate location of the amplicon from this primer pair, as available on the supplier's website (Qiagen, accessed 15/07/2014).³⁶⁷

Name	Rn_Ywhaz_3_SG QuantiTect Primer Assay (QT02382184)
Official symbol	Ywhaz
Official name	tyrosine 3-monooxygenase/tryptophan 5-monooxygenase activation protein, zeta polypeptide
Species	Rat (Rattus norvegicus)
Entrez Gene ID	25578
Detected transcript	NM_013011 (1815 bp)
Ensembl Transcript ID	ENSRNOT00000035628
Amplified exons*	2/3
Amplicon Length	99 bp (NM_013011)
Dye label / detection	SYBR Green

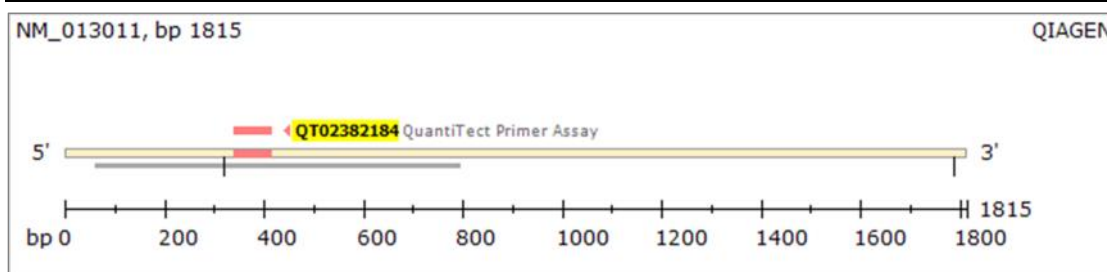


[Table A.1](#) Properties of the QuantiTect™ primer assay used to detect Ywhaz, including schematic diagram illustrating the location of the amplification product within the Ull mRNA transcript.³⁶⁷ The approximate centre of the 99 bp amplicon lies around base 375.

A.2 Urotensin II primer assay

The UII assay used (Qiagen, QT00193018) spanned an exon: exon preventing the amplification of gDNA transcripts. The properties of this primer assay can be found in [Table A.2](#), along with the approximate location of the amplicon from this primer pair, as available on the supplier's website (Qiagen, accessed 15/07/2014).³⁶⁶

Name	Rn_Uts2_1_SG QuantiTect Primer Assay (QT00193018)
Official symbol	Uts2
Official name	urotensin 2
Species	Rat (Rattus norvegicus)
Entrez Gene ID	29180
Detected transcript	NM_019160 (527 bp)
Ensembl Transcript ID	ENSRNOT000000024798
Amplified exons*	3/4
Amplicon Length	82 bp (NM_019160)
Dye label / detection	SYBR Green

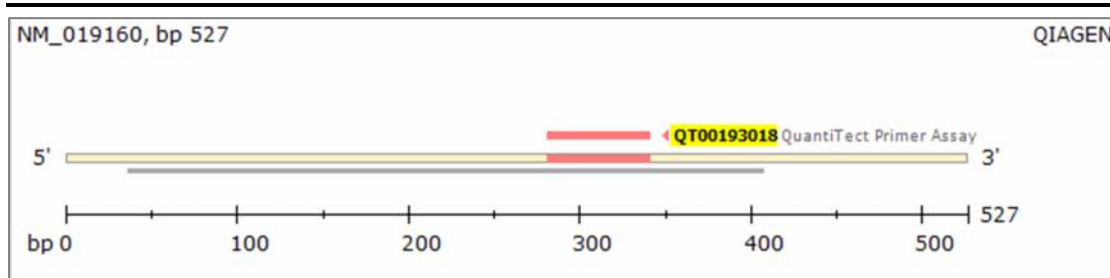


[Table A.2](#) Properties of the QuantiTect™ primer assay used to detect UII, including schematic diagram illustrating the location of the amplification product within the UII mRNA transcript.³⁶⁶ The approximate centre of the 82bp amplicon lies between bases 300 - 325.

A.3 Urotensin II Receptor primer assay

The UT assay used (Qiagen, QT01082690) did not span an exon:exon junction. The properties of this primer assay can be found in [Table A.3](#), along with the approximate location of the amplicon from this primer pair, as available on the supplier's website (Qiagen, accessed 15/07/2014).³⁰⁷

Name	Rn_Uts2r_1_SG QuantiTect Primer Assay (QT01082690)
Official symbol	Uts2r
Official name	urotensin 2 receptor
Species	Rat (Rattus norvegicus)
Entrez Gene ID	57305
Detected transcript	NM_020537 (1161 bp)
Ensembl Transcript ID	Not applicable (this assay may also detect genomic DNA)
Amplicon Length	116 bp (NM_020537)
Dye label / detection	SYBR Green

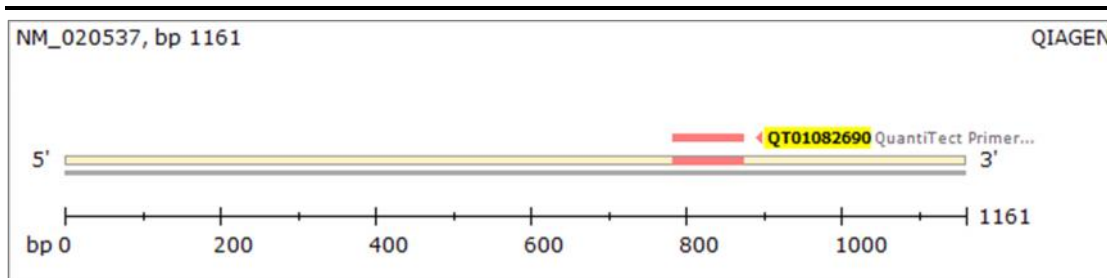


[Table A.3](#) Properties of the QuantiTect™ primer assay used to detect UT, including schematic diagram illustrating the location of the amplification product within the UT mRNA transcript.³⁰⁷ The approximate centre of the 116 bp amplicon lies around base 825.

A.4 Urotensin II - related peptide

The URP assay used (Qiagen, QT00438767) did not span an exon:exon junction. The properties of this primer assay can be found in [Table A.4](#), along with the approximate location of the amplicon from this primer pair, as available on the supplier's website (Qiagen, accessed 15/07/2014).³⁰⁸

.Name	Rn_Uts2b_1_SG QuantiTect Primer Assay (QT00438767)
Official symbol	Uts2b
Official name	urotensin 2B
Species	Rat (Rattus norvegicus)
Entrez Gene ID	378939
Detected transcript	NM_198133 (747 bp)
Ensembl Transcript ID	Not applicable (this assay may also detect genomic DNA)
Amplicon Length	120 bp (NM_198133)
Dye label / detection	SYBR Green

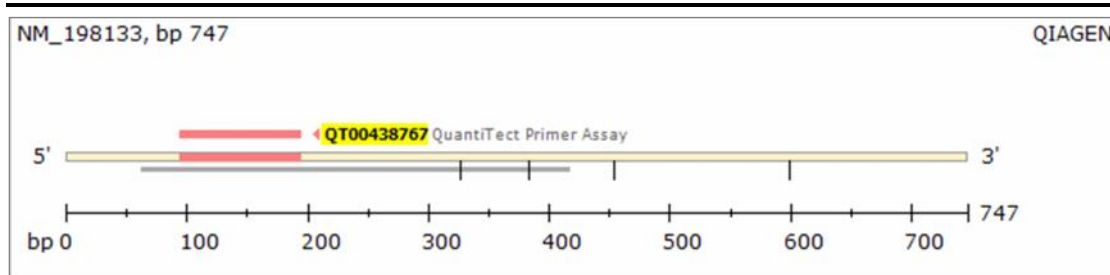


[Table A.4](#) Properties of the QuantiTect™ primer assay used to detect URP, including schematic diagram illustrating the location of the amplification product within the UT mRNA transcript.³⁰⁸ The approximate centre of the 120 bp amplicon lies around base 150.

B: mRNA expression of basement membrane components

The diluted cDNA stocks produced during the qPCR analyses within this thesis (Section 2.13) were used in further QuantiFast® SYBR Green qPCR assays. These assays were kindly performed by Tom Speight under the supervision of Dr. Jo Glazier of the Maternal and Fetal Health Research Centre, University of Manchester.

B.1 Primer specifications

B.1.1 Collagen IV alpha 1 (*Col4a1*)

The Collagen IV alpha 1 assay used (Qiagen QT01620073, *Col4a1*) spanned an exon:exon junction preventing the amplification of gDNA transcripts. A summary Table of the properties of this primer assay can be found below (Table B.1)

Name	Rn_Col4a1_1_SG QuantiTect Primer Assay (QT01620073)
Official symbol	Col4a1
Official name	Collagen, type IV, alpha 1
Species	Rat (<i>Rattus norvegicus</i>)
Entrez Gene ID	290905
Detected transcript	NM_001135009 (6579 bp) XM_001067473 (6579 bp) XM_214400 (6579 bp)
Ensembl Transcript ID	ENSRNOT00000022007
Amplified exons*	37/38
Amplicon Length	66 bp (all transcripts)
Dye label / detection	SYBR Green

Table B.1 Properties of the QuantiTect™ primer assay used to detect Col4a1.³⁸⁶

B.1.2 laminin- β_1 (*Lamb1*)

The laminin- β_1 assay used (Qiagen QT01574531, *Lamb1*) spanned an exon:exon junction preventing the amplification of gDNA transcripts. A summary Table of the properties of this primer assay can be found below ([Table B.2](#)).

.Name	Rn_Lamb1_1_SG QuantiTect Primer Assay (QT01574531)
Official symbol	Lamb1
Official name	Laminin, beta 1
Species	Rat (Rattus norvegicus)
Entrez Gene ID	290905
Detected transcript	NM_001106721 (5837 bp) XM_001075963 (5765 bp) XM_216679 (5626 bp) XM_003750137 (6315 bp) XM_003754198 (5470 bp) XM_006225820 (6165 bp) XM_006239996 (6184 bp) XM_006239997 (6193 bp)
Ensembl Transcript ID	ENSRNOT00000008321
Amplified exons*	28/29
Amplicon Length	121 bp (all transcripts)
Dye label / detection	SYBR Green

[Table B.2](#) Properties of the QuantiTect™ primer assay used to detect *Lamb1*.³⁸⁷

B.1.3 Fibronectin 1 (*Fn1*)

The fibronectin assay used (Qiagen QT00179333, *Fn1*) spanned an exon:exon junction preventing the amplification of gDNA transcripts. A summary table of the properties of this primer assay can be found below ([Table B.3](#))

.Name	Rn_Fn1_1_SG QuantiTect Primer Assay (QT00179333)
Official symbol	Fn1
Official name	Fibronectin 1
Species	Rat (<i>Rattus norvegicus</i>)
Entrez Gene ID	25661
Detected transcript	NM_019143 (8331 bp) XM_006245150 (8260 bp) XM_006245152 (8061 bp) XM_006245153 (7986 bp) XM_006245154 (7975 bp) XM_006245155 (7707 bp) XM_006245158 (7701 bp)
Ensembl Transcript ID	ENSRNOT00000019772
Amplified exons*	32/33
Amplicon Length	92 bp (all transcripts)
Dye label / detection	SYBR Green

[Table B.3](#) Properties of the QuantiTect™ primer assay used to detect *Fn1*.³⁸⁸

B.2 Results, Experiment 1

cDNA samples (provided at 1:100 dilution, [Section 2.13.4](#)) produced from the cortex of SNx rats 7 - 8 weeks (early, EN) post-surgery and at (near, LN) renal failure 30.9 ± 8.5 weeks (mean \pm SD) and time-matched sham controls (EC and LC) were assayed for collagen IV alpha 1 (*Col4a1*), laminin- β_1 (*Lamb1*) and Fibronectin 1 (*Fn1*).

B.2.1 Collagen IV alpha 1 (*Col4a1*)

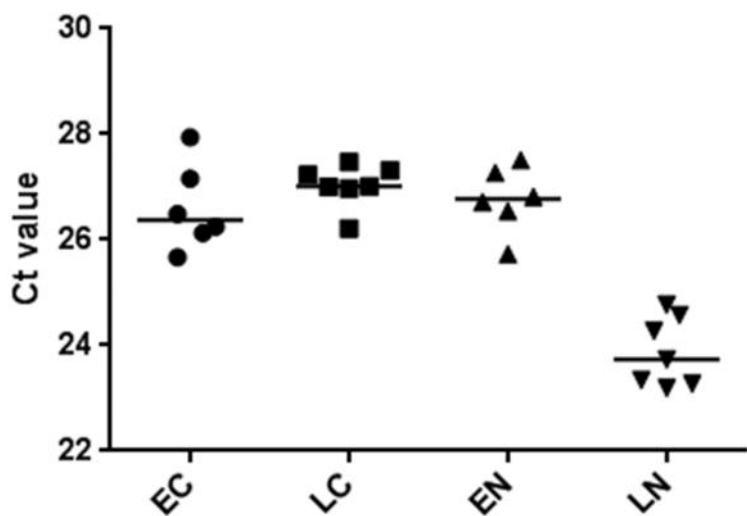


Figure B.1 *Col4a1* appeared to amplify earlier in the samples from renal cortex of late SNx rats (LN) than in early SNx (EN), early sham (EC) or late sham (LC). Each point represents a biological replicate with line at median.

B.2.2 laminin- β_1 (*Lamb1*)

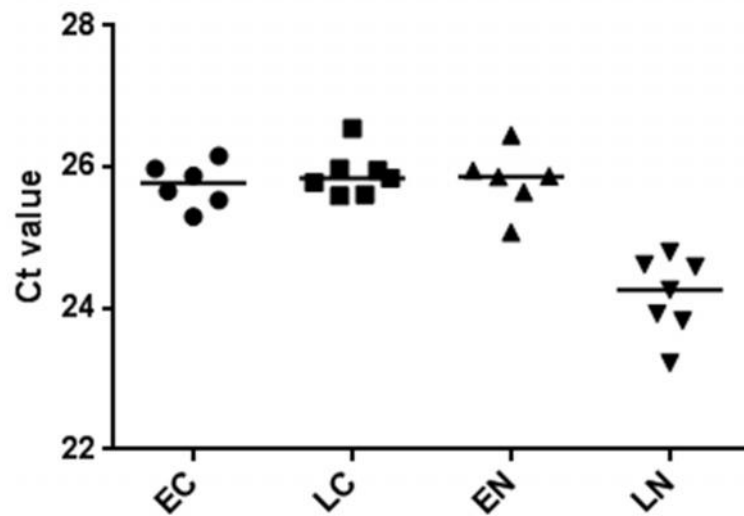


Figure B.2 *Lamb1* appeared to amplify at an earlier cycle in the samples from renal cortex of late SNx rats (LN) than in early SNx (EN), early sham (EC) or late sham (LC). Each point represents a biological replicate with line at median.

B.2.3 Fibronectin 1 (*Fn1*)

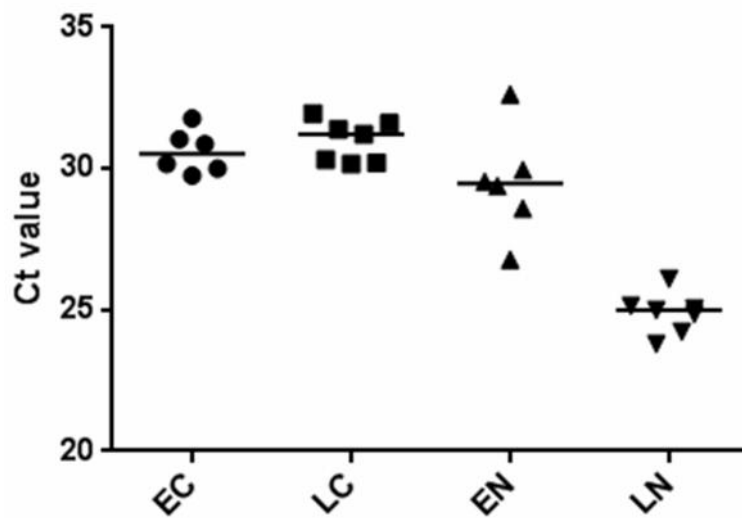
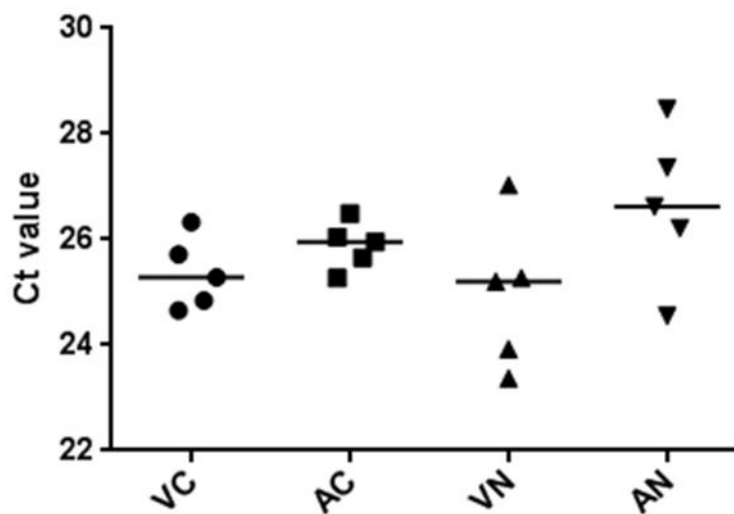


Figure B.3 Ct values for *Fn1* tended to be lower in the samples from renal cortex of late SNx rats (LN) than in early SNx (EN), early sham (EC) or late sham (LC). Each point represents a biological replicate with line at median.

B.3 Results, Experiment 2

cDNA samples (provided at 1:100 dilution, [Section 2.13.4](#)) from the cortex of SNx rats receiving UT-A (NA, n = 5) or vehicle (NV, n = 5) treatment-matched sham controls (SA and SV, n = 5) were assayed for collagen IV alpha 1 (*Col4a1*), laminin- β_1 (Lamb1) and Fibronectin 1 (Fn1).

B.3.1 Collagen IV alpha 1 (*Col4a1*)



[Figure B.4](#) In the *Col4a1* assay Ct values were variable in SNx rats, with some lower Ct values the vehicle treated SNx group (VN) relative to sham controls (VC and VA). Ct values tended to occur later in the UT-A treated SNx (AN) groups. Each point represents a biological replicate with line at median.

B.3.2 laminin- β_1 (*Lamb1*)

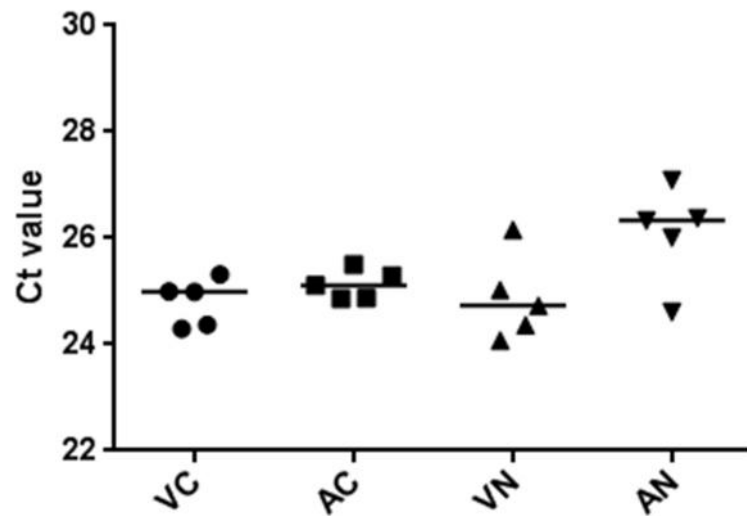


Figure B.5 When amplifying *Lamb1* Ct values tended to be higher in UT-A treated SNx (AN) relative to vehicle treated SNx (VN) and sham controls (VC and VA). Each point represents a biological replicate with line at median.

B.3.3 Fibronectin 1 (*Fn1*)

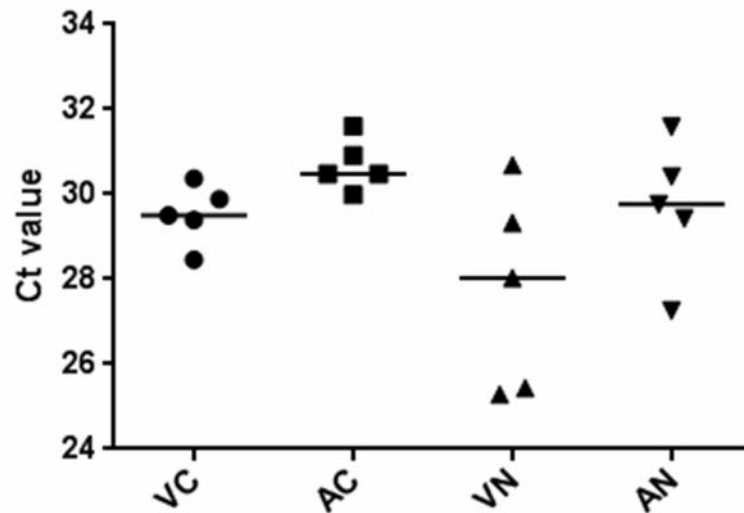


Figure B.6 Ct values for *Fn1* tended to be lower in SNx rats receiving vehicle (VN). Whereas SNx rats receiving UT-A (AN) were comparable to the sham controls (VC and VA). Each point represents a biological replicate with line at median.